

“Spindle organization in three dimensions”

an der Fakultät für Mathematik und Naturwissenschaften der
Technischen Universität Dresden
eingereichte

kumulative

HABILITATIONSSCHRIFT

zur Erlangung des akademischen Grades
doctor rerum naturalium habilitatus
(Dr. rer. nat. habil.)

vorgelegt

von

Dr. sc. nat. Thomas Müller-Reichert

geboren am

3.1.1962

in Frankfurt am Main

Dresden 2006

Für Susanne

Mit dem Wissen wächst der Zweifel.

Johann Wolfgang von Goethe

TABLE OF CONTENTS

SUMMARY	5
ZUSAMMENFASSUNG	6
1 INTRODUCTION	7
1.1 Organization of microtubules in mitotic spindles	7
1.2 Dynamics of microtubules in mitosis	8
1.3 <i>C. elegans</i> as a model system	9
1.4 Electron tomography of spindle components	12
1.5 Aims of this work	13
2 MATERIALS AND METHODS	14
2.1 Laser-induced chemical fixation of isolated <i>C. elegans</i> embryos	14
2.2 High-pressure freezing of whole worms for electron tomography	15
2.3 Correlative light and electron microscopy of single <i>C. elegans</i> embryos ...	17
3 RESULTS	21
3.1 SAS-4 is a <i>C. elegans</i> centriolar protein that controls centrosome size	23
3.2 Morphologically distinct microtubule ends in the mitotic centrosome of <i>Caenorhabditis elegans</i>	37
3.3 Microtubule organization in collapsed mitotic spindles	44
3.4 Role of <i>C. elegans</i> katanin in acentrosomal spindle assembly	57
4 DISCUSSION AND PERSPECTIVES	67
4.1 Application of electron microscopy to study <i>C. elegans</i> ultrastructure	67
4.2 Role of SAS-4 in centriole assembly	69
4.3 Closed microtubule minus ends in the mitotic centrosome	70
4.4 Functional importance of open microtubule minus ends	72
4.5 Spindle assembly in an acentrosomal context	75
5 LITERATURE	78
6 APPENDIX	87
6.1 Related publications	87
6.2 List of publications	130
ERKLÄRUNGEN	132

SUMMARY

During cell division, chromosome segregation takes place on bipolar, microtubule-based spindles. Here, *C. elegans* is used to analyze spindle organization under both mitotic and meiotic conditions. First, the role of SAS-4 in organizing centrosome structure was analyzed. Partial depletion of SAS-4 in early embryos results in structurally defective centrioles. The study of this protein sheds light on the poorly understood role of the centrioles in dictating centrosome size. Second, the ultrastructure of wild-type mitotic spindle components was analyzed by electron tomography. This 3-D analysis reveals morphologically distinct microtubule end morphologies in the mitotic spindle pole. These results have structural implications for models of microtubule interactions with centrosomes. Third, spindle assembly was studied in female meiosis. Specifically, the role of the microtubule severing complex katanin in spindle organization was analyzed. Electron tomography reveals fragmentation of spindle microtubules and suggests a novel katanin-dependent mechanism of meiotic spindle assembly. In this model, relatively long microtubules seen near the meiotic chromatin are converted into numerous short fragments, thus increasing the total number of polymers in an acentrosomal environment. Taken together, these results provide novel insights into the three-dimensional organization of microtubules during spindle assembly.

ZUSAMMENFASSUNG

Die Segregation der Chromosomen während der Zellteilung wird durch bipolare, von Microtubuli-aufgebauten Spindeln gewährleistet. In der vorliegenden Arbeit wird *C. elegans* zur Analyse der Spindelorganisation unter mitotischen und meiotischen Bedingungen herangezogen. Erstens wird die Rolle von SAS-4 in der Organisation von Zentrosomen untersucht. Die partielle Depletierung von SAS-4 in frühen Embryonen führt zu strukturell defekten Zentriolen und wirft somit Licht auf die wenig verstandene Rolle der Zentriolen in der Bestimmung der Zentrosomengröße. Zweitens wird die Ultrastruktur der mitotischen Spindelkomponenten im Wildtyp durch Elektronentomographie untersucht. Diese 3-D-Analyse zeigt, dass im mitotischen Spindelpol unterschiedliche Morphologien der Mikrotubulien zu finden sind. Diese Ergebnisse haben strukturelle Implikationen für Modelle der Mikrotubuli-Zentrosomen-Interaktionen. Drittens wird der Aufbau der Spindel in der weiblichen Meiose, speziell die Rolle des Mikrotubuli-schneidenden Kataninkomplexes in der Spindelorganisation, untersucht. Die Elektronentomographie zeigt hier eine Fragmentierung der Spindelmikrotubuli. Basierend auf diesem Ergebnis wird ein neues Katanin-abhängiges Modell der Formierung der Meiosespindel entwickelt, in dem relativ lange Microtubuli in Nähe des meiotischen Chromatins in zahlreiche kurze Mikrotubuli "zerschnitten" werden. Dies erhöht die Anzahl der verfügbaren Polymere in dieser azentrosomalen Situation. Zusammenfassend bringen diese Ergebnisse neue Einsichten in die räumliche Organisation der Mikrotubuli während des Spindelaufbaus.

1 INTRODUCTION

1.1 Organization of microtubules in mitotic spindles

Microtubules are polar polymers composed of head-to-tail aligned α - and β - tubulin subunits (Hyams and Lloyd, 1994). At the microtubule ends, tubulin subunits are either added during polymerization (growth) or removed during depolymerization (shrinkage). Microtubules are dynamic in that they grow and shrink periodically, a phenomenon described as dynamic instability (Mitchison and Kirschner, 1984). *In vitro* studies have shown that the dynamic state of an individual microtubule is correlated with the morphology of its ends. Growing microtubules exhibit a flared sheet-like structure, whereas shrinking microtubules have curled oligomers with a distinct radius of curvature at their ends (Mandelkow et al., 1991; Chrétien et al., 1995; Müller-Reichert et al., 1998).

In animal cells, microtubules commonly grow from centrosomes with a typical orientation (for reviews see Doxsey, 2001; Bornens, 2002). Microtubule minus ends are located in the centrosome and microtubule plus ends grow away from the centrosome (Fig. 1). The centrosome, composed of a pair of centrioles surrounded by

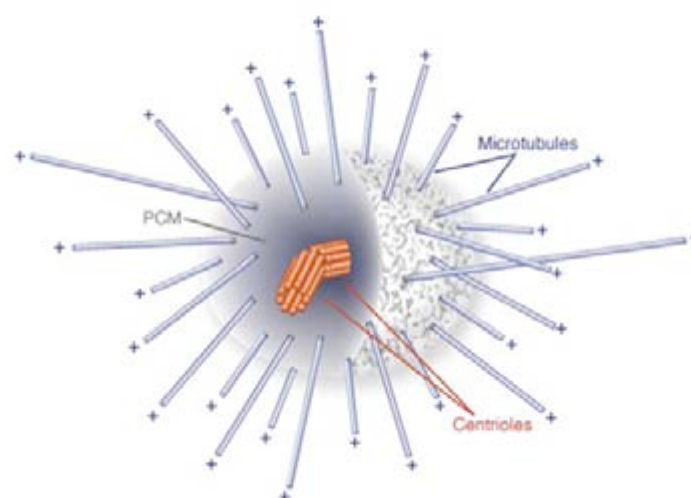


Fig. 1. Orientation of microtubules in the animal centrosome. The diagram shows microtubule minus ends attached to the pericentriolar material (PCM) and microtubule plus ends extending out into the cytoplasm.

pericentriolar material (PCM), provides microtubule nucleation sites (e.g. γ -tubulin and a γ -tubulin ring complex, termed γ -TURC) and a kinetically favorable environment for microtubule polymerization. After nuclear envelope break-down, mitotic spindle assembly starts and microtubules emanating from centrosomes can be divided into those that contact kinetochores (kinetochore microtubules), those that grow towards but do not make contact with chromosomes (non-kinetochore microtubules), and those that grow towards the cell cortex (astral microtubules). Prior to chromosome segregation, the mitotic spindle is under tension as a result of cortical forces that pull on the poles. As anaphase begins, continued forces act on the spindle apparatus to pull the sister chromatids apart (Gönczy et al., 1999; Grill et al., 2003; Afshar et al., 2004; Fisk Green et al., 2004).

1.2 Dynamics of microtubules in mitosis

Previous studies in vertebrate systems have provided some insights into the dynamics of microtubule ends in mitosis (for reviews see Wittmann et al., 2001; Howard and Hyman, 2003). During spindle assembly, microtubule plus ends are selectively stabilized once they associate with kinetochores, causing the rate of microtubule turnover at the plus ends to vary throughout this process. At the minus end of the microtubule, the dynamics is equally complex. For a fraction of microtubules, the minus ends lose subunits while remaining attached to the spindle pole. However, the dynamics and structure of the minus ends, as well as the mechanism by which they maintain a connection to the centrosome, have been less intensively studied and their specific role in spindle assembly remains largely unknown (Dammermann et al., 2003).

Many factors are involved in the regulation of microtubule dynamics throughout mitotic spindle assembly. For instance, microtubule associated proteins (MAPs) are typically implicated in stabilizing microtubules (e.g. XMAP215-like proteins; reviewed in Kinoshita et al., 2002; McNally, 2003). Conversely, some proteins destabilize microtubules by inducing depolymerization (e.g. the kinesin-13 class of kinesins; Desai et al., 1999; reviewed in Moore and Wordeman, 2004), while others

are able to sever intact tubules mid-way along their length, such as katanin (McNally and Vale, 1993). For example, the kinesin-13 family is implicated in microtubule depolymerization at both the plus and minus ends (Desai et al., 1999). At the plus ends, these kinesins cause a rapid depolymerization event, thereby limiting the opportunity for microtubule plus ends to make connections to intracellular structures. At the minus ends, kinesin-13 members have been suggested to promote treadmilling, a phenomenon whereby microtubule subunits are constantly removed from the minus ends and added to the plus ends connected to kinetochores. One good candidate for a microtubule depolymerase in *C. elegans* is KLP-7, a member of the kinesin-13 subfamily. As shown previously, KLP-7 is a centrosomal protein (Oegema et al., 2001) required to limit microtubule outgrowth (Srayko et al., 2005), presumably by depolymerizing microtubule plus ends before they can grow out into the cytoplasm. Microtubule plus ends that grow far enough away from centrosomal KLP-7 activity are no longer vulnerable. Microtubule minus ends, however, are constantly near the centrosome and it is currently unclear if these ends are substrates for KLP-7 activity *in vivo*.

1.3 *C. elegans* as a model system

C. elegans is an excellent model system for studying spindle assembly. Early developmental events are largely invariable from embryo to embryo, i.e. cellular events occur at approximately the same time and in the same manner (Sulston et al., 1983; Wood, 1988; Pelletier et al., 2004a). In the female germ line, mature oocytes are arrested at diakinesis of prophase I. Upon fertilization, meiosis resumes with the formation of two successive acentrosomal spindles to ensure both chromosome segregation and extrusion of polar bodies (Albertson and Thomson, 1993). In these meiotic spindles, microtubules are organized around chromosomes and their minus ends are arranged in acentrosomal spindle poles, lacking typical centrosomal components. It is thought that chromatin-nucleated spindle microtubules are kept short by the action of the katanin-like molecules MEI-1 and MEI-2, which actively sever microtubules (McNally and Thomas, 1998; McNally et al., 2000; Srayko et al., 2000). To date, the mechanisms of this acentrosomal spindle assembly are largely unknown and MEI-1/MEI-2 are the only meiosis-specific factors known so far.

After fusion of female and male haploid genomes, a centrosomal spindle forms in preparation for the first embryonic cell division (Fig. 2; Albertson and Thomson, 1982; Albertson, 1984). The first mitotic spindle in *C. elegans* has attracted much interest, because proteins can easily be depleted by RNA-mediated interference (RNAi), enabling the comparison of wild-type and mutant early embryos.

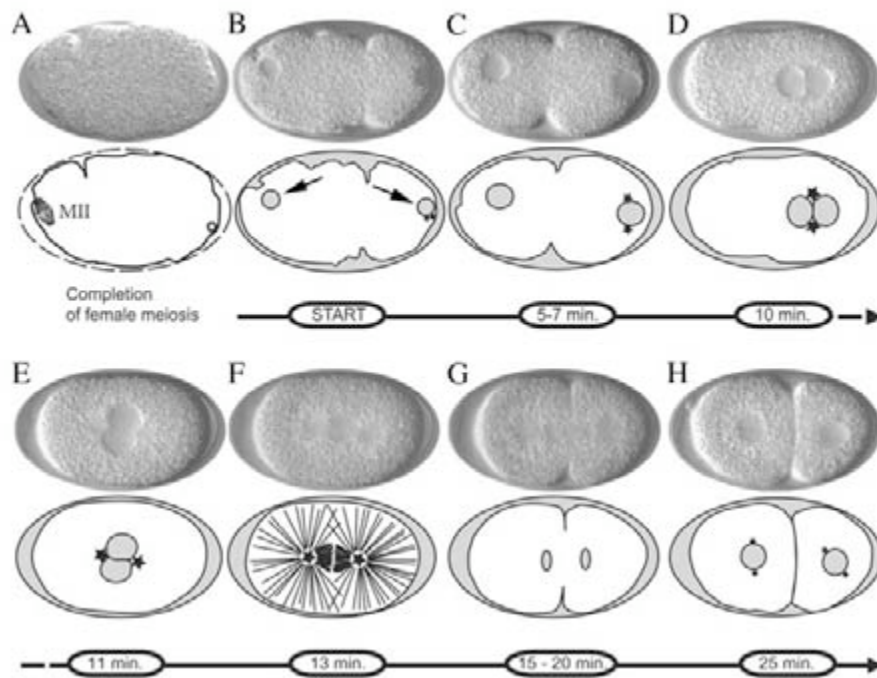


Fig. 2. Early development of the *C. elegans* embryo. Stages are illustrated by DIC images and corresponding schematic drawings (Müller-Reichert et al., 2006). (A) Completion of female meiosis II. (B) Pronuclear appearance. (C) Pronuclear migration. (D) Pronuclear meeting. (E) Pronuclear rotation. (F) Metaphase of the first mitotic division. (G) Telophase. (H) Two-celled embryo. The position and the disappearance of the two pronuclei (arrows) are indicative of specific developmental stages. Asterisks indicate the position of the centrosomes. The *C. elegans* embryo is about 50 μm long and 25 μm high.

To create mutant embryos by RNAi, double-stranded RNA (dsRNA) is introduced in the germ line of *C. elegans* hermaphrodites to give rise to oocytes which are essentially depleted of specific, maternally provided proteins (Fire et al., 1991; Fire et al., 1998). For the purpose of gene discovery, this approach has been applied to conduct a genome-wide cell division screen (Sönnichsen et al., 2005). This genome-wide screen has resulted in the identification of sets of genes required for specific aspects of spindle assembly, such as centriole duplication, microtubule nucleation and centrosome maturation (Oegema and Hyman, 2005). The key components of each process will be introduced briefly.

Centriole duplication in *C. elegans* is under the control of a set of at least 5 genes: ZYG-1 (O'Connell et al., 2001), SAS-4 (Kirkham et al., 2003; Leidel and Gönczy, 2003), SAS-5 (Delattre et al., 2004; Dammermann et al., 2004), SAS-6 (Dammermann et al., 2004), and SPD-2 (Pelletier et al., 2004b). Upon depletion of these proteins (except SPD-2), spindle assembly is indistinguishable from that of wild-type cells during the first mitotic division. During the second mitotic division, however, each of the daughter cells fails to establish a bipolar spindle, but instead assembles a monopolar spindle. SAS-4 has been discovered through a large-scale RNAi-based screen for genes on chromosome III (Gönczy et al. 2000; Zipperlen et al., 2001). Functional analysis suggested that there is a centriolar component whose amount dictates centrosome size.

Microtubule nucleation in *C. elegans* is mainly influenced by the activity of TBG-1, the worm orthologue of γ -tubulin (Bobinnec et al., 2000). In all organisms examined so far, γ -tubulin appears to exist in a heteromeric complex that contains two members of the Spc97/Spc98 protein family conserved from *Drosophila* to humans (Murphy et al., 1998; Gunawardane et al., 2000). This complex, termed the “small” γ -tubulin complex (γ -TuSC), is a subunit of a larger complex referred to as the γ -tubulin ring complex (γ -TuRC) that possesses microtubule capping and nucleating activity *in vitro* (Zheng et al., 1995; Moritz et al., 1995b, Moritz et al., 2000; Oegema et al., 1999). *C. elegans* contains two open reading frames (H04J21.3 and C45G3.3) encoding CeGrip1 and CeGrip2, respectively which probably represent Spc97/Spc98 family members (Hannak et al., 2002). The exact composition of the γ -tubulin complex in *C. elegans*, however, is not known and a *C. elegans* γ -TuRC has yet to be described.

Centrosome maturation in *C. elegans* involves a set of at least four genes, AIR-1, the *C. elegans* aurora A, (Schumacher et al., 1998; Hannak et al., 2001), SPD-2 (O'Connell et al., 2000; Kemp et al., 2004; Pelletier et al., 2004b), SPD-5 (Hamill et al., 2002) and TPXL-1 (Özlü et al., 2005). All of these proteins localize to the centrosome, and are required at different levels for PCM recruitment. TPXL-1, the worm orthologue of TPX-2, is specifically required following nuclear envelope breakdown (NEBD) to establish proper metaphase spindles. Importantly, centrosomes

of *tpxl-1(RNAi)* embryos separate as in wild-type, but collapse together after nuclear envelope breakdown.

1.4 Electron tomography of spindle components

Electron tomography is the method of choice for visualizing the fine structure of cellular organelles with high z-resolution (Fig. 3; reviewed in McEwen and Marko, 2001; Frank et al., 2002; McIntosh et al., 2005). Conceptually similar to CT scans in medical imaging, this method is based on the use of serial tilted views of a semi-thick section (300-400 nm) to create computer-generated reconstructions that can be sliced and imaged in any orientation at ~5 nm resolution in 3-D (reviewed in Frank, 1992). Thus, electron tomography is an ideal method to study complex biological structures, such as the centrosome, and is essential to determine the morphology and three-dimensional distribution of microtubules in both mitotic and meiotic spindles.

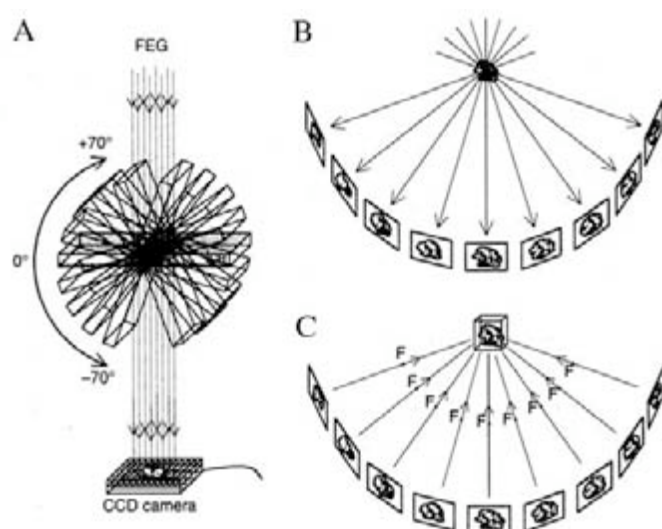


Fig. 3. Principles of electron tomography. (A) Digital collection of tilted views. (B) 2-D representations of a given sample imaged from different orientations. (C) 3-D reconstruction by computed back-projection (after Steven and Aebi, 2003).

Several tomography studies have used isolated centrosomes to provide structural information to correlate with biochemical experiments (Moritz et al., 1995a; Moritz et al., 2000; Vogel et al., 1997; Bullitt et al., 1997; Schnackenberg et al., 1998). Tomographic analysis of isolated centrosomes from *Drosophila* and *Spisula*, revealed the presence of 25 nm diameter ring structures embedded in a 3-D lattice composed of

thin fibers (Moritz et al., 1995a; Schnackenberg et al., 1998). Additional studies using immunolocalization confirmed that γ -tubulin was a component of the 25 nm-ring (Moritz, et al., 1995b; Moritz et al., 2000). Furthermore, isolated centrosomes, treated with high salt, maintained the PCM lattice, or “centromatrix”, but these remnants lacked γ -tubulin rings and were unable to nucleate microtubules. Ring complexes and microtubule nucleating capacity could be recovered upon incubation with extracts containing γ -tubulin (Schnackenberg et al., 1998). These biochemical and structural studies have led to a model showing that the centrosome is formed from a 3-D protein lattice that organizes γ -tubulin and other factors important for microtubule nucleation and anchoring.

Electron tomography has also been applied to study the structure of MTOCs (microtubule-organizing centers) *in vivo*. Comparing wild-type and mutant ultrastructure, this 3-D imaging technique was successfully used to determine the role of specific tubulin isoforms on basal body structure and function in *Chlamydomonas* (O’Toole et al., 2003a). In addition, structure of the *S. cerevisiae* spindle pole body was studied in a wild-type and mutant context to analyze defects in spindle organization (O’Toole et al., 1999; Yoder et al., 2005).

1.5 Aims of this work

Chromosome segregation takes place on bipolar, microtubule-based spindles. *C. elegans* is uniquely suited for structural studies of spindle organization under mitotic (i.e. centrosomal) and meiotic (i.e. acentrosomal) conditions, because both types of division take place in the same cell with a temporal separation of about 20 minutes (Wood, 1988; Pelletier et al., 2004a). Taking advantage of this model system, the following questions are asked: (i) What is the role of specific proteins (i.e SAS-4) in organizing the *C. elegans* centrosome? (ii) How is the wild-type centrosome organized in 3-D? (iii) How is spindle assembly achieved in the absence of centrosomes? To answer these questions, methods for the preparation of *C. elegans* for electron microscopy had to be modified and developed. These methods are described in detail in the next paragraph.

2 MATERIALS AND METHODS

This section describes three different methods for processing *C. elegans* samples for electron microscopy. The first method uses laser-induced chemical fixation (Priess and Hirsh, 1986) to fix isolated embryos at specific mitotic stages. This method takes advantage of time-resolved fixation to investigate centriole duplication. The second method uses high-pressure freezing of whole worms (Rappleye et al., 1999; Müller-Reichert et al., 2003) to analyze the geometry of mitotic spindles in early embryos by electron tomography. This method takes advantage of superior ultrastructural preservation as needed for a high-resolution 3-D study. The third method combines time-resolved fixation with high-pressure freezing to analyze spindle morphology in staged embryos by electron tomography (Müller-Reichert et al., 2006). This method includes containing the isolated embryos in capillary tubes, staging of selected embryos by light microscopy, high-pressure freezing and freeze-substitution of these staged embryos, and 3-D reconstruction of spindle components by electron tomography. Detailed descriptions of these three methods are given in the following paragraphs. Other related methods, such as RNA-mediated interference and specimen preparation for light microscopy, are described in the original publications (except for the analysis of meiotic spindles, see section 3.4).

2.1 Laser-induced chemical fixation of isolated *C. elegans* embryos

A single wild-type or RNAi early embryo was transferred with a mouth pipet to a marked region on an aclar coverslip (Electron Microscopy Sciences) previously glow discharged and coated with 1% poly-L-lysine (Sigma, P1524) in PBS. Water was used to adhere the aclar coverslip to a metal holder before mounting on an inverted microscope (Axiovert 200M, Zeiss). Embryos were imaged through the aclar using DIC until early metaphase. Excess liquid was removed, and the embryo was surrounded with 20 μ l of 1 \times PHEM (60 mM PIPES [pH 6.9], 25 mM HEPES [pH 6.9], 10 mM EGTA, and 2 mM MgCl₂) containing 2% glutaraldehyde and 0.4% tannic acid (O'Connell et al., 2001). A pulsed solid-state UV laser (PowerChip, JDS Uniphase) focused with a 63 \times water immersion objective lens (C-Apochromat, Zeiss) was used for laser permeabilization of the eggshell. About 5 shots were taken at

regions where the vitelline membrane touched the eggshell at the very anterior of the embryo and fixation was monitored by live DIC microscopy. The diffusion of the fixative into the embryo instantly stopped the developing process.

After laser permeabilization, embryos were incubated in fixative on ice for at least 30 min, washed 3-4 times in 1× PHEM, and postfixed in 1% osmium tetroxide and 0.5% $K_3Fe(CN)_6$ in 1× PHEM buffer (O'Connell et al., 2001). The samples were dehydrated through a graded acetone series and gradually infiltrated with Epon/Araldite resin (1 part resin : three parts acetone) for 1 h; 1 : 1 for 2 h; 3 : 1 for 2 h, and 100% resin for 1 h, then overnight, then for 1 h). After infiltration, samples were flat embedded on microscope slides and remounted for thin, serial sectioning. Thin sections (70 nm) were cut using a Leica Ultracut UCT microtome. Sections were collected on Formvar-coated copper grids, poststained with 2% uranyl acetate in 70% methanol followed by aqueous lead citrate and viewed in an FEI TECNAI 12 transmission electron microscope operated at 100 kV.

2.2 High-pressure freezing of whole worms for electron tomography

In preparation for high-pressure freezing, adult wild-type worms containing embryos were selected under a stereomicroscope and transferred to sample holders containing an *E. coli* suspension. About 50-100 worms were placed in the 100- μ m-deep well of a BAL-TEC type A planchette (McDonald, 1999; Engineering Office M. Wohlwend). Samples were covered with the flat side of a complementary planchette (type B) and rapidly frozen using a BAL-TEC HPM 010 (BAL-TEC) high-pressure freezer (Rappleye et al., 1999; Müller-Reichert et al., 2003). Frozen samples were stored in liquid nitrogen until further use.

For freeze-substitution, specimen holders were split under liquid nitrogen and a single planchette type 'A', containing the nematode worms, was transferred to a precooled cryovial (-90 °C) containing the fixative. Freeze-substitution was carried out in anhydrous acetone containing 1% osmium tetroxide and 0.1% uranyl acetate (McDonald and Müller-Reichert, 2002) Using a Leica EM AFS, samples were maintained at -90 °C for 3 days. Freeze-substituted samples were the allowed to warm

to room temperature at a rate of either 5 or 10 °C h⁻¹. At room temperature, specimens were removed from the planchettes and washed three times for 1 h in fresh anhydrous acetone. After the acetone washes, samples were then gradually infiltrated with Epon/Araldite (see section 2.1).

Worms were embedded in thin, optically clean layers of Epon/Araldite on microscope slides (McDonald, 1994). Microscope slides were wiped clean with a soft cloth and coated with Teflon spray (MS-122DF, Miller-Stephenson Chemical Co., Inc., Danbury, CT, USA). Worms were evenly distributed on the cleanly wiped surface of the glass slide. Two layers of Parafilm were used as spacers and coated slides were put on top of the resin samples. After polymerization, worms containing appropriate numbers of early embryos were selected by light microscopy and remounted on 'dummy' blocks for ultramicrotomy. Longitudinal sections through the worms were cut using either a Reichert Ultracut E or a Leica Ultracut UCT Microtome. Semi-thick (300-400 nm) sections were collected on Formvar-coated copper slot grids and post-stained with uranyl acetate followed by Reynold's lead citrate (see section 2.1).

High-voltage electron tomography was carried out essentially as described in O'Toole et al. (1999). Colloidal gold particles (15 nm) were affixed to both surfaces of the semi-thick sections, and the grids were carbon coated to stabilize the samples under the electron beam. Samples were placed in a high-tilt, rotating stage (Gatan model 650, Pleasanton, CA, USA) and imaged using a JEOL JEM1000 microscope operated at 750 kV. Serial, tilted views were collected over a $\pm 60^\circ$ range at 1.5° increments about two orthogonal axes. Images were acquired using a Gatan 1k \times 1k CCD camera at a pixel size of 1.4 nm using an automated image capture software package (Boulder Laboratory for 3-D Fine Structure, CO, USA). Multiple frames, or montages, were collected in order to reconstruct a larger area of the cell (Marsh et al., 2001). Image processing was carried out using the IMOD software package (Ladinsky et al., 1999; O'Toole et al., 1999; Marsh et al., 2001). The serial, tilted views were aligned using the positions of the gold particles, and tomograms were computed using an R-weighted back projection algorithm (Gilbert, 1972). Tomograms from each axis were then aligned to each other and combined (Mastronarde, 1997). The IMOD program was used for image display and 3-D modeling of mitotic features, such as centrioles,

microtubules, microtubule ends and chromatin (Kremer et al., 1996). The ratio of the microtome setting to the final measured thickness of the reconstruction was used to calculate a thinning factor to correct for the collapse of the section during microscopy.

2.3 Correlative light and electron microscopy of single *C. elegans* embryos

To collect isolated early embryos into capillary tubes, ‘loading devices’ were prepared by cutting 2 cm-long pieces of tubing (Hohenberg, 1994), mounting them into gel loader tips, and using nail polish to seal. To cut pieces of tubing of appropriate sizes, a ‘crimping tool’ was made from a scalpel tip by cutting or filing off the final millimeter of the blade, and then shaping it with a whetstone to the shape of a chisel (McDonald et al., 2006). Worms were cut open in small Petri dishes using M-9 buffer containing 20% BSA (Sigma). Embryos were released by cutting the worm in the gonad region with two injection needles (Fig. 4). An early embryo was selected and sucked into the capillary tube, using the loading device mounted on a Pipetman. The tubing was submerged into the BSA-containing M-9 buffer in the Petri dish, then the crimping tool was used to cut the region of the tubing containing the

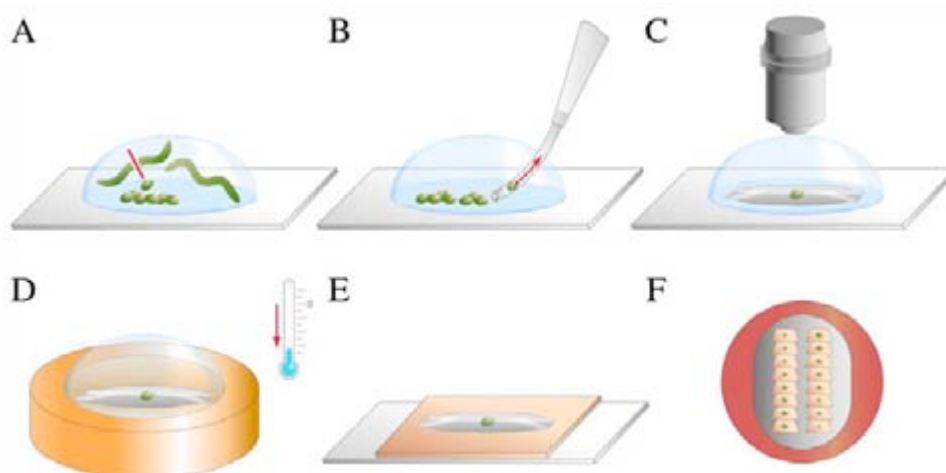


Fig. 4. Diagram illustrating the processing of isolated *C. elegans* embryos for correlative light and electron microscopy. (A) Release of early embryos. (B) Collection of a selected embryo into capillary tubing. (C) Staging of the capillary-contained embryo by light microscopy. (D) Stage-defined fixation by high-pressure freezing. (E) Thin-layer embedding of the freeze-substituted embryo. (F) Serial sectioning for subsequent electron tomography (Müller-Reichert et al., 2006).

early embryo to a final length of about 1 mm. The closed tube was then transferred from the Petri dish to a droplet of BSA-containing M-9 buffer on a glass slide to

observe the further development of the embryo in real time using a light microscope equipped with phase contrast. The developmental history of selected embryos was documented.

To minimize the time-window between observation and freezing, samples were rapidly frozen using an EMPACT2+RTS (Leica) high-pressure freezer, a portable machine that can be easily moved to the site where staging of the embryo is performed. The rapid transfer system (RTS) allows fast loading of the specimen into a pre-loaded high-pressure freezer under standardized conditions (McDonald et al., 2006; Verkade, 2006). In preparation for freezing, the RTS was pre-loaded with a freezing ‘pod’ (Fig. 5). In addition, a specimen carrier, in which the sample has to be placed at an appropriate time point, was pre-mounted in the so-called rapid loader (for details see McDonald et al., 2006; Verkade, 2006). Routinely, 100 μm -deep ‘membrane carriers’ were used, designed to separate the compartment holding the capillary tube from the pressure by a thin ‘membrane’ of copper. Shortly before freezing, the membrane carrier was filled with M-9 buffer containing 20% BSA.

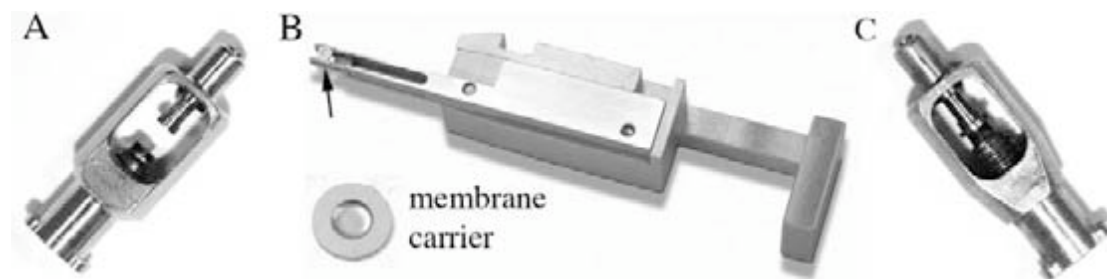


Fig. 5. Loading devices for the rapid transfer system (RTS) of the EMPACT2 high-pressure freezer. (A) The freezing “pod”. (B) “Rapid loader” with pre-mounted specimen carrier (arrow). A “membrane carrier” is shown at higher magnification. (C) Closed freezing “pod” with specimen carrier (Müller-Reichert et al., 2006).

Excess buffer was sucked away with strips of filter paper. At an appropriate developmental stage, the embryo-containing capillary tube was quickly transferred from the microscope slide to the BSA-filled specimen carrier using tweezers. As soon as the capillary tube was loaded in the membrane carrier, the rapid loader was transferred to the RTS. Sliding the rapid loader into the RTS triggered the pod to close automatically and start the ultrarapid freezing procedure. The isolated embryo was transferred from the light microscope to the high-pressure freezer within about 5

seconds. After freezing the membrane carriers were released from the pod and stored in liquid nitrogen until further use.

Freeze-substitution of isolated embryos was carried out essentially as described for whole worms (see section 2.2). The samples were maintained at $-90\text{ }^{\circ}\text{C}$ for a minimum of 8 h and a maximum of 24 h. Freeze-substituted samples were then allowed to warm to room temperature at a rate of $5\text{ }^{\circ}\text{C h}^{-1}$. Specimens were washed in anhydrous acetone and gradually infiltrated with Epon/Araldite resin. Throughout all these steps, the capillary tubes remained in the BSA-filled membrane carriers and were not removed prior to the final flat-embedding step to avoid the loss of the small capillary tubes during rinsing and resin infiltration.

For thin-layer embedding, Teflon-coated slides were polished to get a clean transparent surface and Epon/Araldite (200 – 300 μl) was placed on the microscope slide and allowed to disperse. Subsequently, the membrane carrier containing the capillary tube was placed in the resin droplet and held tightly with appropriate tweezers. The capillary tube was then removed from the specimen carrier with a sharpened tungsten needle and oriented on the glass slide. After polymerization of the resin, samples were observed with a light microscope to re-locate the capillary tubes on the microscope slide. An objective marker with a diamond tip was used to mark a circle around the tube. Using a scalpel, small quadrates of $1 \times 1\text{ mm}$ resin containing the capillary tube were cut out under a stereo microscope. An Epoxy glue was used to remount the samples on ‘dummy’ blocks with the early embryos facing up.

After polymerization, the remounted samples were trimmed for serial sectioning. Semi-thick (300-400 nm) sections were then collected on Formvar-coated copper slot grids and routinely post-stained with uranyl acetate followed by Reynold’s lead citrate (see section 2.1). Stained specimens were then viewed by low-voltage electron microscopy (100 kV) to identify centrosomes in the serial sections.

In preparation for electron tomography, 15-nm colloidal gold particles were affixed to both surfaces of the semi-thick sections. Samples were placed in a high-tilt, tomography stage and imaged with an intermediate-voltage electron microscope

operated at 300 kV. Serial, tilted views were collected over a $\pm 60^\circ$ range at 1° increments about two orthogonal axes and images were acquired using a Gatan 2k \times 2k CCD camera at a pixel size of 1.01 nm using software for automated image capture (SerialEM; Boulder Laboratory for 3-D Fine Structure, CO, USA). Multiple frames, or montages, were collected to reconstruct an area larger than could be seen as a single CCD frame (Marsh et al., 2001). Image processing and 3-D modeling was carried out essentially as described above (section 2.2).

3 RESULTS

Using *C. elegans* as a model system, this chapter describes the regulation of centrosome size, the 3-D organization of the mitotic spindle and the interaction of microtubules with centrosomal components, and the structure and distribution of microtubules in the acentrosomal female meiotic spindle. Each project is briefly summarized and then presented as an original publication (except for section 3.4, manuscript submitted). Other related projects are documented in the “Appendix” (section 6.2).

First, the role of the centriolar protein SAS-4 in the control of centrosome size was analyzed (section 3.1; Kirkham et al., 2003). In summary, spindle assembly during the first mitotic division of fully depleted *sas-4(RNAi)* embryos was indistinguishable from that of wild-type cells. However, each pole of the bipolar *sas-4(RNAi)* spindle contained only a single centriole. In the second mitotic division each of the *sas-4(RNAi)* daughter cells then failed to establish a bipolar spindle, but instead assembled monopolar spindles around the sperm-derived centrioles. This situation in the two-cell embryo changed upon partial depletion of SAS-4. Decreased levels of SAS-4 caused bipolar spindle assembly with an asymmetry in spindle architecture and centrosome size. The asymmetric spindle was organized from single centrioles at each pole. One pole showed an “old” sperm-derived centriole the other pole showed a “new” partially assembled centriole. This partially assembled centriole most likely was composed of a “naked” central tube. Importantly, the partially assembled centrosome accumulated less than wild-type amounts of PCM and it was shown that centrosomal γ -tubulin levels were proportional to the amount of centriolar SAS-4. As a result, a defect in centriole structure caused differences in centrosome size due to a difference in PCM accumulation.

Second, microtubule ends in the mitotic centrosome of *C. elegans* were analyzed by electron tomography (section 3.2; O’Toole et al., 2003b). Briefly, microtubule minus ends were mostly closed but a small population of microtubule ends at the mitotic spindle pole were open. Closed microtubule ends were pointed (or cone-shaped) and uniformly distributed around the centrosome. In contrast, open microtubule ends were

slightly flared and found preferentially on kinetochore-attached microtubules. The “slightly flared” morphology is thought to represent a dynamic state of a microtubule and the closed morphology end a more static state. One hint for a potential source of these open microtubule ends came from an additional study of *tpxl-1(RNAi)* embryos (section 3.3; Özlü et al., 2005). TPXL-1 is the *C. elegans* orthologue of the vertebrate TPX2, a microtubule-associated protein implicated in spindle assembly. Strikingly, in *tpxl-1(RNAi)* embryos, the assembling mitotic spindle collapsed soon after nuclear envelope break-down because the centrosomes were pulled towards the chromatin. Using electron tomography to analyze the collapsed spindle phenotype, a drastic shortening of the kinetochore microtubules was observed. Compared to wild-type spindles, these microtubules exhibited more open minus ends near the chromosome (unpublished observation). Therefore, the *tpxl-1(RNAi)* embryos provided support for the idea that microtubule instability manifests as an open-end morphology.

Third, the 3-D organization of the meiotic spindle and the role of *C. elegans* katanin (MEI-1) in acentrosomal spindle assembly were investigated (section 3.4). In brief, microtubule pole-proximal ends were not focused at a distinct pole in the wild-type female meiosis but were distributed throughout the volume of the spindle. Numerous pole-distal ends were seen at the chromosomes but also at the ends of short microtubules within the spindle. About 30% of the spindle microtubules showed evidence of lateral fragmentation and perforation of the polymer lattice, the later most likely providing a glimpse of the early stages of complete microtubule severing. Importantly, these defects of the microtubule lattice were absent in the *mei-1(null)* mutant.

3.1 SAS-4 is a *C. elegans* centriolar protein that controls centrosome size

M. Kirkham*, T. Müller-Reichert*, K. Oegema*, S. Grill, and A. A. Hyman. 2003. *Cell*. 112, 575-587. (*These authors contributed equally to this work.)

SAS-4 Is a *C. elegans* Centriolar Protein that Controls Centrosome Size

Matthew Kirkham,¹ Thomas Müller-Reichert,¹
Karen Oegema,^{1,2,*} Stephan Grill,
and Anthony A. Hyman*
Max Planck Institute of Molecular Cell Biology
and Genetics
Pfortenhauerstrasse 108
01307 Dresden
Germany

Summary

Centrosomes consist of a centriole pair surrounded by pericentriolar material (PCM). Previous work suggested that centrioles are required to organize PCM to form a structurally stable organelle. Here, we characterize SAS-4, a centriole component in *Caenorhabditis elegans*. Like tubulin, SAS-4 is incorporated into centrioles during their duplication and remains stably associated thereafter. In the absence of SAS-4, centriole duplication fails. Partial depletion of SAS-4 results in structurally defective centrioles that contain reduced levels of SAS-4 and organize proportionally less PCM. Thus, SAS-4 is a centriole-associated component whose amount dictates centrosome size. These results provide novel insight into the poorly understood role of centrioles as centrosomal organizers.

Introduction

Centrioles consist of a polarized central tube surrounded by a 9-fold symmetric array of singlet, doublet, or triplet microtubules (reviewed in Lange et al., 2000; Marshall, 2001; Preble et al., 2000). Centrioles and related structures, referred to as basal bodies or kinetosomes, are found in most extant eukaryotic lineages, including protists, animals, and plants (fungi and higher plants are notable exceptions). Centrioles/basal bodies likely originated in a common ancestor of most eukaryotic lineages where they were components of larger organelles involved in both nuclear division and cell motility (Cavalier-Smith, 2002; Chapman et al., 2000; Mignot, 1996). For their role in nuclear division, the ancestral centriole-containing organelles are thought to have functioned as microtubule organizing centers (MTOCs). The involvement of centrioles in MTOC function by association with pericentriolar material (PCM) that nucleates and organizes microtubules (Gould and Borisy, 1977) and has been retained in one of the most well-studied centriole-containing structures, the animal centrosome (reviewed in Bornens, 2002; Rieder et al., 2001).

In animal cells, mitotic centrosomes consist of a pair of orthogonally connected centrioles surrounded by an

electron dense matrix of PCM. Structural studies in which centrosomes were extracted with chaotropic agents suggest that the PCM contains a matrix of 12–15 nm fibers termed the “centromatrix” (Schnackenberg et al., 1998). The “centromatrix” is tightly associated with the centrioles and directs the recruitment of other centrosomal components including ring-shaped complexes containing γ -tubulin (Moritz et al., 1998; Schnackenberg et al., 1998), a specialized tubulin isoform responsible for the microtubule-nucleating capacity of the PCM (reviewed in Oakley, 2000). Although these studies suggest a mechanism for the targeting of nucleating complexes to centrosomes, the mechanism that links the “centromatrix” to the centrioles remains completely unknown.

In a series of classic experiments, Mazia et al. (1960) demonstrated that a complete centrosome behaves as a pair of “polar organizers”. If experimentally divided, each resulting half centrosome organizes a single spindle pole that cannot be divided further. Subsequent electron microscopy by Sluder and Rieder (1985) showed that the number of “polar organizers” correlates with the number of centrioles present. Compelling evidence for the idea that centrioles act as centrosomal organizers was obtained in a recent experiment in which centrioles were dissolved by injection of an antibody directed against a specific tubulin modification. Dissolution of centrioles resulted in dispersion of the PCM, confirming that centrioles organize PCM to form structurally stable centrosomes (Bobinnec et al., 1998).

The cycles of centriole and centrosome duplication are intimately coupled. Centrioles initiate duplication at the onset of S phase in a process that requires Cdk2 (reviewed in Fry et al., 2000; Lange et al., 2000; Sluder and Hinchcliffe, 1999). At this time a generative disc, a precursor of the daughter centriole, forms at right angles to the proximal end of each mother centriole. Daughter centrioles elongate as the cell cycle progresses, reaching full-length by G2/M. During the G2/M transition the centrosomes also mature, accumulating γ -tubulin and other PCM components, and increasing in size and nucleating capacity (reviewed in Palazzo et al., 2000). Thus, one centrosome containing a pair of centrioles is found at each spindle pole during mitosis. The timing of centrosome splitting and the number of centrioles per centrosome at other cell cycle stages varies between cell types (see Discussion). The cycle of centrosome inheritance and duplication has long fascinated cell biologists, but the mechanisms regulating it are for the most part poorly understood.

The *C. elegans* embryo is uniquely suited for studies of centriole function because of the ease with which powerful functional genomic approaches for gene identification can be combined with high-resolution single cell microscopy-based functional assays. In *C. elegans*, RNA-mediated interference (RNAi) can be used to analyze the first mitotic division that occurs in embryos that have been essentially completely depleted of any targeted gene product (Montgomery and Fire, 1998). Combined with the sequenced genome, this has stimu-

*Correspondence: hyman@mpi-cbg.de (A.A.H.); koegema@ucsd.edu (K.O.)

¹These authors contributed equally to this work.

²Present address: CMM-East 3080, 9500 Gilman Drive, La Jolla, California 92093

lated large-scale RNAi-based approaches that will identify many of the important genes required for cell division (Gönczy et al., 2000; Zipperlen et al., 2001). To date, only one *C. elegans* protein required for centriole function, the atypical protein kinase ZYG-1, has been characterized (O'Connell et al., 2001). Depletion of ZYG-1 by RNAi prevents centriole duplication in the embryo, resulting in a very characteristic phenotype in which a normal first division is followed by assembly of monopolar spindles during the second division (O'Connell et al., 2001; Figure 2A). By looking for this phenotype in an RNAi-based functional genomic screen we identified SAS-4, a novel stably associated centriolar protein. Functional analysis of SAS-4 suggests that it is a centriolar component whose amount dictates centrosome size, providing molecular insight into the role of centrioles as centrosomal organizers.

Results

Centrosome Duplication Fails Prior to the Second Mitotic Division in *sas-4(RNAi)* Embryos

During an RNAi-based screen for genes required for cell division we identified a gene, F10E9.8, whose inhibition results in defects in the second embryonic division (Gönczy et al., 2000). To analyze the nature of the division defect, we performed RNAi of F10E9.8 in a strain expressing GFP- α -tubulin and filmed the embryos using spinning disk confocal microscopy. In all F10E9.8(RNAi) embryos filmed ($n = 15$), microtubule dynamics and spindle assembly were identical to wild-type during the first mitotic division (Figure 1A, top images; see also Supplemental Movies S1 and S2 available at <http://www.cell.com/cgi/content/full/112/4/575/DC1>). However, as F10E9.8(RNAi) embryos entered their second division, each daughter cell assembled only a single centrosomal microtubule aster. These single asters increased normally in size as the cells entered mitosis, and monopolar spindles were formed (Figure 1A, lower right image, and Supplemental Movies S1 and S2 available at above website).

Assembly of monopolar spindles during the second mitotic division suggested that F10E9.8(RNAi) embryos might be defective in centrosome function. We therefore examined centrosome dynamics using a strain co-expressing GFP- γ -tubulin, a centrosomal marker, and GFP-histone (Figure 1B, see also Supplemental Movies S3 and S4 available at above website). In all F10E9.8(RNAi) embryos filmed ($n = 10$), bipolar spindles with wild-type levels of γ -tubulin fluorescence at the spindle poles formed during the first mitotic division (Figure 1B, top images). However, only a single focus of γ -tubulin fluorescence was observed in each daughter cell during the second mitotic division. These single centrosomes accumulated γ -tubulin normally and organized monopolar spindles (Figure 1B, lower right image, and Supplemental Movies S3 and S4 available at above website). Identical results were obtained in fixed F10E9.8(RNAi) embryos stained for three additional centrosomal markers ZYG-9 (Figure 1C; Matthews et al., 1998), AIR-1, and SPD-5 (data not shown; Hamill et al., 2002; Hannak et al., 2001; Schumacher et al., 1998). From these results, we conclude that F10E9.8(RNAi) embryos are defective

in centrosome duplication following the first mitotic division.

Database searches revealed a cDNA, yk425b11, corresponding to F10E9.8. PCR with the *trans*-spliced SL2 leader sequence confirmed that this cDNA contains the full-length coding sequence. F10E9.8 codes for a 92 kDa protein with no obvious homologies or motifs except a central coiled-coil domain (Figure 1D). Because inhibition of F10E9.8 function by RNAi results in failure of spindle assembly at the second mitotic division, this gene has been named *sas-4* for spindle assembly defective.

SAS-4 Is Required for Centriole Duplication

How might the *sas-4(RNAi)* phenotype arise and why does it affect centrosome function during the second but not the first cell division? A previous study of the atypical protein kinase ZYG-1 showed that a normal first division followed by monopolar spindle assembly in the second division is a characteristic phenotype resulting from the inability of RNAi-depleted embryonic cytoplasm to support centriole function (Figure 2A; O'Connell et al., 2001). In *zyg-1(RNAi)* embryos, centriole duplication fails. However, other centriole defects, such as the inability of the daughter centriole to recruit or retain PCM or failure of the daughter centriole to separate from the mother centriole, could also result in a similar defect. To distinguish between these possibilities, we examined wild-type and *sas-4(RNAi)* embryos by correlative differential interference contrast (DIC) microscopy/serial section transmission electron microscopy (TEM; Figures 2B and 2C). Fertilized embryos were filmed using DIC microscopy until metaphase of the first embryonic mitosis. At this stage, embryos were rapidly fixed by laser permeabilization in the presence of glutaraldehyde (Priess and Hirsh, 1986). To count the number of centrioles at each spindle pole, fixed embryos were serially sectioned and analyzed by TEM. Previous work has shown that in wild-type, a pair of centrioles is present at each metaphase spindle pole (Albertson, 1984; O'Connell et al., 2001). We confirmed this in the two wild-type embryos that we sectioned (Figure 2B). Significantly, in the four *sas-4(RNAi)* embryos that we serially sectioned, only one centriole was found at each spindle pole (Figure 2C). From these results, we conclude that SAS-4 is required for centriole duplication in the *C. elegans* embryo.

SAS-4 Localizes to Centrioles Throughout the Cell Cycle

Our phenotypic analysis indicated that SAS-4 is required for centriole duplication, raising the possibility that SAS-4 is a centriolar component. To examine the localization of SAS-4 *in vivo*, we generated an affinity-purified polyclonal antibody and used it for immunofluorescence of whole worms and fixed embryos. In worms, SAS-4 colocalized with γ -tubulin to centrosomes both in sperm and in the syncytial part of the gonad (Figure 3A). Interestingly, SAS-4 staining in the gonad disappeared as the meiotic nuclei cellularized to form oocytes (Figure 3A), presumably marking the point at which the centrioles are lost during oogenesis. At fertilization, a centriole pair enters the oocyte with the sperm (see Figure 2A). In

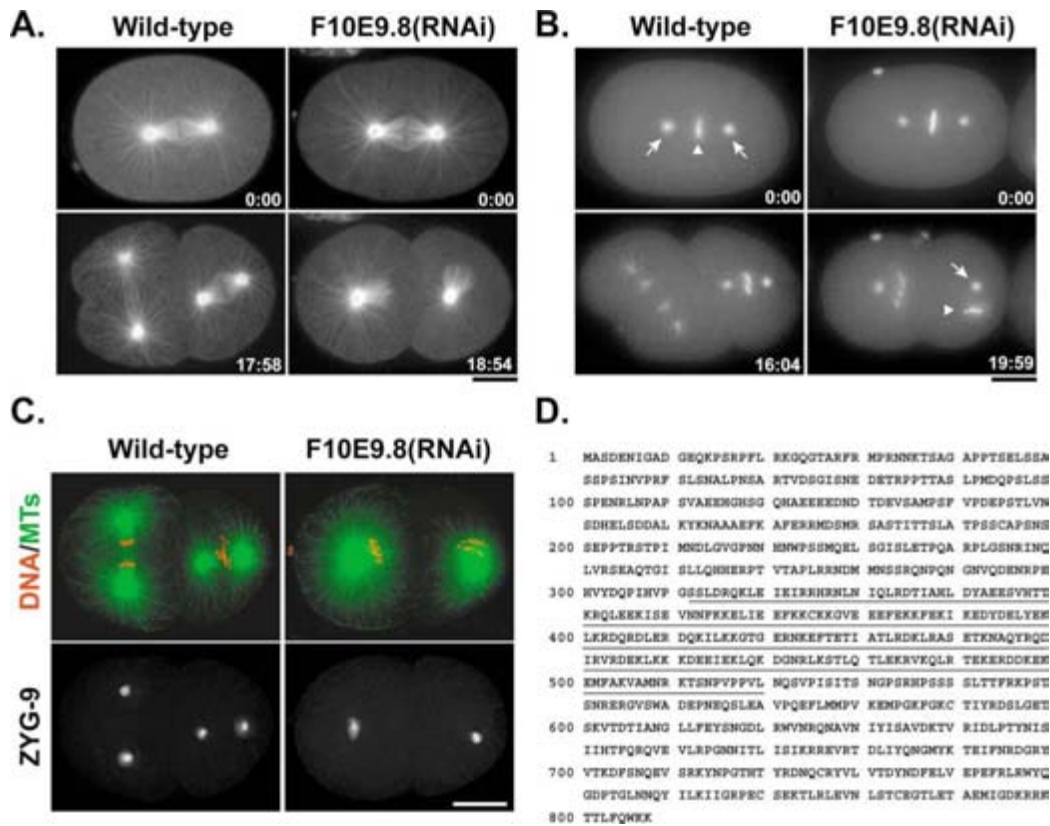


Figure 1. Centrosome Duplication Fails in F10E9.8(RNAi) Embryos

Selected frames from recordings of wild-type and F10E9.8(RNAi) embryos expressing GFP- α -tubulin (A, see also Supplemental Movies S1 and S2 available at <http://www.cell.com/cgi/content/full/112/4/575/DC1>) or co-expressing GFP- γ -tubulin and GFP-histone (B, see also Supplemental Movies S3 and S4 available at above website). In both strains, F10E9.8(RNAi) embryos assemble normal spindles during the first mitotic division (upper right images in A and B) and monopolar spindles during the second mitotic division (lower right images in A and B). The numbers in the lower right corners of each image show time elapsed from metaphase of the first embryonic mitosis. The arrows in the upper left image of (B) point to the two foci of centrosomal γ -tubulin fluorescence, located on either side of the aligned chromosomes (arrowhead). The arrow and arrowhead in lower right image of (B) point to the single focus of γ -tubulin fluorescence and chromosomes, respectively, in a monopolar spindle.

(C) Two-cell stage wild-type and F10E9.8(RNAi) embryos were fixed and stained for microtubules (MTs) and DNA (green and red in upper images) and the centrosomal protein ZYG-9 (lower images). Only one focus of ZYG-9 staining is seen at the pole of the monopolar spindles in F10E9.8(RNAi) embryos.

(D) F10E9.8 codes for a novel 92 kDa protein with a region predicted to form a coiled coil (underlined). Scale bars are 10 μ m.

newly fertilized embryos, SAS-4 is localized to a discrete spot near the sperm-derived pronucleus (Figure 3C, top images). At a slightly later stage, γ -tubulin is recruited to the sperm centrioles forming a focus that colocalizes with SAS-4 (not shown). As the embryo proceeds into mitosis, the amount of γ -tubulin at centrosomes dramatically increases (Hannak et al., 2001; Figure 3C, bottom images). In contrast, the SAS-4 staining remains unchanged as a small dot in the center of the centrosome (Figures 3C and 3E). To confirm the antibody localization, we generated a GFP-SAS-4 expressing strain using microparticle bombardment (Praitis et al., 2001). In living embryos, GFP-SAS-4 fluorescence was observed at a fine focus within centrosomes throughout the cell cycle, similar to the antibody staining (Figures 3B and 3D). From these results, we conclude that SAS-4 localizes to core centrosomal structures, most likely centrioles, throughout the cell cycle.

To examine SAS-4 localization at an ultrastructural level, we performed immunoelectron microscopy on embryos from wild-type hermaphrodites subjected to high-pressure freezing/freeze substitution. In the majority of sections containing centrioles, the secondary antibody conjugated 10 nm colloidal gold particles were observed specifically associated with centriole walls (Figure 3F). In many images, gold particles were detected associated with both mother and daughter centrioles. Cumulatively, the results of the immunofluorescence and immunoelectron microscopy indicate that SAS-4 localizes to centrioles throughout the cell cycle.

SAS-4 Is a Stably Associated Centriole Component that Is Incorporated During Centriole Duplication

To determine if SAS-4 is a stably associated structural component of centrioles, like centriolar tubulin (Kochan-

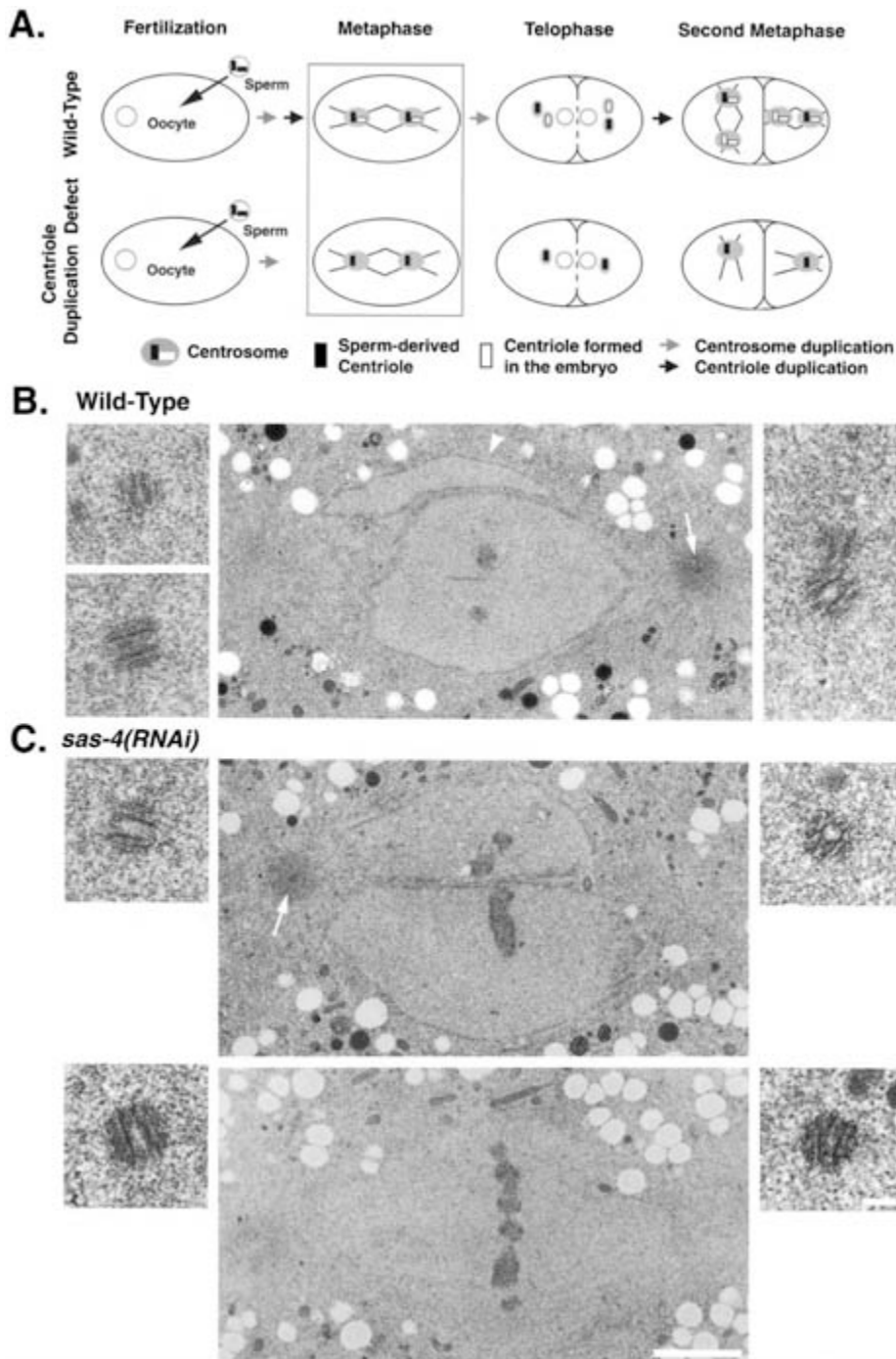


Figure 2. Centriole Duplication Fails in *sas-4(RNAi)* Embryos

(A, top row) Schematic of the centrosome and centriole cycles that follow fertilization in a wild-type *C. elegans* embryo. (Fertilization) During fertilization, the sperm brings a centriole pair into the oocyte, which lacks centrioles (Albertson, 1984; Wolf et al., 1978). (Metaphase) The sperm-derived centriole pair separates and duplicates so that by metaphase of the first mitotic division both spindle poles have a centrosome containing a pair of centrioles (Albertson, 1984; O'Connell et al., 2001). One of the centrioles in each pair was derived from the sperm (black) and the other was formed in the embryonic cytoplasm (white). (Telophase) The centrosomes split (gray arrow) during telophase so that each newly formed daughter cell inherits two centrosomes each containing a single centriole. (Second Metaphase) These centrioles subsequently duplicate (black arrow), so that by metaphase of the second embryonic division each centrosome again contains a pair of centrioles.

(A, bottom row) Schematic of the centrosome and centriole cycles that follow fertilization in an RNAi-depleted embryo that cannot support centriole duplication. Since sperm formation occurs at a developmental stage prior to injection of the interfering dsRNA, a normal centriole pair still enters the oocyte with the sperm during fertilization. These centrioles separate and organize two centrosomes that form the poles of a normal-looking bipolar spindle. However, each metaphase centrosome has only a single sperm-derived centriole. As a consequence of

ski and Borisy, 1990), or whether it is in a dynamic equilibrium with a cytoplasmic pool, we performed a marked mating experiment in which wild-type N2 males were mated to hermaphrodites expressing GFP-SAS-4 (Figure 4). Since male sperm is utilized preferentially over hermaphrodite sperm, this allowed us to introduce centrioles containing exclusively unlabeled SAS-4 into oocyte cytoplasm containing GFP-SAS-4. Embryos were fixed at various times after fertilization and double-label immunofluorescence was performed with the anti-SAS-4 antibody, which detects both the unlabeled SAS-4 and GFP-SAS-4 (Figure 4, total SAS-4), and with an anti-GFP antibody, which selectively detects the GFP-SAS-4 derived from the oocyte cytoplasm (Figure 4, GFP-SAS-4).

In recently fertilized embryos, in which the oocyte pronucleus was still undergoing meiosis, SAS-4 was present as a spot associated with the sperm pronucleus (Figure 4A, total SAS-4). No GFP-SAS-4 was detected, suggesting that SAS-4 associated with the sperm-derived centrioles does not exchange with the cytoplasmic pool (Figure 4A, GFP-SAS-4). By prophase of the first mitotic division, GFP-SAS-4 was detected in the centers of both centrosomes (Figure 4B). The appearance of GFP-SAS-4 coincided with the timing of centriole duplication, presumably reflecting the incorporation of GFP-SAS-4 into daughter centrioles synthesized in the embryo cytoplasm. At metaphase, GFP-SAS-4 continued to be present as a single focus in the center of each centrosome (Figure 4C).

Centrosomes split during telophase, resulting in two centrosomes each of which contains one centriole (see schematic in Figure 4D). This stage is particularly informative because it makes it possible to assay the SAS-4 associated with each centriole independently. Significantly, while both centrosomes contain SAS-4, only one of the centrosomes, most likely the one containing the daughter centriole synthesized in the embryo cytoplasm, contains GFP-SAS-4 (Figure 4D). By prophase of the second mitosis, the centrioles have duplicated again. Both centrosomes now contain at least one centriole that was synthesized in the oocyte cytoplasm and GFP-SAS-4 is detected in the center of both centrosomes (Figure 4E). Interestingly, although the intensity of total SAS-4 staining was equivalent between the two centrosomes in each prophase cell of two-cell embryos, the GFP-SAS-4 staining was asymmetric (Figure 4E). This asymmetry is consistent with one centrosome containing two centrioles formed in the embryo, and the other centrosome containing one unlabeled centriole inherited from the sperm and one centriole formed in

the embryo (see schematic to the right of Figure 4). Thus, SAS-4 is a stably associated centriolar component that, like centriolar tubulin, is incorporated during their duplication.

Partial Depletion of SAS-4 Results in Assembly of Centrosomes That Have Less Than Wild-Type Amounts of PCM

Depletion of either ZYG-1 or SAS-4 leads to failure of centriole duplication. To analyze the relationship between the *zyg-1(RNAi)* and *sas-4(RNAi)* phenotypes, we first performed partial RNAi of *sas-4* by varying the time between injection of dsRNA into hermaphrodites and analysis of newly fertilized embryos. Surprisingly, we found that partial *sas-4(RNAi)* led to intermediate phenotypes not previously observed in *zyg-1(RNAi)* embryos. Following partial RNAi of *sas-4*, asymmetric spindles were observed at the two-cell stage in approximately half of the analyzed embryos (Figure 5A; n = 30 embryos; see also Supplemental Movies S5–S7 available at <http://www.cell.com/cgi/content/full/112/4/575/DC1>). In these spindles, one centrosome had wild-type levels of γ -tubulin whereas the second centrosome had significantly less γ -tubulin and was located closer to the chromosomes. By varying the time of dissection after dsRNA injection, we obtained a continuous range of asymmetric spindles all of which had one normal-looking centrosome and a second centrosome with γ -tubulin levels that varied between normal and barely detectable. These observations suggest that SAS-4 levels dictate the amount of PCM at centrosomes.

To quantitatively compare partial RNAi of *zyg-1* and *sas-4*, we injected hermaphrodites with dsRNA directed against either gene and dissected them after incubation at 16°C for 18, 24, and 28 hr. As a control, we also dissected hermaphrodites injected with *sas-4* RNA that were incubated for 36 hr at 20°C, the conditions used above for stringent RNAi of *sas-4* (Figures 1 and 2). Centrosomes in fixed mitotic two-cell stage embryos were analyzed by staining for γ -tubulin (Figure 5B) and ZYG-9 (not shown). The asymmetry of the centrosome pair in each cell was assessed and classified as either wild-type, asymmetric or, if only one centrosome was present, mono-centrosomal. This analysis revealed that asymmetric spindles are never observed in *zyg-1(RNAi)* embryos. Rather, a threshold level of ZYG-1 is required for centriole duplication to occur (Figure 5C). In contrast, varying SAS-4 levels result in centrosomes of intermediate size (Figures 5B and 5C), suggesting that SAS-4 levels control the amount of PCM at centrosomes.

the failure of centriole duplication, centrosomes fail to split during telophase. Thus, each daughter cell inherits only one centrosome and monopolar spindles form during the second mitotic division.

(B and C) Embryos at the boxed stage in (A) were examined using correlative DIC imaging and serial section TEM. The central images show a single section to give a low-magnification perspective of the analyzed embryo. In wild-type (B), two centrioles were observed at each spindle pole. In the example shown, both centrioles of the right spindle pole were present in the same section (arrow; B, right image); for the left spindle pole, the two centrioles were found in different sections (B, left images).

(C) Two examples of *sas-4(RNAi)* embryos are shown. Only one centriole was found at each spindle pole in all serial sections (shown to the left and right of central images). Note that the nuclear envelopes surrounding the two pronuclei do not completely break down till later in mitosis (the edge of one pronucleus is indicated by an arrowhead in B) and that centrioles in *C. elegans* consist of 9-fold symmetric array of singlet microtubules (Wolf et al., 1978). Scale bars for central overview images are 2.5 μ m; scale bars for higher magnification images are 100 nm.

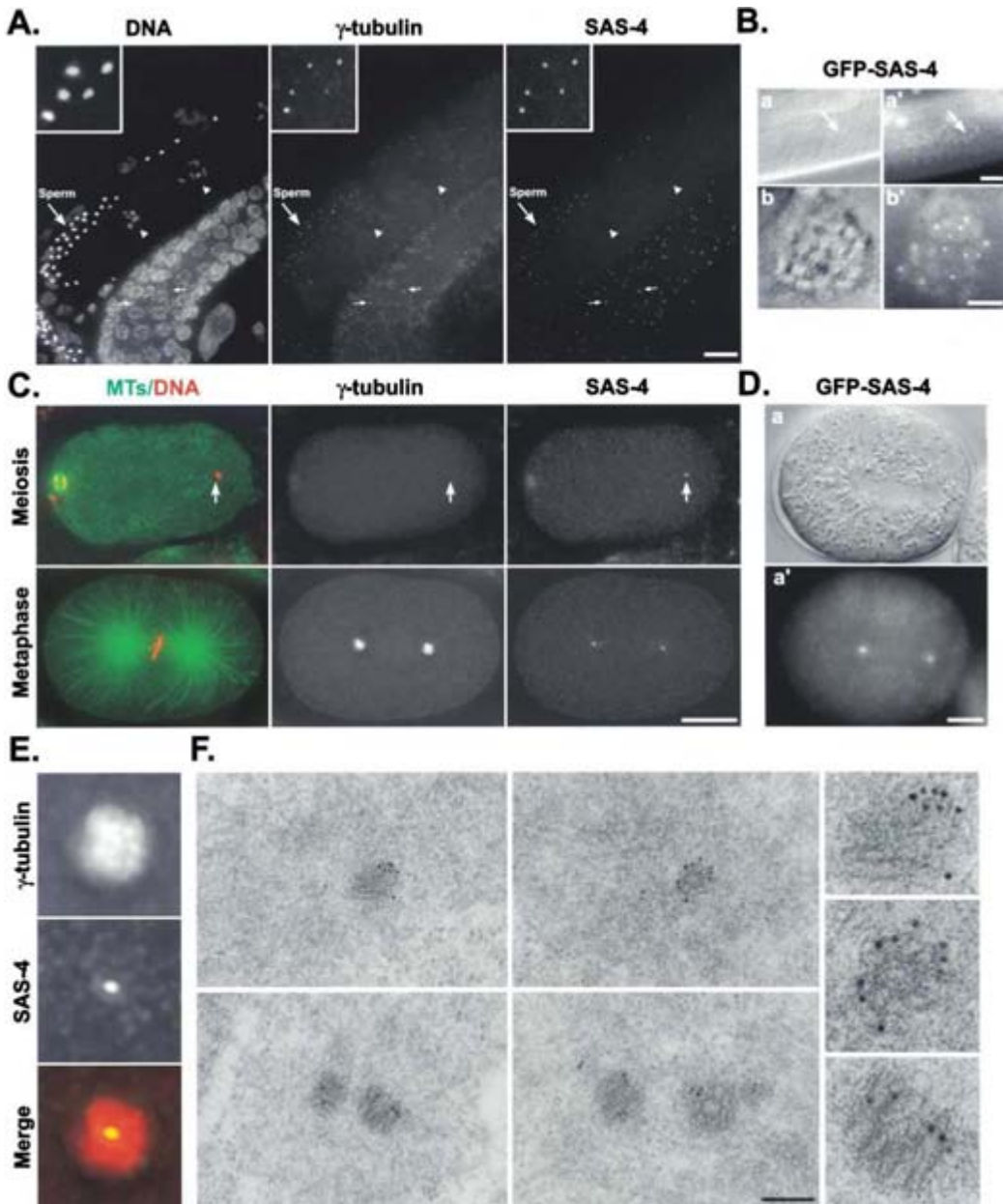


Figure 3. SAS-4 Localizes to Centrosomes Throughout the Cell Cycle

(A) Wild-type hermaphrodites were fixed and stained for DNA, γ -tubulin, and SAS-4. SAS-4 colocalized with γ -tubulin to centrosomes in sperm (arrow on left side of all images and insets) and to centrosomes associated with nuclei in meiotic prophase in the gonad arm (small arrows), but disappeared in oocytes (arrowheads). Insets were magnified 3 \times .

(B) Hermaphrodites expressing GFP-SAS-4 were examined by DIC (a, b) and for GFP fluorescence (a', b'). As was the case for the SAS-4 antibody staining, single punctate fluorescent foci were found in sperm and associated with meiotic nuclei in the gonad arm. Arrows in (a) and (a') indicate the location of a cluster of GFP-SAS-4 foci.

(C) Wild-type embryos were fixed and stained to visualize microtubules (MTs) and DNA (green and red in left images), γ -tubulin (middle images), and SAS-4 (right images). In recently fertilized embryos in which the oocyte nucleus was still completing meiosis (top images), SAS-4 was observed in a single punctate focus associated with the sperm pronucleus (arrows). No colocalizing γ -tubulin staining was observed at these early time points. (C) At metaphase, two small foci of SAS-4 staining are seen in the center of the γ -tubulin staining at each spindle pole.

(D) Stills taken from a time-lapse recording of an embryo expressing GFP-SAS-4. Both DIC (a) and GFP fluorescence (a') are shown. In the DIC image, the mitotic spindle is visible as a region that excludes yolk granules. Punctate foci of GFP-SAS-4 are observed in the center of each spindle pole.

(E) Higher magnification (6.4 \times) view of the right centrosome in the metaphase image in (C). Scale bars in (A–D) are 10 μ m.

(F) Localization of SAS-4 by immunoelectron microscopy. Immunolabeling was found associated with centriole walls. Labeling was detected on both mother and daughter centrioles. Scale bar is 250 nm. Images in the right column show selected centrioles from the images on the left magnified 2.5 \times .

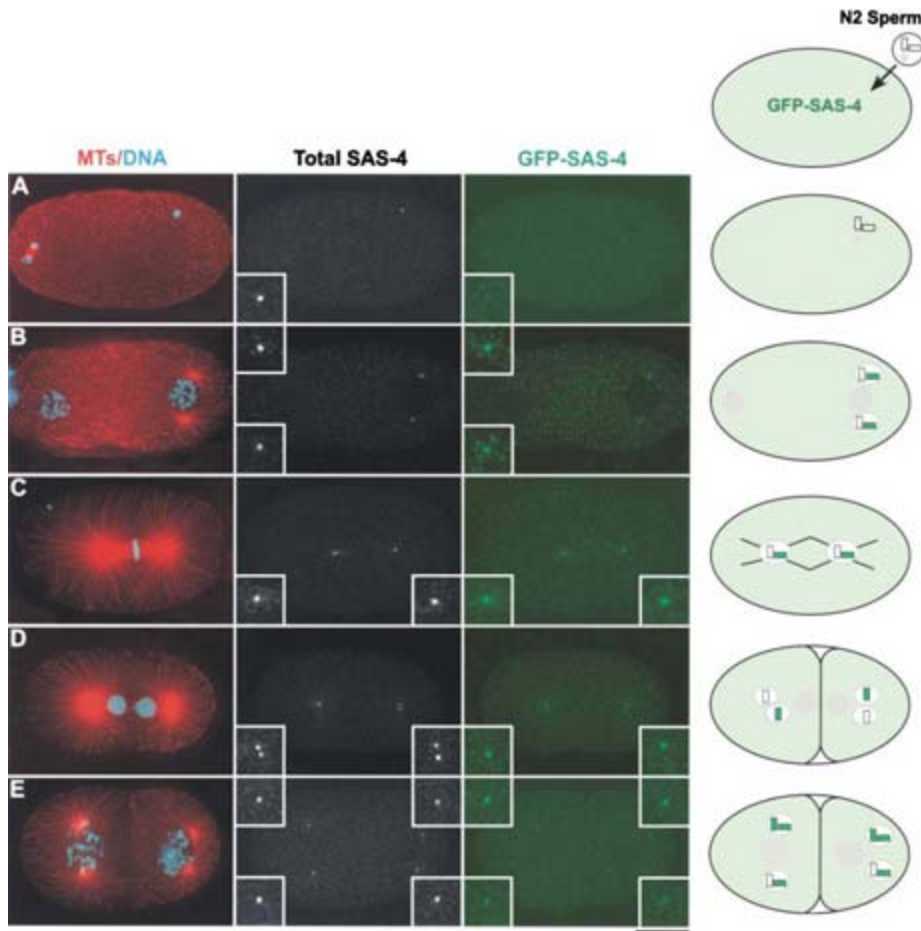


Figure 4. SAS-4 Is Incorporated during Centriole Duplication and Remains Stably Associated Thereafter

Wild-type (N2) males were mated with hermaphrodites expressing GFP-SAS-4. Embryos were fixed at various times after fertilization and stained for microtubules (MTs) and DNA (red and blue in left images) and with antibodies to SAS-4 to detect both the labeled and unlabeled protein (total SAS-4) and to GFP to detect only the GFP-SAS-4 fusion (GFP-SAS-4). Centrosomes are shown in the insets (magnified 3 \times). A schematic of our interpretation of the results is shown on the right.

- (A) In recently fertilized embryos, SAS-4 localizes to the centriole pair associated with the sperm nucleus. There is no staining in the GFP channel.
 (B) By prophase of the first mitotic division, GFP-SAS-4 has been incorporated into both centrosomes.
 (C) GFP-SAS-4 is also detected in a single focus in the center of each centrosome at metaphase.
 (D) When the centrosomes split in telophase, each daughter centrosome inherits one centriole. Both centrosomes have a focus of SAS-4 staining. However, only one of the centrosomes, likely the one containing the daughter centriole synthesized in the embryo, contains GFP-SAS-4.
 (E) By prophase of the two-cell stage the centrioles have duplicated again. All of the centrosomes contain at least one centriole that was synthesized in the oocyte cytoplasm and all contain the GFP-SAS-4 fusion protein. Scale bar is 10 μ m.

Centriolar SAS-4 Levels Correlate with Centrosome Size

Why does partial RNAi of *sas-4* result in centrosomes of intermediate sizes? A simple hypothesis to explain this observation is that the amount of PCM at a centrosome is proportional to the amount of centriolar SAS-4. To see if this is the case, we performed quantitative immunofluorescence of embryos partially depleted of SAS-4 using directly labeled antibodies against SAS-4 and γ -tubulin. In projections of 3D deconvolved images of mitotic two-cell stage embryos, weaker SAS-4 fluorescence appeared to correlate with weaker γ -tubulin fluorescence at the dim centrosome of the asymmetric

centrosome pairs (Figure 6A). To quantify this relationship, we measured total 3D centrosomal SAS-4 and γ -tubulin fluorescence for 14 wild-type and 13 partial *sas-4(RNAi)* centrosome pairs in mitotic two-cell embryos. This analysis confirmed the qualitative observation that the centrosomal fluorescence of both SAS-4 and γ -tubulin at the dim centrosome in *sas-4(RNAi)* embryos was significantly reduced relative to wild-type (Figure 6B, $P < .001$); in contrast, the amount of SAS-4 and γ -tubulin at the bright centrosome of the asymmetric pair in *sas-4(RNAi)* embryos was not significantly different from wild-type (Figure 6B).

To examine the relationship between the amount of

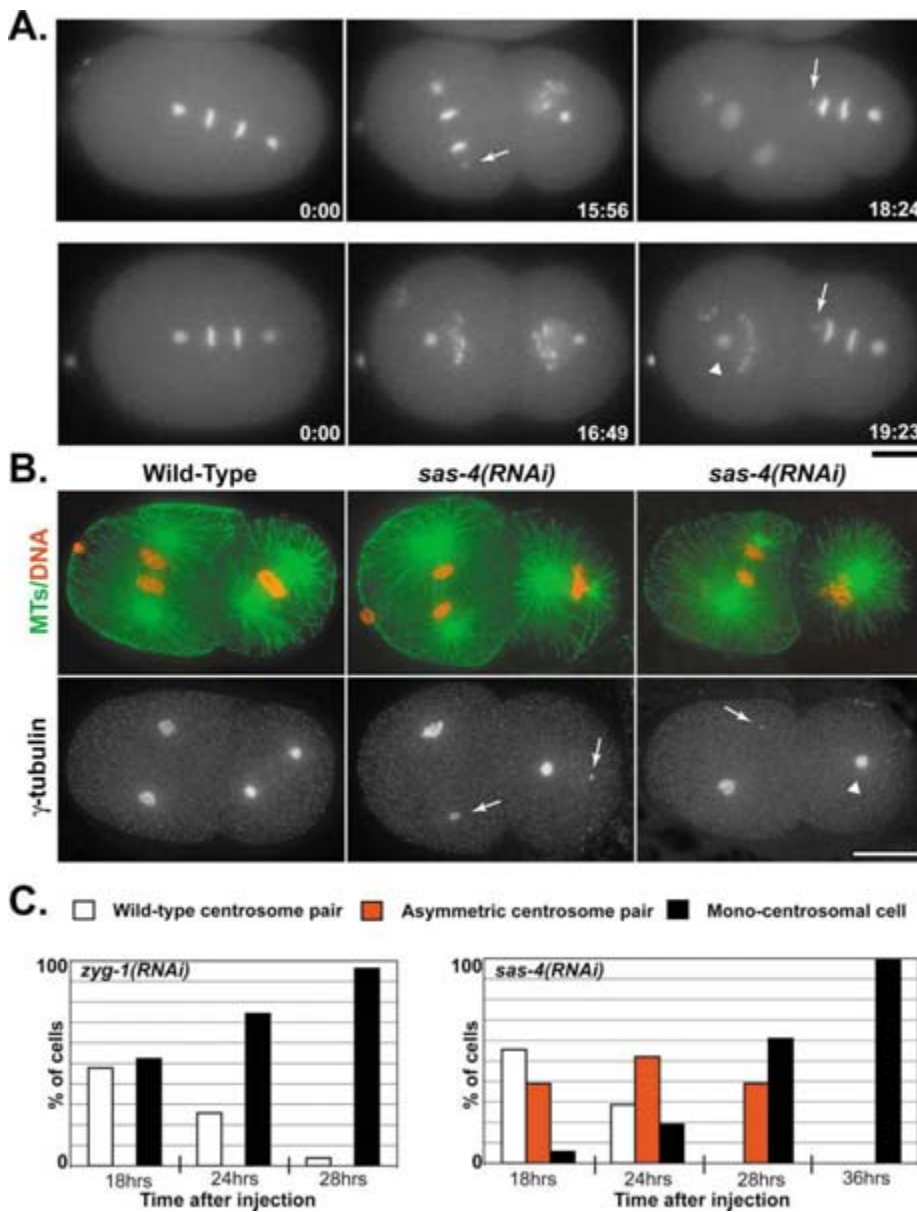


Figure 5. Partial Depletion of SAS-4 Leads to Intermediate Phenotypes Characterized by the Presence of Centrosomes with Less Than Normal Amounts of PCM

(A) Selected frames from two recordings of partial *sas-4(RNAi)* embryos co-expressing GFP- γ -tubulin and GFP-histone (see also Supplemental Movies S5 and S6 available at <http://www.cell.com/cgi/content/full/112/4/575/DC1>). Numbers in the lower right hand corners are elapsed time. Centrosomes that appear smaller than wild-type (arrows) and a single centrosome in a cell with a monopolar spindle (arrowhead) are indicated.

(B) Partially depleted *sas-4(RNAi)* embryos were fixed and stained to visualize microtubules (MTs) and DNA (green and red in upper images) and γ -tubulin (lower images). A wild-type embryo (left images) and two partially depleted *sas-4(RNAi)* embryos (middle and right images) are shown. Centrosomes that appear smaller than wild-type (arrows) and a single centrosome in a cell with a monopolar spindle (arrowhead) are indicated.

(C) Hermaphrodites were injected with *sas-4* or *zyg-1* dsRNA at the L4 larval stage and allowed to develop for 18, 24, or 28 hr at 16°C. As a positive control, L4 hermaphrodites injected with *sas-4* RNA were incubated for 36 hr at 20°C. Embryos were fixed and stained to visualize microtubules (MTs), DNA, γ -tubulin, and ZYG-9. The fluorescence intensity of the pair of centrosomes in each cell of embryos at the two-cell stage was compared and judged to be wild-type, asymmetric or, if only one centrosome was present, mono-centrosomal. Histograms show the percentage of cells in each phenotypic class for each time point. (Left graph) The number of *zyg-1(RNAi)* cells scored in two-cell stage embryos was 44, 70, and 101 at 18, 24, and 28 hr, respectively. At 18 hr, approximately 50% of cells at the second division in *zyg-1(RNAi)* embryos were wild-type and 50% were mono-centrosomal. After 24 and 28 hr, the percentage of mono-centrosomal cells increased to ~75 and 95%, respectively. At all time points, only wild-type or monopolar spindles were observed in *zyg-1(RNAi)* embryos. (Right graph) The number of *sas-4(RNAi)* cells in two-cell stage embryos scored was 36, 42, 46, and 24 at 18, 24, 28, and 36 hr, respectively. After 18 hr, about 40% of cells in *sas-4(RNAi)* embryos contained spindles with asymmetric centrosomes at their poles. After 24 hr, this percentage increased

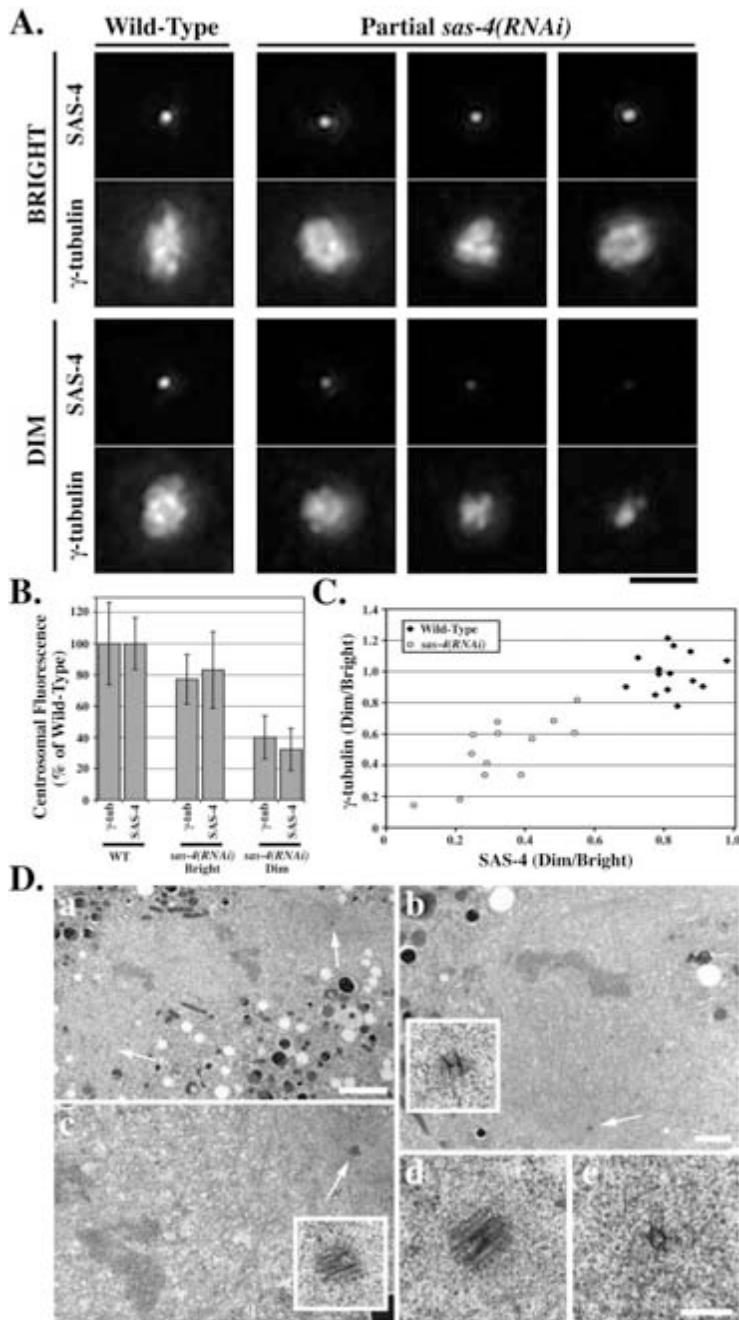


Figure 6. Centrosomal γ -Tubulin Levels Are Proportional to the Amount of Centriolar SAS-4

(A–C) L4 hermaphrodites were injected with *sas-4* RNA and incubated at 20°C for 21–24 hr to produce embryos partially depleted of SAS-4. Embryos were fixed and stained with DAPI to visualize DNA, and with antibodies directly labeled with fluorescent dyes to visualize microtubules, SAS-4, and γ -tubulin. 3D data sets of mitotic embryos at the two-cell stage were collected with an Olympus 100 \times , 1.35 NA lens using 0.15 μ m z steps on a DeltaVision microscope. The centrosomal fluorescence of SAS-4 and γ -tubulin was quantitated in 3D in the deconvolved images (see Experimental Procedures).

(A) Projections of the SAS-4 and γ -tubulin at both centrosomes are shown for one wild-type (left column) and three partial *sas-4(RNAi)* spindles at the two-cell stage. In each case, the centrosome that stained more intensely for SAS-4 (bright) is shown in the top pair of images and the centrosome with weaker SAS-4 staining is shown in the bottom pair of images (dim). As the amount of SAS-4 fluorescence at the dim centrosome decreases, the amount of γ -tubulin fluorescence also decreases.

(B) The average centrosomal γ -tubulin and SAS-4 fluorescence for wild-type and “bright” and “dim” centrosomes in *sas-4(RNAi)* embryos at metaphase is plotted. Error bars are the standard deviation.

(C) For the centrosome pairs in all mitotic wild-type or partial *sas-4(RNAi)* embryos, the ratio of the γ -tubulin fluorescence at the dim centrosome to the fluorescence at the bright centrosome is plotted versus the same ratio for SAS-4.

(D) Centrosomes in partially depleted *sas-4(RNAi)* embryos contain defective centrioles. RNAi was performed by feeding to generate large numbers of worms containing embryos in which SAS-4 was partially depleted. Worms were prepared for TEM by high pressure freezing followed by freeze substitution. (a) Overview showing an anaphase spindle in a two-cell stage embryo. The arrows indicate the approximate positions of the two spindle poles. Scale bar is 2.5 μ m. (b) Enlargement of the spindle half on the right side of the image in (a). (c) Enlargement of the spindle half on the left side of the image in (a). The centrioles in (b) and (c) are indicated with arrows. Higher magnification views of both centrioles are shown in the insets. Each pole has only a single centriole and the two centrioles appear to differ in size. Scale bars are 1 μ m. (d and e) A similar example from a second embryo. The single centrioles observed at the two poles of a spindle at the two-cell stage are shown, illustrating an apparent difference in the size of the two centrioles. Scale bar is 250 nm.

centriolar SAS-4 and the amount of centrosomal γ -tubulin, we plotted the ratio of total γ -tubulin fluorescence at the dim centrosome to that at the bright centrosome versus the same ratio for SAS-4 for all of the wild-type and partial *sas-4(RNAi)* centrosome pairs. Given

that the bright centrosomes in the asymmetric centrosome pairs in *sas-4(RNAi)* embryos are not significantly different from wild-type (Figure 6B), this strategy simplifies the analysis by internally controlling for experimental variations and slight differences in cell cycle state

to just over 50% and cells with monopolar spindles were also observed (~20%). After 28 hr, the number of cells with asymmetric spindles began to decrease (~40%) as the number of cells with monopolar spindles increased to ~60%. After 36 hr at 20°C (the stringent RNAi condition used for *sas-4* in previous experiments), all two-cell embryos had monopolar spindles. Scale bars are 10 μ m.

between embryos (Figure 6C). As expected, for centrosome pairs in wild-type embryos the ratio of γ -tubulin (dim/bright) and the ratio of SAS-4 (dim/bright) were always close to one, suggesting that the two centrosomes in each cell contain similar amounts of SAS-4 and similar amounts of γ -tubulin (the ratio of SAS-4 dim/bright is always slightly less than one because we defined the dim centrosome as the one that contains less SAS-4). Interestingly, in the partial *sas-4(RNAi)* embryos, the ratio of γ -tubulin fluorescence at the two asymmetric centrosomes was proportional to the ratio of the SAS-4 fluorescence over a 10-fold range (Figure 6C). This remarkable proportionality strongly suggests that centriolar SAS-4 levels determine centrosome size.

Partial Depletion of SAS-4 Leads to Assembly of Structurally Defective Centrioles

The fact that SAS-4 is a stably associated centriole component required for centriole duplication suggests that the effect of partial SAS-4 depletion on centrosome size could be the result of an alteration in centriole structure. To test this idea, we prepared large numbers of hermaphrodites containing partially depleted embryos by feeding with bacteria expressing dsRNA directed against *sas-4*. Treated hermaphrodites were high pressure frozen, freeze substituted and selected two-cell stage embryos were serially sectioned for TEM analysis. Two of the four serially sectioned embryos that we analyzed had asymmetric centriolar structures at the two spindle poles (Figure 6D). In these embryos, each spindle pole contained a single centriole, suggesting that one round of centriole duplication occurred but the second round, which normally occurs prior to metaphase of the second division, failed. Interestingly, whereas one of the centrioles in each cell had a normal appearance, the second centriole had a smaller, defective, structural appearance (Figure 6Db and 6De). Although 3D EM tomography will be needed to assess the exact nature of the structural alteration in these defective centrioles, these results suggest that reduction of centriolar SAS-4 leads to the formation of structurally compromised daughter centrioles that organize less than wild-type amounts of PCM.

Discussion

SAS-4 Is A Novel *C. elegans* Centriole Component

SAS-4 localizes to core centrosomal structures at all cell cycle stages in the early *C. elegans* embryo. Unlike the PCM components γ -tubulin and ZYG-9, whose amounts at centrosomes increase dramatically as cells enter mitosis (Hannak et al., 2001), centrosomal SAS-4 fluorescence remains constant. Consistent with this, electron microscopy of sections labeled with immunogold localized SAS-4 to the walls of both mother and daughter centrioles. To investigate the timing and dynamic nature of SAS-4 recruitment, we used mating to introduce unlabeled centrioles into oocytes expressing GFP-SAS-4. This experiment is conceptually analogous to a classic experiment in which biotinylated tubulin was microinjected into tissue culture cells to show that the incorporation of tubulin heterodimers into centriolar microtubules is conservative (Kochanski and Borisy, 1990).

Our results suggest that SAS-4, like centriolar tubulin, is a stably associated structural component of centrioles that is incorporated during their duplication.

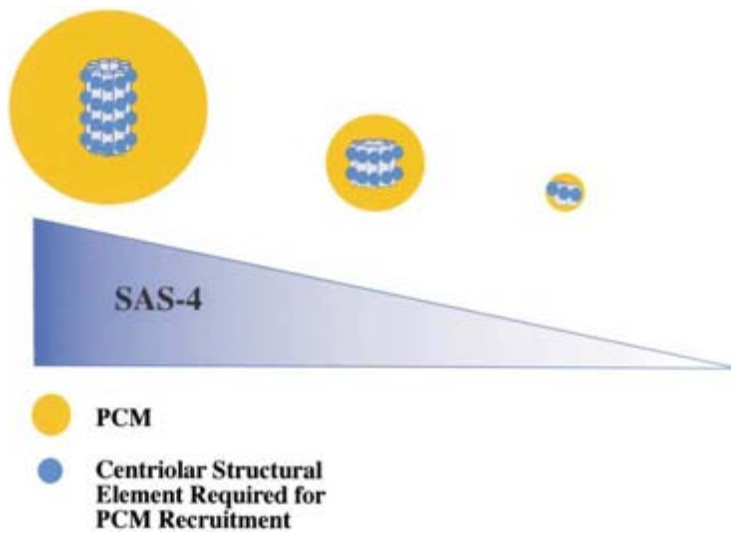
SAS-4 Is Required for Centriole Duplication

Using correlative DIC/TEM microscopy, we have shown that metaphase centrosomes in stringent *sas-4(RNAi)* embryos contain only one instead of the normal two centrioles, demonstrating that SAS-4 is required for centriole duplication. Nevertheless, normal-looking spindles with wild-type levels of γ -tubulin fluorescence at their poles form during the first mitosis in *sas-4(RNAi)* embryos. The lack of a significant difference between centrosomes containing only one centriole and wild-type centrosomes containing two centrioles is consistent with previous work in vertebrate somatic cells demonstrating association of mitotic PCM with only the parent centriole of each pair (reviewed in Vorobjev and Nadezhdina, 1987). In vertebrate somatic cells, daughter centrioles acquire a cloud of fibrillar PCM and the ability to anchor astral microtubules, during prophase of the cell cycle after they are born (Piel et al., 2000; Rieder and Borisy, 1982; Vorobjev and Chentsov, 1982). While our analysis of *sas-4(RNAi)* embryos is consistent with the idea that daughter centrioles do not mature until the cell cycle after their birth, detailed EM analysis of the centriole cycle will be needed to determine the exact timing of daughter centriole maturation in the *C. elegans* embryo.

Our analysis of GFP-SAS-4 in the mating experiment suggests that centriole duplication occurs after centrosome splitting in telophase (Figures 4D and 4E). The centrosome cycle inferred from this result for the *C. elegans* embryo is very similar to the one reported for *Drosophila* embryos (Callaini and Riparbelli, 1990). In both of these embryonic systems, centrosomes contain between 1 and 2 centrioles depending on cell cycle state. The situation is somewhat different in vertebrate somatic cells, where centrosomes contain between 2 and 4 centrioles. In these cells, the mother and daughter centrioles lose their orthogonal orientation in anaphase/telophase (Kuriyama and Borisy, 1981; Rieder and Borisy, 1982; Vorobjev and Chentsov, 1982), but the centrosome does not split because the centrioles are held together until the G2/M transition by a specialized structure that requires the protein C-Nap1 (Fry et al., 1998; Mayor et al., 2000). The similarity of the *C. elegans* and *Drosophila* centrosomal cycles suggests that the centriole-linking structure found in vertebrate somatic cells is not present during embryonic divisions in these systems.

SAS-4 Sheds Light on the Role of Centrioles as Centrosomal Organizers

The amount of SAS-4 at centrioles proportionally dictates the amount of centrosomal PCM. Since stringent RNAi of *sas-4* results in failure of centriole duplication and defective centriolar structures are observed in partial *sas-4(RNAi)* embryos, the effect on centrosome size may be either a direct consequence of depleting SAS-4 or an indirect consequence of perturbing centriole structure. In either case, this work leads to the interesting conclusion that the amount of centrosomal PCM is pro-



portional to the amount of an element of centriolar structure. In support of a direct role for SAS-4, partial RNAi of other genes involved in centriole function does not lead to a SAS-4-like effect on PCM levels. To date, genetic and functional genomic strategies have identified four *C. elegans* genes including *zyg-1* (O'Connell et al., 2001), *sas-4* (this study), and two novel genes (M.K., K.O. and A.A.H., unpublished data), whose inhibition results in the selective failure of spindle assembly at the second mitotic division characteristic of defects in centriole function. Of these, only SAS-4 results in variably sized centrosomes when partially depleted (Figure 5; M.K., K.O., and A.A.H., unpublished data). Testing the hypothesis that SAS-4 has a direct role in regulating PCM levels will be feasible once the entire genomic complement of genes required for centriole function is identified in *C. elegans*.

How does SAS-4 contribute to centriole-directed centrosome assembly? Our results lead us to conclude that there is an element of centriole structure that is proportionally required to organize PCM. SAS-4 could itself constitute this structural element or be proportionally required for its existence (Figure 7). How does this proposed centriolar element control centrosome size? One possibility is that it directly organizes a defined amount of PCM. Therefore, its centriolar stoichiometry would dictate the extent of PCM recruitment. Alternatively, the centriolar stoichiometry of the proposed element may affect the rate of PCM recruitment or the retention of PCM at centrosomes by activating components for assembly or by affecting their turnover. In addition to control by a centriolar structural element, limiting levels of PCM components also influence centrosome size. An effect of PCM component limitation is expected because centrosomes get smaller when the ratio of cytoplasmic volume to centriole number is reduced during embryonic development.

In summary, our work provides evidence for the existence of a centriolar structural element that proportionally dictates centrosome size. Determining the relationship between SAS-4 and this structural element is an important future goal.

Figure 7. Centriolar SAS-4 Levels Determines Centrosome Size

Decreasing levels of centriolar SAS-4 result in structurally defective daughter centrioles that organize progressively smaller quantities of PCM. In stringent *sas-4(RNAi)* embryos, daughter centrioles fail to form and centrosome duplication fails. These results suggest that an element of centriole structure (blue ovals) is proportionally required to organize PCM (orange). This centriolar element could be SAS-4 itself, or may simply be present at a fixed density on centrioles and hence regulated by SAS-4 levels.

Experimental Procedures

Definition of *sas-4* Coding Sequence

The cDNA, yk425b11, corresponding to F10E9.8 was identified from Yuji Kohara's EST database. Sequencing both strands of this cDNA confirmed the predicted coding sequence but did not reveal an inframe stop codon upstream of the first ATG. To unambiguously assign the start codon, we performed PCR with primers directed against the *trans*-spliced SL2 leader (GGTTTTAACCCAGTTACTC AAG) and an internal region of F10E9.8 (CGCGCGCGCGCCGCGCC TATTCGGCAGCTGCATTTTTTA) using *C. elegans* cDNA as template (gift of Martin Srayko, Max Planck Institute of Molecular Cell Biology and Genetics, Dresden, Germany). AT cloning (Promega) and sequencing of the PCR product confirmed that the ATG present in yk425b11 is the start codon.

RNA-Mediated Interference

For production of dsRNA directed against *sas-4* (TTCCAATGGAT CAACCATCA and TTCCTTTCTCCCGTTCCTTT) and *zyg-1* (TTTTTG TGATCTGCTGGAACA TTTTGTGATCTGCTGGAACA), the primers in parentheses with tails containing T3 and T7 promoters were used to amplify regions of genomic N2 DNA. PCR products were transcribed and double-stranded RNA prepared as described (Oegema et al., 2001). For all experiments, except the one presented in Figure 6D, dsRNA was injected into L4 hermaphrodites. For stringent RNAi, injected worms were incubated for 28 hr at 25°C (Figures 1A and 1B) or 36 hr at 20°C (Figure 1C and Figure 2). For partial RNAi, injected worms were incubated for 20–26 hr at 25°C (Figure 3A) or for 18–36 hr at 16/20°C, as indicated (Figures 5B and 5C and Figures 6A–6C). To produce large quantities of partially depleted *sas-4* (RNAi) worms for high pressure freezing (Figure 6D), RNAi was performed by feeding bacteria producing dsRNA to the region of F10E9.8 described above (Timmons et al., 2001).

Generation of GFP-Fusion Expressing Strains and Live Imaging

Strains expressing GFP- α -tubulin and co-expressing GFP- γ -tubulin and GFP-histone H2B were described previously (Oegema et al., 2001). The strain expressing GFP-SAS-4 was constructed by using the primers in parentheses (GCTTCGGCTAGCGCTCCGATGAA AATATCGGTG, CGCTTCGGCTAGCTCATTTTTTCCACTGGAACAAA GTT) to PCR amplify the genomic F10E9.8 locus. The PCR product was digested with NheI, cloned into the plasmid pAZ132 (gift from Judith Austin, University of Chicago, Chicago, Illinois), and bombarded into *unc-119(ed3)* worms as described (Praitis et al., 2001). Live widefield and spinning disk confocal imaging of embryos expressing GFP fusion proteins was performed as described (Oegema et al., 2001).

Antibody Production

6xHis tagged full-length SAS-4 was prepared by amplifying the cDNA, yk425b11, using the following primers: CGCGCGGGATCCGCTTCCGATGAAAATATCGGTG and CGCGCGCTCGAGTCATTTTTTCCACTGGAACAAAGTT, digesting the product with BamHI/XhoI and cloning into pRSET-A (Invitrogen). Antibodies to the fusion protein were generated in rabbits and affinity purified as described (Oegema et al., 2001). The column for the affinity purification was prepared by coupling a mixture of three GST fusion proteins corresponding to three separate 120 amino acid regions of F10E9.8 to a NHS HiTrap column (Amersham Pharmacia). The following 3 sets of primers: GCGCGCGGATCCATGGCTTCCGATGAAAATATC and GCGCGCCTCGAGTCCACTGTGGCCATGCTCT; GCGCGCGGATCCATGGCTTCCGATGAAAATATC and GCGCGCCTCGAGTCCACTGTGGCCATGCTCT; GCGCGCGGATCCATGGCTTCCGATGAAAATATC and GCGCGCCTCGAGTCCACTGTGGCCATGCTCT; GCGCGCGGATCCATGGCTTCCGATGAAAATATC and GCGCGCCTCGAGTCCACTGTGGCCATGCTCT were used to amplify regions of the cDNA yk425b11. Products were digested with BamHI/XhoI and cloned into pGEX-6P-1 (Amersham Pharmacia). GST fusion proteins were purified and coupled as described (Oegema et al., 2001).

Immunofluorescence, Fixed Imaging, and Quantitation of Centrosomal Fluorescence

Antibodies to γ -tubulin and ZYG-9 were described previously (Hannak et al., 2001). Both antibodies were directly labeled with Cy3 and Cy5 as described (Oegema et al., 2001) and were used at a concentration of 1 μ g/ml. DM1 α was used at a dilution of 1:1000 to visualize microtubules and polyclonal rabbit anti-GFP (Molecular Probes) was used at 1 μ g/ml. In four-color immunofluorescence experiments using anti-SAS-4 and anti-GFP antibodies, embryos were incubated with an excess of goat anti-rabbit Fab fragments (5 μ g/ml; Jackson ImmunoResearch Laboratories) to convert the first rabbit antibody to a "goat" antibody before incubation with the second rabbit antibody. For the experiment in Figures 6A–6C, antibodies to SAS-4 were directly labeled with Cy3. Embryos were fixed and processed for immunofluorescence as described (Oegema et al., 2001) and were imaged using a 100 \times , 1.35 NA objective on an Olympus DeltaVision microscope. All fixed images shown are of 3D widefield data sets that were computationally deconvolved and projected using SoftWorx (Applied Precision). Quantitation of centrosomal fluorescence was performed on deconvolved 3D image stacks as described (Hannak et al., 2002).

Correlative DIC/TEM, High Pressure Freezing/Freeze Substitution, and Immunoelectron Microscopy

For the correlative DIC/TEM in Figure 2, a single wild-type or *sas-4(RNAi)* early embryo was transferred with a mouth pipet to a marked region on an aclar coverslip (Electron Microscopy Sciences) previously glow discharged and coated with 1% poly-L-lysine (Sigma, P1524) in PBS. Water was used to adhere the aclar coverslip to a metal holder before mounting on an inverted microscope (Axiovert 200M, Zeiss). Embryos were imaged through the aclar using DIC until early metaphase. Excess liquid was removed, and the embryo was surrounded with 20 μ l of 1 \times PHEM (60 mM PIPES [pH 6.9], 25 mM HEPES [pH 6.9], 10 mM EGTA, and 2 mM MgCl₂) containing 2% glutaraldehyde and 0.4% tannic acid (O'Connell et al., 2001). A pulsed solid-state UV laser (PowerChip, JDS Uniphase) focused with a 63 \times water immersion objective lens (C-Apochromat, Zeiss) was used for laser permeabilization. About 5 shots were taken at regions where the vitelline membrane touches the eggshell at the very anterior of the embryo and fixation was monitored by live DIC microscopy. Laser and microscope control was based on the CCC software (Alfons Riedinger, Nick Salmon, Ernst H.K. Stelzer, EMBL). After laser permeabilization, embryos were incubated in fixative on ice for at least 30 min, washed 3–4 times in 1 \times PHEM, and postfixed in 1% osmium tetroxide and 0.5% K₃Fe(CN)₆ in 1 \times PHEM buffer (O'Connell et al., 2001). The samples were dehydrated through a graded acetone series, flat embedded in epon/araldite, and re-mounted for thin, serial sectioning. Thin sections (70 nm) were cut using a Leica Ultracut UCT microtome. Sections were collected on Formvar-coated copper grids, poststained with 2% uranyl acetate in 70% methanol followed by aqueous lead citrate and viewed in a Philips TECNAI 12 transmission electron microscope operated at

100 kV. For the experiment in Figure 6, partially depleted *sas-4(RNAi)* hermaphrodites prepared by feeding were cryoimmobilized using an HPM 010 high pressure freezer (BAL-TEC). Samples were processed for freeze substitution as described (Rappleye et al., 1999). For immunolabeling experiments, cryoimmobilized wild-type hermaphrodites were freeze substituted at -90°C for 3 days in acetone containing 0.2% glutaraldehyde and 0.1% uranyl acetate. Dehydrated specimens were thin layer embedded in LR White (Lonsdale et al., 2001). Thin sections (50–70 nm) were labeled using anti-SAS-4 diluted in blocking buffer containing 0.8% bovine serum albumin, 0.01% Tween 20, and 0.1% fish scale gelatin (Nycomed, Amersham) in PBS. The secondary goat anti-rabbit IgG antibody was coupled to 10 nm colloidal gold (British BioCell, UK). The antibody complex was stabilized with 1% glutaraldehyde in PBS and the labeled sections were poststained as described.

Acknowledgments

The authors thank Jana Müntler for excellent technical assistance and Arshad Desai for microscopy advice and many helpful discussions during the course of this work. For comments on the manuscript, we thank Arshad Desai and Eva Hannak. We are very grateful to: Yuji Kohara (National Institute of Genetics, Mishima, Japan) for cDNAs used in this study; Geraldine Seydoux (Johns Hopkins University, Baltimore, Maryland) and Judith Austin (University of Chicago, Chicago, Illinois) for vectors and advice on germline expression; Martin Srayko for *C. elegans* cDNA; and Sonja Rybina for help with antibody production. Karen Oegema was supported by a fellowship from the Helen Hay Whitney Foundation.

Received: August 22, 2002

Revised: February 4, 2003

References

- Albertson, D.G. (1984). Formation of the first cleavage spindle in nematode embryos. *Dev. Biol.* 101, 61–72.
- Bobinnec, Y., Khodjakov, A., Mir, L.M., Rieder, C.L., Edde, B., and Bornens, M. (1998). Centriole disassembly in vivo and its effect on centrosome structure and function in vertebrate cells. *J. Cell Biol.* 143, 1575–1589.
- Bornens, M. (2002). Centrosome composition and microtubule anchoring mechanisms. *Curr. Opin. Cell Biol.* 14, 25–34.
- Callaini, G., and Riparbelli, M.G. (1990). Centriole and centrosome cycle in the early *Drosophila* embryo. *J. Cell Sci.* 97, 539–543.
- Cavalier-Smith, T. (2002). The phagotrophic origin of eukaryotes and phylogenetic classification of Protozoa. *Int. J. Syst. Evol. Microbiol.* 52, 297–354.
- Chapman, M.J., Dolan, M.F., and Margulis, L. (2000). Centrioles and kinetosomes: form, function and evolution. *Q. Rev. Biol.* 75, 409–429.
- Fry, A.M., Meraldi, P., and Nigg, E.A. (1998). A centrosomal function for the human Nek2 protein kinase, a member of the NIMA family of cell cycle regulators. *EMBO J.* 17, 470–481.
- Fry, A.M., Mayor, T., and Nigg, E.A. (2000). Regulating centrosomes by protein phosphorylation. *Curr. Top. Dev. Biol.* 49, 291–312.
- Gönczy, P., Echeverri, C., Oegema, K., Coulson, A., Jones, S.J., Copley, R.R., Duperon, J., Oegema, J., Brehm, M., Cassin, E., et al. (2000). Functional genomic analysis of cell division in *C. elegans* using RNAi of genes on chromosome III. *Nature* 408, 331–336.
- Gould, R.R., and Borisy, G.G. (1977). The pericentriolar material in Chinese hamster ovary cells nucleates microtubule formation. *J. Cell Biol.* 73, 601–615.
- Hamill, D.R., Severson, A.F., Carter, J.C., and Bowerman, B. (2002). Centrosome maturation and mitotic spindle assembly in *C. elegans* require SPD-5, a protein with multiple coiled-coil domains. *Dev. Cell* 3, 673–684.
- Hannak, E., Kirkham, M., Hyman, A.A., and Oegema, K. (2001). Aurora-A kinase is required for centrosome maturation in *Caenorhabditis elegans*. *J. Cell Biol.* 155, 1109–1116.
- Hannak, E., Oegema, K., Kirkham, M., Gonczy, P., Habermann, B., and Hyman, A.A. (2002). The kinetically dominant assembly pathway

- for centrosomal asters in *Caenorhabditis elegans* is γ -tubulin dependent. *J. Cell Biol.* **157**, 591–602.
- Kochanski, R.S., and Borisy, G.G. (1990). Mode of centriole duplication and distribution. *J. Cell Biol.* **110**, 1599–1605.
- Kuriyama, R., and Borisy, G.G. (1981). Centriole cycle in Chinese hamster ovary cells as determined by whole-mount electron microscopy. *J. Cell Biol.* **91**, 814–821.
- Lange, B.M., Faragher, A.J., March, P., and Gull, K. (2000). Centriole duplication and maturation in animal cells. *Curr. Top. Dev. Biol.* **49**, 235–249.
- Lonsdale, J.E., McDonald, K.L., and Jones, R.L. (2001). Microwave polymerisation in thin layers of London Resin White allows selection of specimens for immunogold labelling. In *Microwave Techniques and Protocols*, T. Giberson and R.S. Demaree, eds. (Totowa, NJ: Humana Press), pp. 139–153.
- Marshall, W.F. (2001). Centrioles take center stage. *Curr. Biol.* **11**, R487–496.
- Matthews, L.R., Carter, P., Thierry-Mieg, D., and Kemphues, K. (1998). ZYG-9, a *Caenorhabditis elegans* protein required for microtubule organization and function, is a component of meiotic and mitotic spindle poles. *J. Cell Biol.* **141**, 1159–1168.
- Mayor, T., Stierhof, Y.D., Tanaka, K., Fry, A.M., and Nigg, E.A. (2000). The centrosomal protein C-Nap1 is required for cell cycle-regulated centrosome cohesion. *J. Cell Biol.* **151**, 837–846.
- Mazia, D., Harris, P.J., and Bibring, T. (1960). The multiplicity of the mitotic centers and the time-course of their duplication and separation. *J. Biophys. Biochem. Cytol.* **7**, 1–20.
- Mignot, J.P. (1996). The centrosomal big bang: from a unique central organelle towards a constellation of MTOCs. *Biol. Cell* **86**, 81–91.
- Montgomery, M.K., and Fire, A. (1998). Double-stranded RNA as a mediator in sequence-specific genetic silencing and co-suppression. *Trends Genet.* **14**, 255–258.
- Moritz, M., Zheng, Y., Alberts, B.M., and Oegema, K. (1998). Recruitment of the γ -tubulin ring complex to *Drosophila* salt-stripped centrosome scaffolds. *J. Cell Biol.* **142**, 775–786.
- O'Connell, K.F., Caron, C., Kopish, K.R., Hurd, D.D., Kemphues, K.J., Li, Y., and White, J.G. (2001). The *C. elegans* *zyg-1* gene encodes a regulator of centrosome duplication with distinct maternal and paternal roles in the embryo. *Cell* **105**, 547–558.
- Oakley, B.R. (2000). γ -Tubulin. *Curr. Top. Dev. Biol.* **49**, 27–54.
- Oegema, K., Desai, A., Rybina, S., Kirkham, M., and Hyman, A.A. (2001). Functional analysis of kinetochore assembly in *Caenorhabditis elegans*. *J. Cell Biol.* **153**, 1209–1226.
- Palazzo, R.E., Vogel, J.M., Schnackenberg, B.J., Hull, D.R., and Wu, X. (2000). Centrosome maturation. *Curr. Top. Dev. Biol.* **49**, 449–470.
- Piel, M., Meyer, P., Khodjakov, A., Rieder, C.L., and Bornens, M. (2000). The respective contributions of the mother and daughter centrioles to centrosome activity and behavior in vertebrate cells. *J. Cell Biol.* **149**, 317–330.
- Praitis, V., Casey, E., Collar, D., and Austin, J. (2001). Creation of low-copy integrated transgenic lines in *Caenorhabditis elegans*. *Genetics* **157**, 1217–1226.
- Preble, A.M., Giddings, T.M., Jr., and Dutcher, S.K. (2000). Basal bodies and centrioles: their function and structure. *Curr. Top. Dev. Biol.* **49**, 207–233.
- Priess, J.R., and Hirsh, D.I. (1986). *Caenorhabditis elegans* morphogenesis: the role of the cytoskeleton in elongation of the embryo. *Dev. Biol.* **117**, 156–173.
- Rapple, C.A., Paredes, A.R., Smith, C.W., McDonald, K.L., and Aroian, R.V. (1999). The coronin-like protein POD-1 is required for anterior-posterior axis formation and cellular architecture in the nematode *Caenorhabditis elegans*. *Genes Dev.* **13**, 2838–2851.
- Rieder, C.L., and Borisy, G.G. (1982). The centrosome cycle in PtK2 cells: asymmetric distribution and structural changes in the pericentriolar material. *Biol. Cell* **44**, 117–132.
- Rieder, C.L., Faruki, S., and Khodjakov, A. (2001). The centrosome in vertebrates: more than a microtubule-organizing center. *Trends Cell Biol.* **11**, 413–419.
- Schnackenberg, B.J., Khodjakov, A., Rieder, C.L., and Palazzo, R.E. (1998). The disassembly and reassembly of functional centrosomes in vitro. *Proc. Natl. Acad. Sci. USA* **95**, 9295–9300.
- Schumacher, J.M., Ashcroft, N., Donovan, P.J., and Golden, A. (1998). A highly conserved centrosomal kinase, AIR-1, is required for accurate cell cycle progression and segregation of developmental factors in *C. elegans* embryos. *Development* **125**, 4391–4402.
- Sluder, G., and Rieder, C.L. (1985). Centriole number and the reproductive capacity of spindle poles. *J. Cell Biol.* **100**, 887–896.
- Sluder, G., and Hinchcliffe, E.H. (1999). Control of centrosome reproduction: the right number at the right time. *Biol. Cell* **91**, 413–427.
- Timmons, L., Court, D.L., and Fire, A. (2001). Ingestion of bacterially expressed dsRNAs can produce specific and potent genetic interference in *Caenorhabditis elegans*. *Gene* **263**, 103–112.
- Vorobjev, I.A., and Chentsov, Y.S. (1982). Centrioles in the cell cycle. I. Epithelial cells. *J. Cell Biol.* **93**, 938–949.
- Vorobjev, I.A., and Nadezhkina, E.S. (1987). The centrosome and its role in the organization of microtubules. *Int. Rev. Cytol.* **106**, 227–293.
- Wolf, N., Hirsh, D., and McIntosh, J.R. (1978). Spermatogenesis in males of the free-living nematode, *Caenorhabditis elegans*. *J. Ultrastruct. Res.* **63**, 155–169.
- Zipperlen, P., Fraser, A.G., Kamath, R.S., Martinez-Campos, M., and Ahringer, J. (2001). Roles for 147 embryonic lethal genes on *C. elegans* chromosome I identified by RNA interference and video microscopy. *EMBO J.* **20**, 3984–3992.

3.2 Morphologically distinct microtubule ends in the mitotic centrosome of *Caenorhabditis elegans*

E. T. O'Toole, K. L. McDonald, J. Mántler, J. R. McIntosh, A. A. Hyman, and T. Müller-Reichert. 2003b. *J. Cell Biol.* 163, 451-456.

Morphologically distinct microtubule ends in the mitotic centrosome of *Caenorhabditis elegans*

Eileen T. O'Toole,¹ Kent L. McDonald,² Jana Mäntler,³ J. Richard McIntosh,¹ Anthony A. Hyman,³ and Thomas Müller-Reichert³

¹Boulder Laboratory for 3-D Electron Microscopy of Cells, University of Colorado, Boulder, CO 80309

²Electron Microscope Laboratory, University of California, Berkeley, CA 94720

³Max Planck Institute of Molecular Cell Biology and Genetics, D-01307 Dresden, Germany

During mitosis, the connections of microtubules (MTs) to centrosomes and kinetochores are dynamic. From *in vitro* studies, it is known that the dynamic behavior of MTs is related to the structure of their ends, but we know little about the structure of MT ends in spindles. Here, we use high-voltage electron tomography to study the centrosome- and kinetochore-associated ends of spindle

MTs in embryonic cells of the nematode, *Caenorhabditis elegans*. Centrosome-associated MT ends are either closed or open. Closed MT ends are more numerous and are uniformly distributed around the centrosome, but open ends are found preferentially on kinetochore-attached MTs. These results have structural implications for models of MT interactions with centrosomes.

Introduction

In animal cells, microtubules (MTs) commonly grow from centrosomes (for a review see Doxsey, 2001). Following polymer nucleation, each MT minus end generally remains attached to the centrosome, whereas the plus ends extend out into the cytoplasm (reviewed in Wittmann et al., 2001). In interphase, the minus ends tend to be stable; they do not lose or gain tubulin subunits, and most tubulin turnover takes place at the plus ends. In mitosis, much of the MT turnover is still at the plus ends, but the dynamics of minus ends becomes more complex. At least some of the minus ends lose subunits while remaining attached to the spindle pole, which results in MT movement that has been called flux (for a review see Wittmann et al., 2001). Work *in vitro* and *in vivo* has shown that changes in the dynamic properties of MTs are associated with changes in the structure of the ends (for a review see Howard and Hyman, 2003). For instance when MT plus ends are viewed in vitreous ice, growing ends appear as a curved sheet of protofilaments; shrinking ends contain bent or "peeling" protofilaments, known as "rams horns" (Mandelkow et al., 1991; Chrétien et al., 1995). Less work has been done on the structure of

minus ends. MTs nucleated *in vitro* from γ -tubulin, the key regulator of MT nucleation, contain a cone-shaped cap at their minus ends (Keating and Borisy, 2000; Moritz et al., 2000; Wiese and Zheng, 2000). Similar capped structures were previously seen at the minus ends of MTs nucleated from isolated spindle pole bodies of budding yeast (Byers et al., 1978; Rout and Kilmartin, 1990; Bullitt et al., 1997) and centrosomes from *Drosophila* cells (Moritz et al., 1995), suggesting that these polymers too are nucleated and capped by the γ -tubulin complex. It is plausible that MTs nucleated from γ -tubulin complexes are stabilized by this minus-end cap. However, we know little about the distribution of minus-end structures at mitotic spindle poles *in vivo*. The only study to date was in budding yeast cells where all minus ends were found to be capped by structures that resemble the γ -tubulin nucleated ends seen *in vitro* (O'Toole et al., 1999). No data are currently available for MT minus ends in mitotic animal cells. Are there morphologically distinct structures, which could potentially account for the dynamic properties of minus ends attached to a mitotic animal spindle pole? Here, we use high-pressure freezing and electron tomography to examine the end structure of MTs in mitotic spindles of cells from *Caenorhabditis elegans* embryos. We have found variation in centrosome-proximal MT end morphology that is systematically related to the

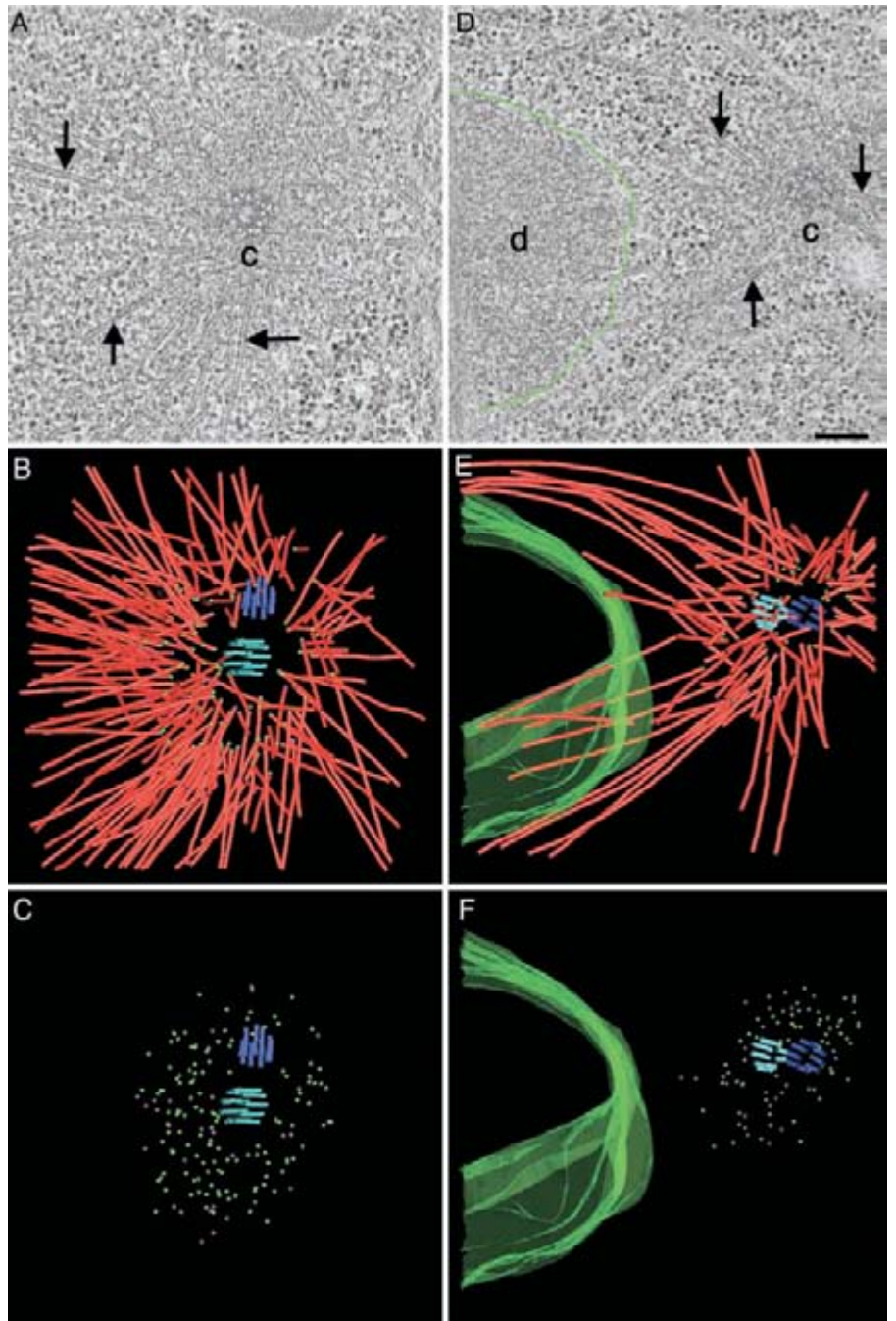
The online version of this article includes supplemental material.

Address correspondence to T. Müller-Reichert, Max Planck Institute of Molecular Cell Biology and Genetics, Pfotenhauerstr. 108, D-01307 Dresden, Germany. Tel.: 49-351-210-1763. Fax: 49-351-210-2000. email: mueller-reichert@mpi-cbg.de

Key words: *Caenorhabditis elegans*; centrosome; electron tomography; mitosis; 3-D reconstruction

Abbreviations used in this paper: 3-D, three-dimensional; KMT, kinetochore MT; MT, microtubule; PCM, pericentriolar material.

Figure 1. MT ends at the centrosome are either closed or open. Distribution of MT minus ends around centrioles in metaphase (A–C) and anaphase (D–F). (A and D) Selected tomographic slices showing MTs (arrows), the centrosome (c), and the condensed DNA (d, DNA surface outlined in green). (B and E) Corresponding 3-D models showing the centrioles (blue and purple), the MTs (red) and the surface of the chromatin (green). MT minus ends are marked by spheres. (C and F) Models showing the distribution of closed (green) and open (purple) MT minus ends. Bar, 200 nm. Also, see Videos 1–4, available at <http://www.jcb.org/cgi/content/full/jcb.200304035/DC1>.



position of the MT plus end and may reflect different mechanisms by which a minus end can be bound to a centrosome.

Results and discussion

Distribution of MT ends in the centrosome

The centrioles in *C. elegans* are morphologically simple (Wolf et al., 1978; Albertson, 1984; O'Connell et al., 2001; Kirkham et al., 2003), but they appear to duplicate and function in a conventional manner (for review see O'Connell, 2000). To characterize the structure of centrosome-proximal MT ends and their distribution to the *C. elegans* centrioles we have examined the overall distribution of MT ends in the vicinity of spindle poles in metaphase and ana-

phase (Fig. 1). A typical array of MTs can be detected in the pericentriolar material (PCM), but MTs do not physically touch the centriole pair. To analyze the MT arrangement, we marked the pole-proximal end of each MT in the reconstructed volumes (Fig. 1, B and E). From these models, it is clear that MTs are centered predominantly around one centriole, which we have designated the "mother" (marked in light blue in Fig. 1).

We then characterized the structure of the centrosome-associated MT ends at higher resolution and found two types embedded in the PCM: the majority of the ends were closed by a cap, but many MT ends were open. Galleries of pole-proximal MT ends are shown in Fig. 2, A and B. The closed ends typically were conical, whereas the open ends were

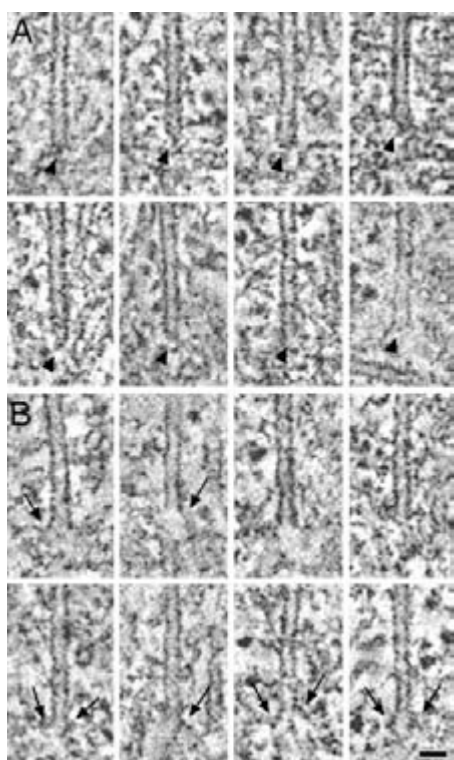


Figure 2. Closed MT minus ends are pointed, open ends are blunt or slightly flared. (A) Capped minus ends. The ends of the MTs are marked by arrowheads. Capped MTs are often pointed and flattened on one side. (B) Open minus ends. Some MT ends show an open, blunt morphology, whereas a few are flared (arrows). Single or double sheet-like extensions can be observed. Bar, 50 nm.

blunt or flared. At some open ends, we observed single or double sheet-like extensions whose curvature varied. None of these open-end morphologies suggested the presence of a protein complex distinct from tubulin subunits. The capped cone-shaped ends, on the other hand, are reminiscent of minus ends observed at yeast spindle pole bodies (Byers et al., 1978; Rout and Kilmartin, 1990; Bullitt et al., 1997; O'Toole et al., 1999) and at isolated *Drosophila* centrosomes (Moritz et al., 1995).

To determine if there was a correlation between MT end structure and position within the centrosome, we marked the closed and open ends in our tomographic volumes with green and purple spheres, respectively (Fig. 1, C and F). The capped MT ends were distributed evenly around the mother centrioles, whereas the open ends were concentrated on one side (the left side in these images). A low magnification view of these cells showed that the chromosomes were also placed to the left of the centrosomes (data not shown). Thus, open MT ends are found preferentially on MTs that point toward the chromosomes.

Fine structure of kinetochore MT (KMT) plus ends

We have used electron tomography to ask whether different minus end structures are associated with specific subpopulations of spindle MTs. First, we identified chromatin-associated ends of spindle MTs. In *C. elegans* this interaction occurs in a ribosome-free zone that surrounds each chromo-

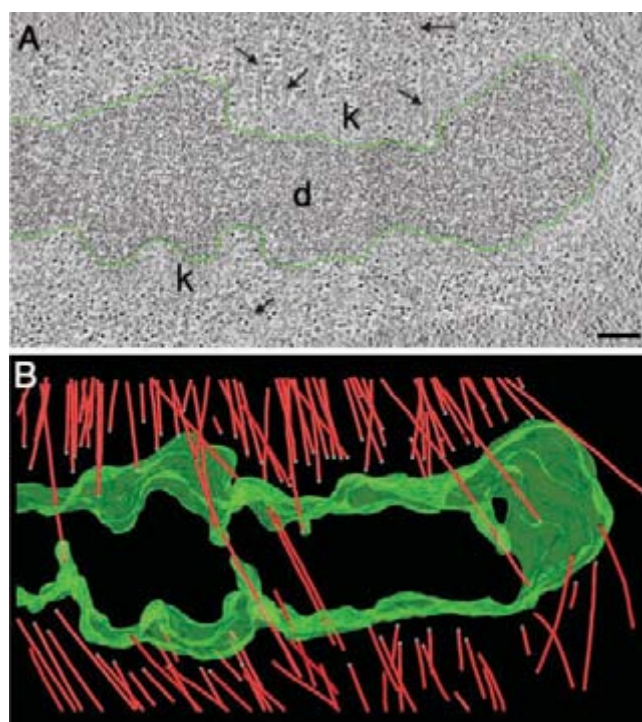


Figure 3. KMTs do not end directly on the condensed chromatin. (A) Selected 2.7-nm thick tomographic slice showing a region at the metaphase plate. MTs (arrows) and the kinetochore regions (k) are indicated. The surface of the DNA (d) is outlined in green. (B) Corresponding 3-D model showing MTs (red) and the surface of the chromatin (green). MT plus ends are marked by blue spheres. Bar, 500 nm. Also, see Videos 5 and 6, available at <http://www.jcb.org/cgi/content/full/jcb.200304035/DC1>.

some (Howe et al., 2001). When chromatin is aligned on the metaphase plate, the two pole-facing regions are peppered with MT ends (Fig. 3 A). In the corresponding three-dimensional (3-D) model, 118 MTs were identified (Fig. 3 B). 85 of these MTs terminated in the ribosome-free zone at the face of the condensed chromatin and were considered to be kinetochore MTs (KMTs). At 6–10 nm resolution we have found no distinct electron-dense protein complex physically linking chromatin to the MTs. Instead, there was a gap between the MT plus ends and the apparent surface of the chromatin. This gap contained a loose mat of fine filaments. KMT ends lay at a mean (\pm SD) distance from the chromatin surface of 115 (\pm 52) nm. The mean width of the ribosome-free zone was 194 (\pm 45) nm. Interestingly, the kinetochores of PtK1 cells prepared by high-pressure freezing/freeze-substitution have been reported to contain a “ribosome-excluded” zone 100–150-nm wide (McEwen et al., 1998), which is similar in appearance and dimension to the zone described here.

The morphological distinctions at the MT minus ends prompted us to investigate the chromosome-associated end morphologies. Fig. 4 A shows a higher magnification tomographic slice from the kinetochore region shown in Fig. 3. Several KMTs can be seen; their ends immersed in the ribosome-free zone. A 3-D model of this region is displayed in Fig. 4 B, and galleries of KMT-proximal ends are shown in Fig. 4, C and D. Of 83 plus ends analyzed in this

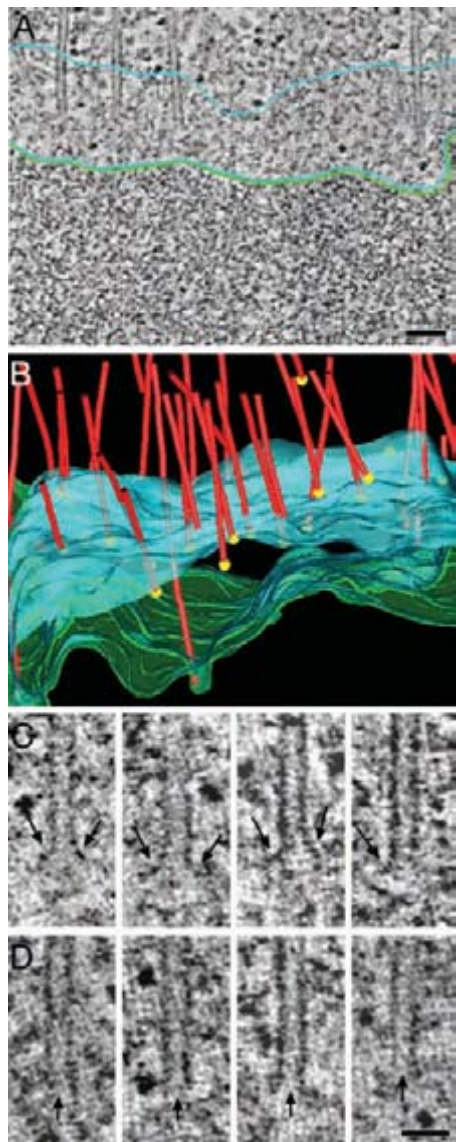


Figure 4. KMT plus ends have an open, flared, or blunt morphology. (A) Detail of a kinetochore region as obtained by high-voltage electron tomography. KMTs terminate in the ribosome-free zone (outlined in light blue). The chromatin surface is indicated by a green line. (B) 3-D model of the kinetochore region showing MTs (red), the position of their plus ends (yellow spheres), the outer boundary of the ribosome-free zone (blue), and the surface of the DNA (green). The mean width of the ribosome-free zone is 194 nm (± 45 nm), and the mean distance of the MT plus end to the chromatin is 115 nm (± 52 nm). Also, see Video 7, available at <http://www.jcb.org/cgi/content/full/jcb.200304035/DC1>. (C) KMT plus ends with an open, flared morphology. Electron tomography revealed double or single extensions (arrows) at the plus ends. (D) Plus ends with an open, blunt morphology. The ends of the open tubes are marked by arrows. Bars: (A) 100 nm; (C) 50 nm.

tomographic volume, all were open, and 78% were flared to some extent. Flared ends often showed an electron-density extension from one or both sides of the MT end. A flared morphology was also observed in late anaphase cells (data not shown). Some KMT plus ends (22%) appeared blunt, but there were no capped MT ends in the kinetochore region.

Connecting KMT plus and minus ends in 3-D

We next looked at the minus end structures of KMTs. KMTs were tracked through tomographic reconstructions from their plus ends at the chromosomes to their minus ends in the PCM. 3-D models generated from two serial, tomographic volumes are shown in Fig. 5. The complete model with presumptive KMTs (white, $n = 48$) and non-KMTs (red, $n = 520$) illustrates the density of MTs forming the mitotic spindle and the arrangement of the spindle fibers by which chromatin is connected to the centrosome (Fig. 5 A). Non-KMTs were defined as those MTs whose pole-distal ends lay outside the volume of the tomogram (though some of the latter may, of course, be KMTs). This partial metaphase reconstruction was first used to perform a neighbor density analysis (Mastrorarde et al., 1993) to determine if there were preferred interfiber distances between any of the spindle MTs. A peak in the distribution of interfiber distance has been considered indicative of interactions between those fiber classes, as has been observed in the non-KMT–KMT interfiber distances in PtK1 spindles (McDonald et al., 1992). We also found no evidence for a preferred spacing between the MTs in a *C. elegans* spindle (data not shown), suggesting that KMTs do not form bundles, as seen in cells of more complex animals. This is presumably because the kinetochores of *C. elegans* are holocentric and the plus-end binding sites are distributed along the chromosomes. In support of this idea, no bundling was seen in the hemipteran insect

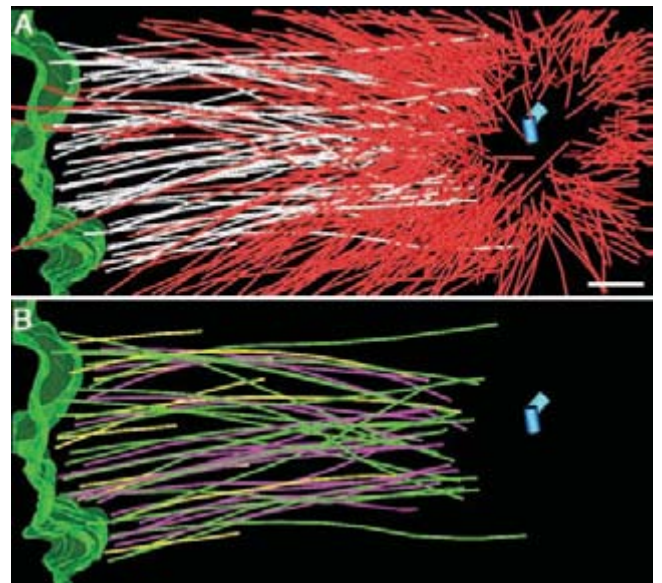


Figure 5. Half of the KMT minus ends are open. (A) Partial reconstruction of a metaphase spindle. The surface of the DNA is outlined in green, and MTs that end in the ribosome-free zone are identified in white. Other spindle MTs are shown in red. The centriole pair is shown as blue cylinders. The mean distance from the mother centriole to the open MT minus end (558 ± 139 nm) was not significantly different from the mean distance of closed MT minus ends (530 ± 137) from the mother centriole. (B) KMTs with closed (green) and open (magenta) minus ends. KMTs with minus ends "outside" the volume of the reconstruction are shown in yellow. Bar, 500 nm. Also, see Video 8, available at <http://www.jcb.org/cgi/content/full/jcb.200304035/DC1>.

Agallia constricta, which also has holocentric kinetochores (Rieder et al., 1990).

We then examined the minus-end structure for those KMTs that could be traced unambiguously from the chromatin to the centrosome (Fig. 5 B). 50% of these KMTs had a closed minus end ($n = 19$), whereas 50% were open ($n = 18$). In contrast, only 20% of all the MTs show open pole-proximal ends. Open minus ends are therefore preferentially associated with kinetochore-attached MTs. Since we are unable to trace the final termination of all centrosomes/MTs in this reconstruction, it is possible that all MTs with open minus ends are KMTs. More complete structural data will be needed to test this possibility.

What is the functional consequence of these different minus-end structures? It seems likely that the capped ends are stable minus ends, nucleated from the centrosome. γ -tubulin appears to be the kinetically dominant nucleator of mitotic centrosomes in *C. elegans* (Hannak et al., 2002), suggesting that these minus ends are capped by γ -tubulin during nucleation. Interestingly, the capped ends make up the majority (~80%) of the minus ends. Open ends, on the other side, are likely to be dynamic, perhaps accounting for the dynamic properties of minus ends at spindle poles. The open minus-end structure could be a structural consequence of MT severing where release of the γ -tubulin cap could then lead to more dynamic behavior of the MT minus ends. MT severing by katanin-like proteins has been documented in meiotic spindles of *C. elegans*, to serve a possible role in limiting the size of MTs in these smaller spindles (Srayko et al., 2000), as well as in mitotic spindles from other systems (McNally et al., 1996; McNally and Thomas, 1998). Possibly, open MTs do not associate with nucleating sites but rather with structures capable of force generation and MT disassembly activity in the PCM. Such ends could be generated by release and anchoring of centrosome-nucleated MTs (for reviews see Bornens, 2002; McIntosh et al., 2002). Dynamic MT minus ends could also participate in poleward MT flux of mitotic spindles (for review see Wittmann et al., 2001). Future experiments combining RNA-mediated interference (RNAi) and tomographic reconstruction of different spindles should distinguish these different possibilities.

Materials and methods

Specimen preparation for electron microscopy

Wild-type *C. elegans* hermaphrodites were cryoimmobilized using a BAL-TEC HPM 010 high-pressure freezer (BAL-TEC). Fixation was performed by freeze substitution over 3 d at -90°C in anhydrous acetone containing 1% OsO_4 and 0.1% uranyl acetate (EM AFS; Leica) (McDonald and Müller-Reichert, 2002). Epon/Araldite infiltrated samples were flat embedded in a thin layer of resin and polymerized for 3 d at 60°C (Rappleye et al., 1999). Worms containing >5 early embryos were selected by light microscopy before remounting. Serial semithick sections (300–400 nm) were cut using a Leica Ultracut UCT Microtome. Sections were collected on Formvar-coated copper slot grids and poststained with 2% uranyl acetate in 70% methanol and Reynold's lead citrate.

High-voltage electron tomography

Electron tomography was performed essentially as described in O'Toole et al. (1999). Briefly, 15-nm colloidal gold particles (Sigma-Aldrich) were attached to both surfaces of the semi-thick sections to serve as fiducial markers for subsequent image alignment. The specimens were placed in a tilt-rotate specimen holder (Model 650; Gatan, Pleasanton, CA) and tomographic datasets recorded using a JEM-1000 high-voltage electron micro-

scope (JEOL, USA) operated at 750 kV. Images were captured every 1.5° over a $\pm 60^{\circ}$ range using a Gatan $1\text{K} \times 1\text{K}$ CCD camera at a pixel size of 1.4 nm. In some instances, montages of 2×1 or 3×1 frames were collected and used to image larger areas (Marsh et al., 2001). For dual axis tomography, the grids were imaged in one tilt series then rotated 90° , and a similar tilt series was acquired. For image processing, images were transferred to a Silicon Graphics workstation, and the tilted views were aligned using the positions of the colloidal gold particles as fiducial points. Tomograms were computed for each tilt axis using the R-weighted back-projection algorithm (Gilbert, 1972). We used the ratio of the section thickness, as defined by the microtome's setting, to the section's thickness measured after microscopy to calculate a "thinning factor," which was then used to correct the tomogram's dimension along the beam axis (O'Toole et al., 1999). For double tilt data sets, the two tomograms were aligned to each other and combined (Mastronarde, 1997). In addition, tomograms computed from adjacent serial sections were aligned and joined to increase the reconstructed volume (Ladinsky et al., 1999; Marsh et al., 2001). We recorded 11 double tilt series of mitotic spindles. In total, we analyzed 5 mitotic centrosomes.

Modeling and analysis of tomographic data

Tomograms were displayed and analyzed using the IMOD software package (Kremer et al., 1996). Features of interest were modeled in the serial slices extracted from the tomogram. An "image slicer" window in IMOD was used to display a slice extracted from the 3-D volume in any position or orientation; this feature was useful for unambiguous tracking of MTs in 3-D (O'Toole et al., 1999). With the slicer window, we analyzed the morphology of MT ends near the centrosomes and kinetochores by extracting a slice of image data 1-voxel thick and adjusting its orientation to contain the axis of the MT in a single view (O'Toole et al., 1999). A projection of the 3-D model was displayed and rotated to study its 3-D geometry. For this display in 3-D, MTs were shown as tubular graphic objects.

A program was written to compute the distance between the points on a selected object and a chosen reference location. The centroid of each centriole was located and used as the reference for positions within the spindle. A single model point was located at the pole-proximal end of each MT, and the 3-D distance of those points from the reference was calculated. A neighbor density analysis was performed to determine if there were preferred inter-fiber distances. These have been seen as indicative of interactions between different classes of MTs in two (McDonald et al., 1992) and three dimensions (Mastronarde et al., 1993; Marsh et al., 2001). MT ends were classified as described (Müller-Reichert et al., 1998).

Online supplemental material

Supplemental videos are available at <http://www.jcb.org/cgi/content/full/jcb.200304035/DC1>. Videos 1 and 2 show the complete tomographic volume of centrosomes in metaphase and anaphase corresponding to Fig. 1, A and D, respectively. Videos 3 and 4 are the projected 3-D models corresponding to Fig. 1, B and C, and E and F, respectively. Video 5 corresponds to Fig. 3 A and shows the tomographic reconstruction of a kinetochore region in metaphase, and Video 6 shows the projected 3-D model displayed in Fig. 3 B. The video sequence associated with Fig. 4 B (Video 7) shows a movie through a tomographic reconstruction of a kinetochore region in greater detail. Video 8, corresponding to Fig. 5, A and B, illustrates the tracing of KMTs in a partially reconstructed metaphase spindle.

We thank Drs. Carrie Cowan, Laurence Pelletier, and Martin Srayko for a critical reading of the manuscript and Drs. Ivan Baines, Michaela Wilsch-Bräuninger, and Paul Verkade for helpful conversations about this work. Drs. David Mastronarde and Richard Gaudette provided essential application software.

This work was supported in part by grant RR00592 from the National Center for Research Resources of the National Institutes of Health to J.R. McIntosh, who is a Research Professor of the American Cancer Society.

Submitted: 7 April 2003

Accepted: 17 September 2003

References

- Albertson, D.G. 1984. Formation of the first cleavage spindle in nematode embryos. *Dev. Biol.* 101:61–72.
- Bornens, M. 2002. Centrosome composition and microtubule anchoring mechanisms. *Curr. Opin. Cell Biol.* 14:25–34.
- Bullitt, E., M.P. Rout, J.V. Kilmartin, and C.W. Akey. 1997. The yeast spindle

- pole body is assembled around a central crystal of Spc42p. *Cell*. 89:1077–1086.
- Byers, B., K. Shriver, and L. Goetsch. 1978. The role of spindle pole bodies and modified microtubule ends in the initiation of microtubule assembly in *Saccharomyces cerevisiae*. *J. Cell Sci.* 30:331–352.
- Chrétien, D., S.D. Fuller, and E. Karsenti. 1995. Structure of growing microtubule ends: two-dimensional sheets close into tubes at variable rates. *J. Cell Biol.* 129:1311–1328.
- Doxsey, S. 2001. Re-evaluating centrosome function. *Nat. Rev. Mol. Cell Biol.* 2:688–698.
- Gilbert, P.F.C. 1972. The reconstruction of a three-dimensional structure from projections and its application to electron microscopy. II. Direct methods. *Proc. R. Soc. Lond. B. Biol. Sci.* 182:89–102.
- Hannak, E., K. Oegema, M. Kirkham, P. Gönczy, B. Habermann, and A.A. Hyman. 2002. The kinetically dominant assembly pathway for centrosomal asters in *Caenorhabditis elegans* is γ -tubulin dependent. *J. Cell Biol.* 157:591–602.
- Howard, J., and A.A. Hyman. 2003. Dynamics and mechanics of the microtubule plus end. *Nature*. 422:753–758.
- Howe, M., K.L. McDonald, D.G. Albertson, and B.J. Meyer. 2001. HIM-10 is required for kinetochore structure and function on *Caenorhabditis elegans* holocentric chromosomes. *J. Cell Biol.* 153:1227–1238.
- Keating, T.J., and G.G. Borisy. 2000. Immunostuctural evidence for the template mechanism of microtubule nucleation. *Nat. Cell Biol.* 2:352–357.
- Kirkham, M., T. Müller-Reichert, K. Oegema, S. Grill, and A.A. Hyman. 2003. SAS-4 is a *C. elegans* centriolar protein that controls centrosome size. *Cell*. 112:575–587.
- Kremer, J.R., D.N. Mastronarde, and J.R. McIntosh, Jr. 1996. Computer visualization of three-dimensional image data using IMOD. *J. Struct. Biol.* 116:71–76.
- Ladinsky, M.S., D.N. Mastronarde, J.R. McIntosh, K.E. Howell, and L.A. Staehelin. 1999. Golgi structure in three dimensions: Functional insights from the normal rat kidney cell. *J. Cell Biol.* 144:1135–1149.
- Mandelkow, E.M., E. Mandelkow, and R.A. Milligan. 1991. Microtubule dynamics and microtubule caps: a time-resolved cryo-electron microscopy study. *J. Cell Biol.* 114:977–991.
- Marsh, B.J., D.N. Mastronarde, K.F. Buttle, K.E. Howell, and J.R. McIntosh. 2001. Organellar relationships in the Golgi region of the pancreatic beta cell line, HIT-T15, visualized by high resolution electron tomography. *Proc. Natl. Acad. Sci. USA*. 98:2399–2406.
- Mastronarde, D.N., K.L. McDonald, R. Ding, and J.R. McIntosh. 1993. Interpolar spindle microtubules in PTK cells. *J. Cell Biol.* 123:1475–1489.
- Mastronarde, D.N. 1997. Dual-axis tomography: An approach with alignment methods that preserve resolution. *J. Struct. Biol.* 120:343–352.
- McDonald, K., and T. Müller-Reichert. 2002. Cryomethods for thin section electron microscopy. *Methods Enzymol.* 351:96–123.
- McDonald, K.L., E.T. O'Toole, D.N. Mastronarde, and J.R. McIntosh. 1992. Kinetochore microtubules in PtK1 cells. *J. Cell Biol.* 118:369–383.
- McEwen, B.F., C.-E. Hsieh, A.L. Mattheyses, and C.L. Rieder. 1998. A new look at kinetochore structure in vertebrate somatic cells using high-pressure freezing and freeze substitution. *Chromosoma*. 107:366–375.
- McIntosh, J.R., E.L. Grishchuk, and R.R. West. 2002. Chromosome-microtubule interactions during mitosis. *Annu. Rev. Cell Dev. Biol.* 18:193–219.
- McNally, F.J., K. Okawa, A. Iwamatsu, and R.D. Vale. 1996. Katanin, the microtubule-severing ATPase, is concentrated at centrosomes. *J. Cell Sci.* 109:561–567.
- McNally, F.J., and S. Thomas. 1998. Katanin is responsible for the M-phase microtubule-severing activity in *Xenopus* eggs. *Mol. Biol. Cell*. 9:1847–1861.
- Moritz, M., M.B. Braunfeld, J.C. Fung, J.W. Sedat, B.M. Alberts, and D.A. Agard. 1995. Three-dimensional structural characterization of centrosomes from early *Drosophila* embryos. *J. Cell Biol.* 130:1149–1159.
- Moritz, M., M.B. Braunfeld, V. Guenebaut, J. Heuser, and D.A. Agard. 2000. Structure of the γ -tubulin ring complex: a template for microtubule nucleation. *Nat. Cell Biol.* 2:365–370.
- Müller-Reichert, T., D. Chrétien, F. Severin, and A.A. Hyman. 1998. Structural changes at microtubule ends accompanying GTP hydrolysis: information from a slowly hydrolyzable analogue of GTP, guanylyl (α,β)methylene-diphosphonate. *Proc. Natl. Acad. Sci. USA*. 95:3661–3666.
- O'Connell, K.F. 2000. The centrosome of the early *C. elegans* embryo: Inheritance, assembly, replication, and developmental roles. *Curr. Top. Dev. Biol.* 49:365–384.
- O'Connell, K.F., C. Caron, K.R. Kopish, D.D. Hurd, K.J. Kempfues, Y. Li, and J.G. White. 2001. The *C. elegans zyg-1* gene encodes a regulator of centrosome duplication with distinct maternal and paternal roles in the embryo. *Cell*. 105:547–558.
- O'Toole, E.T., M. Winey, and J.R. McIntosh. 1999. High-voltage electron tomography of spindle pole bodies and early mitotic spindles in the yeast *Saccharomyces cerevisiae*. *Mol. Biol. Cell*. 10:2017–2031.
- Rappleye, C.A., A.R. Paredes, C.W. Smith, K.L. McDonald, and R.V. Aroian. 1999. The coronin-like protein POD-1 is required for anterior-posterior axis formation and cellular architecture in the nematode *Caenorhabditis elegans*. *Genes Dev.* 13:2838–2851.
- Rieder, C.L., S.S. Bowser, R. Cole, G. Rupp, A. Peterson, and S.P. Alexander. 1990. Diffuse kinetochores and holokinetic anaphase chromatin movement during mitosis in the hemipteran *Agallia constricta* (Leafhopper) cell line AC-20. *Cell Motil. Cytoskeleton*. 15:245–259.
- Rout, M.P., and J.V. Kilmartin. 1990. Components of the yeast spindle and spindle pole body. *J. Cell Biol.* 111:1913–1927.
- Srayko, M., D.W. Buster, O.A. Bazirgan, F.J. McNally, and P.E. Mains. 2000. MEI-1/MEI2 katanin-like microtubule severing activity is required for *Caenorhabditis elegans* meiosis. *Genes Dev.* 14:1072–1084.
- Wiese, C., and Y. Zheng. 2000. A new function for the γ -tubulin ring complex as a microtubule minus-end cap. *Nat. Cell Biol.* 2:358–364.
- Wittmann, T., A. Hyman, and A. Desai. 2001. The spindle: a dynamic assembly of microtubules and motors. *Nat. Cell Biol.* 3:E28–E34.
- Wolf, N., D. Hirsh, and J.R. McIntosh. 1978. Spermatogenesis in males of the free-living nematode, *Caenorhabditis elegans*. *J. Ultrastruct. Res.* 63:155–169.

3.3 Microtubule organization in collapsed mitotic spindles

N. Özlü, M. Srayko, K. Kinoshita, B. Habermann, E. T. O'Toole, T. Müller-Reichert, N. Schmalz, A. Desai, and A. A. Hyman. 2005. *Dev. Cell.* 9, 237-248.

An Essential Function of the *C. elegans* Ortholog of TPX2 Is to Localize Activated Aurora A Kinase to Mitotic Spindles

Nurhan Özlü,^{1,*} Martin Srayko,¹ Kazuhisa Kinoshita,¹ Bianca Habermann,² Eileen T. O'Toole,⁴ Thomas Müller-Reichert,¹ Natalie Schmalz,¹ Arshad Desai,^{1,3} and Anthony A. Hyman^{1,*}

¹Max Planck Institute of Molecular Cell Biology and Genetics

Pfotenhauerstrasse 108
Dresden 01307

Germany

²Scionics Computer Innovation

Pfotenhauerstrasse 110
Dresden 01307

Germany

³Ludwig Institute for Cancer Research

Department of Cellular and Molecular Medicine
University of California, San Diego

9500 Gillman Drive

La Jolla, California 92093

⁴Boulder Laboratory for 3D Electron Microscopy of Cells

University of Colorado
Boulder, Colorado 80309

Summary

In vertebrates, the microtubule binding protein TPX2 is required for meiotic and mitotic spindle assembly. TPX2 is also known to bind to and activate Aurora A kinase and target it to the spindle. However, the relationship between the TPX2-Aurora A interaction and the role of TPX2 in spindle assembly is unclear. Here, we identify TPXL-1, a *C. elegans* protein that is the first characterized invertebrate ortholog of TPX2. We demonstrate that an essential role of TPXL-1 during mitosis is to activate and target Aurora A to microtubules. Our data suggest that this targeting stabilizes microtubules connecting kinetochores to the spindle poles. Thus, activation and targeting of Aurora A appears to be an ancient and conserved function of TPX2 that plays a central role in mitotic spindle assembly.

Introduction

Chromosome segregation takes place on a bipolar, microtubule-based mitotic spindle. During interphase, microtubules radiate from the centrosome, a microtubule-nucleating center. As cells enter mitosis, microtubules reorganize to build a mitotic spindle (reviewed in Wittmann et al., 2001). Microtubules in a mitotic spindle come from two different sources. One source is microtubules nucleated by the centrosome; these grow out from the centrosomes and associate with chromosomes, where they are stabilized. Another source is microtubules nucleated around chromosomes. These

microtubules self-organize into two spindle poles through the action of microtubule-based motors. The relative contributions of these two different pathways vary in different systems (reviewed in Gadde and Heald, 2004).

Mitotic spindles assemble with a characteristic length and shape, which differs in various cell types and organisms. Spindle length can be influenced by the dynamic balance between microtubule stabilization and destabilization within the spindle (Karsenti and Vernos, 2001; Mitchison et al., 2005; Tournebize et al., 2000); changing the global parameters of microtubule dynamics alters the length of spindles (Scholey et al., 2003). In addition, motor proteins acting on microtubules can regulate the length and shape of spindles (Sharp et al., 2000). To date, we understand little about the integration of these different mechanisms in the regulation of spindle length and size.

TPX2, a microtubule-associated protein, is required for mitotic spindle assembly in human cells and *Xenopus* egg extracts (reviewed in Gruss and Vernos, 2004). In *Xenopus* meiotic egg extracts, TPX2 stimulates the formation of microtubules around chromosomes (Groen et al., 2004; Gruss et al., 2001; Schatz et al., 2003). However, we do not know what the role of TPX2 is in mitosis.

A clue as to the possible function of TPX2 came with the discovery that TPX2 binds to the mitotic kinase Aurora A and stimulates its activity (Eyers et al., 2003; Triebelmann et al., 2003; Tsai et al., 2003). In human cells, TPX2 is required for localization of Aurora A to spindles (Kufer et al., 2002). However, the cell cycle arrest phenotype of Aurora A has made it difficult to determine whether an essential function of TPX2 is to localize Aurora A or whether it has other roles (Hirota et al., 2003; Prigent and Giet, 2003). Further complicating the relationship between TPX2's function in spindle assembly and its binding to Aurora A is recent work in *Xenopus* extracts suggesting that the non-Aurora A targeting domain is able to rescue extracts depleted of TPX2 (Brunet et al., 2004).

Although the analysis of TPX2 in mitotic cells indicates a role in spindle function or integrity, it is unclear how these spindle defects manifest over the course of the assembly process. In principle, studying TPX2 in a genetically tractable organism such as yeast, *C. elegans*, or *Drosophila* could help to answer some of these questions. However, to date no TPX2 homolog has been identified in invertebrates. *C. elegans* is an ideal system to identify and study the potential function of Aurora A activators, because Aurora A has a very severe defect in spindle assembly and apparently gives no cell cycle arrest. Here, we use *C. elegans* early embryos to identify TPXL-1, the first known invertebrate ortholog of TPX2. Our results show that the function of TPXL-1 is to activate and localize Aurora A to the mitotic spindle. Comparison of TPXL-1 and Aurora A function further indicates that TPXL-1-mediated activation and localization of Aurora A is necessary to stabilize microtubules connecting kinetochores to spindle poles. These results provide mechanistic insight into

*Correspondence: ozlu@mpi-cbg.de (N.O.); hyman@mpi-cbg.de (A.A.H.)

how the conserved TPX2 protein family contributes to spindle assembly.

Results

TPXL-1 Is a TPX2 Ortholog in *C. elegans* Embryos

To find a *C. elegans* ortholog for TPX2, we screened through genes required for spindle assembly. We identified an uncharacterized gene ORF (Y39G10AR.12) required for spindle assembly, which was initially reported in a Chromosome I RNA interference (RNAi) screen (Fraser et al., 2000). After RNAi of this gene, the separated centrosomes collapse together shortly after nuclear envelope break down (NEBD) and fail to form a robust spindle (Figures 1A and 1B). We name this gene *tpxl-1* (TPX2-like, for reasons stated below).

Sequence alignment with TPX2 showed homology within the N terminus (residues 1–60) (Figures 2A and 2B). This short region of homology was significant because the N-terminal 43 residues of TPX2 have been shown to be sufficient for binding and activating Aurora A kinase (Bayliss et al., 2003). We also determined that the N terminus of TPXL-1 similarly binds *C. elegans* Aurora A, AIR-1. AIR-1 specifically bound to and eluted from a wild-type GST::N-terminal-TPXL-1 (aa 1–63) column but did not bind to mutated TPXL-1 constructs, which should block the interaction between TPXL-1 and AIR-1, based on comparisons to TPX2 (Bayliss et al., 2004, 2003; Evers and Maller, 2004) (Figure 2C; confirmed by mass spectrometry). In agreement with the results shown above, a genome-wide Yeast Two-Hybrid screen of *C. elegans* proteins also identified an interaction between TPXL-1 and AIR-1 (Li et al., 2004).

If TPXL-1 is an ortholog of TPX2, then it should also stimulate the kinase activity of AIR-1. We found that addition of TPXL-1(1–63) dramatically increased the phosphorylation of Histone H3 by AIR-1 kinase, whereas the TPXL-1(1–63) mutant proteins had no effect (Figure 2D). Therefore, we conclude that TPXL-1 binds to and activates Aurora A kinase and that TPXL-1 is an ortholog of vertebrate TPX2.

Interaction of TPXL-1 with AIR-1 Is Required for Spindle Assembly

In human cells, TPX2 is required to localize Aurora A to spindles (Kufer et al., 2002). To test whether *C. elegans* TPX2 is also required to localize *C. elegans* Aurora A, we raised and affinity-purified antibodies to TPXL-1. On Western blots, Anti-TPXL-1 antibodies recognized a single band of approximately 75 kDa that disappeared in *tpxl-1(RNAi)* worm lysate (see Figure S1A in the Supplemental Data available with this article online). Both TPXL-1 immunostaining and live imaging of embryos expressing TPXL-1::GFP showed that TPXL-1 colocalizes with AIR-1 (Figure 3A, see also Movies S3 and S4). We tested for interdependency of their respective intracellular-localization patterns. In *tpxl-1(RNAi)* embryos, AIR-1 was no longer detected on astral microtubules but instead colocalized with γ -tubulin (Figure 3A, see also Movie S5). In contrast, in *air-1(RNAi)* embryos, TPXL-1 was still detected on microtubules (Figure 3B).

Is the main function of TPX2 in spindle assembly to interact with Aurora A? The consequences of depleting

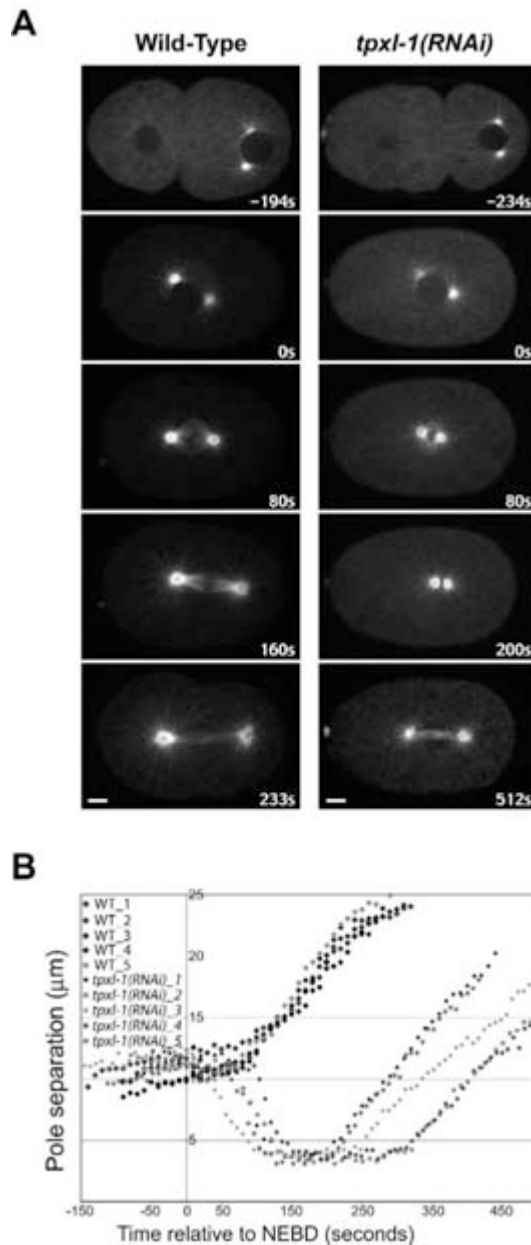


Figure 1. Spindle Poles Collapse in Embryos Depleted of TPXL-1 (A) Summarization of spinning disk confocal time-lapse movies taken from wild-type (left) and *tpxl-1(RNAi)* (right) embryos expressing GFP:: β -tubulin. Times are in seconds relative to NEBD. In the TPXL-1-depleted embryos, centrosomes separate as in wild-type (-234 s). Upon NEBD (0 s), separated centrosomes collapse together (80 s and 200 s). After wild-type embryos initiate anaphase, the spindle in *tpxl-1(RNAi)* embryos elongates but reaches a shorter total spindle length (512 s). See also Movies S1 and S2. (B) Pole-to-pole distances were measured in five wild-type (diamonds) and five *tpxl-1(RNAi)* (circles) embryos. Bars: 5 μ m.

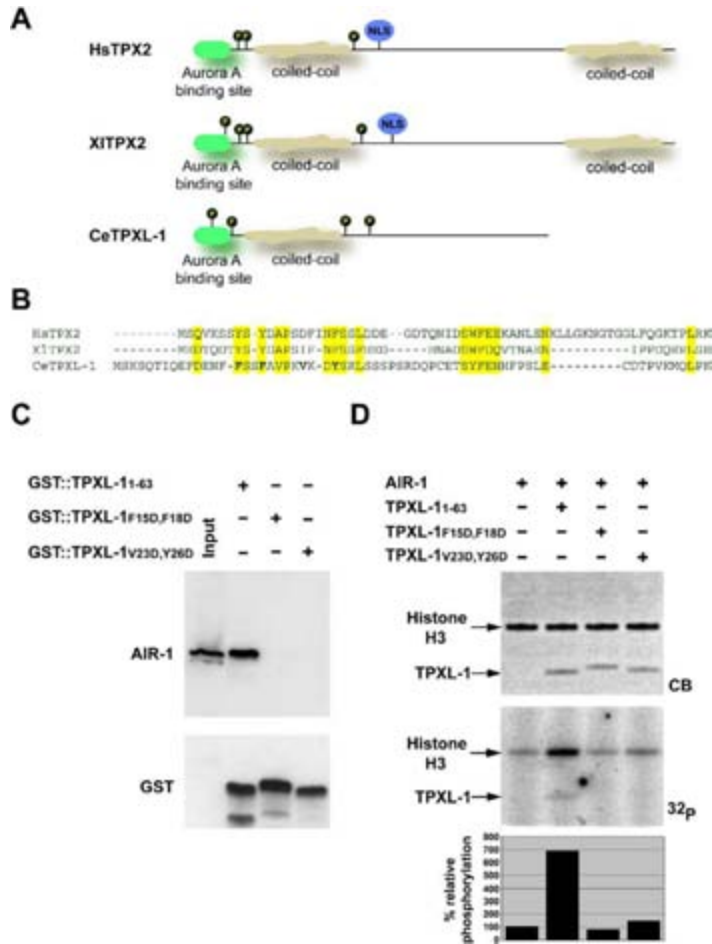


Figure 2. TPXL-1 Binds to and Stimulates AIR-1 Kinase

(A) Common features of *C. elegans* (Ce), *Homo sapiens* (Hs), and *Xenopus laevis* (Xi) TPX2 proteins. TPXL-1 and TPX2 share homology in the minimum Aurora A binding site (green box, aa 1–43; Bayliss et al., 2003). TPX2 contains two coiled-coil domains (Hs aa 213–247 and 664–729; Xi aa 171–216 and 637–696). TPXL-1 possesses one N-terminal coiled-coil domain (aa 150–173). Consensus Aurora A phosphorylation sites (consensus sequence: RX[S/T]); Cheeseman et al., 2002) in the N termini of TPX2 and TPXL-1 are shown by black circles (aa positions in TPXL-1 are 30, 68, 149, and 154). A functional nuclear-localization signal in vertebrates (Schatz et al., 2003) is indicated by blue circles.

(B) Multiple sequence alignment of Aurora A binding domain and the N-terminal regions of TPXL-1 from *C. elegans* (Ce) with TPX2 from human (Hs) and *Xenopus* (Xi). The conserved residues are boxed in yellow. Residues that are mutated in (C) and (D) are indicated with bold lettering.

(C) GST-pulldown assay shows that AIR-1 binds to GST::TPXL-1 (1–63). GST fusions were expressed in *E. coli*, bound to glutathione resin, incubated in worm extract, and eluted with glutathione. Elutions were fractionated by SDS-PAGE and analyzed via Western blotting with anti-AIR-1 (top) and anti-GST (bottom) antibodies. AIR-1 can be detected as a single band (40 kDa) in worm extracts and in the GST::TPXL-1 (1–63) pull-down, but not in the pull-downs performed with the TPXL-1 (1–63) mutants.

(D) TPXL-1 (1–63) stimulates AIR-1 kinase activity. In vitro phosphorylation of histone H3 (determined by ^{32}P -ATP levels) in the presence of AIR-1 and either TPXL-1 (1–63) or the indicated TPXL-1 (1–63) mutants. Coomassie blue stain and autoradiograph of the SDS-PAGE gel are shown. For quantification of histone H3 phosphorylation (bottom), the value of 100% was assigned to the phosphorylation of Histone H3 in the presence of only AIR-1.

TPXL-1 on spindle assembly may reflect both AIR-1-dependent and AIR-1-independent functions. To specifically analyze AIR-1-dependent functions, we generated transgenes expressing either wild-type TPXL-1 or the N-terminal mutant that does not interact with AIR-1 (see Figures 2C and 2D). To specifically remove endogenous TPXL-1 function, the introduced transgenes were engineered to be resistant to RNAi by insertion of silent mutations in the N terminus (Figure 4A). Indeed, immunoblotting of wild-type and mutant transgenic worms showed that *tpxl-1(RNAi)* specifically depleted the endogenous TPXL-1 without affecting RNAi-resistant forms (Figure S1B). In the presence of the wild-type transgene, RNAi of the endogenous *tpxl-1* gene did not affect expression of the transgene and the spindle collapsed only slightly (Figures 4B and 4C). In the presence of the mutated transgene, RNAi of the endogenous *tpxl-1* gene did not affect expression of the transgene (Figure 4B) but the spindle completely col-

lapsed with a similar profile as TPXL-1-depleted embryos (Figures 4B and 4C). Furthermore, depletion of TPXL-1 prevents AIR-1 localization on spindle and astral microtubules and leads to AIR-1 collapse into the same domain of the centrosome as γ -tubulin (Figure 3A). Similarly, in the presence of the mutated transgene, after RNAi of the endogenous *tpxl-1* gene, AIR was no longer detected on microtubules or the peripheral centrosomal region but was collapsed to the inner centrosomal region (Figure 4D). Thus, the interaction between TPXL-1 and AIR-1 targets AIR-1 to the microtubules. The specificity of this experiment suggests that an essential function of TPXL-1 is to target AIR-1 to the spindle microtubules.

To confirm this idea, we compared the phenotypes of TPXL-1 and AIR-1 depletion by RNA interference. AIR-1 is required for cell polarity, centrosome maturation, maintenance of separated centrosomes after NEBD, formation of a robust microtubule aster, spindle

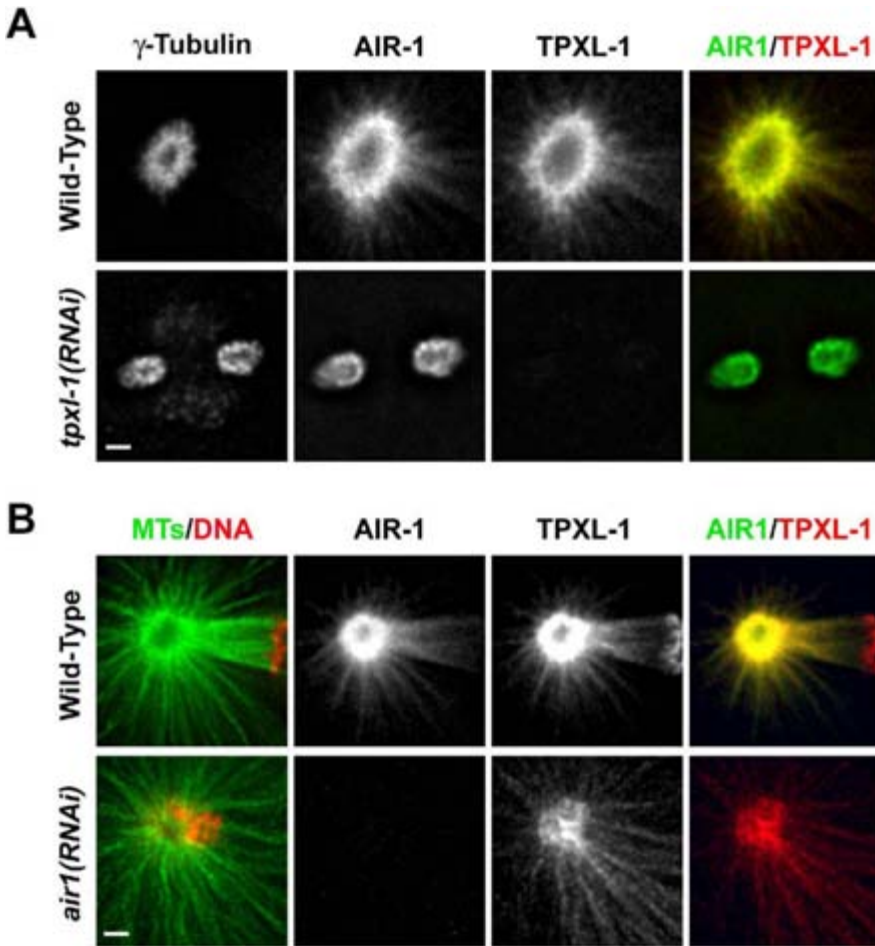


Figure 3. TPXL-1 Is Required for Targeting *C. elegans* Aurora A (AIR-1) to the Spindle

(A) TPXL-1 and AIR-1 colocalize at the centrosome, and TPXL-1 is required for AIR-1 to extend outward from the core centrosome along microtubules. The top row shows a high-magnification view of one centrosome from a wild-type metaphase embryo stained for γ -tubulin, AIR-1, and TPXL-1. AIR-1 and TPXL-1 colocalize on the outer centrosomal layer and extend along centrosomal microtubules. The bottom row shows both mitotic centrosomes in a *tpxl-1(RNAi)* embryo. AIR-1 collapses to colocalize with γ -tubulin after depletion of TPXL-1 and does not extend along centrosomal microtubules.

(B) TPXL-1 still extends onto microtubules in AIR-1-depleted embryos. High-magnification view of one centrosome from a wild-type embryo at the onset of anaphase (top) and an *air1(RNAi)* embryo (bottom) stained for microtubules (green) and DNA (red) (left), AIR-1 (green), and TPXL-1 (red) (right). All images are single z sections of deconvolved wide-field data sets. Bars: 1 μ m.

assembly, and anaphase spindle elongation (Hannak et al., 2001, 2002; Schumacher et al., 1998). Table 1 summarizes the phenotypic comparison of AIR-1- and TPXL-1-depleted embryos. Formation of the PAR domains (data not shown), anaphase spindle elongation (Figures 1A and 1B), and centrosome maturation (Figures S2A and S2B) were normal after depletion of TPXL-1. In both wild-type and *tpxl-1(RNAi)* embryos, γ -tubulin accumulated with similar rates (Figure S2A and S2B). Although this result suggested that centrosome maturation was normal, formation of a robust aster was defective after depletion of TPXL-1 (Figure S2C). The phenotypic differences between *tpxl-1(RNAi)* and *air-1(RNAi)* could represent weakened AIR-1 activ-

ity rather than complete loss of a subset of AIR-1 functions. However, we never observe the characteristic *tpxl-1(RNAi)* phenotype with even partial loss of AIR-1 function (data not shown). Therefore, it seems likely that TPXL-1 is required for a subset of AIR-1 activities, namely formation of a robust mitotic aster and assembly of a mitotic spindle.

The Role of TPXL-1 in Spindle Assembly Is Independent of Chromatin-Stimulated Microtubule Assembly

Why do spindles collapse after depletion of TPXL-1? In *Xenopus* egg extracts, TPX2 stimulates chromatin-dependent microtubule nucleation in a Ran-GTP-depend-

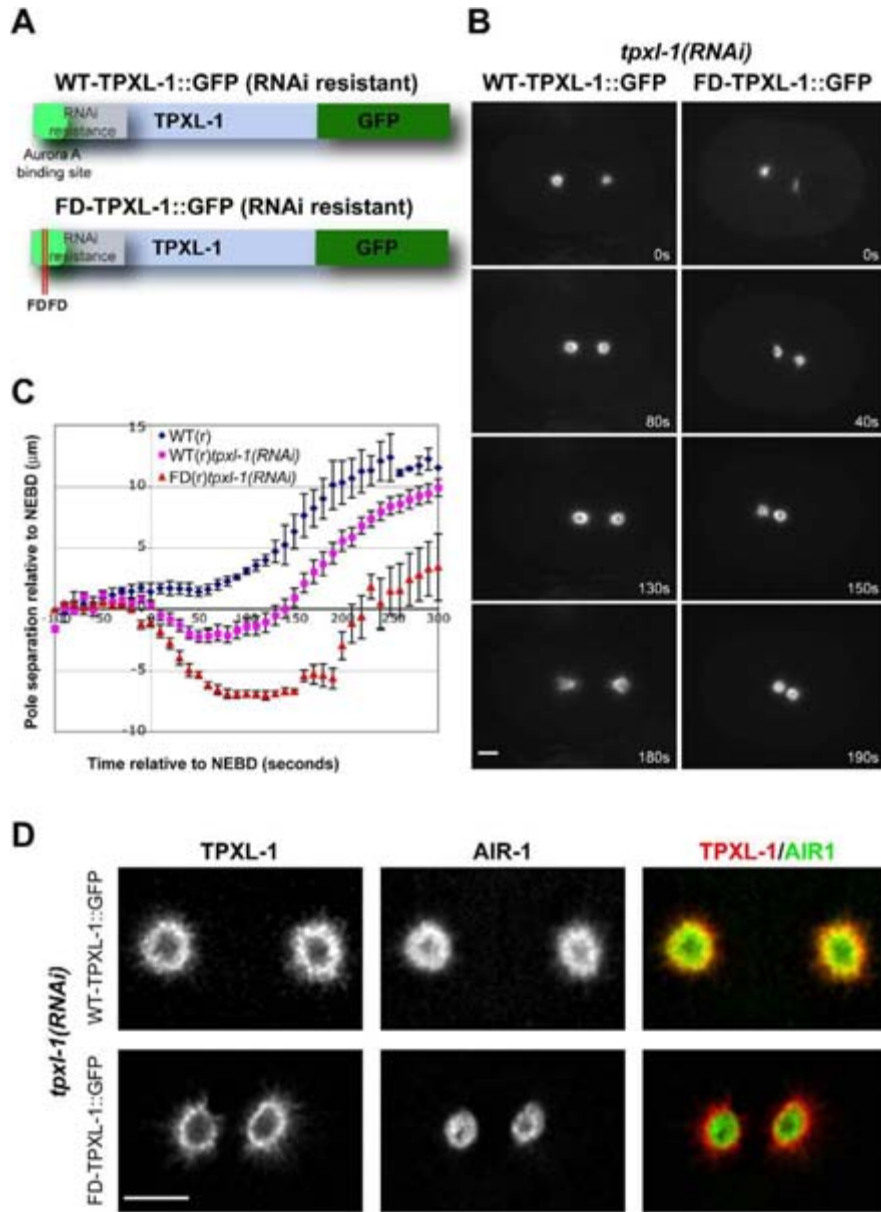


Figure 4. Interaction of TPXL-1 with AIR-1 Is Required for Its Activity In Vivo

(A) Schematic of transgenes: RNAi-resistant wild-type TPXL-1 (blue box) was fused to GFP (dark green box) (top). The Aurora A binding site is indicated in the light green box. The RNAi-resistance tag was created by insertion of silent mutations into the N terminus (gray box). To specifically deplete the endogenous TPXL-1, dsRNA was raised against this region. The RNAi-resistant mutant TPXL-1::GFP transgene (bottom) is as described in the wild-type transgene. F15D and F18D mutations are indicated by red lines in the Aurora A binding site.

(B) Selected panels from time-lapse recordings of wt TPXL-1::GFP(r) and FD TPXL-1::GFP(r)-expressing embryos after *tpxl-1(RNAi)* to remove endogenous TPXL-1. Centrosomal fluorescence intensities are similar in both embryos (Figure S1C). The poles were completely collapsed in the FD TPXL-1::GFP(r)-expressing embryo, but not in the wt TPXL-1::GFP(r)-expressing embryo. Times are in seconds relative to NEBD. See also Movies S6 and S7.

(C) Spindle-pole separation relative to NEBD was tracked for transgenic embryos: wt TPXL-1::GFP(r) ($n = 2$) and FD TPXL-1::GFP(r) ($n = 2$) (plotted together; blue diamonds); *tpxl-1(RNAi)* in wt TPXL-1::GFP(r) ($n = 7$) (pink squares), and *tpxl-1(RNAi)* in FD TPXL-1::GFP(r) ($n = 6$) (red triangles). Average pole-to-pole distance at NEBD was set to zero. Error bars are standard error of the mean (SEM) with a confidence interval of 0.95.

(D) High-magnification view of centrosomes from a metaphase wt TPXL-1::GFP(r)-expressing embryo after RNAi-mediated depletion of endogenous TPXL-1 (top) and from a FD TPXL-1::GFP(r)-expressing embryo after RNAi-mediated depletion of endogenous TPXL-1 (bottom). Embryos were stained for TPXL-1 (red) and AIR-1 (green). In *tpxl-1(RNAi)* wt TPXL-1::GFP(r), AIR-1 localizes to the peripheral centrosomal region. In the *tpxl-1(RNAi)* FD TPXL-1::GFP(r) embryo, AIR-1 localizes to the inner centrosomal region. All images are single z sections of deconvolved wide-field data sets. Abbreviation: r, RNAi resistant. Bars: B, 5 μm ; D, 3 μm .

Table 1. Comparison of AIR-1- and TPXL-1-Depletion Phenotypes (The Cellular Process in the Left Column Is Affected [+] or Not Affected [-] upon Protein Depletion).

	AIR-1	TPXL-1
Cell Polarity	+ ^{a, c}	-
Centrosomal γ -Tubulin Recruitment	+ ^b	-
Robust Aster Formation	+ ^b	+
Spindle Assembly	+ ^{a, b}	+
Spindle Elongation at Anaphase	+ ^b	-

^aSchumacher et al., 1998

^bHannak et al., 2001

^cC. Cowan and A.A.H., unpublished data.

dent manner (Gruss and Vernos, 2004). By using two different tests, we showed that TPXL-1 is not required for chromatin-dependent microtubule nucleation. First, in *spd-5* mutant embryos, which lack functional centrosomes, microtubules assemble around mitotic chromosomes and are unable to form a spindle-like structure (Figure S3A; Hamill et al., 2002). In *spd-5(RNAi);tpxl-1(RNAi)* embryos, we still observed these chromatin-associated microtubules (Figure S3A). Subsequent immunofluorescence assays revealed the efficient depletion of both proteins (Figure S4A). Thus, at the level of depletion in *tpxl-1(RNAi)* embryos in which spindles collapse, noncentrosomal microtubules are still present. Second, during *C. elegans* female meiosis, microtubules nucleate around the chromosomes and subsequently organize into bipolar spindles that lack astral microtubules (Albertson and Thomson, 1993). *tpxl-1(RNAi)* resulted in loss of all meiotic spindle TPXL-1 staining, but meiotic spindle morphology was indistinguishable from wild-type embryos (Figure S3B). Therefore, we conclude that inhibition of chromatin-stimulated microtubule nucleation is unlikely to be the origin of the spindle collapse observed in TPXL-1-depleted embryos. This suggests that the mechanism of spindle stabilization by TPXL-1 is different from that of TPX2 in *Xenopus* extracts.

TPXL-1 Is Not Required for Generation of Astral Forces

Because TPXL-1 is not required for microtubule assembly around chromatin, we searched for an alternate explanation for the observed spindle-collapse phenotype. During spindle assembly, a balance of outward and inward forces exerted on spindle poles controls spindle length. One possibility is that TPXL-1 contributes to cortical pulling forces, transmitted by astral microtubules. In this idea, kinetochore-mediated pulling forces would dominate over weakened astral pulling forces, resulting in spindle collapse. To test if the astral pulling forces are active in *tpxl-1(RNAi)* embryos, we performed spindle-severing experiments with a UV laser (Grill et al., 2001). In wild-type embryos, astral forces pull spindle poles apart after laser-mediated spindle severing (Figures 5A–5C). In TPXL-1-depleted embryos, the spindle poles separated from each other with peak velocities comparable to wild-type (Figure 5C) and the final positions of the centrosomes postablation were similar to wild-type (Figures 5A and 5B). From these results, we conclude that astral forces are not affected by the depletion of TPXL-1.

Kinetochore Microtubules Form after RNAi of TPXL-1

The results so far suggest an intrinsic problem in spindle stability in the absence of TPXL-1. Kinetochore function is required for the formation of a stable spindle by providing a mechanical connection between replicated chromosomes and both spindle poles (Oegema et al., 2001). To resolve the morphology of the collapsed spindles, we performed electron tomography on *tpxl-1(RNAi)* embryos after spindle collapse (Figure 6A). EM-tomography revealed that a spindle is formed and centrosomes are connected to kinetochore microtubules but that these kinetochore microtubules are extremely short.

Spindle Collapse in *tpxl-1(RNAi)* Embryos Depends on Intact Kinetochores, but Not Antiparallel Microtubules

Could kinetochore microtubule instability be causing the spindle collapse? In CeCENP-A-depleted embryos, kinetochore assembly fails and poles separate prematurely before forming a metaphase spindle (Oegema et al., 2001; Figure 6B, compare wild-type and CeCENP-A-depleted 160 s; Figure 6C). In double RNAi, TPXL-1- and CeCENP-A- (Figure 6B) or TPXL-1- and CeCENP-C- (data not shown) depleted embryos, pole separation occurs as in CeCENP-A-depleted embryos, with spindle poles prematurely elongating (Figure 6B, 90 s and 160 s; Figure 6C). Subsequent immunofluorescence assays confirmed that in double RNAi embryos, TPXL-1 was depleted as efficiently as in single *tpxl-1(RNAi)* embryos (Figure S4B). Thus, the spindle collapse in *tpxl-1(RNAi)* embryos is mediated by kinetochores pulling the poles toward the chromosomes.

To check that the spindle collapse in TPXL-1-depleted embryos occurs by destabilization of kinetochore-attached microtubules and not by overlapping antiparallel microtubules emanating from opposite spindle poles, we analyzed spindle formation in *tpxl-1(RNAi)* monopolar spindles. To generate monopolar spindles, we used a *zyg-1(b1)* mutant in which centrosome duplication fails (O'Connell et al., 2001). These mutants make half spindles and therefore have no overlapping antiparallel microtubules. However, spindles still collapse in *tpxl-1(RNAi);zyg-1* double mutants (Figure 6D).

Abnormal Microtubule Behavior at Spindle Poles in *tpxl-1(RNAi)* Embryos

Why are kinetochore microtubules unstable in *tpxl-1(RNAi)*? Aurora A is localized at spindle poles, suggesting that defects in spindle-pole organization could contribute to a lack of kinetochore microtubule stability. To investigate microtubule behavior at spindle poles, we utilized EBP-2::GFP (an EB1 homolog that specifically decorates growing microtubule ends; Srayko et al., 2005). We first examined microtubule nucleation rates. Surprisingly, we found that the microtubule nucleation rate in *tpxl-1(RNAi)* embryos was not significantly different from wild-type embryos ($90 \pm 12\%$ of wild-type metaphase nucleation rates; $p = 0.25$; Figure 7A) despite a reduced microtubule intensity at spindle poles (Figure S2C). This suggested that the decrease in microtubule levels at centrosomes in *tpxl-1(RNAi)* results from a lack of persistence and/or stability of nu-

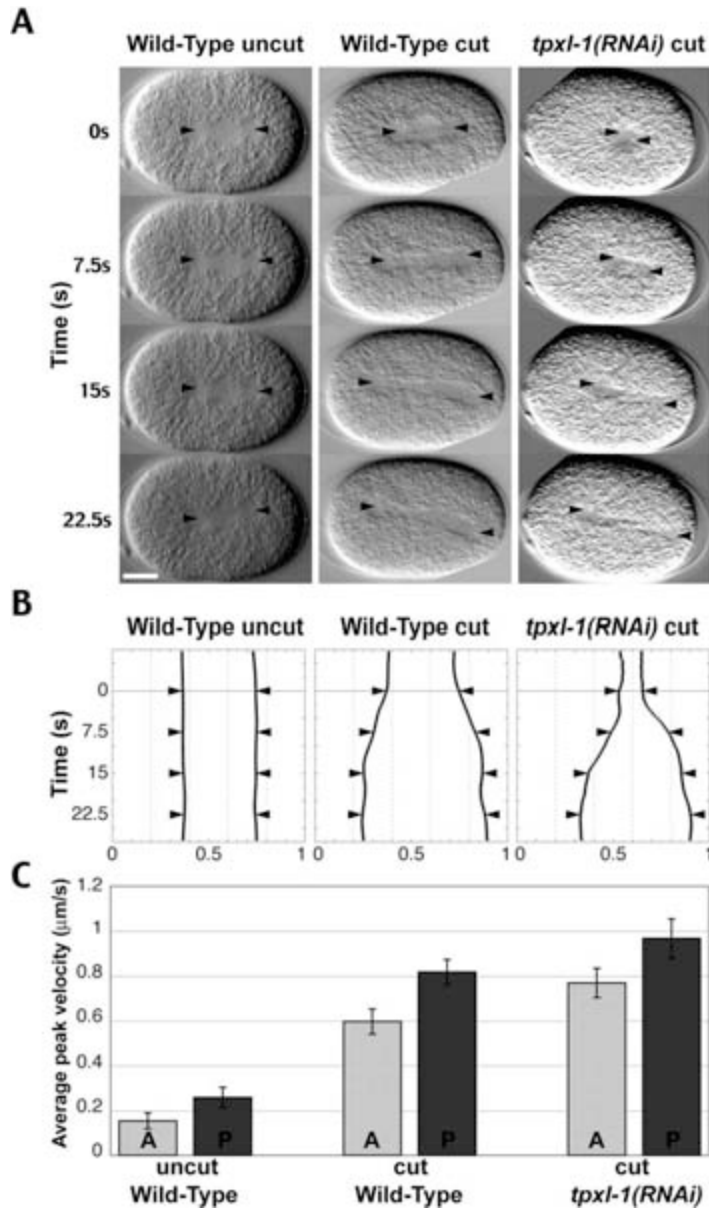


Figure 5. TPXL-1 Is Not Required for Generation of Astral Forces

(A) Laser cutting of spindles to monitor astral pulling forces. Summarization of differential interference contrast (DIC) time-lapse movies of uncut wild-type (left column), laser-cut wild-type (middle column), and laser-cut *tpxl-1(RNAi)* (right column) embryos. The laser-cut was performed at 0 s at the midline between the spindle poles. See also [Movies S12 and S13](#).

(B) Spindle-pole tracking of embryos shown in (A). Position is relative to the embryo length: 0 represents anterior cortex, 1 represents posterior cortex.

(C) Average peak velocities of anterior and posterior spindle poles. Error bars are SEM with a confidence interval of 0.95. Average peak velocities were measured for eight wild-type uncut, 15 wild-type cut, and 23 *tpxl-1(RNAi)* cut. Bar: 10 μm.

cleated microtubules rather than a defect in microtubule nucleation.

We also noticed an increase in the frequency of EBP-2::GFP dots exhibiting a switch from anterograde movement (growth away from centrosomes) to retrograde movement (movement toward centrosomes) (see [Movie S20](#)). The switch occurs at low frequency in wild-type (see [Movie S19](#)). Because EBP-2::GFP only associates with growing microtubule plus ends, retrograde movements are thought to be a consequence of detached microtubule minus ends ([Srayko et al., 2005](#)). In *tpxl-1(RNAi)* embryos, we observed a 6-fold increase in retrograde movements in astral microtubules compared to wild-type ([Figure 7B](#)). We also observed retro-

grade EBP-2::GFP movements in bipolar spindles ([Figure 7C](#), yellow dot) and monopolar spindles (see [Movie S21](#)) of *tpxl-1(RNAi)* embryos, although it was not feasible to quantify the number due to a high density of EBP-2 dots in the spindle. The increased frequency of these movements in *tpxl-1(RNAi)* embryos suggests that the spindle-collapse phenotype observed may arise from a loss of microtubule minus-end stability near the centrosomes.

Discussion

The data presented here provide two key pieces of evidence that identify the first ortholog of TPX2 in inverte-

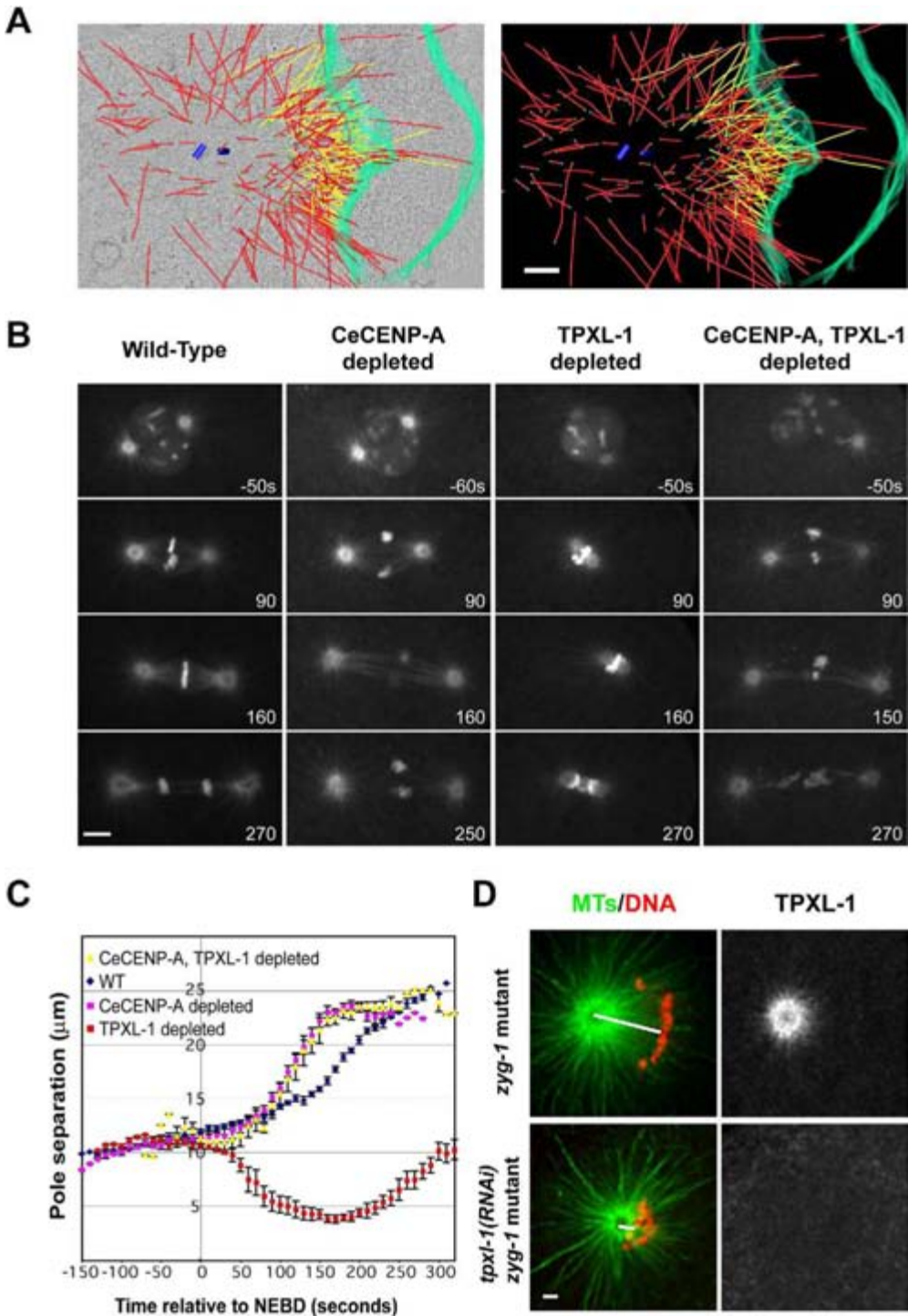


Figure 6. Spindle Collapse in *tpxl-1(RNAi)* Embryos Depends on Intact Kinetochores, but Not Antiparallel Microtubules
(A) Kinetochore microtubules still form in the absence of TPXL-1. Electron tomography of a collapsed *tpxl-1(RNAi)* spindle. The 3D model superimposed on a selected tomographic slice is shown in the left panel. The partial reconstruction was computed from a 2×1 montage. The 3D model (right) shows the boundaries of a kinetosome (green) and the position of spindle microtubules (red, yellow lines). Microtubules that ended on the chromosome were defined as kinetochore microtubules (yellow).

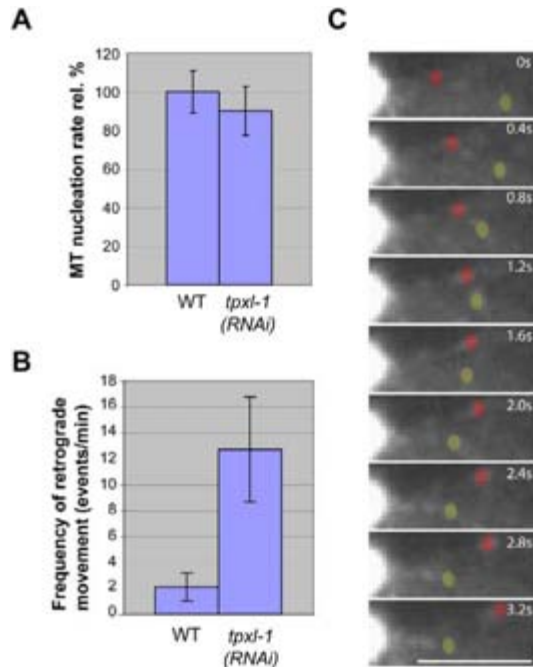


Figure 7. Abnormal Microtubule Behavior at Spindle Poles in *tpxl-1*(RNAi) Embryos

(A) Quantification of astral microtubule nucleation rates in wild-type and *tpxl-1*(RNAi) embryos expressing EBP-2::GFP (an EB1 homolog that specifically decorates growing MT ends). Kymographs from 1 min stream-acquisition movies were used to quantify the number of EBP-2::GFP dots emanating from metaphase centrosomes (Srayko et al., 2005). Nucleation rates are relative to wild-type metaphase (% wt MTs/min). Standard error at 95% confidence is shown; wild-type, n = 16; *tpxl-1*(RNAi), n = 10.

(B) Frequency of retrograde movements (events/min) of EBP-2::GFP dots in wild-type and *tpxl-1*(RNAi) embryos is shown. Standard error at 0.95 confidence is shown; wild-type, n = 16; *tpxl-1*(RNAi), n = 12.

(C) A series of images from a stream-acquisition movie of a EBP-2::GFP dot exhibiting retrograde movement (colored yellow) and a separate dot exhibiting normal anterograde growth movement (colored red) within the mitotic spindle of a *tpxl-1*(RNAi) embryo is shown. Centrosome is on the left (white circle). See also Movie S20, for astral retrograde movements and Movie S21, for retrograde movements in a monopolar spindle. Bar: 5 μ m.

brates. First, both proteins interact with Aurora A and stimulate its kinase activity in vitro (Bayliss et al., 2004; Eyers et al., 2003; Tsai et al., 2003). Second, both proteins are required for the localization of Aurora A to spindle microtubules, but not for the localization of Au-

rorA to the spindle pole (Kufer et al., 2002). However, we have not been able to find any evidence that TPXL-1 is regulated through the Ran pathway, as is the case for TPX2. Although TPXL-1 contains a putative nuclear localization sequence, we do not see prominent nuclear localization. The phenotype of Ran depletion is the failure to form a mitotic spindle, reminiscent of the loss of kinetochore function and unlike the phenotype of TPXL-1 depletion (Askjaer et al., 2002; Bamba et al., 2002). More work is required to characterize the contribution of this pathway to spindle assembly in *C. elegans*.

The identification of a TPX2 ortholog has allowed us to resolve an important question: is a TPX2-Aurora A interaction required for TPX2 function during spindle assembly? In *Xenopus* extracts, the C terminus of TPX2 lacking the Aurora A binding site can complement TPX2 function (Brunet et al., 2004). In human cells, the mitotic arrest induced by Aurora A RNAi has made it difficult to compare the phenotype of Aurora A RNAi and TPX2 RNAi. Our results show that mutated TPXL-1, which cannot bind to Aurora A, does not rescue the spindle-collapse defect. Therefore, in *C. elegans* mitosis, an essential function of the TPX2 ortholog is to target Aurora A to spindles.

Why do spindles collapse in the absence of TPXL-1? In *Xenopus* egg extract, TPX2 is required for chromatin-dependent microtubule nucleation. However, in *C. elegans*, under RNAi conditions in which spindles collapse, microtubule nucleation around chromosomes is unaffected. Thus, TPX2 appears to function differently in *Xenopus* and *C. elegans*. We do not know the reason for this difference. Perhaps TPX2 can activate different kinases in different systems. Alternatively, the C terminus of TPX2 may have functions unrelated to Aurora A activity, and these functions may be more essential in *Xenopus* extracts.

Our data suggest that the most likely reason that spindles collapse in the absence of TPXL-1 is destabilization of kinetochore microtubules. One possibility is that the kinetochore-attached plus ends are unstable in the absence of TPXL-1. Unfortunately, the high-turnover rate of microtubules in *C. elegans* prophase precludes testing this model by FRAP (A.D., unpublished observations; Srayko et al., 2005). The fact that TPXL-1 operates together with Aurora A and Aurora A is localized to spindle poles suggests that the primary defect of *tpxl-1*(RNAi) could be in organization of the spindle pole. Supporting evidence for this is that the number of microtubules at centrosomes is quite reduced, whereas the nucleation rate seems to be the same as wild-type, and that a substantial number of polymerizing microtubules exhibit freedom of movement (visible as retrograde plus-end movement) inconsistent with a stable

(B) Summarization of time-lapse sequences of wild-type (first column), CeCENP-A-depleted (second column), TPXL-1-depleted (third column), and CeCENP-A- and TPXL-1-depleted (fourth column) embryos expressing GFP:: β -tubulin and GFP::histone. Times are in seconds relative to NEBD (left). See also Movies S15–S18.

(C) Spindle pole separation relative to NEBD. The graph shows the average pole-to-pole-distance of wild-type (blue), CeCENP-A-depleted (pink), TPXL-1-depleted (red), and CeCENP-A- and TPXL-1-depleted (yellow) embryos. Error bars are SEM with a confidence interval of 0.95 (n = 4).

(D) Chromosomes in monopolar spindles collapse into the centrosomes after TPXL-1 depletion. Half spindles from a *zyg-1* mutant (top) and a *tpxl-1*(RNAi);*zyg-1* mutant embryo (bottom) stained for microtubules and DNA (left) and TPXL-1 (right) are shown. The white line indicates chromosome-pole distance. Images are single z sections of deconvolved, wide-field data sets. Bars: A, 500 nm; B, 5 μ m; D, 1 μ m.

attachment to centrosomes. Perhaps the minus ends of microtubules are unstable, and this allows the centrosomes to be pulled toward the chromosomes.

Therefore, we propose that in *C. elegans* mitosis, the homolog of TPX2— TPXL-1— targets Aurora A to the spindle, where it phosphorylates downstream targets required for kinetochore microtubule stabilization. These could be centrosome, spindle, or kinetochore components. One possible candidate is TAC-1, a protein implicated in microtubule stability (Bellanger and Gonczy, 2003; Le Bot et al., 2003; Lee et al., 2001; Srayko et al., 2003) whose homologs are known to be an Aurora A substrate (Giet et al., 2002). TPX2 itself is a microtubule binding protein (Wittmann et al., 2000), so it is possible that phosphorylation of TPXL-1 by Aurora A may also contribute to the stabilization activity. The other known substrate of Aurora A, the motor protein Eg5 (Giet et al., 1999), is not required for *C. elegans* spindle assembly (Bishop et al., 2005). Identification of other Aurora A substrates would provide important insights into the mechanisms of spindle assembly.

C. elegans Aurora A has a number of different roles in the first embryonic cell division: (1) cell polarity, (2) centrosome maturation, (3) spindle assembly, and (4) spindle elongation at anaphase. In contrast, TPXL-1 is required only for spindle assembly, and the rescue experiments with wild-type or mutant TPXL-1 indicate that all of the functions of TPXL-1 are contained within a subset of Aurora A functions (Table 1). Thus, it seems that a key role for Aurora A in spindle assembly is to stabilize microtubules nucleated from centrosomes that are bound to kinetochores. Because RNAi is a run-down technique, it is possible that the difference between Aurora A phenotypes and TPX2 phenotypes represents a difference in sensitivity of different Aurora A functions to TPX2 levels. However, we think it is more likely that other Aurora A activation and targeting subunits exist that are responsible for the various functions of Aurora A. In this way, the cell can ensure that Aurora A is targeted at the correct time and to the correct place during the cell cycle to perform its various roles.

Experimental Procedures

RNA-Mediated Interference

For production of *tpxl-1* dsRNA, the gene was amplified from either N2 genomic DNA or the cDNA yk1152d5. RNA synthesis and annealing were performed by using standard procedures (Oegema et al., 2001). Primer sequences are listed in Table S1. L4 hermaphrodites were injected with dsRNA and incubated for 45–48 hr at 16°C, 30–36 hr at 20°C, or 24 hr at 24.5°C before being examined.

GFP Strains and RNAi Resistance Transgenes

The following GFP strains used were as previously described: AZ244, GFP:: β -tubulin, (Praitis et al., 2001); XA3501, GFP::tubulin; GFP::Histone, (Askjaer et al., 2002); and TH24, GFP:: γ -tubulin, (Hannak et al., 2002). TH41 (GFP::AIR-1) was a gift from Carrie Cowan (MPI-CBG, Dresden, Germany). The strain *spd-5(or213ts)* (Hamill et al., 2002) was crossed to the strain AZ244 to obtain *spd-5* mutant embryos expressing GFP:: β -tubulin.

The strain TH53 expressing TPXL-1::GFP was constructed by high-pressure particle bombardment (Bio-Rad) of DP38 [*unc-119(ed3)*] worms with a plasmid (a gift from Andrei Pozniakovski, MPI-CBG, Dresden, Germany) containing a C-terminal TPXL-1::GFP fusion gene under the control of the *pie-1* promoter and *unc-119(+)* as a selection marker (Praitis et al., 2001). TH53 likely contains an

integrated array of the rescuing plasmid due to 100% rescue of progeny for *unc-119*, and all progeny examined express GFP.

RNAi-resistant wild-type and FD TPXL-1::GFP transgenes were made as follows: The first 500 bp of the *tpxl-1* sequence were synthesized by Geneart GmbH (Regensburg, Germany). This sequence contained silent mutations such that the synthetic gene diverged from the original gene at the DNA level (28% divergent), but not at the protein-coding level. Wherever possible, the codon usage was adapted to the codon bias of *Caenorhabditis elegans* genes. A second *tpxl-1(RNAi)*-resistant gene was synthesized containing F15D, F18D mutations. The first 500 bp of the *tpxl-1* sequence in the TPXL-1::GFP construct were then excised by using a unique restriction site and were replaced with newly synthesized genes. The transgenic worms were generated as explained above. To specifically silence the endogenous gene in these transgenic worms, dsRNA was synthesized against 3–393 bp of *tpxl-1*.

Electron Tomography and 3D modeling

Sample preparation for electron tomography was carried out essentially as published (O'Toole et al., 2003). Briefly, RNAi worms were high-pressure frozen (BAL-TEC HPM 010), freeze substituted (Leica EM AFS), and thin-layer embedded in Epon and Araldite for serial sectioning. Electron tomography was performed on 300 nm plastic sections of *tpxl-1(RNAi)* embryos with a TECNAI F30 intermediate-voltage electron microscope operated at 300 kV. Tomograms were computed and analyzed by using the IMOD software package as published (O'Toole et al., 2003).

Time-Lapse Microscopy and Quantification

TPXL-1::GFP-, GFP:: β -tubulin-, and GFP:: β -tubulin;GFP::histone-expressing embryos were imaged with a spinning disk confocal microscope controlled by the Metamorph Imaging software. Images were acquired every 8 or 10 s with an ORCA 100 (Hamamatsu) camera and 63 \times , 1.4 NA PlanApochromat objective with 500–1,000 msec exposure time. GFP:: γ -tubulin-expressing embryos were imaged with a wide-field microscope (Zeiss Axioplan II) equipped as described above. Images were acquired every 10 s with 550 msec exposure time and 2 \times binning. Quantification of centrosomal β -tubulin and γ -tubulin was performed as previously described (Pelletier et al., 2004).

Spindle Severing

Spindle severing was performed as described previously (Grill et al., 2001) with a pulsed, third-harmonic, solid-state UV laser (λ = 354 nm, 4 ns, 12 μ J/Pulse, PowerChip, JDS Uniphase). DIC images were acquired every 0.5 s with an inverted microscope (Axiovert 200M, Zeiss) with a water-immersion lens (C-Apochromat 63 \times , NA 1.2, Zeiss) (Grill et al., 2003). Spindle pole tracking and analysis were performed as described (Grill et al., 2001).

Protein and Antibody Production

For generating antibodies against TPXL-1, the GST::TPXL-1 (aa 1–210) was affinity purified after expression of the appropriate cDNA fragment cloned into pGEX6P-1 (Amersham). Antibodies to the N-terminal TPXL-1 (aa 1–210), the C-terminal 17 amino acids of TPXL-1, and the C-terminal 12 amino acids of AIR-1 were raised, affinity purified, and directly labeled as described (Oegema et al., 2001).

For GST pull-down assays, GST::TPXL-1 (aa 1–63) was affinity purified after expression of the specified cDNA fragment cloned into pGEX-M8 (a gift from Mike Tipsword; MPI-CBG, Dresden, Germany). F15D, F18D GST::TPXL-1 (aa 1–63), and V23D, Y26D GST::TPXL-1 (aa 1–63) site-directed mutants were generated by using the QuikChange protocol (Stratagene). For double mutants, residues were substituted in two steps, and the resulting constructs were confirmed by DNA sequencing (DNA Sequencing Facility, MPI-CBG, Dresden, Germany). GST fusions were expressed in BL21 or BL21 CodonPlus RP *E. Coli* (Stratagene) and purified under native conditions with glutathione agarose beads (Sigma).

Full-length AIR-1 was amplified from first-strand cDNA. The amplified product was subcloned into pGEM-T (Promega) and cloned into pHAT to generate His-tagged AIR-1. His-tagged AIR-1 was ex-

pressed in BL21 *E. Coli* (Stratagene) and purified by using TALON resin (Clontech).

Western Blotting for RNAi and Fixed Imaging

For Western blotting, 20–35 *tpxl-1(RNAi)*-injected worms and an equal number of control worms were washed three times with M9. To 10 μ l of total volume, an equal volume of 2 \times sodium dodecyl sulfate-polyacrylamide gel electrophoresis (SDS-PAGE) sample buffer was added, and tubes were sonicated for 5 min at 80°C in a waterbath sonicator. The entire volume of lysate was loaded onto an SDS-PAGE gel and analyzed by Western blotting by using 1 μ g/ml anti-TPXL-1 and ECL (Amersham) detection of HRP-conjugated anti-rabbit secondary antibody (Bio-Rad Laboratories). For loading control, immunoblots were reprobbed with anti- α -tubulin antibody (DM1 α , Sigma) and detected with either alkaline-phosphatase-conjugated (Jackson ImmunoResearch Laboratories) or HRP-conjugated anti-mouse secondary antibodies.

Immunofluorescence experiments were performed as described previously (Oegema et al., 2001). Antibodies were used at 1 μ g/ml. Images through entire embryos were acquired with a wide-field Delta Vision microscope (Applied Precision), and the images were deconvolved with SoftWorx (Applied Precision).

GST Pulldown Assays

2 μ g of wild-type and mutant GST::TPXL-1 proteins were bound to 40 μ l of glutathione beads. Worm extract was prepared by sonicating 1 g frozen worm pellets in lysis buffer (1 mM EGTA, 1 mM MgCl₂, 50 mM HEPES [pH 7.4], 100 mM KCl, 10% glycerol, 0.05% NP-40, and 1 mM DTT) containing protease inhibitors. Worm extract was incubated with the resin for 1 hr at 4°C, washed four times with lysis buffer, and bound proteins were eluted either by adding reduced glutathione (Sigma) or 40 μ l of 2 \times SDS-PAGE sample buffer. 10 μ l from each sample was loaded on an SDS-PAGE gel and analyzed by Western blotting by using 1 μ g/ml anti-AIR-1 antibodies, HRP-conjugated anti-rabbit secondary antibody, and ECL detection. For comparison of incubated protein levels, immunoblots were also subsequently probed with anti-GST antibody.

In Vitro Kinase Assays

GST::TPXL-1 (1–63) fusions were incubated with Precission protease (Amersham) for 10 hr at 4°C. Cleaved 4 μ M wt and mutant TPXL-1 (1–63) proteins were incubated with HIS-tagged AIR-1 and 0.2 mg/ml Histone H3 (Roche) in kinase buffer (25 mM Hepes [pH 7.4], 100 mM KCl, 5 mM MgCl₂, 0.5 mM EGTA, 1 mM DTT, 0.05% Tween-20, and 0.05 mM ATP) including γ [³²P]-ATP for 15 min at 25°C (Bayliss et al., 2003). Samples were analyzed by SDS-PAGE and autoradiography. Quantification of Histone H3 phosphorylation was performed with a Fujifilm BAS-1800II phosphorimager.

Supplemental Data

Supplemental Data including four figures and 21 movies are available online with this article at <http://www.developmentalcell.com/cgi/content/full/9/2/237/DC1/>.

Acknowledgments

We thank C. Cowan, K. Oegema, L. Pelletier, S. Quintin, A. Schlaitz, J. Stear, and M. Van Breugel for comments on the manuscript. We are very grateful to: E. Conti (European Molecular Biology Laboratory, Heidelberg, Germany) for helpful discussion and Human Aurora A and TPX2 proteins; M. Boxem and M. Vidal (Dana Farber Cancer Institute, Boston, MA) for sharing unpublished data; T. Kapoor (The Rockefeller University, New York, NY) for suggesting the monopolar spindle experiment; S. Grill for help with the laser ablation experiment; Y. Kohara (National Institute of Genetics, Mishima, Japan) for cDNAs used in this study; Neslihan Özlü for help with graphics; C. Cowan, B. Bowerman (University of Oregon, Eugene, OR), and W.M. Saxton (Indiana University, Bloomington, IN) for strains; A. Pozniakovski, M. Tipword, M. Ruer, and S. Rybina for reagents; and the Hyman lab members for many helpful discussions. This work was supported in part by grant RR00592 from the

National Center for Research Resources of the National Institutes of Health to J.R.M.

Received: April 29, 2005

Revised: June 10, 2005

Accepted: July 8, 2005

Published: August 1, 2005

References

- Albertson, D.G., and Thomson, J.N. (1993). Segregation of holocentric chromosomes at meiosis in the nematode, *Caenorhabditis elegans*. *Chromosome Res.* 1, 15–26.
- Askjaer, P., Galy, V., Hannak, E., and Mattaj, I.W. (2002). Ran GTPase cycle and importins alpha and beta are essential for spindle formation and nuclear envelope assembly in living *Caenorhabditis elegans* embryos. *Mol. Biol. Cell* 13, 4355–4370.
- Bamba, C., Bobinsec, Y., Fukuda, M., and Nishida, E. (2002). The GTPase Ran regulates chromosome positioning and nuclear envelope assembly in vivo. *Curr. Biol.* 12, 503–507.
- Bayliss, R., Sardon, T., Vernos, I., and Conti, E. (2003). Structural basis of Aurora-A activation by TPX2 at the mitotic spindle. *Mol. Cell* 12, 851–862.
- Bayliss, R., Sardon, T., Ebert, J., Lindner, D., Vernos, I., and Conti, E. (2004). Determinants for Aurora-A activation and Aurora-B discrimination by TPX2. *Cell Cycle* 3, 404–407.
- Bellanger, J.M., and Gonczy, P. (2003). TAC-1 and ZYG-9 form a complex that promotes microtubule assembly in *C. elegans* embryos. *Curr. Biol.* 13, 1488–1498.
- Bishop, J.D., Han, Z., and Schumacher, J.M. (2005). The *Caenorhabditis elegans* Aurora B kinase AIR-2 phosphorylates and is required for the localization of a BimC kinesin to meiotic and mitotic spindles. *Mol. Biol. Cell* 16, 742–756.
- Brunet, S., Sardon, T., Zimmerman, T., Wittmann, T., Pepperkok, R., Karsenti, E., and Vernos, I. (2004). Characterization of the TPX2 domains involved in microtubule nucleation and spindle assembly in *Xenopus* egg extracts. *Mol. Biol. Cell* 15, 5318–5328.
- Cheeseman, I.M., Anderson, S., Jwa, M., Green, E.M., Kang, J., Yates, J.R., 3rd, Chan, C.S., Drubin, D.G., and Barnes, G. (2002). Phospho-regulation of kinetochore-microtubule attachments by the Aurora kinase Ipl1p. *Cell* 111, 163–172.
- Eyers, P.A., and Maller, J.L. (2004). Regulation of *Xenopus* Aurora A activation by TPX2. *J. Biol. Chem.* 279, 9008–9015.
- Eyers, P.A., Erikson, E., Chen, L.G., and Maller, J.L. (2003). A novel mechanism for activation of the protein kinase Aurora A. *Curr. Biol.* 13, 691–697.
- Fraser, A.G., Kamath, R.S., Zipperlen, P., Martinez-Campos, M., Sohrmann, M., and Ahringer, J. (2000). Functional genomic analysis of *C. elegans* chromosome I by systematic RNA interference. *Nature* 408, 325–330.
- Gadde, S., and Heald, R. (2004). Mechanisms and molecules of the mitotic spindle. *Curr. Biol.* 14, R797–R805.
- Giet, R., Uzbekov, R., Cubizolles, F., Le Guellec, K., and Prigent, C. (1999). The *Xenopus laevis* aurora-related protein kinase pEg2 associates with and phosphorylates the kinesin-related protein XIEg5. *J. Biol. Chem.* 274, 15005–15013.
- Giet, R., McLean, D., Descamps, S., Lee, M.J., Raff, J.W., Prigent, C., and Glover, D.M. (2002). Drosophila Aurora A kinase is required to localize D-TACC to centrosomes and to regulate astral microtubules. *J. Cell Biol.* 156, 437–451.
- Grill, S.W., Gonczy, P., Stelzer, E.H., and Hyman, A.A. (2001). Polarity controls forces governing asymmetric spindle positioning in the *Caenorhabditis elegans* embryo. *Nature* 409, 630–633.
- Grill, S.W., Howard, J., Schaffer, E., Stelzer, E.H., and Hyman, A.A. (2003). The distribution of active force generators controls mitotic spindle position. *Science* 301, 518–521.
- Groen, A.C., Cameron, L.A., Coughlin, M., Miyamoto, D.T., Mitchison, T.J., and Ohi, R. (2004). XRHAMM functions in ran-dependent

- microtubule nucleation and pole formation during anastral spindle assembly. *Curr. Biol.* **14**, 1801–1811.
- Gruss, O.J., and Vernos, I. (2004). The mechanism of spindle assembly: functions of Ran and its target TPX2. *J. Cell Biol.* **166**, 949–955.
- Gruss, O.J., Carazo-Salas, R.E., Schatz, C.A., Guarguagliini, G., Kast, J., Wilm, M., Le Bot, N., Vernos, I., Karsenti, E., and Mattaj, I.W. (2001). Ran induces spindle assembly by reversing the inhibitory effect of importin alpha on TPX2 activity. *Cell* **104**, 83–93.
- Hamill, D.R., Severson, A.F., Carter, J.C., and Bowerman, B. (2002). Centrosome maturation and mitotic spindle assembly in *C. elegans* require SPD-5, a protein with multiple coiled-coil domains. *Dev. Cell* **3**, 673–684.
- Hannak, E., Kirkham, M., Hyman, A.A., and Oegema, K. (2001). Aurora-A kinase is required for centrosome maturation in *Caenorhabditis elegans*. *J. Cell Biol.* **155**, 1109–1116.
- Hannak, E., Oegema, K., Kirkham, M., Gonczy, P., Habermann, B., and Hyman, A.A. (2002). The kinetically dominant assembly pathway for centrosomal asters in *Caenorhabditis elegans* is gamma-tubulin dependent. *J. Cell Biol.* **157**, 591–602.
- Hirota, T., Kunitoku, N., Sasayama, T., Marumoto, T., Zhang, D., Nitta, M., Hatakeyama, K., and Saya, H. (2003). Aurora-A and an interacting activator, the LIM protein Ajuba, are required for mitotic commitment in human cells. *Cell* **114**, 585–598.
- Karsenti, E., and Vernos, I. (2001). The mitotic spindle: a self-made machine. *Science* **294**, 543–547.
- Kufer, T.A., Silje, H.H., Korner, R., Gruss, O.J., Meraldi, P., and Nigg, E.A. (2002). Human TPX2 is required for targeting Aurora-A kinase to the spindle. *J. Cell Biol.* **158**, 617–623.
- Le Bot, N., Tsai, M.C., Andrews, R.K., and Ahringer, J. (2003). TAC-1, a regulator of microtubule length in the *C. elegans* embryo. *Curr. Biol.* **13**, 1499–1505.
- Lee, M.J., Gergely, F., Jeffers, K., Peak-Chew, S.Y., and Raff, J.W. (2001). Msp/XP215 interacts with the centrosomal protein D-TACC to regulate microtubule behaviour. *Nat. Cell Biol.* **3**, 643–649.
- Li, S., Armstrong, C.M., Bertin, N., Ge, H., Milstein, S., Boxem, M., Vidalain, P.O., Han, J.D., Chesneau, A., Hao, T., et al. (2004). A map of the interactome network of the metazoan *C. elegans*. *Science* **303**, 540–543.
- Mitchison, T.J., Maddox, P., Gaetz, J., Groen, A., Shirasu, M., Desai, A., Salmon, E.D., and Kapoor, T.M. (2005). Roles of polymerization dynamics, opposed motors, and a tensile element in governing the length of *Xenopus* extract meiotic spindles. *Mol. Biol. Cell* **16**, 3064–3076.
- O'Connell, K.F., Caron, C., Kopish, K.R., Hurd, D.D., Kempfues, K.J., Li, Y., and White, J.G. (2001). The *C. elegans* zyg-1 gene encodes a regulator of centrosome duplication with distinct maternal and paternal roles in the embryo. *Cell* **105**, 547–558.
- Oegema, K., Desai, A., Rybina, S., Kirkham, M., and Hyman, A.A. (2001). Functional analysis of kinetochore assembly in *Caenorhabditis elegans*. *J. Cell Biol.* **153**, 1209–1226.
- O'Toole, E.T., McDonald, K.L., Mantler, J., McIntosh, J.R., Hyman, A.A., and Muller-Reichert, T. (2003). Morphologically distinct microtubule ends in the mitotic centrosome of *Caenorhabditis elegans*. *J. Cell Biol.* **163**, 451–456.
- Pelletier, L., Ozlu, N., Hannak, E., Cowan, C., Habermann, B., Ruer, M., Muller-Reichert, T., and Hyman, A.A. (2004). The *Caenorhabditis elegans* centrosomal protein SPD-2 is required for both pericentriolar material recruitment and centriole duplication. *Curr. Biol.* **14**, 863–873.
- Praitis, V., Casey, E., Collar, D., and Austin, J. (2001). Creation of low-copy integrated transgenic lines in *Caenorhabditis elegans*. *Genetics* **157**, 1217–1226.
- Prigent, C., and Giet, R. (2003). Aurora A and mitotic commitment. *Cell* **114**, 531–532.
- Schatz, C.A., Santarella, R., Hoenger, A., Karsenti, E., Mattaj, I.W., Gruss, O.J., and Carazo-Salas, R.E. (2003). Importin alpha-regulated nucleation of microtubules by TPX2. *EMBO J.* **22**, 2060–2070.
- Scholey, J.M., Brust-Mascher, I., and Mogilner, A. (2003). Cell division. *Nature* **422**, 746–752.
- Schumacher, J.M., Ashcroft, N., Donovan, P.J., and Golden, A. (1998). A highly conserved centrosomal kinase, AIR-1, is required for accurate cell cycle progression and segregation of developmental factors in *Caenorhabditis elegans* embryos. *Development* **125**, 4391–4402.
- Sharp, D.J., Rogers, G.C., and Scholey, J.M. (2000). Microtubule motors in mitosis. *Nature* **407**, 41–47.
- Srayko, M., Quintin, S., Schwager, A., and Hyman, A.A. (2003). *Caenorhabditis elegans* TAC-1 and ZYG-9 form a complex that is essential for long astral and spindle microtubules. *Curr. Biol.* **13**, 1506–1511.
- Srayko, M., Kaya, A., Stamford, J., and Hyman, A.A. (2005). Identification and characterization of factors required for microtubule growth and nucleation in the early *C. elegans* embryo. *Dev. Cell* **9**, this issue, 223–236.
- Tournebise, R., Popov, A., Kinoshita, K., Ashford, A.J., Rybina, S., Pozniakovskiy, A., Mayer, T.U., Walczak, C.E., Karsenti, E., and Hyman, A.A. (2000). Control of microtubule dynamics by the antagonistic activities of XMAP215 and XKCM1 in *Xenopus* egg extracts. *Nat. Cell Biol.* **2**, 13–19.
- Trieselmann, N., Armstrong, S., Rauw, J., and Wilde, A. (2003). Ran modulates spindle assembly by regulating a subset of TPX2 and Kid activities including Aurora A activation. *J. Cell Sci.* **116**, 4791–4798.
- Tsai, M.Y., Wiese, C., Cao, K., Martin, O., Donovan, P., Ruderman, J., Prigent, C., and Zheng, Y. (2003). A Ran signalling pathway mediated by the mitotic kinase Aurora A in spindle assembly. *Nat. Cell Biol.* **5**, 242–248.
- Wittmann, T., Wilm, M., Karsenti, E., and Vernos, I. (2000). TPX2, A novel *Xenopus* MAP involved in spindle pole organization. *J. Cell Biol.* **149**, 1405–1418.
- Wittmann, T., Hyman, A., and Desai, A. (2001). The spindle: a dynamic assembly of microtubules and motors. *Nat. Cell Biol.* **3**, E28–E34.

3.4 Role of *C. elegans* katanin in acentrosomal spindle assembly

E. T. O'Toole, M. Srayko, A. A. Hyman, and T. Müller-Reichert. 2006. (submitted).

INTRODUCTION

Katanin is a heterodimer that exhibits ATP-dependent microtubule-severing activity (1, 2). In *Xenopus* egg extracts, severing activity of katanin is highest during the transition from interphase to mitosis, suggesting that it might be required for the rapid disassembly of interphase microtubules at the onset of mitosis (3). Other possibilities include mediation of microtubule poleward flux at centrosomes (4) and the release of microtubules from the centrosome during outgrowth of neuronal processes (5). To date we do not completely understand how katanin severs microtubules. Katanin could target the outer surface of the microtubule lattice, the microtubule lumen, or the lateral sides of protofilaments exposed by holes in the lattice (6, 7). Importantly, a detailed description of katanin's effect on the microtubule lattice *in vivo* has not been reported.

Despite the suggested roles for katanin in mitotic systems, the well-characterized katanin complex MEI-1/MEI-2 in *C. elegans* is required specifically for the assembly of the acentrosomal female meiotic spindle (8-10) and is degraded prior to mitosis (11). During meiotic spindle assembly, microtubules initially form around chromatin, and are subsequently organized into a bipolar array (Fig. 1A; 12). In the absence of the catalytic subunit MEI-1 (*mei-1(null)*) microtubules form around chromatin but fail to assemble into a bipolar spindle (Fig. 1B; 10). Furthermore, mutations that prevent MEI-1/MEI-2 degradation after meiosis result in short mitotic spindles that are mispositioned in the posterior of the cell (10). Therefore, the *C. elegans* model provides a unique system to study the effect of katanin on microtubules in both meiotic and mitotic environments.

RESULTS AND DISCUSSION

To examine the effect of katanin on microtubule morphology in meiosis, we applied electron tomography and 3-D modeling of female meiotic spindles in wild-type and *mei-1(null)* mutants lacking katanin activity. We tracked microtubules and identified their ends within a half spindle, built from serial 400 nm thick sections. Surprisingly, pole-facing microtubule ends were not found exclusively at the spindle pole, but were

distributed throughout the volume of the spindle (Fig. 1C, white spheres). Similarly, chromatin-facing microtubule ends were not concentrated at the chromosome surfaces, but were also observed throughout the spindle (Fig. 1C, blue spheres). Both types of microtubule ends were usually open, and were often flared. These observations suggest that the meiotic spindle contains many short microtubules, most of which are aligned and oriented along the spindle axis. The presence of microtubule ends throughout the spindle indicated that many individual microtubules within the reconstructed volume terminate before reaching the pole or chromatin surface.

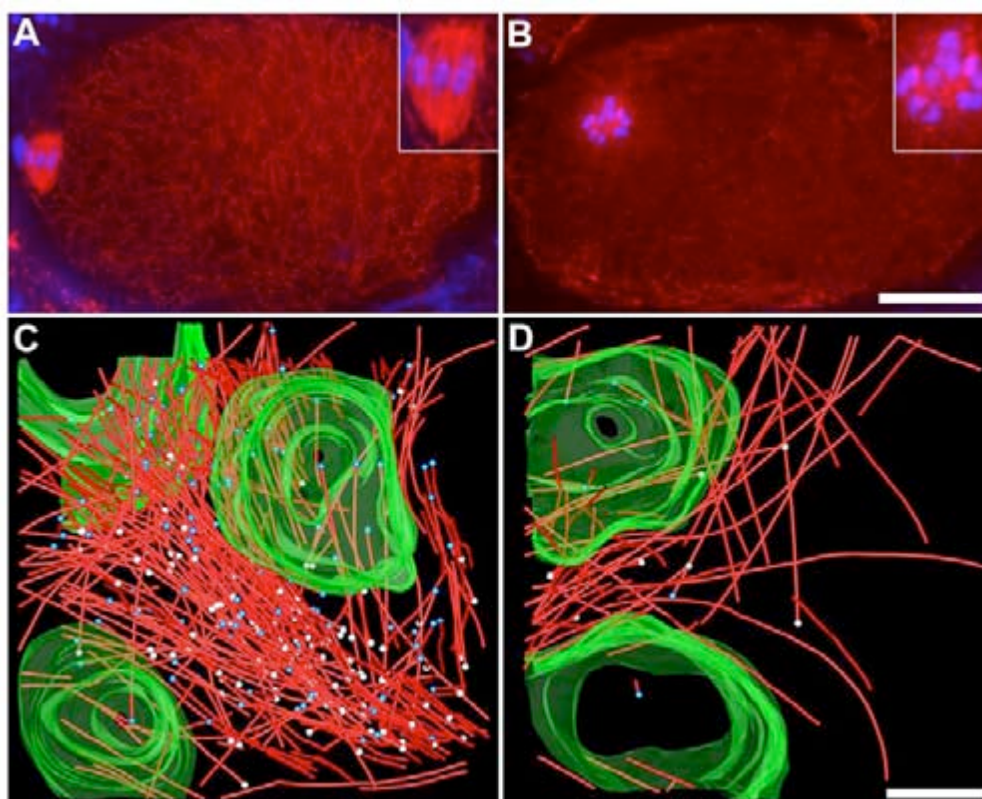


Figure 1. MEI-1 generates numerous microtubules in meiotic spindles. Images of wild-type (A), and *mei-1(null)* (B), embryos fixed and immunostained with anti- α -tubulin (red) are shown. DNA (blue) is visualized with DAPI. The inserts show microtubule organization at higher magnification. Tomographic reconstruction and 3-D modeling of meiotic microtubules in wild-type (C), and the *mei-1(null)* mutant (D). Both tomographic data sets are of equivalent volumes, built from 2 serial 400 nm sections. The wild-type model shows a portion of one half of the spindle (microtubules in red, pole-proximal ends as white spheres, pole-distal ends as blue spheres, chromatin in green). Both types of ends appear throughout the spindle. Tomographic reconstruction of the *mei-1(null)* mutant reveals a disorganized array of long microtubules. Bar is 10 μ m (B), and 500 nm (D).

Next, we looked at microtubules surrounding meiotic chromatin in a *mei-1(null)* mutant. Indirect immunofluorescence of α -tubulin showed a disorganized array of microtubules around meiotic chromatin (Fig. 1B; 8, 10). In contrast to wild type,

meiotic *mei-1(null)* embryos displayed disorganized microtubules in a radial array around chromatin (Fig. 1D). Strikingly, relatively few microtubules were found around the chromatin compared to the wild-type spindle (Fig. 1D, n=73; Fig. 1C, n=348). This suggested that katanin contributes to the increase in microtubule number observed in wild-type meiotic spindles.

In order to determine the effect of katanin on microtubule morphology, we examined individual microtubules in wild-type meiotic spindles and compared these to the *mei-1(null)* mutant. By stepping through serial, 1.6 nm tomographic slices, two morphological differences in microtubules were obvious between the data sets: lateral defects of varying sizes and closely-opposed open microtubule ends. Lateral defects in the protofilament lattice were evident throughout the spindle on 20-30% of the wild-type microtubules (Fig. 2A). In addition, numerous microtubules showed more than one lateral defect along their length. Unlike the curled protofilaments found on microtubules with lateral defects, the closely-opposed microtubule ends usually displayed a blunt morphology (Fig. 2B-D). It is possible that these closely-opposed microtubule ends represent two unrelated microtubules, however, many such paired microtubules were in identical orientations, despite being relatively isolated from neighboring microtubules that might contribute to their alignment. Therefore,

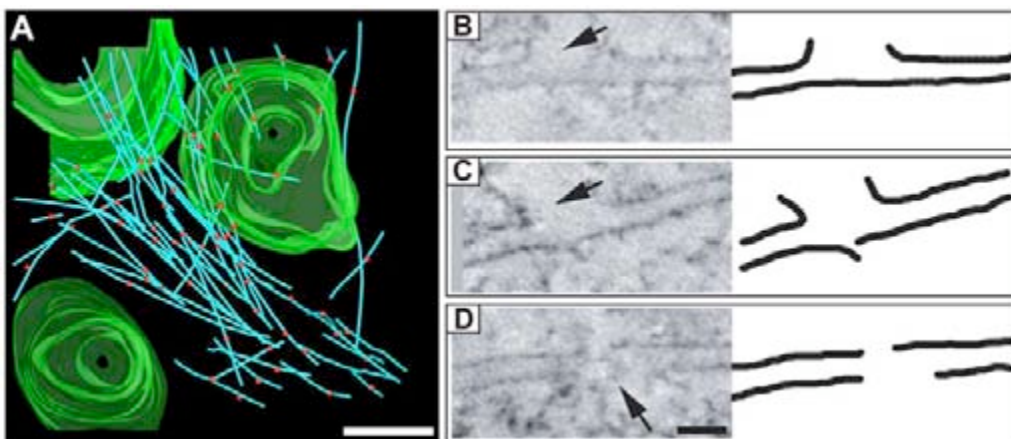


Figure 2. MEI-1 induces lateral defects in spindle microtubules. (A) Deconstruction of the 3-D model given in Fig. 1 C to selectively show spindle microtubules with structural defects. The sites of fragmentation on individual microtubules (blue) are indicated by spheres (red). Numerous microtubules had multiple points of fragmentation along their length. (B-D) Evidence of microtubule fragmentation. Tomographic slices show lateral disruption of the microtubule lattice (B, C), and closely-opposed microtubule ends (D). Points of fragmentation are indicated by arrows. Bar is 500 nm (A), and 50 nm (D).

our interpretation of these structural features is that the lateral defects represent the initiation of katanin-mediated severing, and the closely-opposed ends represent completely severed microtubules. Significantly, we did not observe any of these structures in the *mei-1(null)* mutant. These data provide structural evidence for meiotic katanin activity *in vivo* and suggest a molecular mechanism that involves an initial lateral attack on the microtubule lattice.

The tomographic reconstructions support the notion that microtubule severing during meiosis increases the number of microtubules available for spindle assembly; the wild-type reconstruction contained >300 microtubules, whereas a similar volume reconstructed from the *mei-1(null)* mutant contained only 73 microtubules. Due to the different morphologies of the meiotic microtubule arrays in wild-type and *mei-1(null)* embryos, a direct comparison of microtubule lengths in the meiotic environment was not possible. To quantify katanin's contribution to the fragmentation of spindle microtubules, the total polymer length within the reconstructed volume was divided by the number of lateral defects and closely-opposed ends. In the wild-type reconstruction katanin resulted in an average of 1 lateral defect per 3.01 μm . In contrast, we did not observe any lateral defects or closely-opposed ends in the *mei-1(null)* embryo.

In order to further quantify katanin's effect on microtubule length distribution, we used the gain-of-function mutant *mei-1(gf)*, whereby katanin activity persists into mitosis (Fig. 3; 10) and examined the effect of ectopic katanin on microtubules in a mitotic context. We also tested whether ectopic katanin causes similar defects to those observed on meiotic spindle microtubules. By indirect immunofluorescence of tubulin, the wild-type spindle pole showed a characteristic radial arrangement of microtubules around the pair of centrioles (Fig. 3A). Electron tomography of the spindle pole showed that the majority of microtubules had their pole-distal ends extending beyond the volume of the reconstruction (n=173). The majority of the pole-proximal ends in the centrosome showed capped-end morphologies (n= 166; Fig. 3C; 13). Similar capped-end structures were not detected in the meiotic spindle. As observed previously (13), a smaller population of pole-proximal ends were open and clustered on the chromosome-facing side of the centrosome (n= 61; Fig. 3C). Creation

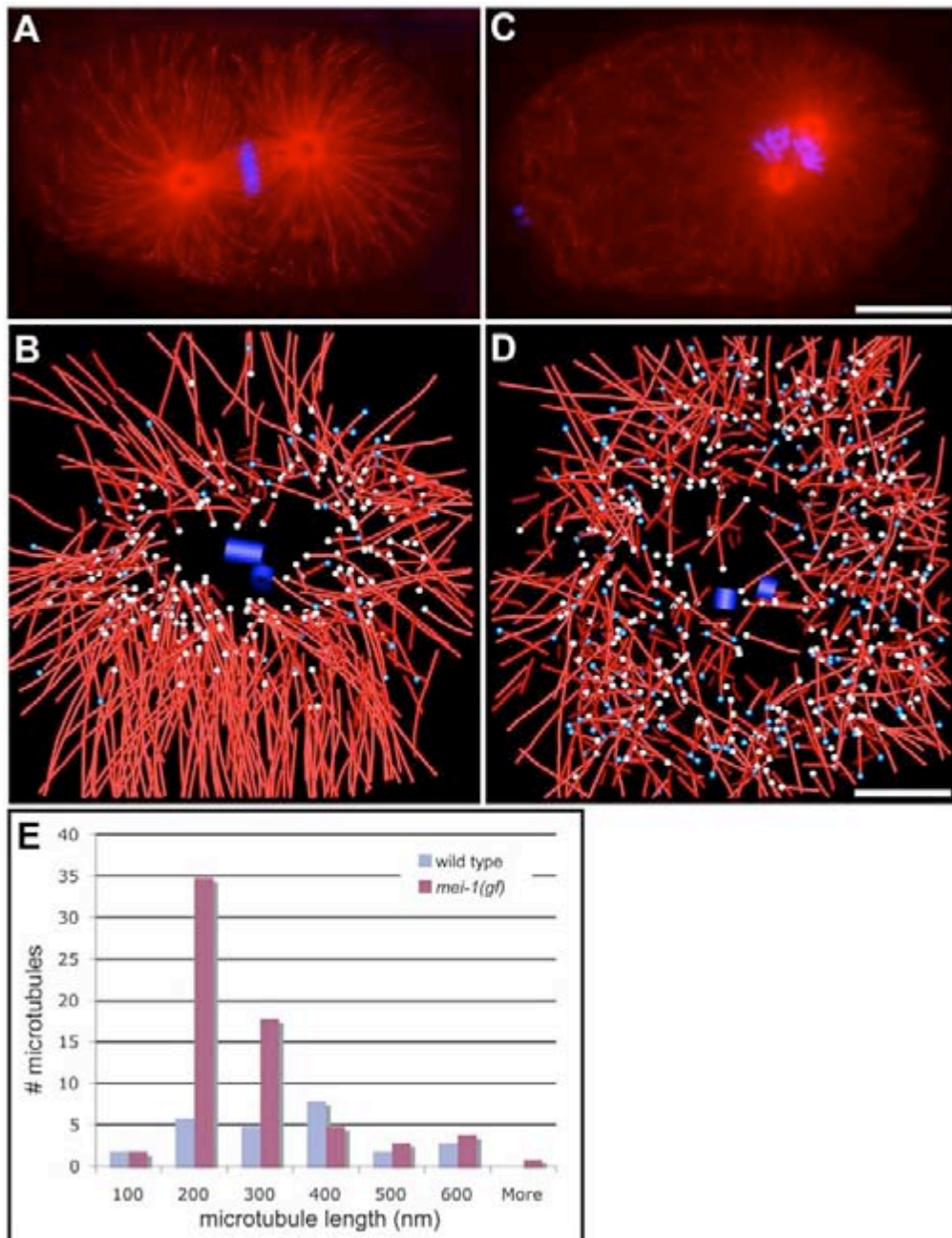


Figure 3. Ectopic MEI-1 activity leads to microtubule fragmentation in mitotic centrosomes. Images of mitotic wild-type (A), and *mei-1(gf)* (B), embryos fixed and immunostained with anti- α -tubulin (red) are shown. DNA (blue) is visualized with DAPI. The *mei-1(gf)* spindle is shorter and mis-positioned, relative to wild type. (C and D) Tomographic reconstruction and 3-D modeling of mitotic spindle poles. Wild-type mitotic centrosome (C), and mitotic *mei-1(gf)* spindle pole (D), are shown (microtubules: red, pole-proximal ends: white spheres, pole-distal ends: blue spheres, centrioles: blue cylinders). (E) A histogram showing the lengths of microtubules contained within the reconstructed volume is shown. Ectopic MEI-1 (*mei-1(gf)*) causes an increase in the number of short (<300 nm) fragments compared to wild type. Bar is 10 μ m (B), and 500 nm (D).

of the open pole-proximal microtubule ends was not dependent on MEI-1 as microtubules with this end-morphology were detected in poles from a MEI-1 loss-of-function mutant. In contrast to meiotic spindles, relatively few pole-distal ends

(likely representing microtubule plus ends) were found within the volume of the mitotic pole reconstruction (n=42; Fig. 3C).

Tomographic reconstruction of the *mei-1(gf)* mitotic spindle pole (Fig. 3B) revealed numerous microtubules (n= 630) surrounding the centrioles (Fig. 3D). Most of these short microtubules were randomly oriented, and had their pole-distal ends contained within the reconstruction, accounting for >3-fold increase in the number of pole-distal ends detected in the *mei-1(gf)* centrosome (n=149; Fig. 3D). In addition, a small population of microtubules (n=22) showed lateral defects. Quantification of microtubule length distributions from microtubules, contained completely within the volume of the reconstruction (n=68), revealed that the majority of microtubules in the *mei-1(gf)* mutant were between 200 and 300 nm in length (Fig. 3E). Wild-type mitotic centrosomes contained fewer microtubules completely contained within the volume of the reconstruction (n=26) and their lengths were more broadly distributed (Fig. 3E). In addition, the vast majority of microtubules emanating from the wild-type pole extended beyond the volume of the reconstruction (Fig. 3B).

In summary, we propose a mechanism of katanin severing that involves microtubule lattice perforation (Fig. 4A). The major consequence of this meiosis-specific katanin activity in *C. elegans* is the conversion of long polymers into two or more smaller polymers, thus contributing to an increase in the total number of microtubules in the meiotic spindle (Fig. 4B; for detailed discussion see section 4.3).

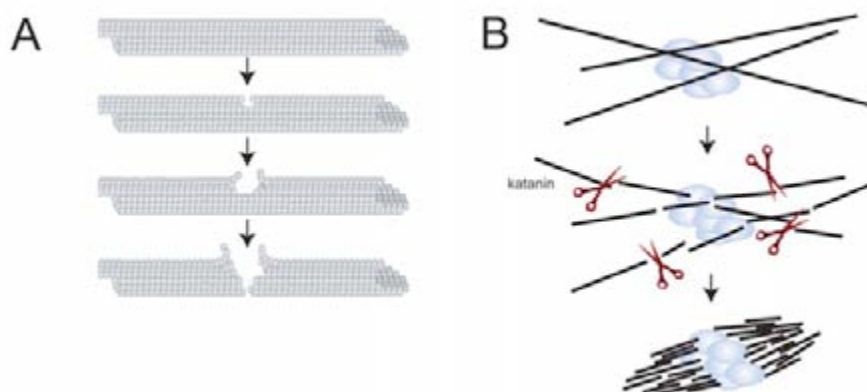


Figure 4. Proposed model of katanin's action and its role in meiotic spindle assembly. (A) Lateral fragmentation leads to protofilament disruption and eventual complete severing of spindle microtubules. (B) Severing of spindle microtubules results in an increase in the total number of fibers during spindle assembly.

MATERIALS AND METHODS

MEI-1 loss-of-function and gain-of-function mutant

To analyze the *mei-1(null)* mutant embryos, Unc segregants from HR311 [*mei-1(ct46ct101) unc-29(e1072)/hT2[bli-4(e937) let(h661)] (I); +/hT2 (III)*] were used (8). *mei-1* gain-of-function mutant embryos were obtained by up-shifting BW729 [*mei-1(ct46ts) unc-29(e1072) (I)*] worms to 25°C (8). *mei-1(ct46ts)* adult worms were maintained at the restrictive temperature until the high-pressure freezing procedure.

Specimen preparation

For wild-type and *mei-1(null)* experiments, whole worms were cryoimmobilized using a HPM 010 high-pressure freezer (BAL-TEC) as previously published (13, 14). For the analysis of wild-type *mei-1(gf)* mitotic poles, hermaphrodites were cut open in M-9 buffer containing 20% BSA. Isolated embryos were collected into capillary tubing and early developmental events were observed using DIC microscopy. At appropriate stages capillary tubes containing single embryos were transferred to specimen carriers and rapidly frozen using an EMPACT2+RTS (15). Both whole worms and isolated embryos were freeze-substituted over 2 days at -90°C in anhydrous acetone containing 1% OsO₄ and 0.1% uranyl acetate (EM AFS, Leica). Specimens were subsequently infiltrated and thin-layer embedded in Epon/Araldite. Serial semi-thick sections (300-400 nm) were cut using a Leica Ultracut UCT Microtome. Sections were collected on Formvar-coated copper slot grids and poststained with 2% uranyl acetate in 70% methanol followed by Reynold's lead citrate.

Intermediate-voltage electron tomography

For electron tomography, 15-nm colloidal gold particles (Sigma-Aldrich) were attached to both surfaces of the semi-thick sections to serve as fiducial markers for subsequent image alignment. The specimens were placed in a tilt-rotate specimen holder (Gatan, Pleasanton, CA) and tomographic data sets recorded using a TECNAI

F30 intermediate-voltage electron microscope (FEI, The Netherlands) operated at 300 kV. Images were captured every 1° over a ± 60° range using a Gatan 2K × 2K CCD camera at a pixel size of 1 nm. For the collection of double tilt data sets the grids were then rotated 90°, and a similar tilt series was acquired. For image processing, images were transferred to a Dell Linux workstation, and the tilted views were aligned using the positions of the colloidal gold particles as fiducial points. Tomograms were computed for each tilt axis using the R-weighted back-projection algorithm (16). For double tilt data sets, the two tomograms were aligned to each other and combined (17). Tomograms were displayed and analyzed using the IMOD software package (18). This program allows the operator to step through serial slices extracted from the tomogram and to track or model objects of interest in 3-D. The ratio of the section thickness, as defined by the microtome's setting to the section's thickness measured after microscopy, was used to calculate a "thinning factor", which was then applied to correct the tomogram's dimension along the beam axis (13). The lengths of microtubules were then extracted from the model contour data using a companion program, IMODINFO.

Modeling and analysis of tomographic data

Using the IMOD software package (18), features, like chromosomes, spindle microtubules, and centrioles were modeled in the serial, tomographic slices. An "image slicer" window in IMOD was used to display a slice extracted from the 3-D volume in any position or orientation, a tool useful for unambiguous tracking of microtubules (13). Structural defects of spindle microtubules were analyzed by extracting a slice of image data 1-voxel thick and adjusting its orientation to contain the axis of the microtubule in a single view (13). A projection of the model was displayed and rotated to study its 3-D geometry. For this display in 3-D, microtubules were shown as tubular graphic objects.

REFERENCES

1. F. J. McNally, R. D. Vale, *Cell* **75**, 419-29 (1993).
2. J. J. Hartman *et al.*, *Cell* **93**, 277-87 (1998).
3. R. D. Vale, *Cell* **64**, 827-39 (1991).

4. F. J. McNally, K. Okawa, A. Iwamatsu, R. D. Vale, *J Cell Sci* **109** (Pt 3), 561-7 (1996).
5. P. W. Baas, A. Karabay, L. Qiang, *Trends Cell Biol* **15**, 518-24 (2005).
6. F. McNally, *Nat Cell Biol* **2**, E4-7 (2000).
7. L. J. Davis, D. J. Odde, S. M. Block, S. P. Gross, *Biophys J* **82**, 2916-27 (2002).
8. M. Srayko, D. W. Buster, O. A. Bazirgan, F. J. McNally, P. E. Mains, *Genes Dev* **14**, 1072-84 (2000).
9. S. Clark-Maguire, P. E. Mains, *Genetics* **136**, 533-46 (1994).
10. S. Clark-Maguire, P. E. Mains, *J Cell Biol* **126**, 199-209 (1994).
11. L. Pintard *et al.*, *Nature* **425**, 311-6 (2003).
12. D. G. Albertson, J. N. Thomson, *Chromosome Res* **1**, 15-26 (1993).
13. E. T. O'Toole *et al.*, *J Cell Biol* **163**, 451-6 (2003).
14. T. Müller-Reichert *et al.*, *J Microsc* **212**, 71-80 (2003).
15. A. Manninen *et al.*, *Mol Cell Biol* **25**, 10087-96 (2005).
16. P. F. C. Gilbert, *Proc R Soc Lond B Biol Sci* **182**, 89-102 (1972).
17. D. N. Mastronarde, *J Struct Biol* **120**, 343-352 (1997).
18. J. R. Kremer, D. N. Mastronarde, J. R. McIntosh, *J Struct Biol* **116**, 71-76 (1996).

4 DISCUSSION AND PERSPECTIVES

The following aspects will be discussed in this section: (i) the methodological aspects of the described techniques for electron microscopy, (ii) the implications of distinct morphologies of microtubule minus ends for mitotic spindle assembly, and (iii) the mechanisms of acentrosomal spindle formation and the specific role of *C. elegans* katanin in this process. This discussion will talk about those aspects that have not been discussed in detail in the original publications and suggest further experiments which might help to answer some of the open questions of spindle assembly.

4.1 Application of electron microscopy to study *C. elegans* ultrastructure

C. elegans is an organism that is considered to be difficult to fix. Strikingly, this nematode worm is able to survive up to 7 h in a solution containing 10% glutaraldehyde (Shepard and Clark, 1976). The *C. elegans* embryo is even more difficult to fix (Müller-Reichert et al. 2003). Here, three different methods were applied to prepare *C. elegans* for electron microscopy. The relevance of each method is briefly discussed below.

To stop the developing *C. elegans* embryo at specific stages of early mitosis, laser-induced chemical fixation has been applied to investigate the role of SAS-4 (Kirkham et al., 2003), SAS-5 and SAS-6 (Dammermann et al., 2004), and SPD-2 (Pelletier et al., 2004b) in centriole duplication. In addition, this technique has been applied to determine the time point of centriole duplication during the first embryonic cell division (data not shown). In general, laser-induced chemical fixation achieves a rapid cessation of the embryonic development and permits a staging of the embryo prior to conventional electron microscopy (Priess and Hirsh, 1986). The major disadvantage of this method, however, is its poor rate of fixation and its insufficient structural preservation of the early embryo; both these issues must be solved for a valuable, high-resolution, 3-D study (for a general discussion on the disadvantages of chemical fixation on cellular fine structure, the reader is referred to Murk et al., 2003).

To achieve excellent ultrastructural preservation, high-pressure freezing has, in the past, been applied to cryoimmobilize the fine structure of the *C. elegans* embryo for both thin-section electron microscopy (Rappleye et al., 1999) and electron tomography (Müller-Reichert et al., 2003). Whole worms have been placed in sample holders for freezing, which can produce a thin layer of embedded nematodes. High-pressure frozen embryos at the desired stages can be identified in serial sections of these longitudinally oriented worms for tomographic analysis. Such prepared samples revealed both open and closed morphologies of centrosome-associated microtubule ends (O'Toole et al., 2003b). However, a disadvantage of this procedure is that whole worms contain populations of embryos at many phases of development, so the stage of mitosis had to be determined later.

A correlative light and electron microscopy (LM/EM) approach has been developed which allows one to combine fixation of selected and staged embryos and high-pressure freezing (Müller-Reichert et al., 2006). Correlative approaches in microscopy are used to obtain complementary information about a given system (Rieder and Cassels, 1999). For example, light microscopy in combination with GFP-tagging, on the one hand, offers the advantage of studying centrosome dynamics in living systems, but with obvious limitations in the obtained resolution. Electron microscopy, on the other hand, delivers high-resolution “snapshot” images of centrosomes, purified (Chrétien et al., 1997), *in vitro* (Schnackenberg et al., 1998), or *in vivo* (O'Toole et al., 2003b), but the yield of information about the dynamics of the process under study is restricted. Based only on “snapshot” images, it is not always possible to unambiguously reconstruct a complex process like the assembly of a cellular structure. The correlative approach described here has been developed to observe spindle dynamics by live-cell imaging and stop the observed process immediately at a specific stage of development by rapid cryofixation, allowing high-resolution analysis by electron tomography.

A prerequisite for this correlative LM/EM technique is that the time between staging by LM and fixation for EM is as short as possible. The ‘standard’ loading procedure for high-pressure freezing (i.e. when using the Leica EMPACT high-pressure freezer) involves loading of the capillary tube into the sample holder, manually closing the

sample holder after insertion into the ‘pod’, insertion of the sample holder into the high-pressure freezer, and starting the freezing process (Verkade, 2006). To minimize the time required for specimen loading, the use of the newly developed RTS associated with the EMPACT2 high-pressure freezer (Leica) is advantageous (McDonald et al., 2006; Verkade, 2006). When the rapid loader is used for automatic insertion of the sample holder into the pre-loaded pod, the RTS reduces the time between observation and freezing to about 5 seconds. Moreover, the automatic closure of the pod allows standardization of the loading/freezing procedure, thereby contributing to the high reproducibility of the method. It should be noted here that freezing of the isolated embryos is by no means restricted to the EMPACT2+RTS. The question, however, is, whether very fast loading times can be achieved with the other commercially available high-pressure freezers. In summary, the freezing method described here gives excellent and reproducible results for isolated and staged early *C. elegans* embryos. In this study, correlative LM/EM has been applied for the analysis of ectopic katanin in wild-type and mutant mitotic embryos (section 3.4). In addition, this method is currently used for a detailed tomography study of intermediate products of centriole assembly (see below).

4.2 Role of SAS-4 in centriole assembly

The embryonic centrioles in *C. elegans* possess a rather simple morphology and the process of their assembly is largely unknown. These centrioles are composed of nine singlet microtubules surrounding a central tube (Wolf et al., 1978; Albertson, 1984; Kirkham et al., 2003). Several lines of evidence suggest that SAS-4 is a structural component of this ‘simple’ centriole (Kirkham et al., 2003). (1) SAS-4 appears to be associated with the centriole throughout the cell cycle. (2) Immuno-electron microscopy has shown a ring-like pattern of gold staining on centrioles imaged in cross-section. (3) Centrioles of *sas-4(RNAi)* embryos in thin section EM images appear to be defective in the assembly of the centriole microtubules. How could the study of SAS-4 function in *C. elegans* contribute to a deeper understanding of centriole formation? High-pressure freezing and electron microscopy has shown that centrioles in partially depleted two-cell *sas-4(RNAi)* embryos show an apparent difference in the size (Fig. 6D in Kirkham et al., 2003). The structurally defective

centrioles of the small poles are obviously composed of the central tube only. This suggests that assembly of the *C. elegans* centriole is initiated from the central tube onto which nine singlet microtubules are attached. To decipher this assembly process, it will be important to analyze centriole structure in asymmetric metaphase spindles of partially depleted two-cell *sas-4(RNAi)* embryos by electron tomography. It is very likely that intermediate centrioles indeed fail to assemble the full number of nine singlet microtubules. Such a tomographic analysis of *sas-4(RNAi)* intermediate phenotypes is currently under investigation and here it is important to apply the newly developed correlative LM/EM approach for the analysis of staged embryos.

4.3 Closed microtubule minus ends in the mitotic centrosome

Electron tomography has revealed closed and open microtubule ends in the mitotic centrosome of *C. elegans*. Are closed (capped) minus end more stable and open (flared) ends more dynamic? In this section, the implications of minus end capping are discussed. The origin and function of the open minus ends will be discussed in the next section (4.4).

Closed microtubule ends in the mitotic centrosome of *C. elegans* are pointed (or cone-shaped). This “pointed” morphology is likely due to γ -tubulin in a complex with other proteins, as indicated by cone-shaped structures at closed minus ends of microtubules nucleated from γ -tubulin *in vitro* (Keating and Borisy, 2000; Moritz et al., 2000; Wiese and Zheng, 2000). Closed, cone-shaped structures have also been observed at the minus ends of microtubules nucleated from isolated spindle pole bodies of budding yeast (Byers et al., 1978; Rout and Kilmartin, 1990; Bullitt et al., 1997) and centrosomes from *Drosophila* cells (Moritz et al., 1995a). In addition, capped minus-end structures were observed *in situ* in budding yeast (O’Toole et al., 1999; Yoder et al., 2005). The crucial experiment, however, to assess minus end morphology *in vivo* after depletion of γ -tubulin has not been performed so far. Is γ -tubulin required for the formation of capped microtubule minus ends? It would be interesting to directly visualize the distribution and structure of microtubule minus ends in isolated and staged *tbg-1(RNAi)* embryos (see section 2.3). Upon γ -tubulin depletion, one would

expect that most of the capped minus-end structures would disappear. In other words, minus-end morphology should significantly shift from closed (wild-type) to open (γ -tubulin-depletion). This would provide direct evidence for the hypothesis that closure of microtubule minus ends by a pointed cap most likely represents γ -TuRC-mediated blocking of minus end polymerization and depolymerization.

The situation, however, might be more complicated. Although the kinetically dominant assembly pathway for centrosomal asters in *C. elegans* is γ -tubulin dependent, other mechanisms that nucleate microtubules obviously exist (Hannak et al., 2002). Therefore, the possibility can't be excluded that closed microtubule minus ends are still present in γ -tubulin-depleted embryos. In this case, where alternative nucleating mechanisms lead to the presence of capped ends, one key might be to look at severely versus moderately affected *tbg-1(RNAi)* embryos (Strome et al., 2001). Interestingly, γ -tubulin depletion does not prevent the nucleation of astral microtubules. Using light microscopic resolution, however, severe RNAi embryos display a collapsed diastral array of microtubules with little or no evidence of kinetochore or interpolar microtubules. In contrast, moderate RNAi embryos show bipolar but stunted spindles with disorganized microtubules between the poles. At higher resolution it appears plausible to analyze the minus end morphologies of a microtubule subpopulation only, i.e. those microtubules positioned between the centrosomal asters. Again, such experiments can be performed using the described correlative approach (section 2.3). Under severe conditions it is expected that those microtubules display open minus ends exclusively. In any case, such experiments would provide useful structural information about γ -tubulin-dependent and -independent nucleating mechanisms.

Another interesting aspect is that γ -tubulin can interact with β -tubulin (Leguy et al., 2000), the exposed subunit of the tubulin heterodimer at microtubule plus ends (Nogales et al., 1999). Depletion of γ -tubulin might also affect microtubule plus end dynamics and structure. Interestingly, a failure of appropriate kinetochore attachments has been attributed to an increase in microtubule stability (Paluh et al., 2000). When

assessing minus end morphology in *tbg-1(RNAi)* embryos, it would, therefore, also be interesting to analyze plus end morphology, preferably of kinetochore microtubules.

In summary, depletion of γ -tubulin will likely provide an explanation for the morphological difference of closed versus open microtubule minus ends, but will not address the issue of how the open ends arise preferentially on kinetochore microtubules during spindle assembly. This issue will be discussed in the next section.

4.4 Functional importance of open microtubule minus ends

Open minus ends in the mitotic centrosome of *C. elegans* are preferentially associated with kinetochore microtubules (O'Toole et al., 2003b). In addition, a drastic shortening of the kinetochore microtubules was observed in collapsed *tpxl-1(RNAi)* embryos (Özlü et al., 2005). Compared to wild-type spindles, these microtubules exhibited more open minus ends near the chromosome (unpublished observations). What is the functional significance of open microtubule minus ends? The open morphology could be a consequence of microtubule-kinetochore attachment on chromatin, and possibly the pulling forces that later ensue. Alternatively, the open ends may arise by a mechanism at the centrosome that is independent of the kinetochore attachment. The possible involvement of key components in the generation of these open minus ends is discussed below.

4.4.1 Factors that could contribute to open minus ends, dependent on kinetochore-microtubule attachment

Do open minus ends form in the absence of functional kinetochores? During spindle assembly, microtubules grow towards chromatin, make contact with kinetochores, and are selectively stabilized. Pulling forces on the centrosomes provide the mechanism by which sister chromatids segregate via their attachment to these kinetochore microtubules. The open-end morphology observed on kinetochore microtubules could be a consequence of the microtubules-kinetochore attachment. This could be tested directly by removing kinetochore function with *CENP-C(RNAi)*.

As reported previously, *CENP-C(RNAi)* results in a kinetochore-null phenotype (Oegema et al., 2001). Depletion of CENP-C could, therefore, result in a loss of open end morphology during early spindle assembly, because the kinetochore microtubules are no longer attached to chromosomes. A reduction or loss of open minus ends would suggest a role for kinetochore attachment in the generation of the open ends, but would not rule out a causal role for pulling forces by kinetochore microtubules.

Do pulling forces acting on the spindle contribute to the formation of open ends? One possible explanation for the open microtubule ends is that forces exerted on kinetochore microtubules during spindle assembly pull microtubules away from the centrosome. *gpr-1/2(RNAi)* results in a severe reduction in astral pulling force on the spindle (Afshar et al., 2004; Grill et al., 2003). Using *gpr-1/2(RNAi)* the contribution of astral forces to the creation of open microtubule ends could be tested. In addition, mutations in the *zyg-1* gene result in failed centriole duplication and lead to the formation of a monopolar spindle (O'Connell et al., 2001). This mutation could also be used to test for the contribution of pulling forces in the generation of open microtubule minus ends. In addition, this assay would independently test whether a bipolar spindle is required for the open microtubule ends. If pulling forces would be required to generate the open ends, this would provide a novel explanation to account for the diversity of microtubule end morphologies observed during spindle assembly.

4.4.2 Factors that could contribute to open minus ends, independent of kinetochore-microtubule attachment

Is the microtubule depolymerizing kinesin KLP-7 involved in the generation of open ends? KLP-7 is a member of the kinesin-13 family, which is implicated in depolymerization of microtubules. Other members of this kinesin family have been shown to exhibit depolymerizing activity at both plus and minus ends of microtubules (Desai et al., 1999). Therefore, it is possible that the microtubule ends in the *C. elegans* centrosome are potential targets of KLP-7 and that KLP-7 contributes to the open-end morphology by destabilizing the minus ends. It could be hypothesized that the minus ends are normally protected from the KLP-7 depolymerizing activity, for instance γ -tubulin may provide a protective role (section 4.3). The open ends observed

in wild-type embryos might represent unstable microtubule ends that are attacked by the depolymerizing activity of KLP-7. *klp-7(RNAi)* could be used to directly test whether KLP-7 is involved in the creation of these open ends. Importantly, *klp-7(RNAi)* embryos assemble a spindle and undergo chromosome segregation during anaphase, although the chromosomes segregate at a higher velocity than in wild type. Interestingly, the centrosomes snap apart in anaphase, but chromosomes still segregate with high fidelity. Contrary to the γ -tubulin experiments, *klp-7(RNAi)* should result in less open ends. If no open ends would be observed in association with kinetochore microtubules, this would suggest a role for KLP-7 in the creation of the open ends, and further suggest that open ends are not required for spindle assembly, but possibly play a role during anaphase.

Does Ran play a role in the asymmetric distribution of open ends towards the chromatin? The small GTPase Ran is required for spindle assembly in all systems studied, although the molecular mechanisms of its action remain obscure (reviewed in Gruss and Vernos, 2004). In *Xenopus* egg extracts, Ran is required for chromatin-mediated microtubule stabilization. In *C. elegans*, Ran is not required for chromatin-mediated spindle assembly (Askjaer et al., 2002; Bamba et al., 2002), but it is required for a microtubule outgrowth bias towards chromosomes during early spindle formation (Srayko et al., 2005). It is possible that the open-end morphology is related to this phenomenon; there may be a link between the turnover of microtubules emanating from the centrosome and the frequency of microtubule open ends near the centrosome. If fewer open ends are observed in *ran-1(RNAi)* embryos, it would suggest that Ran influences the dynamics and morphology of the minus end, providing a potentially novel explanation for the distribution of open ends during spindle assembly and a novel role for Ran at the minus ends of microtubules. However, kinetochore attachment of microtubules is also defective in *ran-1(RNAi)*, so any conclusions from the Ran experiments would be weighed against the results from experiments on the role of kinetochore attachment (see above).

In the future, it will be important to further combine RNAi technology and electron tomography of staged early embryos to test these different hypotheses for open

microtubule minus-end origin and function. Importantly, the early *C. elegans* embryo allows to do so in a systematic manner.

4.5 Spindle assembly in an acentrosomal context

As in other animal systems the female meiotic spindle forms in the absence of centrosomes (Sawada & Schatten, 1988; Theurkauf and Hawley, 1992; Gard, 1992; Albertson and Thomson, 1993). Using chromatin-based pathways, microtubules are initially formed around the meiotic chromatin (Tournebize et al., 1997). Subsequently, the microtubules are organized from the ‘inside-out’, most likely by plus-end directed motor proteins, implicated in pushing microtubule minus ends away from chromatin (Afshar et al., 1995; Vernos et al., 1995; Wang and Adler, 1995; Walczak et al., 1998). The resulting radially-symmetric microtubule array is then focused into two opposing poles, likely by minus end-directed motors with microtubule tethering properties (Matthies et al., 1996; Walczak et al., 1998). Importantly, the mechanisms of this acentrosomal spindle assembly and the proteins involved in this process are largely unknown. To date, the katanin complex MEI-1/MEI-2 is the only known meiosis-specific factor in *C. elegans* (Srayko et al., 2000). How does *C. elegans* katanin contribute to spindle organization?

Electron tomography has revealed fragmentation of microtubules and perforation of the polymer lattice in wild-type meiotic spindles. These structural defects on microtubules were not observed in the *mei-1(null)* embryo, indicating a role for katanin in their creation. Lateral defects likely represent intermediate states of complete severing. These data support a mechanism of katanin severing that involves an early stage of microtubule lattice perforation during meiotic spindle formation. Breaks in the microtubule lattice could be stress-related because the meiotic spindle in *C. elegans* is barrel-shaped and the curvature of its microtubules is suggestive of internal tension (Albertson and Thomson, 1982). However, most of the microtubules having these defects did not exhibit kinking or excessive bending, rather, the microtubules were relatively straight regardless of the extent of damage to their lattice.

Localization data, based on indirect immunofluorescence of MEI-1-specific antibodies and *in vivo* GFP-MEI-1, suggest that katanin is most concentrated at chromatin and to a lesser degree at the poles (Clark-Maguire and Mains 1994a; Clark-Maguire and Mains 1994b; Srayko et al., 2000). The results presented here indicate that katanin activity is not restricted to these zones, rather katanin severing is evident throughout the spindle. Possibly MEI-1/katanin is loaded onto microtubules at chromatin but severs the microtubules some distance away from chromatin. *In vitro* experiments and computer modeling have suggested that katanin targets relatively rare defects in the lattice that might arise from changes in protofilament number (Davis et al., 2002). Although such protofilament variability cannot directly be observed by electron tomography, this *in vitro* finding raises the possibility that katanin severing activity may not necessarily correlate with its distribution pattern or concentration.

Female meiotic spindles lack centrosomes, the primary sites of microtubule nucleation in mitosis. During meiosis, microtubules initially appear around chromatin after oocyte nuclear envelope break-down and throughout the cytoplasm in early meiotic embryos (Yang et al., 2003). In *spd-2* or *spd-5* mutant embryos, microtubule nucleation from centrosomes is drastically reduced (Hamill et al., 2002; Dammermann et al., 2004; Srayko et al., 2005). After nuclear envelope break-down, microtubules will also form around mitotic chromatin, however, the amount observed around chromatin is significantly lower than the amount generated by wild-type centrosomes (Hamill et al., 2002; Dammermann et al., 2004; Srayko et al., 2005), suggesting that microtubule nucleation by chromatin is relatively inefficient in *C. elegans*. Importantly, in meiosis *mei-1(null)* embryos have fewer microtubules directly associated with chromatin than the wild-type embryos. Assuming that katanin does not have a direct role in nucleation, this result suggests that the nucleating capacity of chromatin during meiosis is also relatively inefficient compared to centrosomes.

In conclusion, the presented data suggest that the major consequence of meiosis-specific katanin activity in *C. elegans* is the conversion of long polymers into two or more smaller polymers, thus increasing the total number of microtubules in the

meiotic spindle. An alternative method to shorten microtubules is to alter microtubule end dynamics, for instance, to increase depolymerization and/or decrease growth rate (Mitchison and Kirschner, 1984). This end-wise mechanism, however, would not be expected to change the number of polymers in the system. In order to account for increased polymer accumulation during spindle assembly, severed microtubules might not immediately depolymerize after severing; specific microtubule stabilizing factors could be involved in preventing depolymerization of the newly-exposed microtubule ends.

5 LITERATURE

Afshar, K., F. S. Willard, K. Colombo, C. A. Johnston, C. R. McCudden, D. P. Siderovski, and P. Gönczy. 2004. RIC-8 is required for GPR-1/2-dependent Galpha function during asymmetric division of *C. elegans* embryos. *Cell*. 119, 219-230.

Albertson, D. G. 1984. Formation of the first cleavage spindle in nematode embryos. *Dev. Biol.* 101, 61-72.

Albertson, D. G., and J. N. Thomson. 1982. The kinetochores of *Caenorhabditis elegans*. *Chromosoma*. 86, 409-428.

Albertson, D. G., and J. N. Thomson. 1993. Segregation of holocentric chromosomes at meiosis in the nematode, *Caenorhabditis elegans*. *Chromosome Res.* 1, 15-26.

Askjaer, P., V. Galy, E. Hannak, and I. W. Mattaj. 2002. Ran GTPase cycle and importins alpha and beta are essential for spindle formation and nuclear envelope assembly in living *Caenorhabditis elegans* embryos. *Mol. Biol. Cell*. 13, 4355-4370.

Bamba, C., Y. Bobinnec, M. Fukuda, and E. Nishida. 2002. The GTPase Ran regulates chromosome positioning and nuclear envelope assembly *in vivo*. *Curr. Biol.* 12, 503-507.

Bobinnec, Y., M. Fukuda, and E. Nishida. 2000. Identification and characterization of *Caenorhabditis elegans* γ -tubulin in dividing cells and differentiated tissues. *J. Cell Sci.* 113 Pt 21:3747-3759.

Bornens, M. 2002. Centrosome composition and microtubule anchoring mechanisms. *Curr. Opin. Cell Biol.* 14, 25-34.

Bullitt, E., M. P. Rout, J. V. Kilmartin, and C. W. Akey. 1997. The yeast spindle pole body is assembled around a central crystal of Spc42p. *Cell*. 89, 1077-1086.

Byers, B., K. Shriver, and L. Goetsch. 1978. The role of spindle pole bodies and modified microtubule ends in the initiation of microtubule assembly in *Sacharomyces cerevisiae*. *J. Cell Sci.* 30, 331-352.

Chrétien, D., B. Buendia, S. D. Fuller, and E. Karsenti. 1997. Reconstruction of the centrosome cycle from cryoelectron micrographs. *J. Struct. Biol.* 120, 117-133.

Chrétien, D., S. D. Fuller, and E. Karsenti. 1995. Structure of growing microtubule ends: two-dimensional sheets close into tubes at variable rates. *J. Cell Biol.* 129, 1311-1328.

Clark-Maguire, S., and P. E. Mains. 1994a. Localization of the mei-1 gene product of *Caenorhabditis elegans*, a meiotic-specific spindle component. *J. Cell Biol.* 126, 199-209.

- Clark-Maguire, S., and P. E. Mains. 1994b. *mei-1*, a gene required for meiotic spindle formation in *Caenorhabditis elegans*, is a member of a family of ATPases. *Genetics*. 136, 533-546.
- Dammermann, A., A. Desai, and K. Oegema. 2003. The minus end in sight. *Curr. Biol.* 13, R614-R624.
- Dammermann, A., T. Müller-Reichert, L. Pelletier, B. Habermann, A. Desai, and K. Oegema. 2004. Centriole assembly requires both centriolar and pericentriolar material proteins. *Dev. Cell.* 7, 815-829.
- Davis, L. J., D. J. Odde, S. M. Block, and S. P. Gross. 2002. The importance of lattice defects in katanin-mediated microtubule severing in vitro. *Biophys. J.* 82, 2916-2927.
- Delattre, M., S. Leidel, K. Wani, K. Baumer, J. Bamat, H. Schnabel, R. Feichtinger, R. Schnabel, and P. Gönczy. 2004. Centriolar SAS-5 is required for centrosome duplication in *C. elegans*. *Nat. Cell Biol.* 6, 656-664.
- Desai, A., S. Verma, T. J. Mitchison, and C. E. Walczak. 1999. Kin I kinesins are microtubule-destabilizing enzymes. *Cell.* 96, 69-78.
- Doxsey, S. 2001. Re-evaluating centrosome function. *Nat. Rev. Mol. Cell Biol.* 2, 688-698.
- Fire, A., D. Albertson, S. W. Harrison, and D. G. Moerman. 1991. Production of antisense RNA leads to effective and specific inhibition of gene expression in *C. elegans* muscle. *Development.* 113, 503-514.
- Fire, A., S. Xu, M. K. Montgomery, S. A. Kostas, S. E. Driver, and C. C. Mello. 1998. Potent and specific genetic interference by double-stranded RNA in *Caenorhabditis elegans*. *Nature.* 391, 806-811.
- Fisk Green, R., M. Lorson, A. J. Walhout, M. Vidal, and S. Van Den Heuvel. 2004. Identification of critical domains and putative partners for the *Caenorhabditis elegans* spindle component LIN-5. *Mol. Genet. Genomics.* 271, 532-544.
- Frank, J. 1992. Introduction: principles of electron tomography. *In* Electron tomography: three dimensional imaging with the transmission electron microscope. J. Frank, editor. Plenum Press, N.Y. 1-13.
- Frank J. T. Wagenknecht, B. F. McEwen, M. Marko, C. Hsieh, and C. A. Mannella. 2002. Three-dimensional imaging of biological complexity. *J. Struct. Biol.* 138, 85-91.
- Gard, D. L. 1992. Microtubule organization during maturation of *Xenopus* oocytes: assembly and rotation of the meiotic spindles. *Dev. Biol.* 151, 516-530.

Gilbert, P. F. C. 1972. The reconstruction of a three-dimensional structure from projections and its application to electron microscopy. II. Direct methods. *Proc. R. Soc. Lond. B Biol. Sci.* 182, 89-102.

Gönczy, P., C. Echeverri, K. Oegema, A. Coulson, S. J. Jones et al. 2000. Functional genomic analysis of cell division in *C. elegans* using RNAi of genes on chromosome III. *Nature*. 408, 331-336.

Gönczy, P., S. Pichler, M. Kirkham, and A. A. Hyman. 1999. Cytoplasmic dynein is required for distinct aspects of MTOC positioning, including centrosome separation, in the one cell stage *Caenorhabditis elegans* embryo. *J. Cell Biol.* 147, 135-50.

Grill, S. W., J. Howard, E. Schaffer, E. H. Stelzer, and A. A. Hyman. 2003. The distribution of active force generators controls mitotic spindle position. *Science*. 301, 518-21.

Gruss, O. J., and I. Vernos. 2004. The mechanism of spindle assembly: functions of Ran and its target TPX2. *J. Cell Biol.* 166, 949-55.

Gunawardane, R. N., O. C. Martin, K. Cao, L. Zhang, K. Dej, A. Iwamatsu, and Y. Zheng. 2000. Characterization and reconstitution of *Drosophila* γ -tubulin ring complex subunits. *J. Cell Biol.* 151, 1513-1524.

Hamill, D. R., A. F. Severson, J. C. Carter, and B. Bowerman. 2002. Centrosome maturation and mitotic spindle assembly in *C. elegans* require SPD-5, a protein with multiple coiled-coil domains. *Dev. Cell*. 3, 673-684.

Hannak, E., M. Kirkham, A. A. Hyman, and K. Oegema. 2001. Aurora-A kinase is required for centrosome maturation in *Caenorhabditis elegans*. *J. Cell Biol.* 155, 1109-1115.

Hannak, E., K. Oegema, M. Kirkham, P. Gönczy, B. Habermann, and A. A. Hyman. 2002. The kinetically dominant assembly pathway for centrosomal asters in *Caenorhabditis elegans* is γ -tubulin dependent. *J. Cell Biol.* 157, 591-602.

Hohenberg, H., K. Mannweiler, and U. B. Sleytr. 1994. High pressure freezing of cell suspensions in cellulose capillary tubes. *J. Microsc.* 175, 34-43.

Howard, J., and A. A. Hyman. 2003. Dynamics and mechanics of the microtubule plus end. *Nature*. 422, 753-758.

Hyams, J. S. and C. W. Lloyd. 1994. Microtubules. *Modern Cell Biology* (ed. By J. B. Harford). Wiley-Liss, New York.

Keating, T. J., and G. G. Borisy. 2000. Immunostuctural evidence for the template mechanism of microtubule nucleation. *Nat. Cell Biol.* 2, 352-357.

- Kemp, C. A., K. R. Kopish, P. Zipperlen, J. Ahringer, and K. F. O'Connell. 2004. Centrosome maturation and duplication in *C. elegans* require the coiled-coil protein SPD-2. *Dev. Cell.* 6, 511-523.
- Kinoshita, K., B. Habermann, and A. A. Hyman. 2002. XMAP215: a key component of the dynamic microtubule cytoskeleton. *Trends Cell Biol.* 12, 267-73.
- Kirkham, M., T. Müller-Reichert, K. Oegema, S. Grill, and A. A. Hyman. 2003. SAS-4 is a *C. elegans* centriolar protein that controls centrosome size. *Cell.* 112, 575-587.
- Kremer, J. R., D. N. Mastronarde, and J. R. McIntosh. 1996. Computer visualization of three-dimensional image data using IMOD. *J. Struct. Biol.* 116, 71-76.
- Ladinsky, M. S., D. N. Mastronarde, J. R. McIntosh, K. E. Howell, and L. A. Staehelin. 1999. Golgi structure in 3 dimensions: functional insights from the NRK cell. *J. Cell Biol.* 144, 1135-1149.
- Leguy, R., R. Melki, D. Pantaloni, and M. F. Carrier. 2000. Monomeric gamma-tubulin nucleates microtubules. *J. Biol. Chem.* 275, 21975-21980.
- Leidel, S., and P. Gönczy. 2003. SAS-4 is essential for centrosome duplication in *C. elegans* and is recruited to daughter centrioles once per cell cycle. *Dev. Cell.* 4, 431-439.
- Mandelkow, E. M., E. Mandelkow, and R. A. Milligan. 1991. Microtubule dynamics and microtubule caps: a time-resolved cryo-electron microscopy study. *J. Cell Biol.* 114, 977-991.
- Marsh, B. J., D. N. Mastronarde, K. F. Buttle, K. E. Howell, and J. R. McIntosh. 2001. Organellar relationships in the Golgi region of the pancreatic beta cell line, HIT-T15, visualized by high resolution electron tomography. *Proc. Natl. Acad. Sci. USA.* 98, 2399-2406.
- Mastronarde, D. N. 1997. Dual-axis tomography: An approach with alignment methods that preserve resolution. *J. Struct. Biol.* 120, 343-352.
- Matthies, H. J., H. B. McDonald, L. S. Goldstein, and W. E. Theurkauf. 1996. Anastral meiotic spindle morphogenesis: role of the non-claret disjunctonal kinesin-like protein. *J. Cell Biol.* 134, 455-464.
- McDonald, K. L. 1994. Electron microscopy and EM immunohistochemistry. *Meth. Cell Biol.* 44, 411-444.
- McDonald, K. 1999. High-pressure freezing for preservation of high resolution fine structure and antigenicity for immunolabeling. *Electron Microscopy Methods and Protocols* (ed. By N. Hajibagheri), pp. 77-97. Humana Press, Totowa, NJ.
- McDonald, K., and T. Müller-Reichert. 2002. Cryomethods for thin section electron microscopy. *Meth. Enzymol.* 351, 96-123.

- McDonald, K. L., M. Morphew, P. Verkade, and T. Müller-Reichert. 2006. Some practical observations regarding high pressure freezing. *Meth. Mol. Biol.* (in press).
- McEwen, B. F., and M. Marko. 2001. The emergence of electron tomography as an important tool for investigating cellular ultrastructure. *J. Histochem. Cytochem.* 49, 553-563.
- McIntosh, R., D. Nicastro, and D. Mastronarde. 2005. New views of cells in 3D: an introduction to electron tomography. *Trends Cell Biol.* 15, 43-51.
- McNally, F. 2003. Microtubule dynamics: new surprises from an old MAP. *Curr. Biol.* 13, R597-599.
- McNally, F. J., and S. Thomas. 1998. Katanin is responsible for the M-phase microtubule-severing activity in *Xenopus* eggs. *Mol. Biol. Cell.* 9, 1847-1861.
- McNally, F. J., and R. D. Vale. 1993. Identification of katanin, an ATPase that severs and disassembles stable microtubules. *Cell.* 75, 419-29.
- McNally, K. P., O. A. Bazirgan, and F. J. McNally. 2000. Two domains of p80 katanin regulate microtubule severing and spindle pole targeting by p60 katanin. *J. Cell Sci.* 113, 1623-1633.
- Mitchison, T., and M. Kirschner. 1984. Dynamic instability of microtubule growth. *Nature.* 312, 237-242.
- Moore, A., and L. Wordeman. 2004. The mechanism, function and regulation of depolymerizing kinesins during mitosis. *Trends Cell Biol.* 14, 537-46.
- Moritz, M., M. B. Braunfeld, J. C. Fung, J. W. Sedat, B. M. Alberts, and D. A. Agard 1995a. Three-dimensional structural characterization of centrosomes from early *Drosophila* embryos. *J. Cell Biol.* 130, 1149-1159.
- Moritz, M., M. B. Braunfeld, J. W. Sedat, B. Alberts, and D. A. Agard. 1995b. Microtubule nucleation by γ -tubulin-containing rings in the centrosome. *Nature.* 378, 638-640.
- Moritz, M., M. B. Braunfeld, V. Guenebaut, J. Heuser, and D. A. Agard. 2000. Structure of the γ -tubulin ring complex: a template for microtubule nucleation. *Nat. Cell Biol.* 2, 365-370.
- Müller-Reichert, T., D. Chrétien, F. Severin, and A. A. Hyman. 1998. Structural changes at microtubule ends accompanying GTP hydrolysis: information from a slowly hydrolyzable analogue of GTP, guanylyl (α,β)methylenediphosphonate. *Proc. Natl. Acad. Sci. USA.* 95, 3661-3666.
- Müller-Reichert, T., H. Hohenberg, E. T. O'Toole, and K. McDonald. 2003. Cryoimmobilization and three-dimensional visualization of *C. elegans* ultrastructure. *J. Microsc.* 212, 71-80.

- Müller-Reichert, T., M. Srayko, A. A. Hyman, E. O'Toole, and K. McDonald. 2006. Correlative light and electron microscopy of early *C. elegans* embryos in mitosis. *Cellular Electron Microscopy* (ed. by J. R. McIntosh). (submitted).
- Murk, J. L., G. Posthuma, A. J. Koster, H. J. Geuze, A. J. Verkleij, M. J. Kleijmeer, and B. Humbel. 2003. Influence of aldehyde fixation on the morphology of endosomes and lysosomes: quantitative analysis and electron tomography. *J. Microsc.* 212, 81-90.
- Murphy, S. M., L. Urbani, and T. Stearns. 1998. The mammalian gamma-tubulin complex contains homologues of the yeast spindle pole body components spc97p and spc98p. *J. Cell Biol.* 141, 663-674.
- Nogales, E., M. Whittaker, R. A. Milligan, and K. H. Downing. 1999. High-resolution model of the microtubule. *Cell.* 96, 79-88.
- O'Connell, K. F. 2000. The centrosome of the early *C. elegans* embryo: Inheritance, assembly, replication, and developmental roles. *Curr. Top. Dev. Biol.* 49, 365-384.
- O'Connell, K. F., C. Caron, K. R. Kopish, D. D. Hurd, K. J. Kemphues, Y. Li, and J. G. White. 2001. The *C. elegans zyg-1* gene encodes a regulator of centrosome duplication with distinct maternal and paternal roles in the embryo. *Cell.* 105, 547-558.
- O'Toole, E. T., M. Winey, and J. R. McIntosh. 1999. High-voltage electron tomography of spindle pole bodies and early mitotic spindles in the yeast *Saccharomyces cerevisiae*. *Mol. Biol. Cell.* 10, 2017-2031.
- O'Toole, E. T., T. H. Giddings, J. R. McIntosh, and S. K. Dutcher. 2003a. Three-dimensional organization of basal bodies from wild-type and δ -tubulin deletion strains of *Chlamydomonas reinhardtii*. *Mol. Biol. Cell.* 14, 2999-3012.
- O'Toole, E. T., K. L. McDonald, J. Mäntler, J. R. McIntosh, A. A. Hyman, and T. Müller-Reichert. 2003b. Morphologically distinct microtubule ends in the mitotic centrosome of *Caenorhabditis elegans*. *J. Cell Biol.* 163, 451-456.
- Oegema, K., and T. Hyman. 2005. Cell division. *WormBook*, (ed. by J. M. Kramer and D. G. Moerman). The *C. elegans* Research Community, WormBook, doi/10.1895/wormbook.1.72.1, <http://www.wormbook.org>.
- Oegema, K., A. Desai, S. Rybina, M. Kirkham, and A. A. Hyman. 2001. Functional analysis of kinetochore assembly in *Caenorhabditis elegans*. *J. Cell Biol.* 153, 1209-1226.
- Oegema, K., C. Wiese, O. C. Martin, R. A. Milligan, A. Iwamatsu, T. J. Mitchison, and Y. Zheng. 1999. Characterization of two related *Drosophila* γ -tubulin complexes that differ in their ability to nucleate microtubules. *J. Cell Biol.* 144, 721-733.
- Özlu, N., M. Srayko, K. Kinoshita, B. Habermann, E. T. O'Toole, T. Müller-Reichert, N. Schmalz, A. Desai, and A. A. Hyman. 2005. An essential function of the C.

C. elegans ortholog of TPX2 is to localize activated aurora A kinase to mitotic spindles. *Dev. Cell.* 9, 237-48.

Paluh, J. L., E. Nogales, B. R. Oakley, K. McDonald, A. L. Pidoux, and W. Z. Cande. 2000. A mutation in γ -tubulin alters microtubule dynamics and organization and is synthetically lethal with kinesin-like protein Pkl1p. *Mol. Biol. Cell.* 11,1225-1239.

Pelletier, L., T. Müller-Reichert, M. Srayko, N. Özlü, A.-L. Schlaitz, and A. A. Hyman. 2004a. The *C. elegans* centrosome during early embryonic development. *Centrosomes in Development and Disease* (ed. by E. Nigg), pp. 227-250. Wiley-VCH, Weinheim.

Pelletier, L., N. Özlü, E. Hannak, C. Cowan, B. Habermann, M. Ruer, T. Müller-Reichert, and A. A. Hyman. 2004b. The *Caenorhabditis elegans* centrosomal protein SPD-2 is required for both pericentriolar material recruitment and centriole duplication. *Curr. Biol.* 14, 863-873.

Priess, J. R., and D. I. Hirsh. 1986. *Caenorhabditis elegans* morphogenesis: the role of the cytoskeleton in elongation of the embryo. *Dev. Biol.* 117, 156-173.

Rappleye, C. A., A. R. Paredez, C. W. Smith, K. L. McDonald, and R. V. Aroian. 1999. The coronin-like protein POD-1 is required for anterior-posterior axis formation and cellular architecture in the nematode *Caenorhabditis elegans*. *Genes Dev.* 13, 2838-2851.

Rieder, C. L., and G. Cassels. 1999. Correlative light and electron microscopy of mitotic cells in monolayer cultures. *Meth. Cell Biol.* 61, 297-315.

Rout, M. P., and J. V. Kilmartin. 1990. Components of the yeast spindle and spindle pole body. *J. Cell Biol.* 111, 1913-1927.

Sawada, T., and G. Schatten. 1988. Microtubules in ascidian eggs during meiosis, fertilization, and mitosis. *Cell Motil. Cytoskeleton.* 9, 219-230.

Schnackenberg, B. J., A. Khodjakov, C. L. Rieder, and R. E. Palazzo. 1998. The disassembly and reassembly of functional centrosomes *in vitro*. *Proc. Natl. Acad. Sci. USA.* 95, 9295-9300.

Schumacher, J. M., N. Ashcroft, P. J. Donovan, and A. Golden. 1998. A highly conserved centrosomal kinase, AIR-1, is required for accurate cell cycle progression and segregation of developmental factors in *Caenorhabditis elegans* embryos. *Development.* 125, 4391-4402.

Shepard, B., and C. Clark. 1976. Structure of the anterior alimentary tract of the passively feeding nematode: *Pratylenchus penetrans* (Nematoda: Pratylenchidae). *Nematologica.* 31, 321-334.

Sönnichsen, B., Koski, L.B., Walsh, A., Marshall, P., Neumann et al. (2005). Full-genome RNAi profiling of early embryogenesis in *Caenorhabditis elegans*. *Nature.* 434, 462-469.

- Srayko, M., D. W. Buster, O. Bazirgan, F. J. McNally, and P. E. Mains. 2000. MEI-1/MEI-2 katanin-like microtubule severing activity is required for *Caenorhabditis elegans* meiosis. *Genes Dev.* 14, 1072-1084.
- Srayko, M., A. Kaya, J. Stamford, and A. A. Hyman. 2005. Identification and characterization of factors required for microtubule growth and nucleation in the early *C. elegans* embryo. *Dev. Cell.* 9, 223-36.
- Steven, A. C., and U. Aebi. 2003. The next ice age: cryo-electron tomography of intact cells. *Trends Cell Biol.* 13, 107-110.
- Strome, S., J. Powers, M. Dunn, K. Reese, C. J. Malone, J. White, G. Seydoux, and W. Saxton. 2001. Spindle dynamics and the role of γ -tubulin in early *Caenorhabditis elegans* embryos. *Mol. Biol. Cell.* 12, 1751-1764.
- Sulston, J. E., E. Schierenberg, J. G. White, and J. N. Thomson. 1983. The embryonic cell lineage of the nematode *Caenorhabditis elegans*. *Dev. Biol.* 100, 64-119.
- Theurkauf, W. E., and R. S. Hawley. 1992. Meiotic spindle assembly in *Drosophila* females: behavior of nonexchange chromosomes and the effects of mutations in the nod kinesin-like protein. *J. Cell Biol.* 116, 1167-1180.
- Tournebize, R., S. S. Andersen, F. Verde, M. Doree, E. Karsenti, A. A. Hyman. 1997. Distinct roles of PP1 and PP2A-like phosphatases in control of microtubule dynamics during mitosis. *EMBO J.* 16, 5537-5549.
- Verkade, P. 2006. An automated sample transfer system for the Leica EMPACT2 high pressure freezer or new instruments and techniques. *J. Microsc. (Oxford)*. submitted.
- Vernos, I., J. Raats, T. Hirano, J. Heasman, E. Karsenti, and C. Wylie. 1995. Xklp1, a chromosomal *Xenopus* kinesin-like protein essential for spindle organization and chromosome positioning. *Cell.* 81, 117-127.
- Vogel, J. M., T. Stearns, C. L. Reider, and R. E. Palazzo. 1997. Centrosomes isolated from *Spisula solidissima* oocytes contain rings and an unusual stoichiometric ratio of α/β tubulin. *J. Cell Biol.* 137, 193-202.
- Walczak, C. E., I. Vernos, T. J. Mitchison, E. Karsenti, and R. Heald. 1998. A model for the proposed roles of different microtubule-based motor proteins in establishing spindle bipolarity. *Curr. Biol.* 8, 903-913.
- Wang, S. Z., and R. Adler. 1995. Chromokinesin: a DNA-binding, kinesin-like nuclear protein. *J. Cell Biol.* 128, 761-768.
- Wiese, C., and Y. Zheng. 2000. A new function for the for the γ -tubulin ring complex as a microtubule minus-end cap. *Nat. Cell Biol.* 2, 358-364.

Wittmann, T., A. Hyman, and A. Desai. 2001. The spindle: a dynamic assembly of microtubules and motors. *Nature Cell Biol.* 3, E28-E34.

Wolf, N., D. Hirsh, and J. R. McIntosh. 1978. Spermatogenesis in males of the free-living nematode, *Caenorhabditis elegans*. *J. Ultrastruct. Res.* 63, 155-169.

Wood, W. B. 1988. The Nematode *Caenorhabditis elegans*. Cold Spring Harbour Laboratory.

Yang, H.-Y., K. McNally, and F. J. McNally. 2003. MEI-1/katanin is required for translocation of the meiosis I spindle to the oocyte cortex in *C. elegans*. *Dev. Biol.* 260, 245-259.

Yoder, T. J., M. A. McElwain, S. E. Francis, J. Bagley, E. G. Muller, B. Pak, E. T. O'Toole, M. Winey, and T. N. Davis. 2005. Analysis of a spindle pole body mutant reveals a defect in biorientation and illuminates spindle forces. *Mol. Biol. Cell.* 16, 141-152.

Zheng, Y., M. L. Wong, B. Alberts, and T. Mitchison. 1995. Nucleation of microtubule assembly by a γ -tubulin-containing ring complex. *Nature.* 378, 578-583.

Zipperlen, P., A. G. Fraser, R. S. Kamath, M. Martinez-Campos, and J. Ahringer. 2001. Roles for 147 embryonic lethal genes on *C. elegans* chromosome I identified by RNA interference and video microscopy. *EMBO J.* 20, 3984-3992.

6 APPENDIX

6.1 Related publications

The following related research articles are attached:

Dammermann, A., T. Müller-Reichert, L. Pelletier, B. Habermann, A. Desai, and K. Oegema. 2004. *Dev. Cell.* 7, 815-829.

Pelletier, L., N. Özlü, E. Hannak, C. Cowan, B. Habermann, M. Ruer, T. Müller-Reichert, and A. A. Hyman. 2004b. *Curr. Biol.* 14, 863-873.

Müller-Reichert, T., H. Hohenberg, E. T. O'Toole, and K. McDonald. 2003. *J. Microsc.* 212, 71-80.

Müller-Reichert, T., D. Chrétien, F. Severin, and A. A. Hyman. 1998. *Proc. Natl. Acad. Sci. USA.* 95, 3661-3666.

Centriole Assembly Requires Both Centriolar and Pericentriolar Material Proteins

Alexander Dammermann,^{1,*}
Thomas Müller-Reichert,² Laurence Pelletier,²
Bianca Habermann,³ Arshad Desai,¹
and Karen Oegema^{1,*}

¹Ludwig Institute for Cancer Research
Department of Cellular and Molecular Medicine
University of California, San Diego
9500 Gilman Drive
La Jolla, California 92093

²Max Planck Institute for Molecular Cell Biology
and Genetics (MPI-CBG)
Pfortenauerstrasse 108
01307 Dresden
Germany

³Scionics Computer Innovation
Pfortenauerstrasse 110
01307 Dresden
Germany

Summary

Centrioles organize pericentriolar material to form centrosomes and also template the formation of cilia. Despite the importance of centrioles in dividing and differentiated cells, their assembly remains poorly understood at a molecular level. Here, we develop a fluorescence microscopy-based assay for centriole assembly in the 1-cell stage *C. elegans* embryo. We use this assay to characterize SAS-6, a centriolar protein that we identified based on its requirement for centrosome duplication. We show that SAS-6, a member of a conserved metazoan protein family, is specifically required for new centriole assembly, a result we confirm by electron microscopy. We further use the centriole assembly assay to examine the roles of three pericentriolar material proteins: SPD-5, the kinase aurora-A, and γ -tubulin. Our results suggest that the pericentriolar material promotes daughter centriole formation by concentrating γ -tubulin around the parent centriole. Thus, both centriolar and pericentriolar material proteins contribute to centriole assembly.

Introduction

Centrioles are eukaryotic organelles that have two divergent functions: (1) they organize centrosomes, cellular organelles that nucleate and anchor microtubules (Bornens, 2002; Rieder et al., 2001); and (2) they template the formation of cilia, microtubule-based projections that perform a variety of motile and sensory functions (Snell et al., 2004).

Centrioles are cylindrical structures, \sim 100–200 nm in diameter and \sim 100–400 nm in length (Marshall, 2001; Preble et al., 2000), composed of a 9-fold symmetric

array of stabilized microtubules (singlet, doublet, or triplet, depending on organism and tissue). New centrioles usually form adjacent to pre-existing centrioles, which are thought to template their assembly (reviewed in Delattre and Gonczy, 2004). Electron microscopy has defined a morphological pathway for centriole assembly (Anderson and Brenner, 1971, and references therein). First, a disc of fibrous material forms adjacent to the proximal end of the parental centriole. Next, a “cartwheel,” consisting of a set of 9-fold symmetric spokes connected to a central axis, appears within this material. Centriolar microtubules assemble at the tips of each of the cartwheel spokes, and the structure elongates to form the mature centriole. In dividing cells, parental centrioles template the formation of 1 centriole per cell cycle. However, in ciliated tissues, up to 8 centrioles can form simultaneously, generally in a radial array around the base of the parent centriole. New centrioles can also form in association with other structures, notably the deuterosome during ciliogenesis in vertebrates (Anderson and Brenner, 1971) and the blepharoplast during spermatogenesis in ferns (Mizukami and Gall, 1966).

In the context of the centrosome, centrioles recruit pericentriolar material (PCM) to form a focal body (Bobinnec et al., 1998) that nucleates and anchors microtubules. Centrioles therefore determine centrosome number (Mazia et al., 1960; Sluder and Rieder, 1985), and assembly of new centrioles is a prerequisite for centrosome duplication (Delattre et al., 2004). Studies of extracted centrosomes indicate that centrioles are tightly associated with a fibrous matrix that directs the recruitment of other PCM components including the microtubule nucleator γ -tubulin (Moritz et al., 1998; Schnackenberg et al., 1998). In addition to its role in nucleating and organizing microtubules, pericentriolar material may also play a role in centriole assembly. When centrosomes are destroyed by laser ablation in vertebrate somatic cells, foci of pericentriolar material reform first, and new centrioles subsequently assemble de novo within these foci (Khodjakov et al., 2002). Although this topic has received less attention, PCM proteins may also be involved in centriole assembly during ciliogenesis (Kubo et al., 1999).

The identification of proteins required for centriole assembly has been hindered by their essential role in cell division and their small size, which has necessitated the use of serial-section EM to confidently score centriole number. Nevertheless, a number of proteins have been identified that directly function in centriole assembly. These include centrin-2 in vertebrates (Salisbury et al., 2002); SAS-4 (Kirkham et al., 2003; Leidel and Gonczy, 2003), SPD-2 (Kemp et al., 2004; Pelletier et al., 2004), and the kinase ZYG-1 (O’Connell et al., 2001) in *C. elegans*; and Bld10p in *Chlamydomonas* (Matsuura et al., 2004). In organisms whose centrioles have doublet or triplet microtubules, δ - and ϵ -tubulin are also required for centriole assembly (reviewed in Dutcher, 2003). The PCM protein γ -tubulin has also been implicated in basal body assembly based on studies in *Paramecium* and

*Correspondence: adammernann@ucsd.edu (A.D.), koegema@ucsd.edu (K.O.)

Tetrahymena (Ruiz et al., 1999; Shang et al., 2002). However, the essential functions of γ -tubulin in cell growth and division have complicated analysis of its role in centriole assembly.

The *C. elegans* embryo is well suited for studies of centriole function. RNA-mediated interference (RNAi) can be used to generate oocytes containing cytoplasm >95% depleted of a targeted gene product independent of intrinsic protein turnover (Montgomery and Fire, 1998). Fertilization introduces a single centriole pair, whose capacity to duplicate and recruit pericentriolar material in the depleted cytoplasm can be assayed. The ease of RNAi combined with the sequenced genome has prompted genome-wide screens (Grant and Wilkinson, 2003) that have identified ~1600 genes required for embryonic viability, which would include proteins required for centriole assembly. These screens, as well as forward genetics and characterization of homologs of proteins identified in other systems, are rapidly generating a catalog of proteins required for centriole and pericentriolar material function.

To study centriole duplication in *C. elegans*, we developed a fluorescence microscopy assay for centriole assembly based on incorporation of a GFP fusion with the centriolar structural protein SAS-4. Using this assay, we show that SAS-6, a member of a conserved family of centriolar proteins, is specifically required for centriole assembly. We further use our assay to examine the role of the pericentriolar material in this process. Our results suggest that the pericentriolar material promotes centriole assembly by providing a localized source of γ -tubulin. Thus, both centriole components and pericentriolar material contribute to centriole assembly.

Results

Development of a Fluorescence-Based Assay for Centriole Assembly

During *C. elegans* fertilization, the sperm brings a pair of centrioles into the oocyte, which lacks centrioles. The sperm-derived centrioles separate and a new “daughter” centriole forms adjacent to each of them, so that by metaphase each spindle pole has a centrosome containing two full-length centrioles (Kirkham et al., 2003). Newly formed daughters remain closely associated with their parent and individual centrioles cannot be resolved by light microscopy until the centriole pair separates in late anaphase/telophase. Therefore, to specifically monitor the assembly of new centrioles, we used mating to introduce unlabeled sperm centrioles into oocytes expressing a GFP fusion with the centriolar structural component, SAS-4 (Figure 1A). Like α/β -tubulin (Kochanski and Borisy, 1990), SAS-4 is incorporated into centrioles during their assembly and does not subsequently exchange with the cytoplasmic pool (Kirkham et al., 2003; Leidel and Gonczy, 2003). Furthermore, SAS-4 is required for formation of the centriolar cylinder, and the amount of centriolar SAS-4 is proportional to at least one measure of centriole function (the amount of PCM that a centriole can recruit; Kirkham et al., 2003), suggesting that GFP:SAS-4 incorporation provides a reliable readout for the extent of centriole assembly. New centriole assembly was assayed in fixed embryos by

immunofluorescence with antibodies to GFP (to detect newly formed centrioles) and SAS-4 (to detect all centrioles, both new and sperm derived). Since *C. elegans* is a hermaphrodite, false positives in this assay could result from self-fertilization with GFP-containing sperm. To avoid this problem, we constructed a strain expressing GFP:SAS-4 that also carries a temperature-sensitive mutation in *fem-1*, a gene required for sperm production (Nelson et al., 1978). Thus, all embryos produced by hermaphrodites raised at the nonpermissive temperature are derived from fertilization of GFP:SAS-4-expressing oocytes with wild-type unlabeled sperm.

We first used this assay to examine the timing of new centriole assembly in the *C. elegans* embryo (Figures 1B and 1C). Foci of GFP:SAS-4 first became detectable concomitant with the onset of chromosome condensation during the first mitotic division (Figure 1B). Classifying embryos into early, middle, and late prophase based on their DNA morphology (see Supplemental Figure S1 at <http://www.developmentalcell.com/cgi/content/full/7/6/815/DC1/>) revealed that both the number of centrioles with a detectable GFP signal (Figure 1C) and the intensity of the signal (Figure 1B) gradually increased concurrent with chromosome condensation during prophase. During this time interval, centrosomes also mature in preparation for mitosis, with both the amount of PCM surrounding the centrioles and the number of centrosomally organized microtubules increasing ~5-fold (Hanak et al., 2001). By late prophase, when the chromosomes were fully condensed, clear foci of GFP:SAS-4 were associated with both sperm centrioles in all embryos examined (Figures 1B and 1C). In anaphase/telophase, when the accumulated mitotic PCM disperses and the paired centrioles separate in preparation for another round of duplication, GFP:SAS-4 is clearly visible associated with the newly formed centriole at each spindle pole, while the other, sperm-derived centriole remains unlabeled, confirming that centriolar SAS-4 does not exchange with the cytoplasmic pool (Figure 1B). Thus, this assay allows us to use fluorescence microscopy to monitor the assembly and fate of new centrioles that form in the oocyte cytoplasm. Our analysis indicates that centriole assembly occurs concurrent with chromosome condensation and centrosome maturation, during the last 12 min of the ~40 min period between fertilization and metaphase of the first mitotic division.

Identification of Two Proteins Required for Centrosome Duplication

Previous work identified two *C. elegans* proteins specifically required for centrosome duplication, SAS-4 and the kinase ZYG-1 (Kirkham et al., 2003; Leidel and Gonczy, 2003; O’Connell et al., 2001). Depletion of either protein results in an apparently normal first division followed by assembly of monopolar spindles in both daughter cells during the second division. In a differential interference contrast (DIC) microscopy-based RNAi screen for genes required for cell division, we identified two additional genes, F35B12.5 and Y45F10D.9, whose inhibition results in spindle assembly defects first apparent during the second division. By analogy with *sas-4*, these genes were named *sas-5* and *sas-6*, respectively (reflecting their role in bipolar spindle assembly).

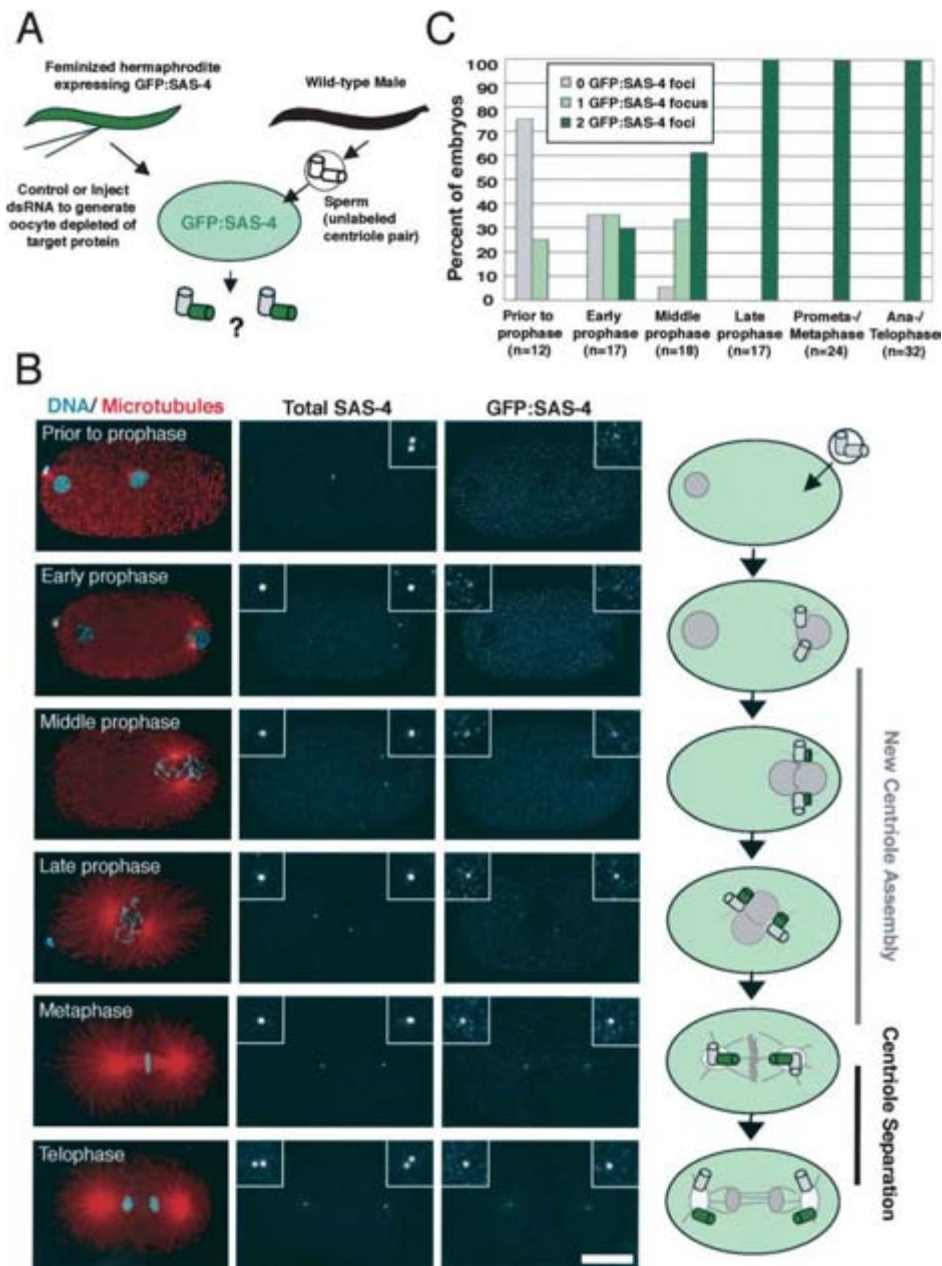


Figure 1. A Fluorescence Assay for Centriole Assembly

(A) Feminized hermaphrodites expressing a GFP fusion with the centriolar structural protein SAS-4 are mated with wild-type males. Fertilization introduces a pair of unlabeled centrioles (gray) into an oocyte containing GFP:SAS-4. Sperm centrioles separate, and assembly of new GFP-containing centrioles (green) adjacent to each of the sperm centrioles is scored. To test if specific proteins are required for centriole assembly, hermaphrodites are injected with dsRNA prior to mating to generate oocytes expressing GFP:SAS-4 that are depleted of the targeted protein. (B) Centrioles assemble during prophase of the first mitotic division. Embryos resulting from mating feminized hermaphrodites expressing GFP:SAS-4 to wild-type males were fixed and stained for DNA, microtubules, SAS-4, and GFP. Schematics illustrate the progression of new centriole assembly suggested by incorporation of GFP:SAS-4. Scale bar equals 10 μ m. Insets are magnified 3.5 \times . (C) The number of new centrioles (foci staining for both SAS-4 and GFP) was quantified in embryos of the indicated cell cycle states.

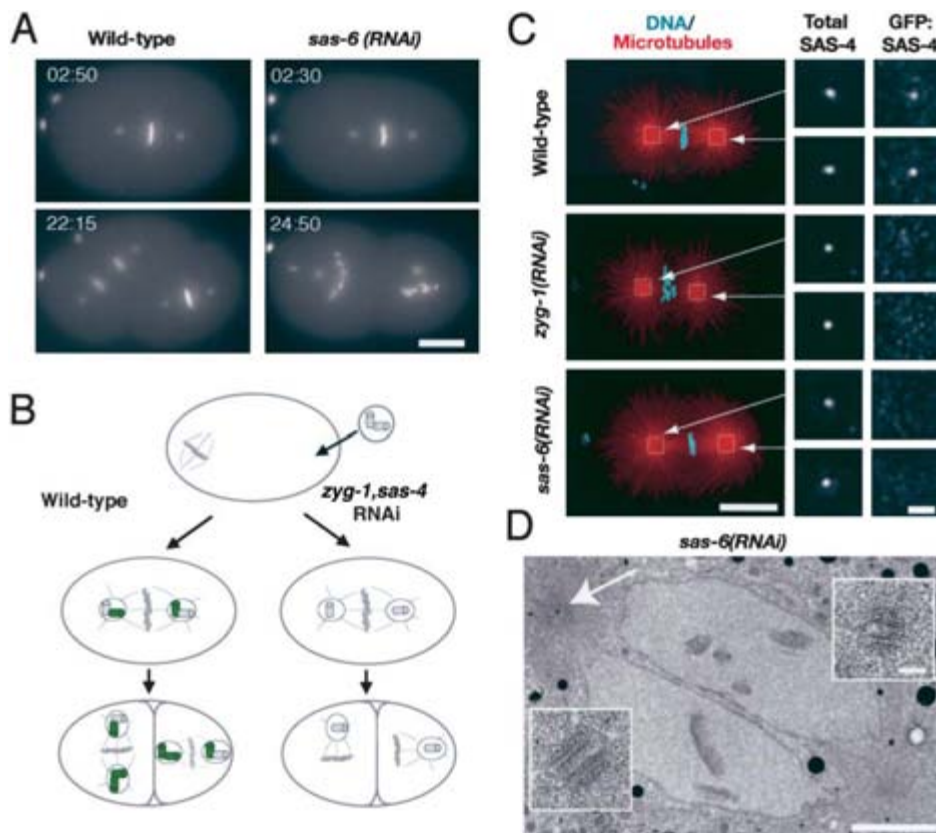


Figure 2. SAS-6 Is Specifically Required for Centriole Assembly

(A) Stills from time-lapse sequences of wild-type and *sas-6(RNAi)* embryos expressing GFP:histone and GFP: γ -tubulin (see also Supplemental Movies S1–S6). Times are minutes after nuclear envelope breakdown. Scale bar equals 10 μ m.

(B) The centrosome duplication failure previously described for ZYG-1 and SAS-4-depleted embryos results from a failure of new centriole assembly (Kirkham et al., 2003; O’Connell et al., 2001).

(C) Results of centriole assembly assays performed on embryos depleted of SAS-6 or ZYG-1. Embryos were fixed and stained for DNA and microtubules (left), total SAS-4 (middle), and GFP:SAS-4 (right). Total SAS-4 and GFP:SAS-4 panels are higher magnification views of the indicated regions. Scale bars equal 10 and 1 μ m, respectively.

(D) Correlative DIC/transmission EM confirms that each spindle pole in *sas-6(RNAi)* embryos contains only a single centriole ($n = 5$). Overview image illustrates the mitotic state of the chromatin. The position of a single centriole present in this section is indicated by an arrow. Insets are higher magnification views taken from sections containing the single centriole found at each spindle pole. Scale bars equal 2.5 μ m and 100 nm, respectively.

To further analyze SAS-5 and SAS-6, we used RNAi to deplete them in embryos coexpressing GFP: γ -tubulin and GFP:histone to simultaneously monitor centrosomes and chromosomes (Figure 2A; Supplemental Figure S2A and Supplemental Movies S1–S3). In all *sas-5* and *sas-6(RNAi)* embryos filmed ($n = 6$ for each), bipolar spindles with levels of centrosomal γ -tubulin fluorescence similar to wild-type formed during the first mitotic division. However, during the second division, monopolar spindles with only a single focus of γ -tubulin fluorescence were observed in each daughter cell. We also analyzed depleted embryos coexpressing GFP:histone and GFP: β -tubulin to examine the microtubule cytoskeleton (Supplemental Movies S4–S6). Spindle assembly appeared identical to wild-type during the first mitotic division in both *sas-5* and *sas-6(RNAi)* embryos. However, as the embryos entered their second division, each daughter cell assembled only a single centrosomal microtubule aster. These asters increased normally in size

during mitotic entry and monopolar spindles were formed. Depletion of either SAS-5 or SAS-6 therefore results in a specific defect in centrosome duplication identical to that observed in embryos depleted of ZYG-1 or SAS-4. SAS-5 was independently discovered in a mutational screen, and a characterization of this protein was recently published (Delattre et al., 2004). In Supplemental Figure S2 we present our analysis of this protein, which confirms and extends this prior study. Here, we focus on the previously uncharacterized SAS-6.

SAS-6 Is Specifically Required for Centriole Assembly

Serial-section transmission EM of *sas-4(RNAi)* and *zyg-1* mutant embryos has shown that their centrosome duplication defects result from a failure of centriole assembly (Kirkham et al., 2003; O’Connell et al., 2001). During the apparently normal first division in these embryos, each

pole is organized by a centrosome containing a single sperm-derived centriole instead of the normal centriole pair (Figure 2B). Since each daughter cell inherits only one centriole, only one centrosome can form, resulting in monopolar spindles in the second mitotic division. The phenotype in *sas-6(RNAi)* embryos could result from a similar failure of centriole assembly. However, other defects could also give rise to this phenotype. For example, new centrioles may assemble and separate from the sperm-derived centrioles normally but fail to recruit pericentriolar material to organize a new centrosome. Alternatively, centriole separation may be defective, so that the sperm-derived and newly assembled centrioles remain together, forming a single centrosome during the second mitotic division.

To distinguish between these possibilities, we used our fluorescence centriole assembly assay. Double-stranded RNA (dsRNA) was injected into feminized hermaphrodites prior to mating (Figure 1A) to generate oocytes expressing GFP:SAS-4 that were depleted of SAS-6 or ZYG-1. We examined embryos at stages between late prophase and metaphase of the first mitotic division, when all wild-type embryos have foci of GFP:SAS-4 associated with both sperm centrioles (Figure 1C; $n = 41$). In ZYG-1-depleted embryos, each centrosomal aster contained a focus of SAS-4, corresponding to a single sperm centriole, but no associated foci of GFP:SAS-4 were detected ($n = 22$; Figure 2C). SAS-6-depleted embryos similarly failed to form GFP:SAS-4 foci, either associated with the sperm centrioles or elsewhere in the embryo cytoplasm ($n = 26$ embryos; Figure 2C).

To confirm that no centrioles formed in the absence of detectable SAS-4 incorporation, we performed correlative DIC/serial-section transmission EM on *sas-6(RNAi)* embryos (Figure 2D). Fertilized embryos were filmed by DIC microscopy until metaphase of the first embryonic mitosis, when they were rapidly fixed by laser permeabilization in the presence of glutaraldehyde. Serial-section transmission EM was used to count the number of centrioles at each spindle pole. While wild-type embryos contain two centrioles at each spindle pole in metaphase (Kirkham et al., 2003), *sas-6(RNAi)* embryos contained only a single centriole at each pole ($n = 5$). Thus, SAS-6 is specifically required for new centriole assembly, as is also the case for ZYG-1 (O'Connell et al., 2001), SAS-4 (Kirkham et al., 2003; Leidel and Gonczy, 2003), and SAS-5 (Delattre et al., 2004; see also correlative DIC/serial-section transmission EM in Supplemental Figure S2C). Furthermore, the agreement between the results of our fluorescence assay and the analysis of embryos depleted of ZYG-1, SAS-5, and SAS-6 by serial-section EM validates the use of our assay for monitoring centriole assembly.

SAS-6 Localizes to Centrioles

To determine if SAS-6 acts at centrioles, we examined its localization using affinity-purified antibodies. Embryos were also stained for SAS-4, which was previously localized to centrioles by immuno-EM (Kirkham et al., 2003). SAS-6 colocalized with SAS-4 to small focal structures in the center of the centrosome throughout the embryonic cell cycle (Figure 3A). SAS-6 also colocalized with SAS-4 in sperm (Figure 3B). To confirm that SAS-6

localizes to centrioles, we performed immuno-EM on embryos from wild-type hermaphrodites prepared by high-pressure freezing/freeze substitution. In sections containing centrioles, gold particles were observed associated with the centriolar cylinders (Figure 3C). We also performed immuno-EM for SAS-5 and found that it too localizes to the centriolar cylinders (Supplemental Figure S2D). The combination of light microscopy and EM analysis indicates that SAS-6, like SAS-4 and SAS-5, is a bona fide centriolar protein.

Centriole assembly occurs primarily in prophase (Figure 1C), but ZYG-1, which is required for centriole assembly, was previously reported to localize to centrioles only transiently between metaphase and telophase (O'Connell et al., 2001). To resolve this apparent contradiction, we re-examined ZYG-1 localization. Using our antibodies, we could detect ZYG-1 staining at centrioles throughout the cell cycle (Figure 3A). This localization was observed with two different antibodies as well as in a transgenic line expressing GFP:ZYG-1 (data not shown). However, unlike SAS-4 and SAS-6, no ZYG-1 staining was observed in sperm (Figure 3B). In summary, ZYG-1, like SAS-4, SAS-5, and SAS-6, localizes to centrioles at a time consistent with its role in centriole assembly.

SAS-6 Is a Member of a Conserved Family of Centriolar Proteins

SAS-6 is a 56 kDa protein with no obvious sequence motifs other than a centrally located coiled-coil domain. Database searches using the N-terminal, coiled-coil-free region of SAS-6 identified human DKFZp761A078 and *Drosophila* CG15524 as potential SAS-6 homologs (Figure 4A). Interestingly, the putative human homolog was present in the proteomic catalog of the mammalian centrosome, recently defined using mass spectrometry (Andersen et al., 2003). To test whether HsSAS-6 localizes to centrioles, we transiently transfected a construct directing expression of a YFP fusion. YFP:HsSAS-6 localized to small foci in the center of the PCM (defined by γ -tubulin staining), consistent with centriolar localization (Figure 4B). Thus, SAS-6 is a member of a widely conserved centriolar protein family.

Centrosome Maturation Is Not Required for New Centriole Assembly

Our analysis of GFP:SAS-4 incorporation (Figures 1B and 1C) indicates that centrioles assemble concurrent with the recruitment of additional PCM during mitotic entry (centrosome maturation). SPD-2, a protein that localizes to both centrioles and the PCM, has recently been shown to be required for both centrosome maturation and centriole assembly (Kemp et al., 2004; Pelletier et al., 2004), suggesting a link between these two processes. To determine if the recruitment of additional PCM during centrosome maturation is required for centriole assembly, we examined embryos depleted of the aurora-A kinase, AIR-1. Like SPD-2, AIR-1 is required for centrosome maturation (Hannak et al., 2001). In embryos depleted of either protein, sperm centrioles acquire a small amount of PCM following fertilization, but the dramatic accumulation of additional PCM that normally accompanies mitotic entry fails to occur (Figures 5A and

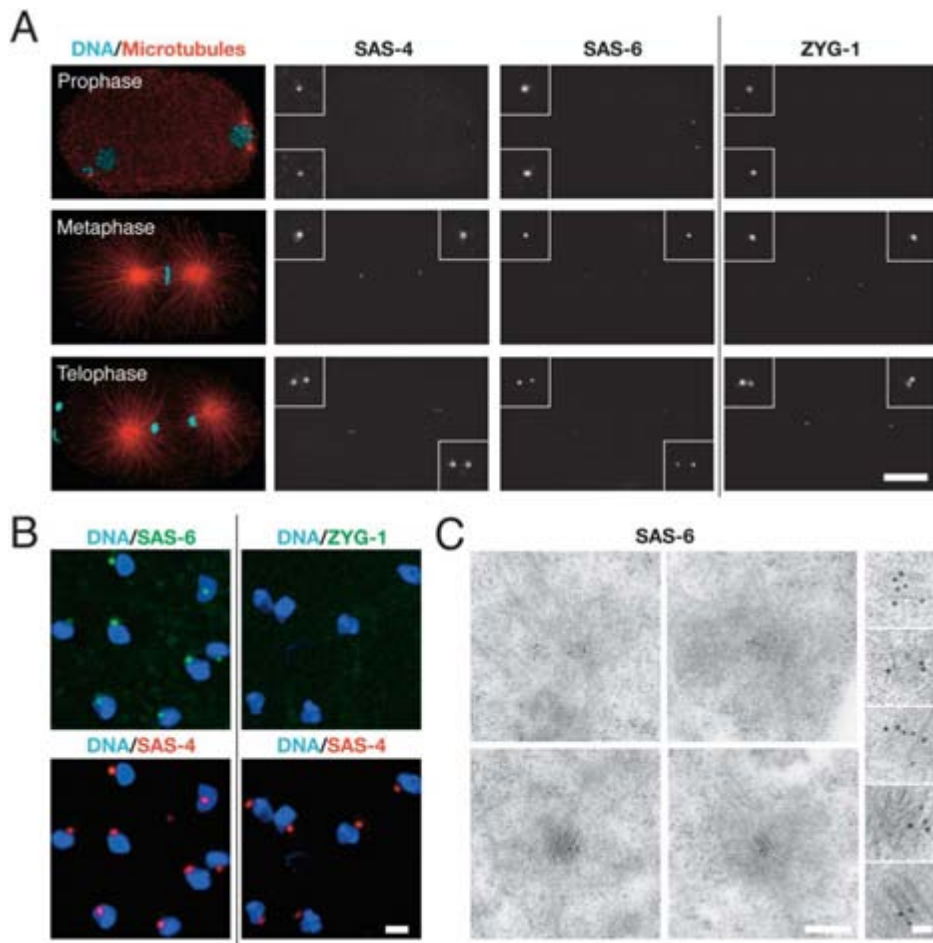


Figure 3. SAS-6 and ZYG-1 Colocalize with SAS-4 at Centrioles throughout the Cell Cycle

(A) Fixed embryos were stained for DNA, microtubules, SAS-4, and either SAS-6 or ZYG-1. DNA/microtubule, SAS-4, and SAS-6 images are from the same embryos. The ZYG-1 panels are from different embryos at similar cell cycle stages. Scale bar equals 10 μm . Insets are magnified 3.5 \times .

(B) SAS-6, but not ZYG-1, colocalizes with SAS-4 to a single focus on the nuclear periphery in mature sperm. Scale bar equals 1 μm .

(C) SAS-6 localizes to centrioles by immunoelectron microscopy. Scale bar equals 200 nm, insets 50 nm.

5B; Hannak et al., 2001; Pelletier et al., 2004; Kemp et al., 2004). We examined embryos in late prophase/prometaphase of the first mitotic division, which can be identified following even severe perturbations of centrosome function (see Experimental Procedures). At this stage, GFP:SAS-4 incorporation is observed associated with all sperm centrioles in wild-type embryos (Figure 1C). As expected, no foci of GFP:SAS-4 were detected in *spd-2(RNAi)* embryos ($n = 20$), either associated with the sperm centrioles or elsewhere in the cytoplasm. In contrast, GFP:SAS-4 incorporation occurred normally in AIR-1-depleted embryos (Figure 5C; $n = 11$), despite the failure of centrosome maturation. From these results, we can conclude that the mitosis-specific accumulation of PCM is not required for centriole assembly.

A Role for the Pericentriolar Material in Centriole Formation

Although PCM levels do not increase during mitotic entry in AIR-1-depleted embryos, sperm centrioles do acquire a basal level of PCM following fertilization. To determine whether this basal level contributes to centriole assembly, we analyzed embryos depleted of the pericentriolar material protein SPD-5 (Hamill et al., 2002). SPD-5 is an essential component of the PCM matrix; in *spd-5(RNAi)* embryos, no γ -tubulin or other pericentriolar material components accumulate around the centrioles at any cell cycle stage (Figure 6A; Hamill et al., 2002). In *spd-5(RNAi)* embryos, new centriole assembly did occur but was highly abnormal (Figure 6B). In wild-type embryos, both sperm centrioles are associated

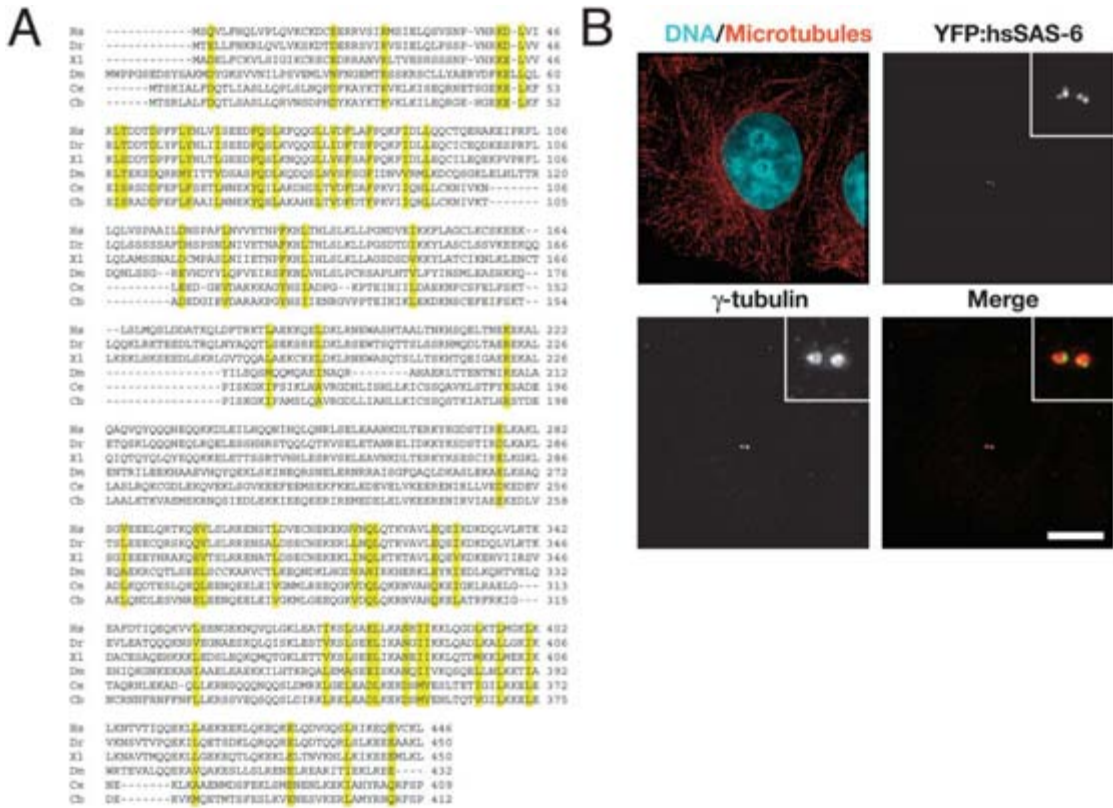


Figure 4. SAS-6 is a Member of a Conserved Metazoan Centriolar Protein Family

(A) Partial sequence alignment of putative SAS-6 homologs. Conserved residues are highlighted in yellow. Abbreviations and accession numbers (in parentheses) of protein sequences: Hs, *Homo sapiens* (NP_919268.1); Dr, *Danio rerio* (NP_998603.1); XI, *Xenopus laevis* (AAH70784.1); Dm, *Drosophila melanogaster* (NP_651756.1, CG15524-PA); Ce, *Caenorhabditis elegans* (NP_502660.1); Cb, *Caenorhabditis briggsae* (CAE74596.1). (B) YFP:hsSAS-6 expressed in T98G human cultured cells localizes to two small foci within the larger PCM positive for γ -tubulin. Scale bar equals 10 μ m. Insets magnified 4 \times .

with a focus of GFP:SAS-4 by late prophase/prometaphase, indicating that they have initiated the formation of a daughter centriole (Figure 1C). In contrast, only 29% of *spd-5(RNAi)* embryos at this stage contained two GFP:SAS-4 foci. In 43% of embryos, only a single GFP:SAS-4 focus was present, and in 29% of embryos no GFP:SAS-4 foci were detected, indicating that both new daughter centrioles failed to initiate assembly (Figure 6B). Thus, when the assembly of pericentriolar material around the sperm centrioles is blocked by depletion of SPD-5, new daughter centrioles fail to initiate ~50% of the time.

The partial failure to initiate new centriole assembly in *spd-5(RNAi)* embryos is in contrast to the complete block observed following depletion of ZYG-1, SAS-5, SAS-6, and SPD-2. To address whether residual centriole assembly might be due to inadequate depletion, we performed quantitative Western blotting and immunofluorescence. Western blots of injected worms revealed that total SPD-5 protein levels were reduced to ~1.5% of that in wild-type (Figure 6C). Similarly, the amount

of SPD-5 detected at centrosomes in depleted mitotic 1-cell stage embryos was reduced by more than 99% (0.23% of wild-type levels; n = 24 wild-type embryos, 30 *spd-5(RNAi)* embryos). Thus, the partial disruption of new centriole assembly likely reflects the complete loss-of-function phenotype for SPD-5.

γ -Tubulin Promotes the Initiation of Centriole Assembly

SPD-5 could have a direct role in centriole assembly distinct from its role in PCM formation. Alternatively, the centriole assembly defect in *spd-5(RNAi)* embryos could result from failure to recruit another PCM component that promotes centriole assembly. An attractive candidate for such a component is γ -tubulin, a specialized tubulin required for centrosomal microtubule nucleation (Hannak et al., 2002). To test this idea, we analyzed the role of γ -tubulin in centriole assembly. Surprisingly, the GFP:SAS-4 incorporation assay revealed a defect in γ -tubulin-depleted embryos that was remarkably similar to that in embryos depleted of SPD-5 (Figure 7A). In

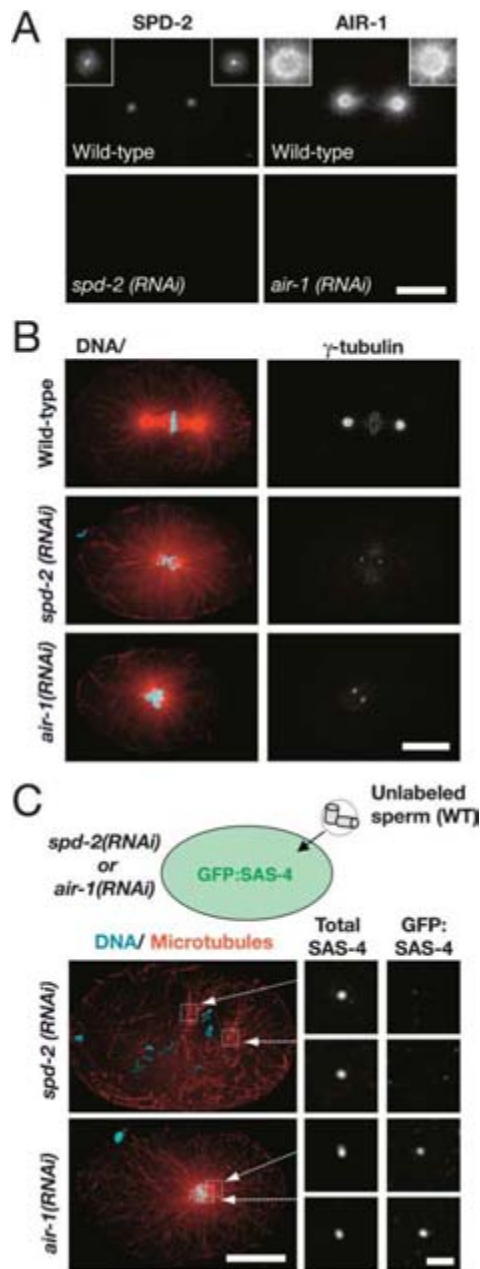


Figure 5. The Mitosis-Specific Accumulation of Pericentriolar Material Is Not Required for Centriole Assembly

(A) Wild-type, *spd-2(RNAi)*, and *air-1(RNAi)* embryos were fixed and stained for SPD-2 and AIR-1, as indicated. SPD-2 localizes to centrioles and weakly to the PCM. In contrast, AIR-1 localizes to the periphery of the centrosomes and extends out along astral microtubules. Both proteins are depleted beyond the detection limit following RNAi. Scale bar equals 10 μ m. Insets magnified 2.5 \times .

(B) Wild-type, *spd-2(RNAi)*, and *air-1(RNAi)* embryos were fixed and stained for DNA and microtubules (left) and γ -tubulin (right). Mitotic centrosomes in depleted embryos remain small, reflecting a failure to recruit additional PCM during mitotic entry. Mitotic centrosomal microtubule asters also remain small and spindle assembly fails (Hannak et al., 2001; Kemp et al., 2004; Pelletier et al., 2004; see also

32% of late prophase/prometaphase γ -tubulin-depleted embryos, no foci of GFP:SAS-4 were detected, indicating that both new daughter centrioles failed to initiate assembly. In 58% of embryos, only a single GFP:SAS-4 focus was present, and only 11% of embryos contained two GFP:SAS-4 foci (Figure 7B). These results indicate that new daughter centrioles failed to initiate assembly \sim 60% of the time in γ -tubulin-depleted embryos. A quantitative comparison of γ -tubulin and SPD-5-depleted embryos further underscores the similarity of the defect in the initiation of new centriole assembly (Figure 7B).

No γ -tubulin is detected around the sperm centrioles in SPD-5-depleted embryos (Figure 6A). Western blots revealed that γ -tubulin protein levels are unchanged following SPD-5 depletion (Figure 6C), indicating that γ -tubulin has not been destabilized, but rather fails to target to centrosomes. In contrast, depletion of γ -tubulin does not block PCM assembly, and centrosomal SPD-5 accumulates to normal levels in γ -tubulin-depleted embryos (Figure 7C). These results lead us to conclude that γ -tubulin is the key component of the PCM that is required to promote centriole assembly. The role of SPD-5 in centriole assembly is likely due to its role in targeting γ -tubulin to centrosomes.

Centrioles that Form in γ -Tubulin- or SPD-5-Depleted Embryos Are Aberrant

During our analysis of SPD-5- and γ -tubulin-depleted embryos, we found that when new centrioles did form, they often failed to remain in close proximity to their parent sperm-derived centrioles (Figure 7B). Premature separation of centriole pairs was observed in both SPD-5- and γ -tubulin-depleted embryos as early as late prophase, prior to nuclear envelope breakdown. By prometaphase/metaphase, 80% of new centrioles ($n = 12/15$) had separated from their parent in *spd-5(RNAi)* embryos and 60% ($n = 6/10$) had separated in γ -tubulin (*RNAi*) embryos. In contrast, paired centrioles in wild-type embryos never separate before late anaphase/telophase ($n = 0/48$; Figure 8A). The new centrioles (GFP-positive) in SPD-5- and γ -tubulin-depleted embryos also appeared to contain less total SAS-4 than the parental sperm-derived centrioles (Figure 8A). To determine if new centrioles were ultimately able to reach normal size, we quantified the ratio of total SAS-4 in the new centrioles to that in the old centrioles in telophase embryos, when centriole pairs have separated in wild-type (Figure 1). In control embryos, as well as in embryos depleted of AIR-1 (which is not required for the initiation of new centriole assembly; Figure 5B), this ratio is \sim 1, indicating that the new centrioles have reached full size. In contrast, in embryos depleted of SPD-5 or γ -tubulin, this ratio was \sim 0.6, suggesting that the new centrioles that do form fail to reach full size (Figures 8B and 8C).

Supplemental Movies S7–S9. Scale bar equals 10 μ m.

(C) AIR-1 is not required for centriole assembly. Results of centriole assembly assays performed on embryos depleted of SPD-2 or AIR-1. Embryos were fixed and stained for DNA and microtubules (left), total SAS-4 (middle), and GFP:SAS-4 (right). Total SAS-4 and GFP:SAS-4 panels are higher magnification views of the indicated regions. Scale bars equal 10 and 1 μ m, respectively.

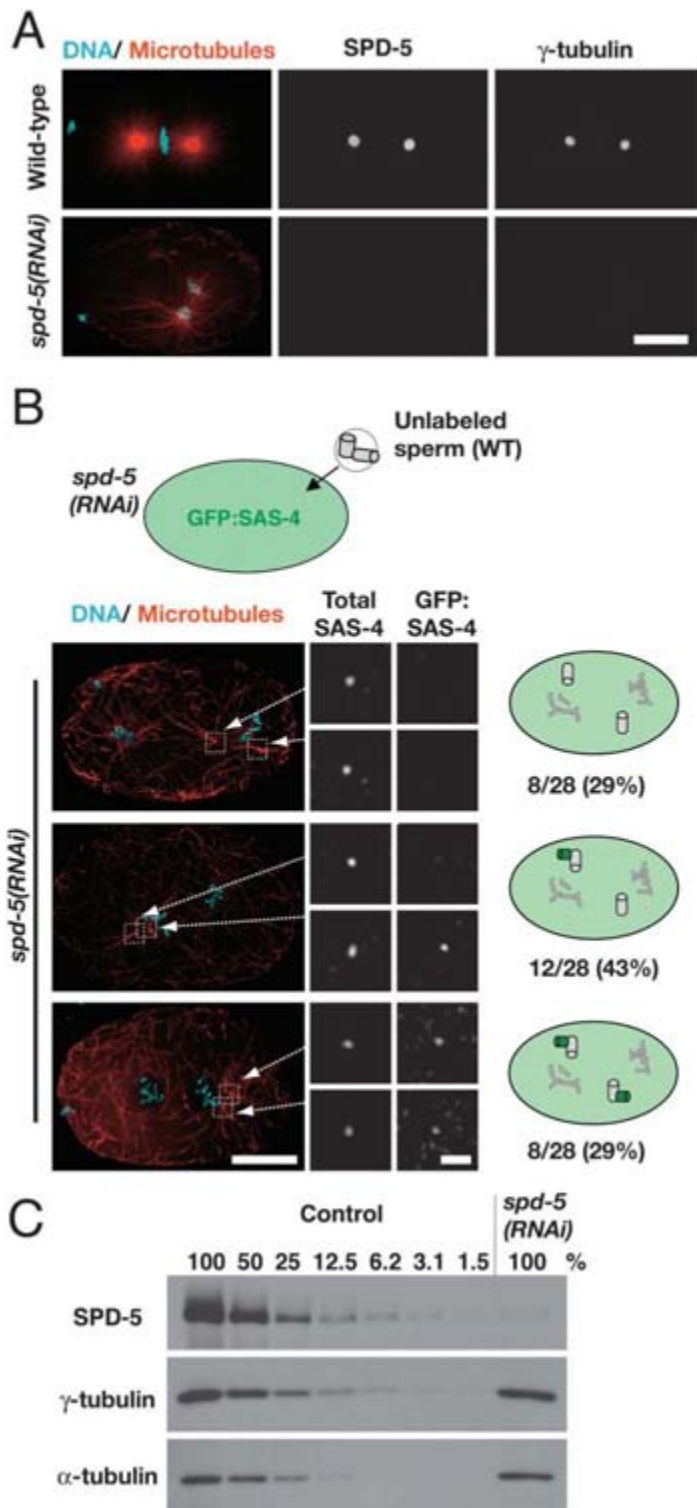


Figure 6. The Pericentriolar Material Protein SPD-5 Is Required for Proper Initiation of Centriole Assembly

(A) Wild-type and *spd-5(RNAi)* embryos were fixed and stained for DNA and microtubules (left), SPD-5 (middle), and γ -tubulin (right). SPD-5 colocalizes with γ -tubulin to the PCM in wild-type embryos. No γ -tubulin or other PCM components accumulate around the centrioles at any cell cycle stage in *spd-5(RNAi)* embryos (Hamill et al., 2002). Although weak microtubule asters form around the chromatin following nuclear envelope breakdown, no centrosomal microtubule asters form and spindle assembly fails (Hamill et al., 2002; see also Supplemental Movies S7 and S10).

(B) Results of centriole assembly assays performed on embryos depleted of SPD-5. Embryos were fixed and stained for DNA and microtubules (left), total SAS-4 (middle), and GFP:SAS-4 (right). Three classes of embryos, in which 0, 1, or 2 centrioles had duplicated, were observed as illustrated in the schematics to the right. Scale bars equal 10 and 1 μ m (insets).

(C) Western blot comparing extract prepared from *spd-5(RNAi)* worms with serial dilutions of extract prepared from wild-type worms (numbers indicate percentage of amount loaded in 100% lane). SPD-5 is depleted to \sim 1.5% of wild-type levels. γ -tubulin levels are not affected by depletion of SPD-5. The same blot was probed for α -tubulin as a loading control.

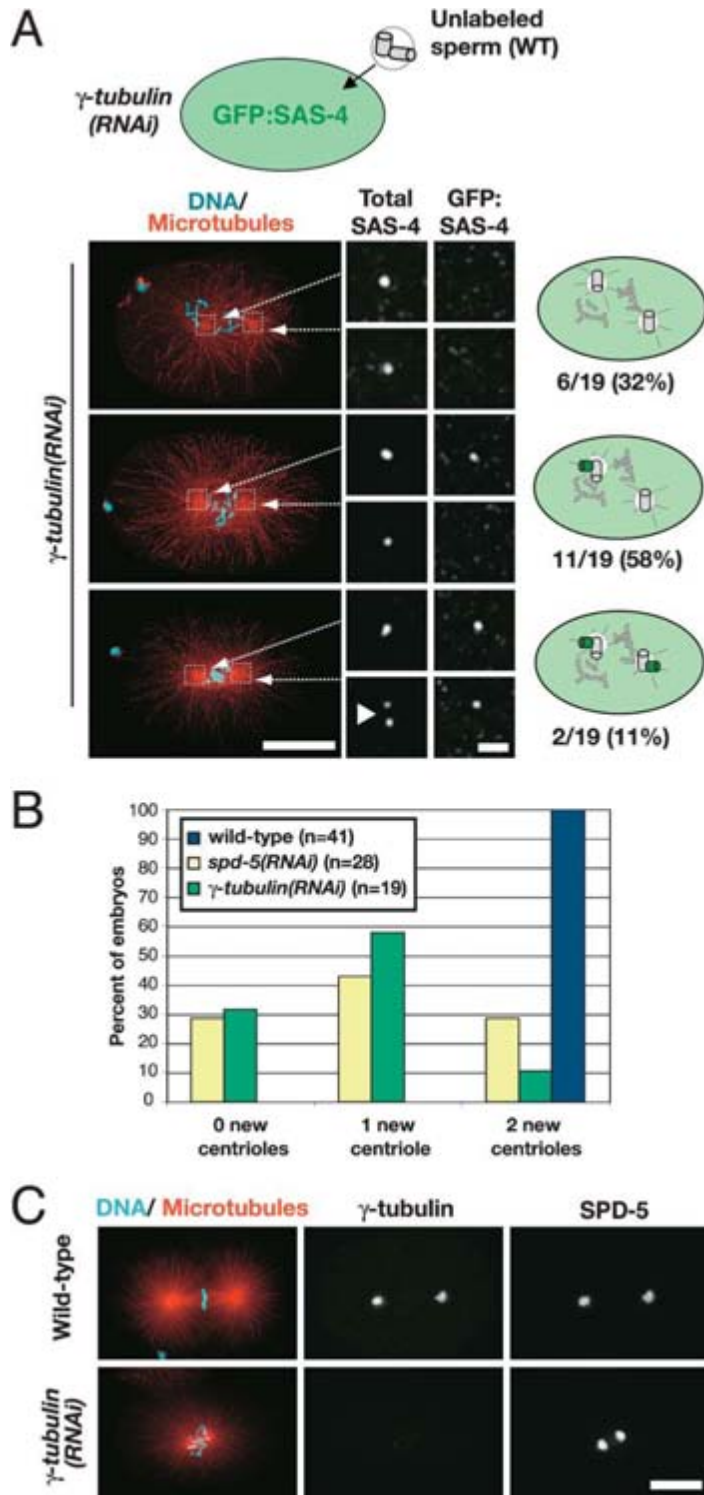


Figure 7. Depletion of γ -Tubulin Recapitulates the Centriole Assembly Defect Observed in *spd-5(RNAi)* Embryos

(A) Results of centriole assembly assays performed on embryos depleted of γ -tubulin. Embryos were fixed and stained for DNA and microtubules (left), total SAS-4 (middle), and GFP:SAS-4 (right). Three classes of embryos, in which 0, 1, or 2 centrioles had duplicated, were observed as illustrated in the schematics to the right. Arrowhead in lower panel highlights the premature separation of a new centriole from its parent (see Figure 8). Scale bars equal 10 and 1 μ m (insets).

(B) The percentage of late prophase/prometaphase embryos that had formed 0, 1, and 2 new centrioles was quantified for wild-type, *spd-5(RNAi)*, and γ -*tubulin(RNAi)* embryos.

(C) Wild-type and γ -*tubulin(RNAi)* embryos were fixed and stained for DNA and microtubules (left), γ -tubulin (middle), and SPD-5 (right). Normal levels of SPD-5 assemble around centrioles in γ -*tubulin(RNAi)* embryos. Centrosomal microtubule asters form but centrosomal microtubule nucleation is severely compromised and spindle assembly fails (Hannak et al., 2002; see also Supplemental Movies S7 and S11).

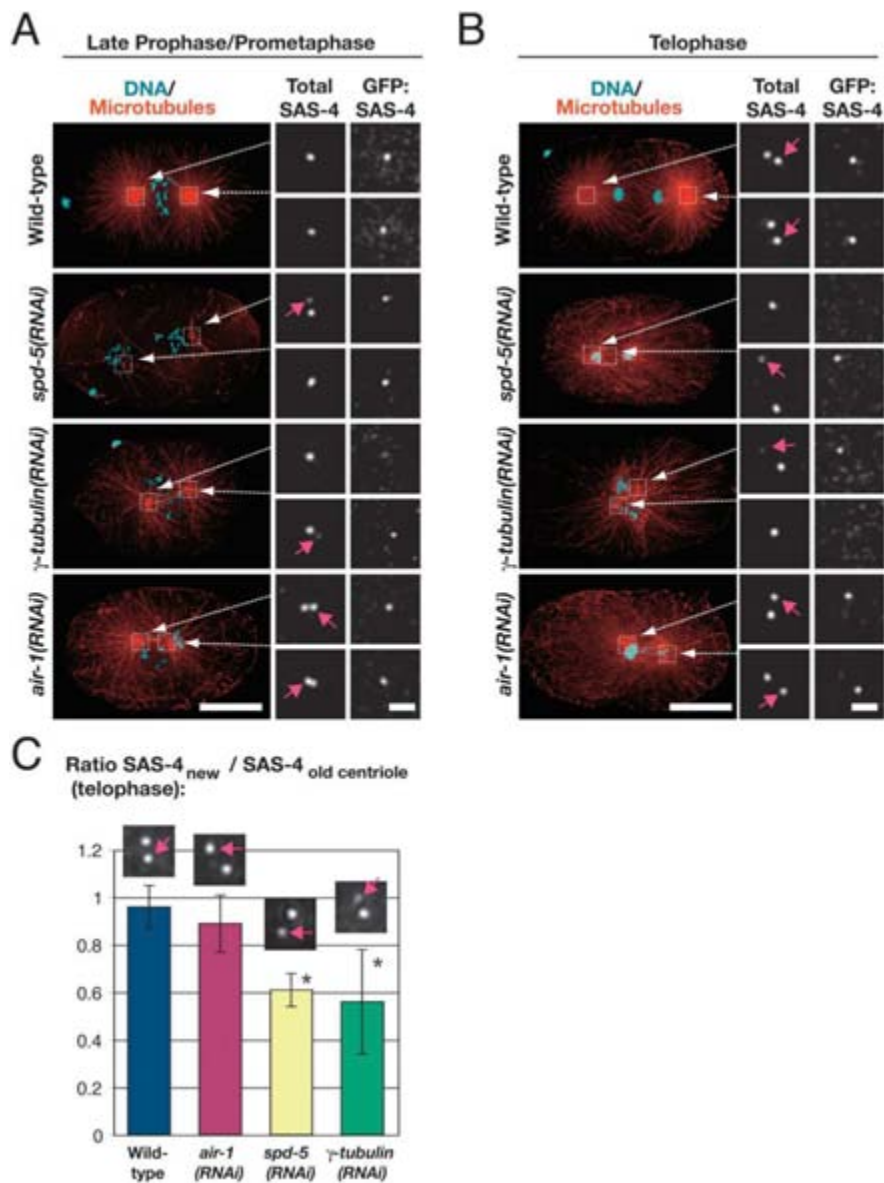


Figure 8. New Centrioles that Form in *spd-5* and γ -tubulin(RNAi) Embryos Are Aberrant

(A) In embryos depleted of SPD-5, γ -tubulin, or AIR-1, new centrioles often prematurely separate from their parent. Embryos were stained for DNA and microtubules (left), total SAS-4 (middle), and GFP:SAS-4 (right). New centrioles (containing GFP:SAS-4) are indicated with arrows in the total SAS-4 images. Scale bars equal 10 and 1 μ m (insets).

(B) New centrioles that form in *spd-5* and γ -tubulin(RNAi) embryos fail to reach full size. Embryos in late anaphase/telophase (as assessed by DNA/microtubule morphology, see Experimental Procedures) were stained for DNA and microtubules (left), total SAS-4 (middle), and GFP:SAS-4 (right).

(C) Quantification of total centriolar SAS-4 fluorescence in anaphase/telophase-stage embryos. The ratio of total SAS-4 fluorescence on the new centriole (also positive for GFP) to that on the sperm-derived parental centriole was measured for 32 wild-type, 17 *spd-5(RNAi)*, 9 γ -tubulin(RNAi), and 18 *air-1(RNAi)* centriole pairs. The average is plotted for each condition; error bars represent the SEM with a confidence interval of 0.95. Insets show representative images of SAS-4 staining (arrows point to the newly formed centrioles). Asterisks indicate statistically significant differences from wild-type (t test, $p < 0.001$).

New centrioles formed in γ -tubulin- and SPD-5-depleted embryos exhibit two distinct defects: premature separation from their parent and failure to reach full size. It seemed possible that the premature separation of

immature new centrioles from their parent might prevent completion of their assembly. However, premature separation of centriole pairs was also observed following depletion of AIR-1 (Figure 8A; $n = 11/14$ centriole pairs

in prometaphase/metaphase embryos) without affecting the extent of SAS-4 incorporation (Figures 8B and 8C). Therefore, premature separation cannot explain the centriole assembly defect observed in SPD-5- or γ -tubulin-depleted embryos. In summary, our results indicate that depletion of SPD-5 or γ -tubulin results in a severe defect in centriole assembly. New centrioles fail to initiate ~50%–60% of the time, and the centrioles that do form contain less SAS-4 than wild-type, suggesting that they are incomplete or structurally defective.

Discussion

A Light Microscopic Assay for Centriole Assembly

Here we report the development of a fluorescence assay for centriole assembly based on incorporation of a GFP fusion with the centriolar protein SAS-4. The use of this assay is validated by our analysis of embryos depleted of four proteins shown to be required for new centriole formation by serial-section EM, ZYG-1 (O'Connell et al., 2001), SPD-2 (Pelletier et al., 2004), SAS-5 (Supplemental Figure S2), and SAS-6 (Figure 2). In all cases, no GFP:SAS-4 incorporation was detected in association with the sperm centrioles or elsewhere in the embryo.

We have used our ability to monitor centriole assembly at the light microscopic level to define a kinetic profile for this process during the first mitotic division of the *C. elegans* embryo. This allowed us to extend prior EM analysis, which showed the presence of full-length new centrioles at metaphase spindle poles (Kirkham et al., 2003). We have further used our fluorescence assay to characterize the role of the pericentriolar material in centriole assembly. This analysis relied on our ability to monitor centriole assembly following severe perturbations of centrosome structure and to find even defective centrioles that had prematurely separated from their parent. In addition, the assay allows analysis of large numbers of embryos, which would be prohibitively difficult using serial-section EM.

SAS-6 Is an Evolutionarily Conserved Protein Specifically Required for Centriole Assembly

Here, we report the identification of SAS-6, a centriolar component that, like ZYG-1 (O'Connell et al., 2001), SAS-4 (Kirkham et al., 2003; Leidel and Gonczy, 2003), and SAS-5 (Delattre et al., 2004, and this study), is specifically required for centriole assembly. To date, SAS-6 is the only member of this class of centriolar proteins to have identifiable homologs in other metazoans. We further show that the human homolog, HsSAS-6, is present on small foci within the PCM, consistent with localization to centrioles (Figure 4). Functional characterization of HsSAS-6 will be needed to determine if the essential role of SAS-6 in centriole assembly has also been conserved.

SAS-5 and SAS-6 colocalize with SAS-4 throughout the embryonic cell cycle and are associated with centrioles by immuno-EM (Figure 3 and Supplemental Figure S2). Unlike the other three proteins, ZYG-1 was previously reported to localize to centrioles only transiently between metaphase and telophase (O'Connell et al., 2001). In contrast, we found ZYG-1 to be localized to centrioles throughout the embryonic cell cycle (Figure

3). The previously reported antibody was raised against a ZYG-1 peptide (O'Connell et al., 2001), raising the possibility that this discrepancy is due to variations in epitope accessibility during the cell cycle. Thus, all four proteins specifically required for centriole assembly localize to centrioles at a time consistent with a role in their formation.

Partial depletion of SAS-4 results in defective centrioles that contain less SAS-4 and recruit proportionally less pericentriolar material (Kirkham et al., 2003). The high frequency with which intermediate phenotypes were observed following SAS-4 depletion is consistent with its proposed role as a structural component that is gradually incorporated during elongation. Similar depletions of ZYG-1 were reported to not result in intermediate phenotypes (Kirkham et al., 2003). However, we have recently found that assembly of defective centrioles that contain less than wild-type levels of SAS-4 and recruit less than wild-type amounts of γ -tubulin can also occur following partial depletions of SAS-5 and SAS-6 as well as ZYG-1, albeit at much lower frequencies than with SAS-4 (data not shown; see also Delattre et al., 2004). This may suggest that these three proteins play fundamentally different roles in centriole assembly (e.g., in initiation of centriole assembly rather than elongation) or simply reflect their different depletion kinetics.

Role of the Pericentriolar Material in Centriole Assembly

Our fluorescence assay made it technically feasible to perform a detailed analysis of the role of the PCM in centriole assembly. The timing of SAS-4 incorporation during the first mitotic division indicates that centriole assembly occurs concurrent with the recruitment of additional PCM during mitotic entry (centrosome maturation). However, centrioles form normally in *air-1(RNAi)* embryos in which centrosome maturation does not occur (Hannak et al., 2001), demonstrating that centriole assembly does not require the mitosis-specific recruitment of PCM. Conversely, centrosome maturation occurs normally in embryos depleted of ZYG-1, SAS-4, SAS-5, and SAS-6, in which centriole assembly fails (O'Connell et al., 2001; Kirkham et al., 2003; Leidel and Gonczy, 2003; Delattre et al., 2004; and this study). Thus, centriole assembly and the recruitment of additional PCM during centrosome maturation are independent events.

Although maturation is not required, our data do provide strong evidence for a role for the PCM in centriole assembly. We show that two proteins that localize to the PCM, SPD-5 (required for the formation of the PCM; Hamill et al., 2002) and γ -tubulin (required for centrosomal microtubule nucleation; Hannak et al., 2002; Strome et al., 2001), contribute to the formation of new centrioles. A role for γ -tubulin in centriole assembly is consistent with previous work in *Tetrahymena* and *Paramecium*, where inhibition of γ -tubulin expression caused defects in basal body duplication (Ruiz et al., 1999; Shang et al., 2002). The fact that we observe a defect in a rapidly dividing embryonic system in which γ -tubulin depletion does not halt cell growth or cell cycle progression (Hannak et al., 2002; Strome et al., 2001) strongly supports the idea that γ -tubulin has a direct role in centriole assembly.

Following depletion of γ -tubulin or SPD-5, new daughter centrioles fail to initiate ~50% of the time and the new centrioles that do form contain less SAS-4 than wild-type centrioles. The fact that centriole assembly is not completely blocked in our assay is consistent with previous work showing that older SPD-5-depleted embryos often contain multiple centrioles (Kemp et al., 2004; Pelletier et al., 2004). The partial defect in centriole assembly in SPD-5- and γ -tubulin-depleted embryos is in contrast to the complete block observed following depletion of SAS-4, SAS-5, SAS-6, ZYG-1, and SPD-2 (O'Connell et al., 2001; Kirkham et al., 2003; Leidel and Gonczy, 2003; Delattre et al., 2004; and this study). Previously, we have shown that our γ -tubulin RNAi conditions reduce the amount of centrosomal γ -tubulin to ~2% of wild-type levels (Hannak et al., 2002). Here we show that centrosomal SPD-5 is similarly depleted following SPD-5 RNAi (0.23% of wild-type levels). Although we cannot exclude the possibility that the residual centriole assembly that we observe results from a small amount of remaining protein, the interpretation we favor is that the partial defect in centriole assembly in SPD-5- and γ -tubulin-depleted embryos represents the complete loss-of-function phenotypes for these proteins.

What is the nature of the centriole assembly defect in γ -tubulin/SPD-5-depleted embryos? Our previous characterization of SAS-4 demonstrated that partial reduction of the level of centriolar SAS-4 results in the assembly of partial centrioles, as assayed by serial-section EM and by reduced ability to recruit PCM components such as γ -tubulin (Kirkham et al., 2003). This analysis strongly supports the idea that the centrioles containing reduced levels of SAS-4 that form in γ -tubulin/SPD-5-depleted embryos are either less than full length or structurally defective. One possibility is that γ -tubulin/SPD-5 contribute to the generation of a template that directs new centriole assembly. In depleted embryos, some centriole assembly occurs, but the resulting structures are abnormal. Alternatively, γ -tubulin/SPD-5 might normally function to accelerate the kinetics of centriole assembly. In this case, new centrioles may be structurally normal but fail to elongate to their normal length within the time constraints imposed by the rapid cell cycles of the early *C. elegans* embryo. Resolving this issue is an important future direction that will require structural analysis by 3D EM tomography.

One of our most intriguing findings is a role in centriole formation for SPD-5. In SPD-5-depleted embryos, all of the PCM components that have been tested, including γ -tubulin, fail to concentrate around the centrioles (Hammill et al., 2002; Kemp et al., 2004; Pelletier et al., 2004). One attractive possibility suggested by our data is that assembly of PCM around the parent centriole is required to generate a local concentration of γ -tubulin, which in turn promotes centriole formation. Consistent with this idea, depletion of γ -tubulin alone can recapitulate the centriole assembly defect seen in SPD-5-depleted embryos without preventing the recruitment of other PCM proteins.

Experimental Procedures

Worm Strains and Culture Conditions

Strains coexpressing GFP:histone and GFP: γ -tubulin (TH32), and GFP:histone and GFP: β -tubulin (XA3501), were described previously

(Askjaer et al., 2002; Desai et al., 2003). The centriole assembly assay strain OD19 was obtained by mating BA17 and DP38 to generate a *fem-1(hc17)*, *unc-119(ed3)* strain. Males expressing GFP:SAS-4 (TH26; Kirkham et al., 2003) were mated to this strain, F2 individuals were singled, and a line homozygous for the temperature-sensitive female-sterile mutation *fem-1(hc17)* and positive for the GFP:SAS-4 transgene was identified. Strain genotypes are listed in Supplemental Table S1. Strains were maintained at 16°C (OD19) or 20°C (TH32, XA3501). For the SAS-4 incorporation assay, OD19 was shifted to 25°C as L4 larvae. L4 progeny of shifted worms were injected with dsRNA and mated to wild-type (N2 Bristol) males. OD19 worms raised to the L4 larval stage at 25°C remain female-sterile even if returned to the permissive temperature (16°C).

RNA-Mediated Interference

dsRNA was prepared as described (Oegema et al., 2001). DNA templates were prepared by using the primers listed in Supplemental Table S2 to amplify regions of genomic N2 DNA or specific cDNAs, as indicated. For depletion of γ -tubulin and AIR-1, the RNAi conditions described previously that led to penetrant depletion were used (Hannak et al., 2001, 2002). For all other depletions, L4 larvae were incubated at 16°C for 48 hr following dsRNA injection, prior to analysis of their embryos.

Live Imaging

Live imaging of embryos coexpressing GFP: γ -tubulin and GFP:histone was performed as described (Desai et al., 2003).

Immunofluorescence, Fixed Imaging, and Quantification of Centrosomal Fluorescence

Antibodies to γ -tubulin and AIR-1 were described previously (Hannak et al., 2001). Goat anti-GFP was a gift from David Drechsel (MPI-CBG, Dresden, Germany). Polyclonal antibodies against SAS-4 (residues 181–300), ZYG-1 (201–402), SAS-5 (1–210), SPD-2 (2–200), and SPD-5 (392–550) as well as peptide antibodies to the C-terminal 17 amino acids of SAS-5 and the C-terminal 19 amino acids of SAS-6 were raised, affinity-purified, and directly labeled as described (Oegema et al., 2001). DM1 α (Sigma) was used at a dilution of 1:1000. All other antibodies were used at a concentration of 1 μ g/ml. Embryos were fixed and processed for immunofluorescence as described (Oegema et al., 2001). 3D widefield data sets collected using a 100 \times 1.3 NA PlanApochromat lens on a DeltaVision microscope were computationally deconvolved and projected using SoftWorx software (Applied Precision). Quantification of centrosomal fluorescence was performed on deconvolved 3D image stacks as described (Hannak et al., 2002).

Staging of Fixed Embryos

Embryos were assigned to early, middle, and late prophase based on DNA and microtubule morphology (see Supplemental Figure S1). AIR-1, SPD-2, γ -tubulin, and SPD-5-depleted embryos were considered to be in late prophase of the first mitotic division if they had the expected number of fully condensed chromosomes, but the nuclear envelope was still intact (as assessed by exclusion of cytoplasmic GFP and tubulin fluorescence). Prometaphase/metaphase embryos had a similar DNA morphology to late prophase embryos, but the nuclear envelope had broken down. Prometaphase and metaphase embryos were grouped together because we could not distinguish between these stages in the absence of an intact spindle. Embryos at a stage analogous to anaphase/telophase in wild-type were identified by their DNA and microtubule morphology. Exit from mitosis was marked by aggregation of chromosomes and a marked increase in microtubule assembly in the vicinity of the chromatin. Separated sister chromatids were also frequently observed. DNA decondensation was further evident in late telophase embryos. This analysis was facilitated by comparison with aligned time-lapse sequences taken in the GFP: β -tubulin and GFP:histone line (see examples in Supplemental Movies S7–S11). Note that none of the molecular perturbations performed blocked cell cycle progression.

Correlative DIC/Transmission Electron Microscopy and Immunoelectron Microscopy

Correlative DIC/transmission EM and immuno-EM using the SAS-5 and SAS-6 peptide antibodies were performed as described (Kirkham et al., 2003).

Immunoblotting

Western blotting of *spd-5(RNAi)* and wild-type control worms was performed as described (Hannak et al., 2001).

Bioinformatics

BLASTP searches against the nonredundant database (May 2004 release) were performed using the NCBI-BLAST stand-alone software package. Multiple sequence alignments generated using ClustalX were manually refined.

Cloning of HsSAS-6 and Localization in Human Cells

Full-length HsSAS-6 was amplified by PCR from a HeLa cDNA library (provided by Jagesh Shah, UCSD, CA) and cloned into the expression vector pEYFP-C1 (Clontech). T98G human glioblastoma multiforme cells were maintained in DMEM supplemented with 10% FBS in a humidified 37°C, 5% CO₂ atmosphere. Transient transfections were performed by calcium phosphate precipitation. Cells were fixed for 10 min in methanol at -20°C 24 hr after transfection. For these experiments, γ -tubulin and microtubules were visualized using mouse (GTU-88, Sigma) and rat (YOL1/34, Abcam) monoclonal antibodies, respectively.

Acknowledgments

We thank Tony Hyman and the members of the Oegema, Desai, and Hyman labs for their support. We are grateful to Jagesh Shah (UCSD, CA), David Drechsel, Mike Tipword, and Martine Ruer (MPI-CBG, Dresden, Germany) for reagents; Anne Schwager for technical assistance; the *Caenorhabditis* Genetics Center (University of Minnesota, Minneapolis, MN) for strains; and Yuji Kohara (National Institute of Genetics, Mishima, Japan) for gene-specific cDNAs. This work is supported by funding from the Ludwig Institute for Cancer Research to K.O. and A.D. L.P. is supported by a postdoctoral fellowship from the HFSP. A.D. is a Damon Runyon Scholar supported by the Damon Runyon Cancer Research Foundation (DRS 38-04). K.O. is a Pew Scholar in the Biomedical Sciences.

Received: June 23, 2004

Revised: September 9, 2004

Accepted: October 12, 2004

Published: December 6, 2004

References

- Andersen, J.S., Wilkinson, C.J., Mayor, T., Mortensen, P., Nigg, E.A., and Mann, M. (2003). Proteomic characterization of the human centrosome by protein correlation profiling. *Nature* **426**, 570–574.
- Anderson, R.G.W., and Brenner, R.M. (1971). The formation of basal bodies (centrioles) in the rhesus monkey oviduct. *J. Cell Biol.* **50**, 10–34.
- Askjaer, P., Galy, V., Hannak, E., and Mattaj, I.W. (2002). Ran GTPase cycle and importins alpha and beta are essential for spindle formation and nuclear envelope assembly in living *Caenorhabditis elegans* embryos. *Mol. Biol. Cell* **13**, 4355–4370.
- Bobinnec, Y., Khodjakov, A., Mir, L.M., Rieder, C.L., Edde, B., and Bornens, M. (1998). Centriole disassembly in vivo and its effect on centrosome structure and function in vertebrate cells. *J. Cell Biol.* **143**, 1575–1589.
- Bornens, M. (2002). Centrosome composition and microtubule anchoring mechanisms. *Curr. Opin. Cell Biol.* **14**, 25–34.
- Delattre, M., and Gonczy, P. (2004). The arithmetic of centrosome biogenesis. *J. Cell Sci.* **117**, 1619–1630.
- Delattre, M., Leidel, S., Wani, K., Baumer, K., Bamat, J., Schnabel, H., Feichtinger, R., Schnabel, R., and Gonczy, P. (2004). Centriolar SAS-5 is required for centrosome duplication in *C. elegans*. *Nat. Cell Biol.* **6**, 656–664.
- Desai, A., Rybina, S., Muller-Reichert, T., Shevchenko, A., Hyman, A., and Oegema, K. (2003). KNL-1 directs assembly of the microtubule-binding interface of the kinetochore in *C. elegans*. *Genes Dev.* **17**, 2421–2435.
- Dutcher, S.K. (2003). Long-lost relatives reappear: identification of

new members of the tubulin superfamily. *Curr. Opin. Microbiol.* **6**, 634–640.

Grant, B.D., and Wilkinson, H.A. (2003). Functional genomic maps in *Caenorhabditis elegans*. *Curr. Opin. Cell Biol.* **15**, 206–212.

Hamill, D.R., Severson, A.F., Carter, J.C., and Bowerman, B. (2002). Centrosome maturation and mitotic spindle assembly in *C. elegans* require SPD-5, a protein with multiple coiled-coil domains. *Dev. Cell* **3**, 673–684.

Hannak, E., Kirkham, M., Hyman, A.A., and Oegema, K. (2001). Aurora-A kinase is required for centrosome maturation in *Caenorhabditis elegans*. *J. Cell Biol.* **155**, 1109–1116.

Hannak, E., Oegema, K., Kirkham, M., Gonczy, P., Habermann, B., and Hyman, A.A. (2002). The kinetically dominant assembly pathway for centrosomal asters in *Caenorhabditis elegans* is gamma-tubulin dependent. *J. Cell Biol.* **157**, 591–602.

Kemp, C.A., Kopish, K.R., Zipperlen, P., Ahringer, J., and O'Connell, K.F. (2004). Centrosome maturation and duplication in *C. elegans* require the coiled-coil protein SPD-2. *Dev. Cell* **6**, 511–523.

Khodjakov, A., Rieder, C.L., Sluder, G., Cassels, G., Sibon, O., and Wang, C.L. (2002). De novo formation of centrosomes in vertebrate cells arrested during S phase. *J. Cell Biol.* **158**, 1171–1181.

Kirkham, M., Muller-Reichert, T., Oegema, K., Grill, S., and Hyman, A.A. (2003). SAS-4 is a *C. elegans* centriolar protein that controls centrosome size. *Cell* **112**, 575–587.

Kochanski, R.S., and Borisy, G.G. (1990). Mode of centriole duplication and distribution. *J. Cell Biol.* **110**, 1599–1605.

Kubo, A., Sasaki, H., Yuba-Kubo, A., Tsukita, S., and Shiina, N. (1999). Centriolar satellites: molecular characterization, ATP-dependent movement toward centrioles and possible involvement in cilio-genesis. *J. Cell Biol.* **147**, 969–980.

Leidel, S., and Gonczy, P. (2003). SAS-4 is essential for centrosome duplication in *C. elegans* and is recruited to daughter centrioles once per cell cycle. *Dev. Cell* **4**, 431–439.

Marshall, W.F. (2001). Centrioles take center stage. *Curr. Biol.* **11**, R487–R496.

Matsuura, K., Lefebvre, P.A., Kamiya, R., and Hirono, M. (2004). Bld10p, a novel protein essential for basal body assembly in *Chlamydomonas*: localization to the cartwheel, the first ninefold symmetrical structure appearing during assembly. *J. Cell Biol.* **165**, 663–671.

Mazia, D., Harris, P., and Bibring, T. (1960). The multiplicity of the mitotic centers and the time-course of their duplication and separation. *Biophys. Biochem. Cytol.* **7**, 1–20.

Mizukami, I., and Gall, J. (1966). Centriole replication. II. Sperm formation in the fern, *Marsilea*, and the cycad, *Zamia*. *J. Cell Biol.* **29**, 97–111.

Montgomery, M.K., and Fire, A. (1998). Double-stranded RNA as a mediator in sequence-specific genetic silencing and co-suppression. *Trends Genet.* **14**, 255–258.

Moritz, M., Zheng, Y., Alberts, B.M., and Oegema, K. (1998). Recruitment of the gamma-tubulin ring complex to *Drosophila* salt-stripped centrosome scaffolds. *J. Cell Biol.* **142**, 775–786.

Nelson, G.A., Lew, K.K., and Ward, S. (1978). Intersex, a temperature-sensitive mutant of the nematode *Caenorhabditis elegans*. *Dev. Biol.* **66**, 386–409.

O'Connell, K.F., Caron, C., Kopish, K.R., Hurd, D.D., Kempfues, K.J., Li, Y., and White, J.G. (2001). The *C. elegans* zyg-1 gene encodes a regulator of centrosome duplication with distinct maternal and paternal roles in the embryo. *Cell* **105**, 547–558.

Oegema, K., Desai, A., Rybina, S., Kirkham, M., and Hyman, A.A. (2001). Functional analysis of kinetochore assembly in *Caenorhabditis elegans*. *J. Cell Biol.* **153**, 1209–1226.

Pelletier, L., Özlü, N., Hannak, E., Cowan, C., Habermann, B., Ruer, M., Müller-Reichert, T., and Hyman, A.A. (2004). The *Caenorhabditis elegans* centrosomal protein SPD-2 is required for both pericentriolar material recruitment and centriole duplication. *Curr. Biol.* **14**, 863–873.

Preble, A.M., Giddings, T.M., Jr., and Dutcher, S.K. (2000). Basal bodies and centrioles: their function and structure. *Curr. Top. Dev. Biol.* **49**, 207–233.

- Rieder, C.L., Faruki, S., and Khodjakov, A. (2001). The centrosome in vertebrates: more than a microtubule-organizing center. *Trends Cell Biol.* *11*, 413–419.
- Ruiz, F., Beisson, J., Rossier, J., and Dupuis-Williams, P. (1999). Basal body duplication in *Paramecium* requires gamma-tubulin. *Curr. Biol.* *9*, 43–46.
- Salisbury, J., Suino, K., Busby, R., and Springett, M. (2002). Centrin-2 is required for centriole duplication in mammalian cells. *Curr. Biol.* *12*, 1287–1292.
- Schnackenberg, B.J., Khodjakov, A., Rieder, C.L., and Palazzo, R.E. (1998). The disassembly and reassembly of functional centrosomes in vitro. *Proc. Natl. Acad. Sci. USA* *95*, 9295–9300.
- Shang, Y., Li, B., and Gorovsky, M.A. (2002). *Tetrahymena thermophila* contains a conventional gamma-tubulin that is differentially required for the maintenance of different microtubule-organizing centers. *J. Cell Biol.* *158*, 1195–1206.
- Sluder, G., and Rieder, C.L. (1985). Centriole number and the reproductive capacity of spindle poles. *J. Cell Biol.* *100*, 887–896.
- Snell, W.J., Pan, J., and Wang, Q. (2004). Cilia and flagella revealed; from flagellar assembly in *Chlamydomonas* to human obesity disorders. *Cell* *117*, 693–697.
- Strome, S., Powers, J., Dunn, M., Reese, K., Malone, C.J., White, J., Seydoux, G., and Saxton, W. (2001). Spindle dynamics and the role of gamma-tubulin in early *Caenorhabditis elegans* embryos. *Mol. Biol. Cell* *12*, 1751–1764.

Note Added in Proof

While this manuscript was in press, Raynaud-Messina et al. reported similar defects in centriole assembly following γ -tubulin depletion in *Drosophila* S2 cells (Raynaud-Messina, B., Mazzolini, L., Moisand, A., Cirinesi, A.M., and Wright, M. (2004). Elongation of centriolar microtubule triplets contributes to the formation of the mitotic spindle in γ -tubulin-depleted cells. *J. Cell Sci.* *117*, 5497–5507).

The *Caenorhabditis elegans* Centrosomal Protein SPD-2 Is Required for both Pericentriolar Material Recruitment and Centriole Duplication

Laurence Pelletier,^{1,*} Nurhan Özlü,¹ Eva Hannak,^{1,2}
Carrie Cowan,¹ Bianca Habermann,³
Martine Ruer,¹ Thomas Müller-Reichert,¹
and Anthony A. Hyman¹

¹Max Planck Institute of Molecular Cell Biology
and Genetics
Pfotenhauerstrasse 108
01307 Dresden
Germany

Summary

Background: The centrosome is composed of a centriole pair and pericentriolar material (PCM). By marking the site of PCM assembly, the centrioles define the number of centrosomes present in the cell. The PCM, in turn, is responsible for the microtubule (MT) nucleation activity of centrosomes. Therefore, in order to assemble a functional bipolar mitotic spindle, a cell needs to control both centriole duplication and PCM recruitment. To date, however, the molecular mechanisms that govern these two processes still remain poorly understood.

Results: Here we show that SPD-2 is a novel component of the *C. elegans* centrosome. SPD-2 localizes to the centriole throughout the cell cycle and accumulates on the PCM during mitosis. We show that SPD-2 requires SPD-5 for its accumulation on the PCM and that in the absence of SPD-2, centrosome assembly fails. We further show that centriole duplication is also defective in *spd-2(RNAi)* embryos, but not in *spd-5(RNAi)* embryos, where PCM recruitment is efficiently blocked.

Conclusions: Taken together, our results suggest that SPD-2 may link PCM recruitment and centriole duplication in *C. elegans*. SPD-2 shares homology with a human centrosome protein, suggesting that this key component of the *C. elegans* centrosome is evolutionarily conserved.

Introduction

The centrosome, or microtubule organizing center (MTOC), is the major site of microtubule (MT) nucleation in animal cells (For reviews see [1, 2]). It is responsible for the organization of the interphase array of MTs and, during mitosis, the organization of the two spindle poles. Defects in centrosome function can lead to an inability to correctly assemble a mitotic spindle and, therefore, contribute to genomic instability and cancer progression [3].

Centrosomes are composed of a pair of orthogonally oriented centrioles surrounded by an electron-dense proteinaceous lattice termed the pericentriolar material

(PCM). The PCM is the major site of MT nucleation and anchoring both in interphase and mitosis [4]. During interphase, the centrosomes contain a relatively small amount of PCM components. In preparation for mitosis, the centrosomes accumulate 3- to 5-fold more PCM components, thereby increasing their size and MT nucleation capacity (a process called centrosome maturation) [5, 6]. The onset of centrosome maturation coincides with the activation of Cdk-1 and is regulated, at least in part, through Aurora-A and Polo-like kinases [7–10, 44].

The centrioles define the site of PCM assembly, and therefore, by controlling the centriole duplication cycle, a cell ensures it has a single centrosome during interphase and two during mitosis. In mammalian cells, centrosome duplication is initiated by the disorientation of the mother and daughter centrioles and is regulated by the cyclin-dependent kinase Cdk2 and cyclin A/E [11, 12]. After centriole disorientation, a precursor of the daughter centrioles forms at right angles to the mother centrioles where the daughter centrioles begin elongating, reaching their full-length by G2/M. The cohesion between the original mother and daughter centrioles is maintained by C-Nap1 [13, 14], the phosphorylation of which by Nek2 is thought to initiate the separation of the duplicated centrosomes [15, 16]. At the time of nuclear envelope breakdown (NEBD), the separated centrosomes begin organizing the poles of the mitotic spindle, with each pole containing a centriole pair.

Caenorhabditis elegans has proven to be an amenable system to study centrosome assembly. The centrioles in *C. elegans*, rather than containing the usual nine triplet MTs with associated appendages, are instead composed of nine singlet MTs with much less-prominent appendages [17]. To date, two *C. elegans* centriolar components have been identified; the core centriolar protein SAS-4 [18, 19], which remains associated with the centriole once it has formed, and ZYG-1 [20], a kinase that controls centriole duplication by localizing transiently to the centrioles at anaphase. In *C. elegans*, the centrioles are eliminated during oogenesis and are provided by the sperm upon fertilization [21]. SAS-4 is present on the sperm centriole, and its intensity stays relatively constant as one or two bright dots at the center of the centrosome after fertilization and throughout the cell cycle [18, 19]. After fertilization, PCM components are recruited to the sperm-provided centrioles [21–24]. The most upstream component implicated in PCM recruitment so far identified is SPD-5, a protein with multiple coiled-coil domains [22]. SPD-5 directs the recruitment of other known PCM components in *C. elegans*, including γ -tubulin, ZYG-9, and AIR-1 [22]. As the embryos progress further into mitosis the rate of PCM recruitment increases significantly in a process called centrosome maturation, which is regulated, at least in part, by the *C. elegans* ortholog of Aurora-A, AIR-1 [23].

To date, most of the known *C. elegans* centrosomal components identified are required for normal spindle assembly in the early embryo [20, 22–27]. To identify

*Correspondence: pelletie@mpi-cbg.de

²Present address: Department of Molecular and Cell Biology, University of California, Berkeley, 315 LSA, Berkeley, CA 94720-3200.

³Present address: Scionics Computer Innovation, Pfotenhauerstrasse 110, 01307 Dresden, Germany.

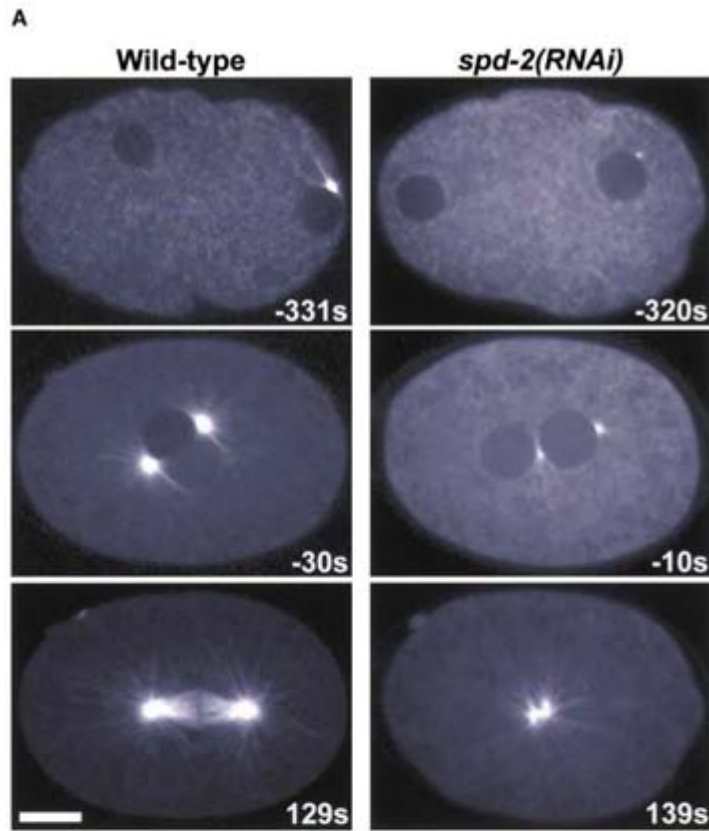
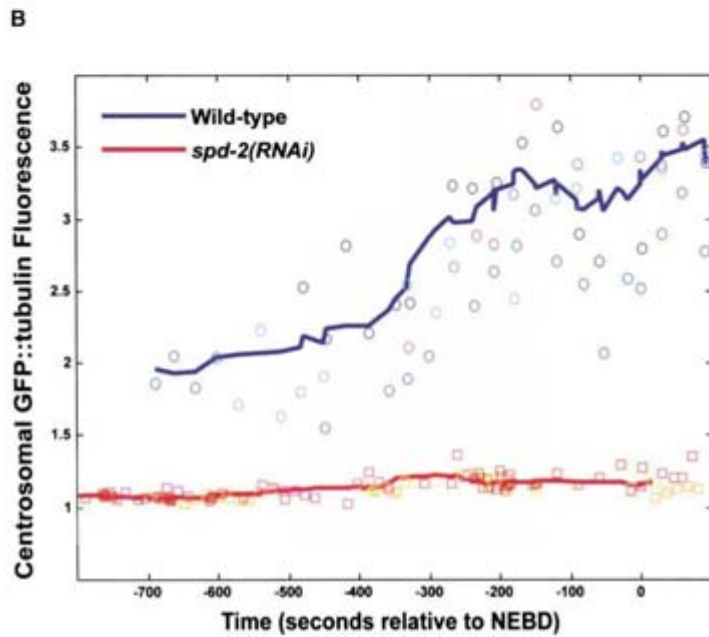


Figure 1. SPD-2 Is Required for Spindle Assembly

(A) Panels summarizing time-lapse movies of wt and *spd-2(RNAi)* embryos expressing GFP:: β -tubulin. In wt embryos, MT asters were detected at an early stage and increased in size as the embryos progressed through mitosis, reaching a maximum at the metaphase/anaphase transition. In *spd-2(RNAi)* embryos, although detectable, MT asters did not increase significantly in size, and spindle assembly failed. The indicated times are in seconds relative to NEBD. Also see Movies 1 and 2 in the Supplemental Data. (B) The fluorescence intensity of GFP:: β -tubulin at centrosomes in wt ($n = 4$) and *spd-2(RNAi)* embryos ($n = 4$) was quantified and shown either as individual data points (circles are wt, squares are *spd-2(RNAi)* embryos) or as a running average for wt (blue line) or *spd-2(RNAi)* (red line) embryos. Note the absence of MT build-up at the centrosomes prior to NEBD in *spd-2(RNAi)* embryos.



novel centrosomal components, we began analyzing genes exhibiting such defects when targeted by RNAi. Here we characterize *spd-2* (F32H2.3), a gene previously shown to be required for spindle assembly by differential interference contrast (DIC) time-lapse microscopy in which mutants have been identified [28–30] ([46], NCBI accession number AAQ17186). Here we show that SPD-2 is a component of the *C. elegans* centrosome required not only for PCM recruitment but also for centriole duplication. In addition, we provide bioinformatics evidence suggesting that this key component of the *C. elegans* centrosome is conserved in humans.

Results

F32H2.3(RNAi) and *spd-2* embryos have previously been shown to fail in spindle assembly and to lack conspicuous sperm asters prior to polarization [29, 30]. Sequencing of *spd-2* mutants alleles revealed that F32H2.3 is *spd-2*, and we shall therefore refer to it as *spd-2* [46]. To better understand the role of SPD-2 in the formation of MT asters, we looked at spindle assembly in *spd-2*(RNAi) embryos expressing β -tubulin tagged with GFP (Figure 1A). Our results confirmed the spindle assembly defect previously observed by DIC but, in addition, showed that the amount of MTs at centrosomes in *spd-2*(RNAi) embryos did not increase significantly prior to NEBD, remaining 2- to 3.5-fold lower than in wt embryos throughout the cell cycle (Figures 1A and 1B and Movies 1 and 2). Upon NEBD, MTs began associating with the condensed chromosomes, a situation also observed in *spd-2* and *spd-5* mutants that may represent a chromatin-based mode of MT nucleation [22, 30]. Together these results suggests that the spindle assembly defect observed in *spd-2*(RNAi) embryos may be due to the inability of centrosomes to efficiently nucleate MTs, although enough MTs remain to promote centrosome separation.

SPD-2 Is a Centrosomal Component

In early *C. elegans* embryos, SPD-2 exhibited a two-tiered distribution: a bright, central spot surrounded by a peripheral dimmer halo (Figure 2A, wild-type). The staining pattern was specific for SPD-2, since no labeling above background could be observed in mitotic *spd-2*(RNAi) embryos (Figure 2A, *spd-2*(RNAi)), and was blocked by preincubating the antibody with soluble GST::SPD-2 (Figure S1). The bright, central spot suggested that SPD-2 was centriole associated. To verify this we performed immuno-electron microscopy (immuno-EM) and found that gold labeling was observed on the centrioles (Figure 2B, magnification of the boxed region) and also in the periphery of the centrioles in the area corresponding to the PCM (Figure 2B, arrows). The density of gold labeling was highest within a 100 nm radius from the center of the centrioles and quickly diminished further away from the centrioles (Figure 2B, graph). Therefore, we conclude that SPD-2 is a centrosomal component that localizes to the centrioles and also the PCM.

We compared the spatial and temporal distribution of SPD-2 to known centrosome and centriole components. In mature sperm, SPD-2 colocalized with SAS-4 on the

sperm centriole (Figure 2C). The fact that centriolar labeling was lost after the fertilization of *spd-2*(RNAi) embryos suggests that SPD-2 is not stably associated with the centriolar structure (Figure 2A). Labeling was also observed surrounding the sperm nucleus, although we could not confirm the specificity of this labeling by *spd-2*(RNAi) given that RNAi does not work efficiently in the sperm (Figure 2C). Shortly after fertilization, during female meiosis, the amount of SPD-2 on the centriole remained largely unchanged. SPD-5 or γ -tubulin were not detected on the centrosome and no MT nucleation was observed (Figure 2D, top, and data not shown). Upon the completion of meiosis, SPD-2 levels began increasing, coincident with the accumulation of SPD-5 and the onset of MT nucleation (Figure 2D, middle and bottom). As the embryos entered mitosis, SPD-2 maintained its centriolar localization but, during centrosome maturation, accumulated on the PCM, coincident with the increase of γ -tubulin and SPD-5 levels (Figures 3A and S2B).

SPD-2 May Be an Evolutionary Conserved Centrosomal Component

To determine if *C. elegans* SPD-2 had homologs in other species, we performed database searches with the sequence of the *Caenorhabditis briggsae* ortholog of SPD-2. One human protein (KIAA1569 and FLJ00145) and one *Drosophila melanogaster* protein (CG17286) with homology to SPD-2 were identified (Figure 3B). Back-Blast searches with these two proteins identified *C. elegans* SPD-2, thereby confirming the homology. Six putative CDK phosphorylation sites conserved in both nematodes were identified (Figure 3B). Interestingly, the human homolog of SPD-2 was recently shown to be a component of the mammalian centrosome [31]. We therefore would like to propose that KIAA1569 and CG17286 represent the human and *D. melanogaster* orthologs of SPD-2. The homology between the putative SPD-2 orthologs is restricted to a 200 amino acid domain that we named the SPD-2 domain. In nematodes, this domain is present in the C-terminal part of the proteins. The SPD-2 domains of *C. elegans* and *C. briggsae* share 46% identity and 63% similarity. This is consistent with the high degree of divergence observed between a subset of orthologous proteins in nematodes, mostly in protein families that have essential functions [32] (Figure 3B). The percent identity/similarity between the *C. elegans* SPD-2 domain and its human and fly orthologs are 15%/36% and 14%/34%, respectively (Figure 3B). Like *C. elegans* SPD-2, its orthologs possess a large, predicted coiled-coil domain adjacent to the SPD-2 domain. Further analysis of the SPD-2 domain revealed that its first 100 amino acids also share homology to members of the abnormal spindle proteins (Asp, Figure 3C), which have also been associated with centrosome function [33–36]. In this case, the percent identity/similarity between *C. briggsae*, which is more closely related in sequence to humans than is *C. elegans*, and the human and mouse Asp proteins are 20%/35% and 24%/38%, respectively. Although not addressed experimentally, these results suggest that SPD-2 is an evolutionarily conserved centrosomal component and that the function of the SPD-2 domain may also be conserved.

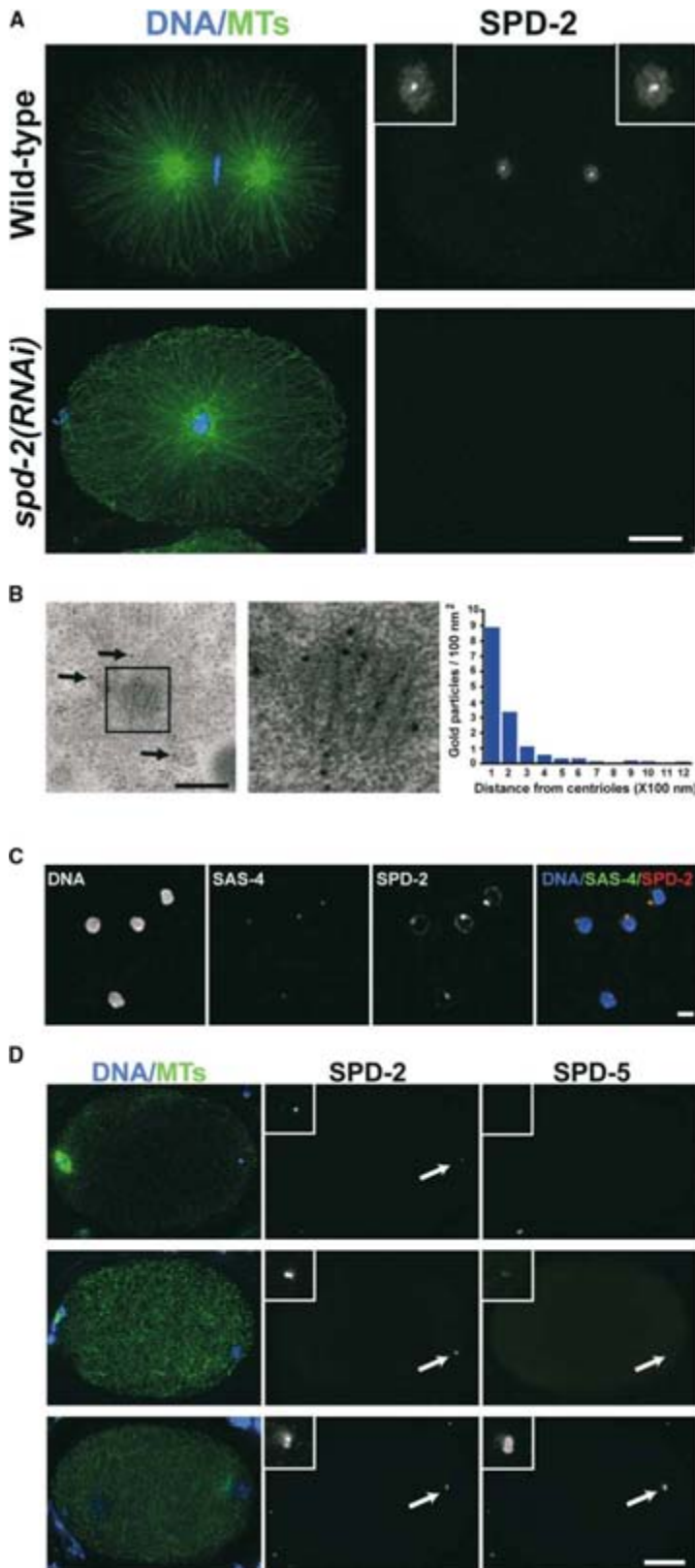


Figure 2. SPD-2 Is a Component of the *C. elegans* Centrosome

(A) wt and *spd-2(RNAi)* embryos were labeled for DNA (blue), MTs (green), and SPD-2. Labeling of SPD-2 in wt embryos was restricted to the centrosome and was two tiered; a bright, central spot was surrounded by a dimmer halo. No labeling could be detected in *spd-2(RNAi)* embryos confirming the specificity of our antibody. Merged images of the DNA and MT labelings are shown. Bar is 10 μ m.

(B) Immuno-EM of wt embryos using SPD-2 antibodies. Labeling was observed on the centrioles (see higher magnification of boxed region) and in the periphery of centrioles, in the region corresponding to the PCM (arrows). The density of gold labeling is plotted against the distance from the centriole (gold particles/100 nm²). The labeling density was highest within 100 nm of the centriole. Bar is 250 nm.

(C) Mature sperms were labeled for DNA (blue), SAS-4 (green), and SPD-2 (red). Note that SPD-2 and SAS-4 are both found on the sperm centriole. Bar is 1 μ m.

(D) Embryos shortly after fertilization (top), further into female meiosis (middle), and shortly after the completion of female meiosis (bottom) were labeled for DNA (blue), MTs (green), SPD-2, and SPD-5. Note that SPD-5 localizes to the centrosomes after SPD-2. Merged images of the DNA and MT labelings are shown. Bar is 10 μ m.

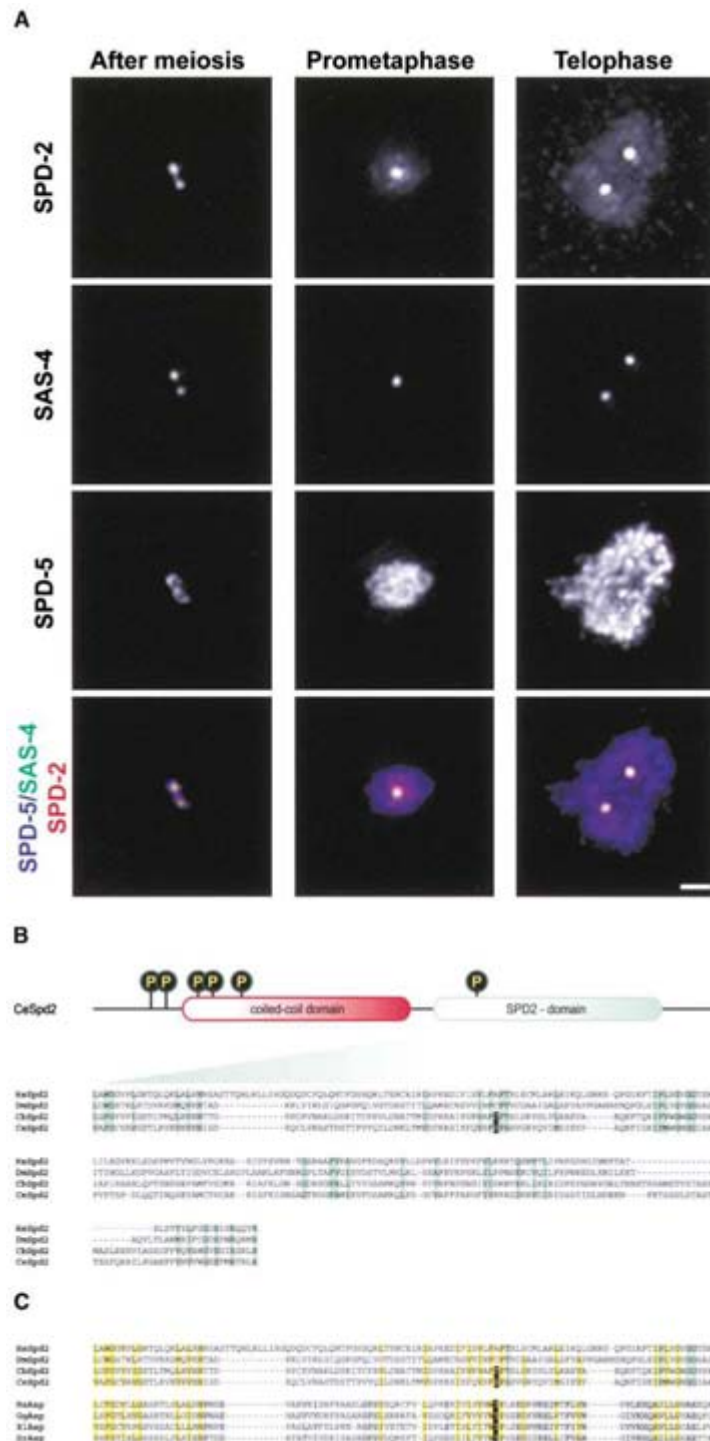


Figure 3. Centrosomal Distribution of SPD-2 during the First Cell Division and the Domain Structure of SPD-2 Homologs

(A) wt embryos after meiosis, at prometaphase, and at telophase were stained for DNA (not shown), SPD-2 (red), SAS-4 (green), and SPD-5 (blue). See Figure S2A for the stages analyzed. Merged images at the three different stages are also shown. Bar is 1 μ m. Note that SPD-2 localizes to both the PCM and the centrioles.

(B) Domain structure of *C. elegans* SPD-2 and multiple sequence alignment of the putative SPD-2 orthologs. SPD-2 contains a coiled-coil domain (aa 200–470, red box) and a SPD-2 domain (aa 484–714, green box) defined by similarity to its orthologs in other species. By comparing *C. elegans* and *C. briggsae* SPD-2, we identified six conserved CDK phosphorylation sites (consensus sequence: [ST]-P, indicated by black circles; aa positions 143, 171, 220, 233, 259 and 545 in *C. elegans* SPD-2). The putative phosphorylation site within the SPD-2 domain that is conserved in nematodes is not present in other eukaryotes. The conserved residues are boxed in green; the putative CDK phosphorylation sites are boxed in black with yellow lettering.

(C) Multiple sequence alignment of the N-terminal region of the SPD-2 domain with the homologous region of vertebrate abnormal spindle proteins (Asp). Nearly all conserved residues present within the N-terminal region of the SPD-2 domain and Asp proteins are highlighted in yellow, those that are only specific for the SPD-2 domain are boxed in green, and those that are only specific for the Asp N-terminal domain are boxed in gray. Abbreviations: Hs, *Homo sapiens*; Dm, *Drosophila melanogaster*; Cb, *Caenorhabditis briggsae*; Ce, *Caenorhabditis elegans*; Gg, *Gallus gallus*; Xi, *Xenopus laevis*; and Dr, *Danio rerio*. Additional information about the alignments and accession numbers of the sequences used can be found in the Supplemental Data.

SPD-2 and SPD-5 Are Mutually Required for Their Accumulation on Centrosomes

To determine whether SPD-5 was required for the centrosomal accumulation of SPD-2, we generated

transgenic worms expressing SPD-2 tagged with GFP (GFP::SPD-2). Time-lapse imaging of wt embryos showed that the level of SPD-2 present on the centrosome increased over time, reaching a maximum at the

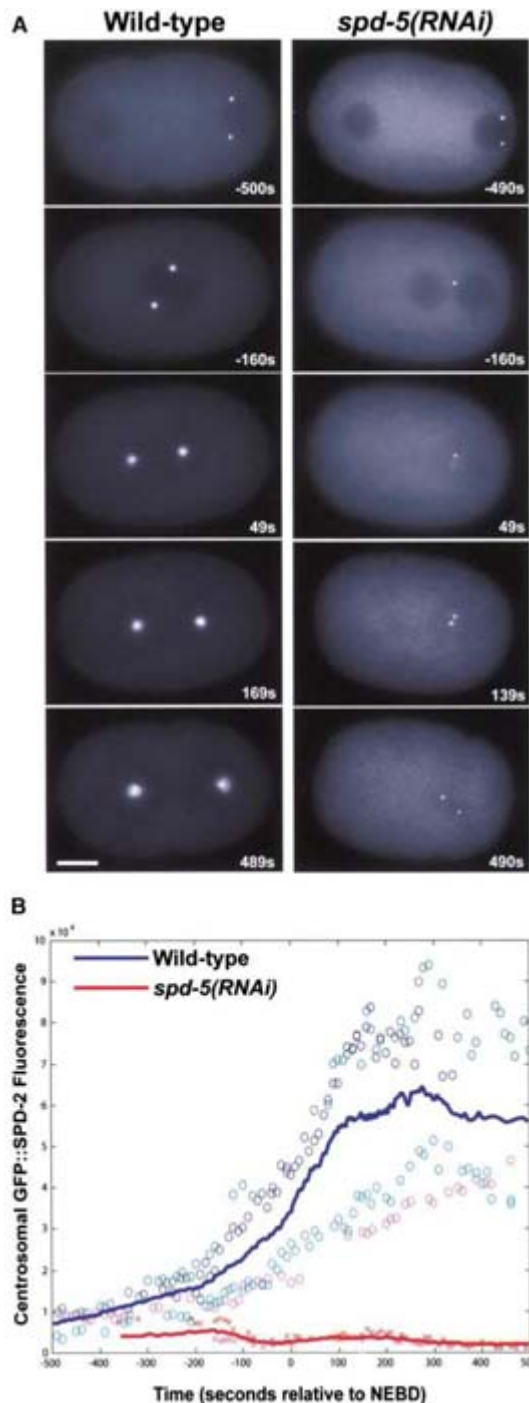


Figure 4. The Centrosomal Accumulation of SPD-2 during Centrosome Maturation Requires SPD-5

(A) wt and *spd-5(RNAi)* embryos from GFP::SPD-2 transgenic worms were submitted to time-lapse microscopy. Images acquired at different times (seconds relative to NEBD) are shown.

(B) The fluorescence intensity of wt ($n = 4$) and *spd-5(RNAi)* embryos ($n = 4$) was quantified and shown either as individual data points (circles represent wt, crosses represent *spd-5(RNAi)* embryos) or as a running average for wt (blue line) or *spd-5(RNAi)* embryos (red

metaphase to anaphase transition (Figures 4A and 4B, wild-type, and Movies 3 and 4). In *spd-5(RNAi)* embryos, no accumulation of GFP-SPD-2 could be detected as the cell progressed through mitosis, although a small structure was always present (Figures 4A and 4B, *spd-5(RNAi)*, and Movies 5 and 6). In a separate set of experiments, SPD-2 labeling was restricted to the centriolar region in *spd-5(RNAi)* embryos, as judged by its colocalization with the centriolar protein SAS-4 (data not shown). Together, these results suggest that SPD-5 is required for the accumulation of SPD-2 on the PCM, but not for its centriolar association. However, we cannot be certain that this is not due to undetectable residual SPD-5 left after RNAi. It was previously shown that the amount of SPD-5 and γ -tubulin on mitotic centrosomes is reduced in *spd-2* mutants [22, 30]. In *spd-2(RNAi)* embryos, we also observed low levels of SPD-5 on mitotic centrosomes and, consequently, low levels of γ -tubulin confirming the previously published work (Figures S3A–S3B) [22, 30]. Together, the results presented here in combination to those previously described in *spd-2* mutants, suggest that SPD-2 and SPD-5 are mutually required for their localization to the centrosome.

SPD-2 Is Required for Centriole Duplication

The prominent centriolar localization of SPD-2 suggested that it might be required for centriole function. To follow centriole duplication, we used SAS-4 as a marker of centriole number. In wt embryos at telophase, two SAS-4-positive structures could be detected at each pole of the mitotic spindle, indicating that the centrioles had duplicated and disjoined (Figure 5A, wild-type). In *spd-2(RNAi)* embryos, only two structures labeling for SAS-4 could be detected at any stage during the first cell division (Figure 5A, *spd-2(RNAi)*). In older *spd-2* embryos, in which multiple rounds of failed mitoses had occurred, no more than two structures labeling for SAS-4 could be observed (Figure 5A, *spd-2(RNAi)*).

The analysis of SAS-4 staining in *spd-2(RNAi)* embryos suggested that SPD-2 is required for centriole duplication. However other possibilities exist that can explain this observation. For instance, the centrioles could duplicate normally, but not disjoin, making the daughter centrioles undetectable at the light microscope level. Another possibility is that SAS-4 does not accumulate on the daughter centriole in the absence of maternal SPD-2. Therefore, we examined centriole number by using EM. In wt embryos, duplicated centrioles were observed at metaphase (Figure S4B). Since *spd-2* embryos do not have a bona fide metaphase, we allowed *spd-2(RNAi)* embryos to undergo pronuclear migration, pronuclear meeting, and NEBD before processing them for EM. In the four *spd-2(RNAi)* embryos serially sectioned and analyzed, only two single centrioles per embryo were observed (Figures 5B and S4C). Taken together, our immunofluorescence and EM data show conclusively that SPD-2 is required for centriole duplication in *C. elegans*.

line). Note that in the absence of SPD-5, SPD-2 does not accumulate on the centrosome. See Movies 3 and 4 (wt) and Movies 5 and 6 (*spd-5(RNAi)*) in the Supplemental Data.

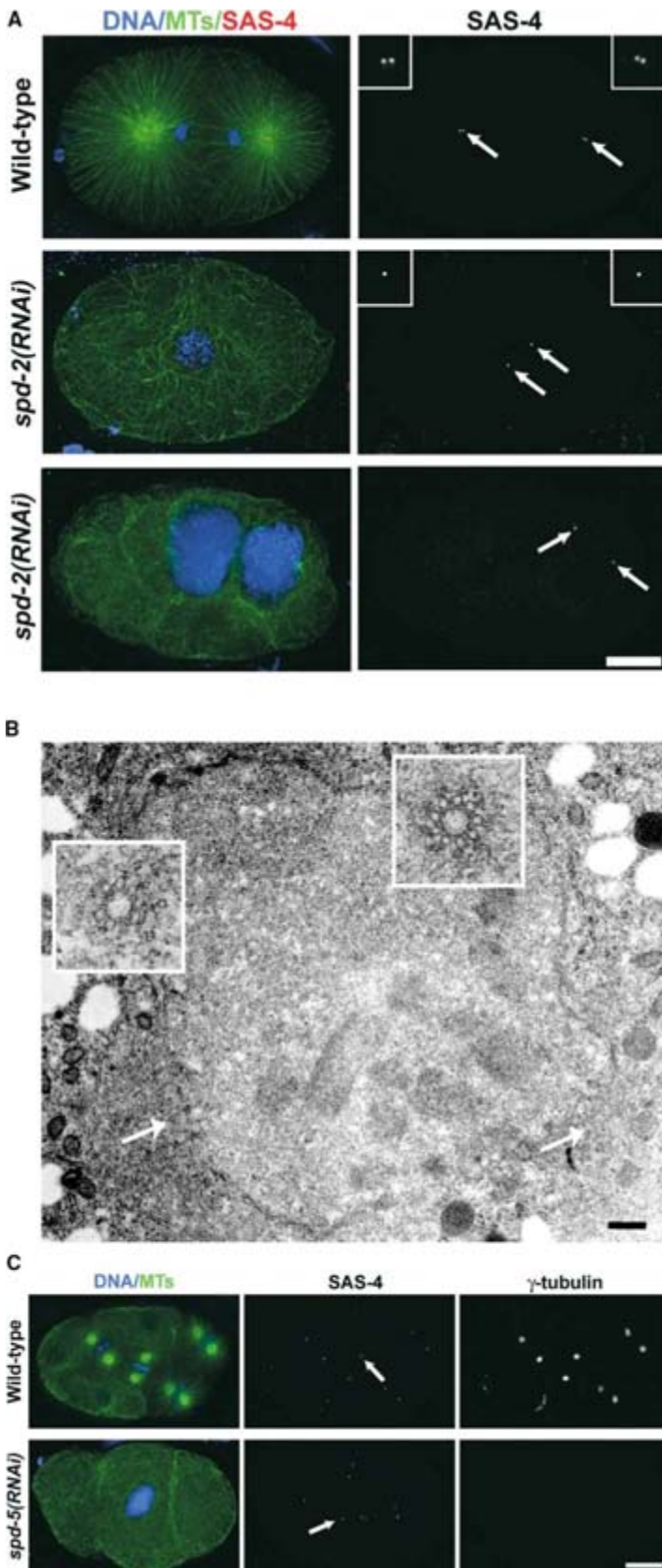


Figure 5. Centriole Duplication Also Fails in *spd-2(RNAi)* Embryos

(A) wt and *spd-2(RNAi)* embryos were fixed and stained for DNA (blue), MTs (green), and the centriolar protein SAS-4 (red). Note that in wt embryos at telophase, four structures labeling for SAS-4 were observed, two at each pole of the mitotic spindle (insets). In *spd-2(RNAi)* embryos at the end of the first cell division, only two SAS-4 positive structures were observed, suggesting that centriole duplication did not occur. In *spd-2(RNAi)* embryos allowed to undergo numerous rounds of failed mitoses, only two structures labeling for SAS-4 could be observed. Merged images of the DNA, MT, and SAS-4 labelings are shown. Bar is 10 μ m.

(B) In serially sectioned *spd-2(RNAi)* embryos, only two single centrioles were found ($n = 4$). Arrows point to the approximate position of the centrioles relative to their position in other sections. Bar is 1 μ m.

(C) wt and *spd-5(RNAi)* embryos were labeled for DNA (blue), MTs (green), SAS-4, and γ -tubulin. In a wt embryo at the 8-cell stage, two structures labeling for SAS-4 could be observed per cell (wt, SAS-4), and the centrosomes contained variable amounts of γ -tubulin depending on their cell cycle stage (wild-type, γ -tubulin). In *spd-5(RNAi)* embryos allowed to undergo numerous rounds of failed mitoses, multiple centrioles could be observed, even in the absence of γ -tubulin recruitment. Merged images of the DNA and MTs labeling are shown. Bar is 10 μ m.

We next wanted to determine if the centriole duplication defect observed in *spd-2(RNAi)* embryos was due to their failure to recruit PCM or to a more direct role of SPD-2 in centriole duplication. Since *spd-5(RNAi)* embryos are unable to recruit PCM components [22], we asked if centriole duplication still occurred in the absence of SPD-5. We allowed *spd-5(RNAi)* embryos to undergo multiple rounds of failed mitoses before looking at centriole number. Several SAS-4 structures were detected in *spd-5(RNAi)* embryos, while no significant γ -tubulin staining was observed, confirming that PCM recruitment was efficiently blocked (Figure 5C). Four GFP::SPD-2 dots were also observed at a similar stage in GFP::SPD-2 embryos derived from hermaphrodites exposed to *spd-5* dsRNA (see Movies 5 and 6). Although we cannot unequivocally refute that undetectable amounts of SPD-5 sufficient to promote centriole duplication still remain after RNAi, it should be noted that in *spd-2(RNAi)* embryos, a significant amount of SPD-5 is still present on the centriole, but centriole duplication still fails (Figure S3A). Together these results suggest that centriole duplication can still occur in the absence of SPD-5 and that the centriole duplication defect observed in *spd-2(RNAi)* embryos may be due to a specific role of SPD-2 in centriole duplication rather than a general effect caused by the failure to recruit PCM.

Discussion

In this paper we show that *C. elegans* SPD-2 is required for both centrosome assembly and centriole duplication. Through bioinformatics, we found that SPD-2 shares sequence homology to a human protein recently shown to be a component of the mammalian centrosome [31]. We have shown that spindle assembly most likely fails in *spd-2(RNAi)* embryos because centrioles are unable to efficiently recruit PCM components, a situation also observed in *spd-2* mutants [22, 30]. Three lines of evidence make us believe that the primary role of SPD-2 in PCM assembly is through the recruitment of SPD-5. First, SPD-2 is present on the sperm centriole before and after fertilization, while SPD-5 is only recruited to the centrosome after meiosis, coincident with the onset of MT nucleation [22]. Second, SPD-2 is required for the recruitment of SPD-5 to the PCM. Third, in *spd-5(RNAi)* embryos, low levels of SPD-2 are present on the centrosome, but no MT nucleation is observed, while in *spd-2(RNAi)* embryos, some SPD-5 is present and, concomitantly, low levels of MT nucleation is observed. Therefore, the MT nucleation activity of centrosomes seems to relate to the amount of SPD-5 present. We did observe that during centrosome assembly, the recruitment of SPD-2 to the PCM requires SPD-5. This suggests other possible roles for SPD-2; for instance, that SPD-2 and SPD-5 associate with the PCM as a protein complex. However, the weak PCM localization when compared to the prominent centriolar labeling suggests that this PCM localization may be secondary to its function in centrosome assembly.

The fact that spindle assembly fails in the absence of either SPD-2 or SPD-5 [22] strengthens the idea that mitotic spindle assembly requires functional centro-

somes in *C. elegans*. This is in contrast to results obtained in vitro with *Xenopus* egg extracts [37] and also in other species, such as *Drosophila*, plants and mammals, where centrosomes seem to be dispensable for spindle assembly [38–41]. One possibility is that SPD-2 and SPD-5 are also required for non centrosome-dependent spindle assembly. The other possibility is that spindles in *C. elegans* require centrosomes. It will prove interesting to further analyze if a noncentrosome spindle assembly pathway exists in *C. elegans* and, if so, why this pathway is unable to compensate for the absence of functional centrosomes.

In addition to its role in PCM recruitment, SPD-2 localizes to the centrioles and is required for their duplication. Although SPD-2 could be a core component of the centriole structure, the centriolar association of SPD-2 differs from the known core centriole protein SAS-4 [18, 19]. Both SPD-2 and SAS-4 are present on the sperm centrioles, and in both cases RNAi does not affect this localization because RNAi is largely ineffective in the male germ line [18, 19]. After exposure of hermaphrodites to *sas-4* dsRNA, the embryos produced contain SAS-4, provided by the sperm, which remains stably associated with the centriole throughout the cell cycle [18, 19]. In contrast, after exposure of hermaphrodites to *spd-2* dsRNA, the sperm-provided SPD-2 rapidly falls off the centrioles. Taken together this suggests, using the *C. elegans* definition, that unlike SAS-4, SPD-2 is not a core centriolar component but is instead associated with the centriole. While the definition of a centriole versus PCM component is somewhat semantic, in *C. elegans* embryos it does allow the comparison of components that are probably built into the centriole structure when it is being assembled and those that bind to the centriole to perform downstream functions.

Taken together, our data suggest that SPD-2 binds to the fully-formed centrioles to recruit PCM components necessary for MT nucleation and centriole duplication. Thus, SPD-2 is a good candidate to be a primary scaffolding protein that links assembly of the centriole structure to its downstream effectors. Recruitment of PCM components appears to proceed through the recruitment of SPD-5 [22]. However, since SPD-5 is not necessary for centriole duplication, SPD-2 may recruit other factors that initiate centriole duplication. To date, no such factors have been identified in *C. elegans*, but by analogy with work in mammalian cells, SPD-2 may be required to recruit CDK kinases [42, 43]. Future work on the *C. elegans* and mammalian homologs of these proteins should shed more light on this process.

Experimental Procedures

Time-Lapse Microscopy and Quantification

To generate GFP::SPD-2 transgenic worms, primers (5'-AACTAG TAATCTCTGTAATGAA-3', 5'-GGCTTAAGTTACTTCTATTCTGA-3') containing SpeI or AflIII sites (bold) were used in a PCR reaction using N2 genomic DNA as a template. The resulting fragment, corresponding to amino acids 8–828 of SPD-2, was cloned in frame to GFP to generate an N-terminal GFP::SPD-2 gene fusion in a vector containing *pie-1* promoter sequence to ensure expression of the transgene in the germline and spliced *unc-119(+)* as a selection marker. The TH42 worm strain was constructed by high-pressure ballistic bombardment (BioRad) of DP38 *unc-119(ed3)* homozygotes. Considering that 100% of the progeny were rescued for *unc-*

119 and expressed GFP, we conclude that TH42 contains an integrated copy of the transgene.

For live imaging of GFP::SPD-2, embryos were mounted as previously described [45] and imaged by using a Zeiss Axioplan II microscope equipped with a Orca 100 camera (Hamamatsu) and a 63× 1.4 NA PlanApoChromat objective (Zeiss) controlled by the Metamorph software package (Universal Imaging Corporation). Images were acquired every 10 s by using a 550 ms exposure time and 2× binning. For the quantification of centrosomal GFP:SPD-2 fluorescence, the bright centrosomal regions were circled and the average fluorescence intensity of that region along with that of an identically sized background region determined by using the Metamorph software package (Visitron Systems); from these values, the integrated fluorescence intensity was determined. To generate the graph in Figure 5B, the data for the individual experiments was combined and sorted by the time reference. A running average of the fluorescence intensity data was calculated by using a window size corresponding to 1/10 of the number of data points for wt and *spd-5(RNAi)*, and both the individual data points and the running averages were plotted using MatLab (v5.1). For time-lapse imaging of GFP::β-tubulin worms, embryos were mounted and imaged on a Zeiss Axioplan II microscope equipped with a spinning-disc confocal head (QLC100; Visitech International), an Orca 100 camera (Hamamatsu), and a 63× 1.4 NA PlanApoChromat objective (Carl Zeiss) controlled by the Metamorph software package (Universal Imaging Corp.). Images were acquired every 10 by using an 800 ms exposure time and 2× binning. For the quantification of MT build-up at centrosomes, images of wt embryos were acquired every 15 s by using a 500 ms exposure time and 2× binning ($n = 4$). For *spd-2(RNAi)* embryos, images were acquired every 10 s by using a 939 ms exposure time and 2× binning ($n = 4$). Given that different imaging parameters were used for wt and *spd-2(RNAi)* embryos, the ratio between the integrated fluorescence intensity value of the centrosomal region over that of a background region of identical area was calculated and plotted over time. The results are shown as both individual data points and running averages as described above.

Electron Microscopy

Correlative DIC/TEM was carried out as described [18]. A single wt or *spd-2(RNAi)* early embryo was transferred to a marked region on an aclar coverslip (Electron Microscopy Sciences) that was previously glow discharged and coated with 1% poly-L-lysine (Sigma, P1524) in PBS. The aclar coverslip was mounted on an inverted Zeiss Axiovert 200M microscope, and the embryos were imaged through the aclar by using DIC. Embryos were placed in fixing solution (1× PHEM buffer (60 mM PIPES [pH 6.9], 25 mM HEPES [pH 6.9], 10 mM EGTA, and 2 mM MgCl₂ containing 2% glutaraldehyde and 0.4% tannic acid) [20] and the eggshell permeabilized by using a pulsed solid-state UV laser (PowerChip, JDS Uniphase) focused with a 63× 1.2 NA C-Apochromat water immersion-objective lens (Carl Zeiss). After permeabilization, the embryos were incubated at 4°C for an additional 30 min in fixing solution, washed three to four times in 1× PHEM buffer, and postfixed in 1× PHEM containing 1% osmium tetroxide and 0.5% K₃Fe(CN)₆ [20]. The samples were dehydrated through a graded series of acetone baths, flat embedded in Epon/Araldite, and remounted for thin, serial sectioning (Leica Ultracut UCT microtome). Thin sections (70 nm) were collected on Formvar-coated copper grids, poststained with 2% uranyl acetate in 70% methanol followed by aqueous lead citrate, and viewed in an FEI TECNAI 12 transmission electron microscope (Phillips) operated at 100 kV.

Immuno-EM was performed as previously published [18]. wt hermaphrodites were cryoimmobilized by using an HPM 010 high-pressure freezer (BAL-TEC). Samples were freeze substituted at -90°C for 3 days in acetone containing 0.2% glutaraldehyde and 0.1% uranyl acetate. The temperature was then raised progressively to room temperature over a 48 hr period in an automatic freeze substitution machine (Leica). Dehydrated specimens were embedded in LR White for thin sectioning. Thin sections (50–70 nm) were cut with a Leica ULTRACUT UCT microtome and collected on Formvar-

coated copper grids. For on-section immunolabeling, primary antibodies against SPD-2 were diluted in blocking buffer containing 0.8% bovine serum albumin, 0.01% Tween 20, and 0.1% fish scale gelatin (Nycomed, Amersham, Inc.) in PBS. The secondary goat anti-rabbit IgG antibody was coupled with 10 nm colloidal gold (British BioCell, England). The antibody complex was stabilized by 1% glutaraldehyde in PBS. Immunolabeled sections were poststained with 2% uranyl acetate in 70% methanol for 4 min followed by aqueous lead citrate for 2.5 min. Samples were imaged by using a TECNAI 12 transmission electron microscope operated at 100 kV (Phillips). For the quantification of immunogold labeling, the distance of 160 individual gold particles from the center of the centrosome (centriole) taken from 15 randomly selected images was determined and grouped as shown in Figure 2B.

Bioinformatics

A BLAST-search using the *C. briggsae* ortholog of SPD-2 identified *C. elegans* SPD-2, with an E value of 1E-50, as the first and only hit. The two nematode sequences align from N to C terminus and share overall identity/similarity of 43% and 59%, respectively, with an alignment score of 1E-167. The SPD-2 gene has apparently undergone a high degree of divergence consistent with what is usually observed between the two nematodes [32], yet the similarity of the two proteins is highly significant. The SPD-2 domain of the nematodes shares 46% identity and 63% similarity and is therefore slightly more conserved than the rest of the protein. The vertebrate and *Drosophila* orthologs were confidently identified by a PSI-BLAST search against the nonredundant database. Likewise, back-PSI-BLASTs by using the human sequence of the SPD-2-domain identified the *C. elegans* and *D. melanogaster* sequence. The percentages of identical and similar residues between *C. briggsae* and human are 21% and 41%, respectively, and the E value after the fourth iteration is 1E-81. The percent identity/similarity between the *C. briggsae* SPD-2 domain and its fly ortholog is 18%/41% (Figure 3B). We would like to note that the search query had to be *C. briggsae* SPD-2, since the protein sequence of *C. briggsae* SPD-2 was at the time not present in the nonredundant database, and at least two homologs are required to carry out a successful PSI-BLAST search. The N terminus of the Asp proteins is confidently identified by PSI-BLAST searches, and the SPD2-domain is identified by back-BLASTs with the Asp N-terminal domain. The fact that the residues that are conserved between the different species of the Spd2-family are also conserved in the Asp proteins further strengthens the hypothesis that these two domains are related and fulfill a similar function. Accession numbers and domain boundaries for the SPD-2 orthologs are as follow: HsSpd2, Bab13395.1 (374–599); DmSpd2, NP_648906.1 (707–928); CbSpd2, ENSCBRP00000013151 (494–733); and CeSpd2: NP_492414.1 (484–714). Accession numbers and amino acid positions (if known) in the Asp proteins are as follows: HsAsp, NP_060606.2 (50–144); GgAsp, BU107436 (source: dbEST); XAsp, BJ031648 (source: dbEST); and DrAsp, BF156705 (source: dbEST).

Supplemental Data

Supplemental Data including Experimental Procedures, figures, and movies are available at <http://www.current-biology.com/cgi/content/full/14/10/863/DC1/>.

Acknowledgments

The authors would like to thank Karen Oegema for antibodies to SPD-2 and SPD-5; Michael Glotzer for communicating unpublished observations; David Drechsel and Mike Tipsword for protein expression; Jana Mántler for EM; Andrei Pozniakovsky for bombardment vectors; Glenis Wiebe for DNA sequencing; Andrea Zinke and Anne Schwager for laboratory assistance; Carsten Höge, Friederike Quittnat, and Martin Srayko for comments on the manuscript; and Cornelia Lorenz for secretarial assistance. Certain strains used were provided by the *C. elegans* Genetics Center funded by the National Institutes of Health National Center for Research Resources (NCRR). During the course of this work, L.P. was supported by postdoctoral fellowships from the European Molecular Biology Organization and the Human Frontiers Science Program.

Received: January 22, 2004
Revised: April 1, 2004
Accepted: April 2, 2004
Published online: April 15, 2004

References

- Bornens, M. (2002). Centrosome composition and microtubule anchoring mechanisms. *Curr. Opin. Cell Biol.* **14**, 25–34.
- Doxsey, S. (2001). Re-evaluating centrosome function. *Nat. Rev. Mol. Cell Biol.* **2**, 688–698.
- Nigg, E.A. (2002). Centrosome aberrations: cause or consequence of cancer progression? *Nat. Rev. Cancer* **2**, 815–825.
- Dammermann, A., Desai, A., and Oegema, K. (2003). The minus end in sight. *Curr. Biol.* **13**, R614–R624.
- Khodjakov, A., and Rieder, C.L. (1999). The sudden recruitment of γ -tubulin to the centrosome at the onset of mitosis and its dynamic exchange throughout the cell cycle, do not require microtubules. *J. Cell Biol.* **146**, 585–596.
- Palazzo, R.E., Vogel, J.M., Schnackenberg, B.J., Hull, D.R., and Wu, X. (2000). Centrosome maturation. *Curr. Top. Dev. Biol.* **49**, 449–470.
- Glover, D.M., Hagan, I.M., and Tavares, A.A. (1998). Polo-like kinases: a team that plays throughout mitosis. *Genes Dev.* **12**, 3777–3787.
- Dutertre, S., Descamps, S., and Prigent, C. (2002). On the role of aurora-A in centrosome function. *Oncogene* **21**, 6175–6183.
- Berdnik, D., and Knoblich, J.A. (2002). *Drosophila* Aurora-A is required for centrosome maturation and actin-dependent asymmetric protein localization during mitosis. *Curr. Biol.* **12**, 640–647.
- Lane, H.A., and Nigg, E.A. (1996). Antibody microinjection reveals an essential role for human polo-like kinase 1 (Plk1) in the functional maturation of mitotic centrosomes. *J. Cell Biol.* **135**, 1701–1713.
- Hinchcliffe, E.H., Li, C., Thompson, E.A., Maller, J.L., and Sluder, G. (1999). Requirement of Cdk2-cyclin E activity for repeated centrosome reproduction in *Xenopus* egg extracts. *Science* **283**, 851–854.
- Meraldi, P., Lukas, J., Fry, A.M., Bartek, J., and Nigg, E.A. (1999). Centrosome duplication in mammalian somatic cells requires E2F and Cdk2-cyclin A. *Nat. Cell Biol.* **1**, 88–93.
- Mayor, T., Stierhof, Y.D., Tanaka, K., Fry, A.M., and Nigg, E.A. (2000). The centrosomal protein C-Nap1 is required for cell cycle-regulated centrosome cohesion. *J. Cell Biol.* **151**, 837–846.
- Mayor, T., Hacker, U., Stierhof, Y.D., and Nigg, E.A. (2002). The mechanism regulating the dissociation of the centrosomal protein C-Nap1 from mitotic spindle poles. *J. Cell Sci.* **115**, 3275–3284.
- Fry, A.M. (2002). The Nek2 protein kinase: a novel regulator of centrosome structure. *Oncogene* **21**, 6184–6194.
- Faragher, A.J., and Fry, A.M. (2003). Nek2A kinase stimulates centrosome disjunction and is required for formation of bipolar mitotic spindles. *Mol. Biol. Cell* **14**, 2876–2889.
- O'Toole, E.T., McDonald, K.L., Mantler, J., McIntosh, J.R., Hyman, A.A., and Muller-Reichert, T. (2003). Morphologically distinct microtubule ends in the mitotic centrosome of *Caenorhabditis elegans*. *J. Cell Biol.* **163**, 451–456.
- Kirkham, M., Muller-Reichert, T., Oegema, K., Grill, S., and Hyman, A.A. (2003). SAS-4 is a *C. elegans* centriolar protein that controls centrosome size. *Cell* **112**, 575–587.
- Leidel, S., and Gonczy, P. (2003). SAS-4 is essential for centrosome duplication in *C. elegans* and is recruited to daughter centrioles once per cell cycle. *Dev. Cell* **4**, 431–439.
- O'Connell, K.F., Caron, C., Kopish, K.R., Hurd, D.D., Kempthues, K.J., Li, Y., and White, J.G. (2001). The *C. elegans zyg-1* gene encodes a regulator of centrosome duplication with distinct maternal and paternal roles in the embryo. *Cell* **105**, 547–558.
- Bobinnec, Y., Fukuda, M., and Nishida, E. (2000). Identification and characterization of *Caenorhabditis elegans* γ -tubulin in dividing cells and differentiated tissues. *J. Cell Sci.* **113**, 3747–3759.
- Hamill, D.R., Severson, A.F., Carter, J.C., and Bowerman, B. (2002). Centrosome maturation and mitotic spindle assembly in *C. elegans* require SPD-5, a protein with multiple coiled-coil domains. *Dev. Cell* **3**, 673–684.
- Hannak, E., Kirkham, M., Hyman, A.A., and Oegema, K. (2001). Aurora-A kinase is required for centrosome maturation in *Caenorhabditis elegans*. *J. Cell Biol.* **155**, 1109–1116.
- Strome, S., Powers, J., Dunn, M., Reese, K., Malone, C.J., White, J., Seydoux, G., and Saxton, W. (2001). Spindle dynamics and the role of γ -tubulin in early *Caenorhabditis elegans* embryos. *Mol. Biol. Cell* **12**, 1751–1764.
- Hannak, E., Oegema, K., Kirkham, M., Gonczy, P., Habermann, B., and Hyman, A.A. (2002). The kinetically dominant assembly pathway for centrosomal asters in *Caenorhabditis elegans* is γ -tubulin dependent. *J. Cell Biol.* **157**, 591–602.
- Schumacher, J.M., Ashcroft, N., Donovan, P.J., and Golden, A. (1998). A highly conserved centrosomal kinase, AIR-1, is required for accurate cell cycle progression and segregation of developmental factors in *Caenorhabditis elegans* embryos. *Development* **125**, 4391–4402.
- Matthews, L.R., Carter, P., Thierry-Mieg, D., and Kempthues, K. (1998). ZYG-9, a *Caenorhabditis elegans* protein required for microtubule organization and function, is a component of meiotic and mitotic spindle poles. *J. Cell Biol.* **141**, 1159–1168.
- Fraser, A.G., Kamath, R.S., Zipperlin, P., Martinez-Campos, M., Sohrmann, M., and Ahringer, J. (2000). Functional genomic analysis of *C. elegans* chromosome I by systematic RNA interference. *Nature* **408**, 325–330.
- Zipperlin, P., Fraser, A.G., Kamath, R.S., Martinez-Campos, M., and Ahringer, J. (2001). Roles for 147 embryonic lethal genes on *C. elegans* chromosome I identified by RNA interference and video microscopy. *EMBO J.* **20**, 3984–3992.
- O'Connell, K.F., Maxwell, K.N., and White, J.G. (2000). The *spd-2* gene is required for polarization of the anteroposterior axis and formation of the sperm asters in the *Caenorhabditis elegans* zygote. *Dev. Biol.* **222**, 55–70.
- Andersen, J.S., Wilkinson, C.J., Mayor, T., Mortensen, P., Nigg, E.A., and Mann, M. (2003). Proteomic characterization of the human centrosome by protein correlation profiling. *Nature* **426**, 570–574.
- Stein, L.D., Bao, Z., Blasiar, D., Blumenthal, T., Brent, M.R., Chen, N., Chinwalla, A., Clarke, L., Clee, C., Coghlan, A., et al. (2003). The genome sequence of *Caenorhabditis briggsae*: a platform for comparative genomics. *PLoS Biol* **1**(2): e45 DOI:10.1371/journal.pbio.0000045.
- do Carmo Avides, M., and Glover, D.M. (1999). Abnormal spindle protein, Asp, and the integrity of mitotic centrosomal microtubule organizing centers. *Science* **283**, 1733–1735.
- Bond, J., Roberts, E., Mochida, G.H., Hampshire, D.J., Scott, S., Askham, J.M., Springell, K., Mahadevan, M., Crow, Y.J., Markham, A.F., et al. (2002). ASPM is a major determinant of cerebral cortical size. *Nat. Genet.* **32**, 316–320.
- Ripoll, P., Pimpinelli, S., Valdivia, M.M., and Avila, J. (1985). A cell division mutant of *Drosophila* with a functionally abnormal spindle. *Cell* **41**, 907–912.
- Gonzalez, C., Saunders, R.D., Casal, J., Molina, I., Carmena, M., Ripoll, P., and Glover, D.M. (1990). Mutations at the *asp* locus of *Drosophila* lead to multiple free centrosomes in syncytial embryos, but restrict centrosome duplication in larval neuroblasts. *J. Cell Sci.* **96**, 605–616.
- Heald, R., Tournebise, R., Blank, T., Sandaltzopoulos, R., Becker, P., Hyman, A., and Karsenti, E. (1996). Self-organization of microtubules into bipolar spindles around artificial chromosomes in *Xenopus* egg extracts. *Nature* **382**, 420–425.
- Khodjakov, A., Rieder, C.L., Sluder, G., Cassels, G., Sibon, O., and Wang, C.L. (2002). De novo formation of centrosomes in vertebrate cells arrested during S phase. *J. Cell Biol.* **158**, 1171–1181.
- Bonaccorsi, S., Giansanti, M.G., and Gatti, M. (2000). Spindle assembly in *Drosophila* neuroblasts and ganglion mother cells. *Nat. Cell Biol.* **2**, 54–56.
- Smirnova, E.A., and Bajer, A.S. (1992). Spindle poles in higher plant mitosis. *Cell Motil. Cytoskeleton* **23**, 1–7.
- Smirnova, E.A., and Bajer, A.S. (1998). Early stages of spindle

- formation and independence of chromosome and microtubule cycles in *Haemaphysalis endosperm*. *Cell Motil. Cytoskeleton* **40**, 22–37.
42. Hinchcliffe, E.H., and Sluder, G. (2001). Centrosome duplication: three kinases come up a winner! *Curr. Biol.* **11**, R698–R701.
 43. Hinchcliffe, E.H., and Sluder, G. (2002). Two for two: Cdk2 and its role in centrosome doubling. *Oncogene* **21**, 6154–6160.
 44. Carmena, M., and Earnshaw, W.C. (2003). The cellular geography of aurora kinases. *Nat. Rev. Mol. Cell Biol.* **4**, 842–854.
 45. Gonczy, P., Pichler, S., Kirkham, M., and Hyman, A.A. (1999). Cytoplasmic dynein is required for distinct aspects of MTOC positioning, including centrosome separation, in the one cell stage *Caenorhabditis elegans* embryo. *J. Cell Biol.* **147**, 135–150.
 46. Kemp, C.A., Kopish, K.R., Zipperlen, P., Ahringer, J., and O'Connell, K.F. (2004). Centrosome maturation and duplication in *C. elegans* require the coiled-coil protein SPD-2. *Dev. Cell* **6**, 511–523.

Cryoimmobilization and three-dimensional visualization of *C. elegans* ultrastructure

T. MÜLLER-REICHERT, H. HOHENBERG*, E. T. O'TOOLE† & K. MCDONALD‡

Max Planck Institute for Molecular Cell Biology and Genetics, Pfotenhauerstr. 108, D-01307 Dresden, Germany

*Heinrich Pette Institute of Experimental Virology and Immunology, Martinistr. 52, D-20251 Hamburg, Germany

†Boulder Laboratory for 3-D Fine Structure, University of Colorado, Boulder, CO 80309, U.S.A.

‡Electron Microscope Laboratory, 26 Giannini Hall, University of California, Berkeley, CA 94720, U.S.A.

Key words. 3-D reconstruction, *C. elegans*, electron tomography, freeze-substitution, high-pressure freezing, immunolabelling.

Summary

Caenorhabditis elegans is one of the most important genetic systems used in current biological research. Increasingly, these genetics-based research projects are including ultrastructural analyses in their attempts to understand the molecular basis for cell function. Here, we present and review state-of-the-art methods for both ultrastructural analysis and immunogold localization in *C. elegans*. For the initial cryofixation, high-pressure freezing is the method of choice, and in this article we describe two different strategies to prepare these nematode worms for rapid freezing. The first method takes advantage of transparent, porous cellulose capillary tubes to contain the worms, and the second packs the worms in *E. coli* and/or yeast paste prior to freezing. The latter method facilitates embedding of *C. elegans* in a thin layer of resin so individual worms can be staged, selected and precisely orientated for serial sectioning followed by immunolabelling or electron tomography.

Introduction

In the past few years, extremely efficient sequencing techniques have provided complete genetic information for several model organisms, including the nematode *Caenorhabditis elegans*. Currently, various techniques, including RNA-mediated interference (RNAi), are applied to answer fundamental questions related to molecular, cell and developmental biology. Importantly, for a description of *C. elegans* biology, the analysis of wild-type and mutant fine structure and the ultrastructural localization of gene products are crucial.

Using conventional methods of specimen preparation for electron microscopy, *C. elegans* is an organism that is considered to be difficult to fix. When transferred into a buffered fixative, this nematode can respond very quickly and prevent fixative from entering its tissues. By blocking the diffusion of fixatives through the cuticle, *C. elegans* is able to survive up to 7 h in a solution containing 10% glutaraldehyde (Shepard & Clark, 1976). In order to permit penetration of the chemical reagents into the nematode, the worms have to be cut into pieces (Ward *et al.*, 1975; Hall, 1995) or warmed by microwave treatment (Jones & Gwynn, 1992). Compared with whole worms, it is even more difficult to fix isolated early embryos of *C. elegans*. To allow adequate chemical fixation by glutaraldehyde, the eggshell of the embryo has to be either digested enzymatically or treated with bleach (Rappleye *et al.*, 1999) or made porous with a laser beam (Priess & Hirsh, 1986; Kirkham *et al.*, 2003). Such problems related to the diffusion of chemical reagents can be avoided when high-pressure freezing in combination with freeze-substitution is applied. These high-pressure frozen/freeze-substituted samples are suitable for both morphological (Dernburg *et al.*, 1998; Rappleye *et al.*, 1999; Howe *et al.*, 2001; Kirkham *et al.*, 2003) and immunogold studies (Favre *et al.*, 1995; Kirkham *et al.*, 2003).

In this article, we describe and discuss two different methods for cryoprocessing of *C. elegans* samples. The first method takes advantage of transparent, porous cellulose capillary tubes with an inner diameter of 200 µm to contain the worms, which are drawn into the tubes by capillary action (Hohenberg *et al.*, 1994). In the second method, worms are packed in *E. coli* and/or yeast paste prior to high-pressure freezing/freeze-substitution and then embedded in a thin layer of polymerized resin. Using this method, individual worms can

Correspondence: Thomas Müller-Reichert. Tel.: +49 351 210 1763; fax: +49 351 210 2000; e-mail: mueller-reichert@mpi-cbg.de

be viewed by high-resolution light microscopy to preselect particular stages of development for precisely orientated sectioning (Rapplepey *et al.*, 1999; Lonsdale *et al.*, 2001).

Materials and methods

C. elegans was cultivated on plates or in suspension according to published procedures (Brenner, 1974). Worms were prepared for high-pressure freezing using either the 'capillary tube' or 'thick paste' method.

Capillary tube method

Filling the capillary tubes. The capillary tube method was carried out as described (Hohenberg *et al.*, 1994). Briefly, the tip of a capillary tube (hollow cellulose fibre; type LD OC O2; Microdyn, Wuppertal, Germany) was inserted into a droplet of a nematode suspension and the nematodes were drawn into the tube by capillary action. The capillary was kept in place by a clamping mechanism (Fig. 1). A piece of filter paper was held against the opposite end of the capillary tube, and nematodes were trapped and concentrated in the capillary tube by passing medium out into the filter paper. After about 10 s, 2 mm of the capillary tube was packed densely with the worms. Suitably filled segments of the tubes were submerged in 1-hexadecene and cut with a scalpel. This cutting process sealed the ends of the segments. When there were low nematode concentrations inside the tube, the application of non-penetrating cryoprotectants was necessary. To achieve this, the tubes were filled with nematodes as described above. In addition, either a 10% solution of HES (hydroxy ethyl starch; Echlin *et al.*, 1977) or 10% Dextran (molecular weight $M_r \sim 40\,000$) was drawn into the tube by capillary action, displacing the cultivation medium prior to high-pressure freezing. This process of medium displacement and the preservation of nematode

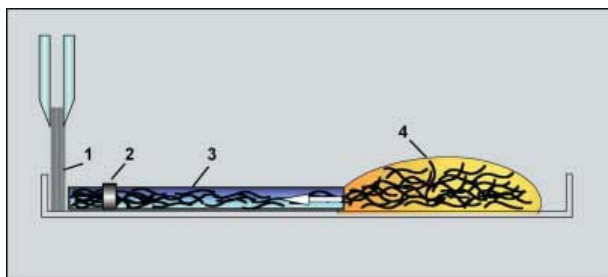


Fig. 1. Using capillary tubes for specimen preparation. The tip of a capillary tube is inserted into a drop of nematode suspension to fill the cellulose tube. Nematodes are drawn into the tube by capillary action. The capillary tube is kept in place by a clamping mechanism. A piece of filter paper is held against the opposite end of the tube to trap and concentrate the specimens. Suitably filled segments of the tube can be cut and sealed prior to freezing: 1, filter paper; 2, clamping mechanism; 3, capillary tube; 4, nematode suspension.

vitality can easily be monitored by light microscopy as a result of the transparency of the capillary tubes.

High pressure freezing. The 2-mm segments of the capillary tubes were fitted into the cavity (depth 200 μm) of the standard aluminium planchette (type A; Engineering Office M. Wohlwend, Sennwald, Switzerland) filled with 1-hexadecene. 1-Hexadecene is a hydrophobic and chemically inert paraffin oil of rather low viscosity. Therefore, cavities are easily filled (Studer *et al.*, 1989). Type A planchettes were sandwiched with the flat side of a complementary type B planchette. The sandwich was then inserted into the holder of the high-pressure freezer (BAL-TEC HPM 010, BAL-TEC, Liechtenstein; Moor, 1987) and frozen. The frozen sandwiches were stored in liquid nitrogen until further use.

Freeze-substitution, embedding and electron microscopy. Freeze-substitution was performed in anhydrous acetone containing 2% osmium tetroxide (van Harreveld & Crowell, 1964). The frozen capillary tubes were freed mechanically from adhering 1-hexadecene at $-90\text{ }^\circ\text{C}$ in the substitution medium. At $-90\text{ }^\circ\text{C}$, 1-hexadecene is not soluble in acetone, methanol or ethanol, thereby possibly preventing the substitution of the aqueous phase. As a consequence, adequately frozen samples may be damaged by subsequent ice crystal growth, if substitution occurs only at elevated temperatures. The capillary tubes, freed from 1-hexadecene, were then transferred to 1.5-mL Eppendorf tubes containing the substitution medium pre-cooled to $-90\text{ }^\circ\text{C}$. A miniature 'transfer basket' was used to transfer the capillary tubes and change solutions during freeze-substitution (for details see Hohenberg *et al.*, 1994). The samples were kept at -90 , -60 and $-30\text{ }^\circ\text{C}$ for 8 h at each step and finally brought to $20\text{ }^\circ\text{C}$ for 1 h in a freeze-substitution unit (Leica EM AFS, Vienna, Austria). The samples were then washed three times in anhydrous acetone and embedded stepwise in Spurr's resin (30% and 70% resin in acetone) at $25\text{ }^\circ\text{C}$ for 4 h at each concentration (Spurr, 1969). The capillary tubes were orientated either parallel or perpendicular to the rim of the embedding form prior to polymerization at $60\text{ }^\circ\text{C}$ for 24 h. Thin sections (50 nm) were cut using a Leica Ultracut UCT Microtome (Leica), post-stained with 2% uranyl acetate followed by Reynold's lead citrate and imaged in a Philips CM 120 transmission electron microscope (FEI, The Netherlands) operated at 60 kV.

Thick paste method

Sample loading and high-pressure freezing. In preparation for high-pressure freezing, adult wild-type worms containing embryos were selected under a stereomicroscope and transferred to sample holders containing an *E. coli* suspension. Alternatively, a thick paste of yeast was made from dry bakers yeast and 10% methanol and worms were mixed with this paste and loaded into the high-pressure freezing planchette. About 50–

100 worms were placed in the 100- μ m-deep well of a BAL-TEC type A planchette (McDonald, 1999; Engineering Office M. Wohlwend). Samples were covered with the flat side of a complementary planchette (type B) and rapidly frozen using a BAL-TEC HPM 010 high-pressure freezer (BAL-TEC). Frozen samples were stored in liquid nitrogen until further use.

Freeze-substitution and infiltration with resin. For freeze-substitution, specimen holders were split under liquid nitrogen and a single planchette type 'A', containing the nematode worms, was transferred to a precooled cryovial (-90°C) containing the fixative. For morphological studies, freeze-substitution was carried out in anhydrous acetone containing 1% osmium tetroxide and 0.1% uranyl acetate (McDonald & Müller-Reichert, 2002). For immunolabelling studies, we used a 'cocktail' containing 0.2% glutaraldehyde and 0.1% uranyl acetate in anhydrous acetone (McDonald, 1999). Using a Leica EM AFS, samples were maintained at -90°C for 3 days. Freeze-substituted samples were then allowed to warm to room temperature at a rate of 5°C h^{-1} . At room temperature, specimens were removed from the planchettes and washed three times for 1 h in fresh anhydrous acetone. After the acetone washes, samples were then gradually infiltrated with either Epon/Araldite resin (1 part resin : three parts acetone) for 1 h; 1 : 1 for 2 h; 3 : 1 for 2 h, and 100% resin for 1 h, then overnight, then for 1 h, or LR White resin (1 part resin : 1 part acetone for 2 h; 100% resin 4×2 h and overnight).

Thin-layer embedding. Worms were embedded in thin, optically clear layers of resin on microscope slides. For Epon/Araldite embedding (McDonald, 1994; Fig. 2A), microscope slides were wiped clean with a soft cloth and coated with Teflon® spray (MS-122DF, Miller-Stephenson Chemical Co., Inc., Danbury, CT, USA). Worms in Epon/Araldite were evenly distributed on the cleanly wiped surface of the glass slide. Two layers of Parafilm® were used as spacers and coated slides were put on top of the resin samples. For LR White embedding (Fig. 2B), we used the methods described in Lonsdale *et al.* (2001). Briefly, a microscope slide was coated with Teflon spray as above, then wiped clean. A piece of Thermanox® 22 mm square from which an 18-mm square had been removed from the centre was glued to the slide with a Crazy Glue® Pen and allowed to dry for at least 1 h. Worms in pure LR White resin were placed in the 18-mm square cavity and covered with a 25-mm square piece of Aclar® plastic such that no air bubbles were trapped in the cavity. The slide was then placed in a container flooded with dry nitrogen gas, which was then sealed and put into a 60°C oven for 1–2 days. The Aclar plastic was peeled off and selected worms were cut out and remounted for sectioning.

Remounting, sectioning and electron microscopy. Worms containing appropriate numbers of early embryos were selected by light microscopy and remounted on 'dummy' blocks for ultramicrotomy (Fig. 2C–E). Longitudinal sections through the

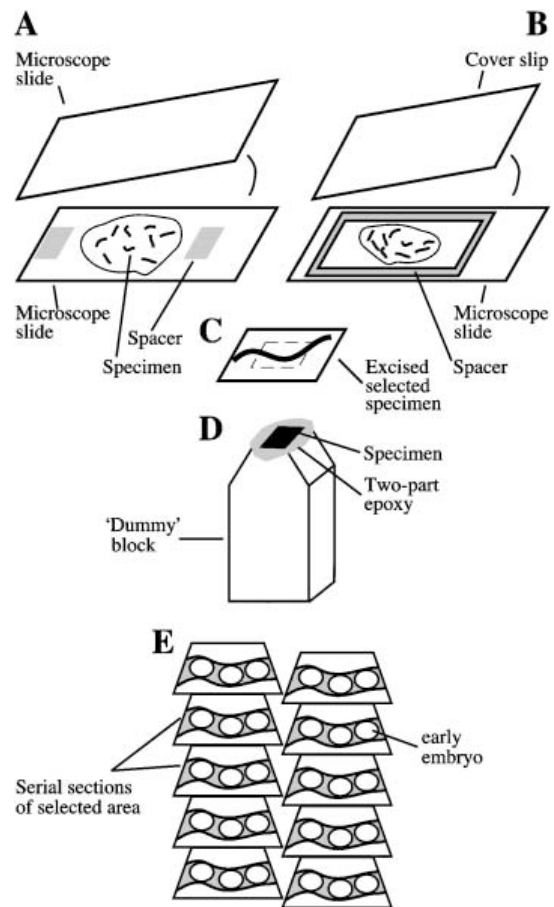


Fig. 2. Selection of thin-layer embedded worms for electron microscopy. (A) Epon/Araldite-infiltrated worms are sandwiched between two Teflon®-coated microscope slides. Spacers are used to hold the slides apart. (B) Worms infiltrated with LR White are placed in slide moulds made of a microscope slide and a Thermanox® spacer. Slide moulds are closed using an Aclar® cover slip. After polymerization of the resin, selected specimens are excised (C) and remounted on 'dummy' blocks (D) for serial sectioning (E).

worms were cut using either a Reichert Ultracut E or a Leica Ultracut UCT Microtome (Leica). Both thin (60–70 nm) and semi-thick (300–400 nm) Epon/Araldite sections were collected on Formvar-coated copper slot grids. Thin sections (50–70 nm) for immunolabelling were collected on Formvar-coated rhodium/copper slot grids. Sections were post-stained with 2% uranyl acetate in 70% methanol followed by Reynold's lead citrate and imaged in a TECNAI 12 transmission electron microscope (FEI) operated at 100 kV.

On-section immunolabelling. All steps of immunolabelling were performed in a humid chamber at room temperature. The samples were floated on blocking buffer containing 0.8% bovine serum albumin, 0.01% Tween 20 and 0.1% fish skin

gelatin (Nycomed, Amersham Inc.) in physiologically buffered saline (PBS) for 20 min. Samples were then transferred to blocking buffer containing the diluted primary polyclonal antibody (1 : 1200). After 45 min the grids were rinsed three times each for 5 min in PBS and transferred to blocking buffer containing the secondary antibody. The secondary goat anti-rabbit IgG antibody (British BioCell, U.K.), coupled to 10-nm colloidal gold, was diluted 1 : 40 in blocking buffer. After rinsing in blocking buffer and PBS (three times each for 5 min), samples were fixed for 5 min using 1% glutaraldehyde in PBS, then rinsed three times each for 1 min in dH₂O, and post-stained as described above.

Tomographic reconstruction of mitotic spindle components in early C. elegans embryos. High-voltage electron tomography was carried out essentially as described in O'Toole *et al.* (1999). Briefly, 15-nm colloidal gold particles were affixed to both surfaces of semi-thick (300–400 nm) sections, and the grids were carbon coated to stabilize the sample under the electron beam. Samples were placed in a high-tilt, rotating stage (Gatan model 650, Pleasanton, CA, U.S.A.) and imaged using a JEOL JEM1000 microscope operating at 750 kV. Serial, tilted views were collected over a $\pm 60^\circ$ range at 1.5° increments about two orthogonal axes. Images were acquired using a Gatan

1k × 1k CCD camera at a pixel size of 1.4 nm using an automated image capture software package developed in the Boulder Laboratory for 3-D Fine Structure. Multiple frames, or montages, were collected in order to reconstruct a larger area of the cell as described in Marsh *et al.* (2001). Image processing was carried out using the IMOD software package (Ladinsky *et al.*, 1999; O'Toole *et al.*, 1999; Marsh *et al.*, 2001). The serial, tilted views were aligned using the positions of the gold particles, and tomograms computed using an R-weighted back projection algorithm. Tomograms from each axis were then aligned to each other and combined (Mastrorade, 1997). The IMOD modelling program was used for image display and modelling (Kremer *et al.*, 1996). The ratio of the microtome setting to the final measured thickness of the reconstructions was used to calculate a thinning factor to correct for the collapse of the section during microscopy.

Results

Cellulose capillary tubes

A transverse section through a high-pressure frozen *C. elegans* hermaphrodite prepared in a capillary tube is shown in Fig. 3(A). Excellent ultrastructural preservation is indicated

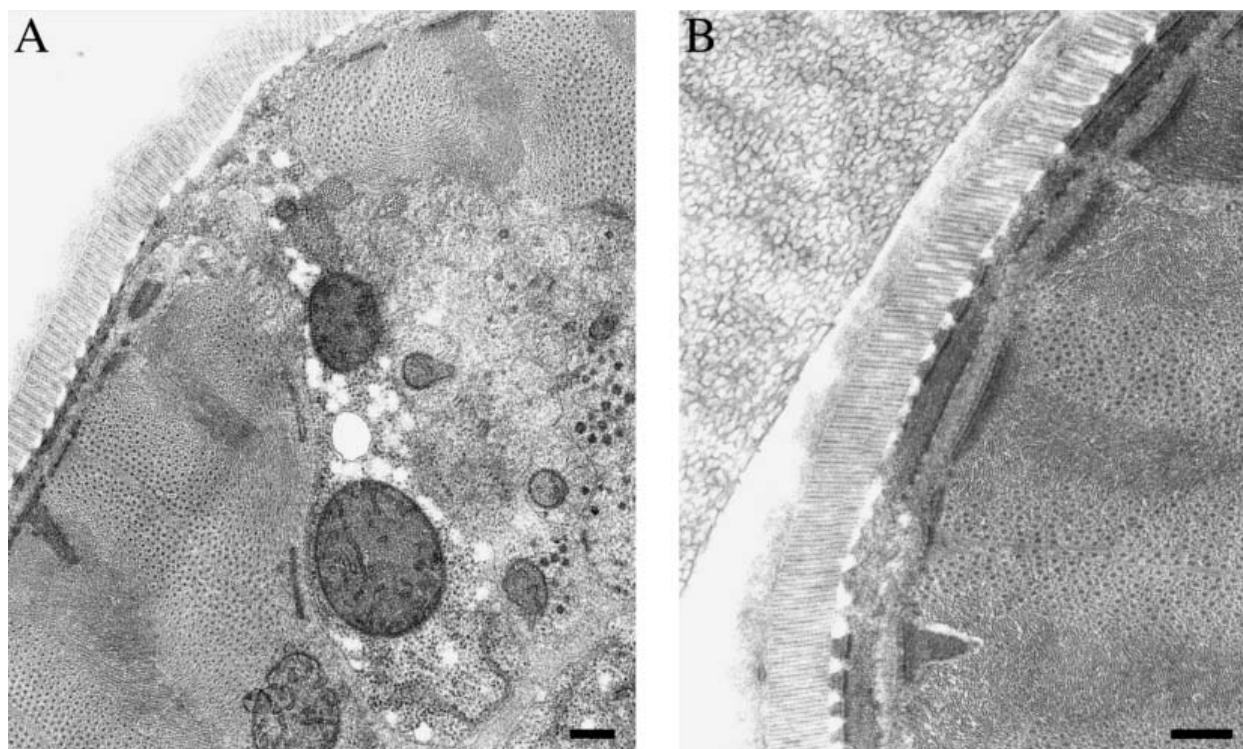


Fig. 3. Nematode worms frozen in capillary tubes. (A) Ultrastructure of a wild-type worm in cross-section. (B) Worm ultrastructure in the presence of 10% dextran. High-pressure frozen worms were freeze-substituted in acetone containing 2% osmium tetroxide. Worms were embedded in Spurr's resin. Scale bars = 0.1 μ m.

by the nematode cuticle, which shows the sharply delineated and highly ordered striations (Hohenberg *et al.*, 1994). The outer somatic muscles as well as structures in the centre of the worm are free of detectable segregation patterns. This method adequately cryofixed nematodes, suspended in their natural medium, by high-pressure freezing throughout the entire length of the capillary tubes (diameter of 200 μ m, over a length of 2 mm). Even low concentrations of nematodes, frozen in an HES or Dextran solution, showed good freezing results although in some cases more than 80% of the capillary lumen was filled with an aqueous solution of the respective cryoprotectant (see Hohenberg *et al.*, 1994). As shown in Fig. 3(B), a single nematode surrounded by an ice crystal pattern is well preserved and shows no intracellular ice crystal formation of detectible size. Only at the outer part of the cuticle are patterns of structural damage visible.

Thick paste method and thin-layer embedding

To analyse the ultrastructure of early *C. elegans* embryos, an alternative method of specimen preparation was applied. Adult worms were frozen in a 'thick paste' of *E. coli* and/or bakers yeast and subsequently thin-layer embedded after applying high-pressure freezing/freeze-substitution. Embedding of whole worms in a thin layer of Epon/Araldite allowed us to screen for worms with appropriate numbers of early embryos. A low-magnification image of an early embryo, showing cells in interphase as well as in mitosis, is given in Fig. 4(A). At higher magnification, spindle components of a cell in telophase are visualized (Fig. 4B). The condensed chromatin and the centrioles of the spindle poles are indicated. The mitotic spindle apparatus is shown in Fig. 4(C). This electron microscope image shows spindle microtubules, the condensed DNA and a nuclear envelope, which is partially dispersed at the spindle pole.

To localize specific gene products in the *C. elegans* embryo by immunogold labelling, thin-layer embedding in LR White resin was performed. When looking for specific labelling of mitotic spindle components it is crucial to screen a number of labelled embryos. Again, thin-layer embedding was useful because worms with appropriate numbers of embryos could be selected for immunostaining. On-section immunolabelling of spindle components in the early *C. elegans* embryo is illustrated in Fig. 5. The micrograph shows one half of a bipolar spindle with spindle microtubules and condensed DNA. Details of the immunola-

labelling at higher magnification are shown in Fig. 5(B). The polyclonal primary antibody (gift of Dr K. Oegema, University of California, San Diego), raised against the kinetochore component Knl-1p, recognized antigens along the 'surface' of the chromatin (Desai *et al.*, 2003). Arrows mark the 10-nm gold particles.

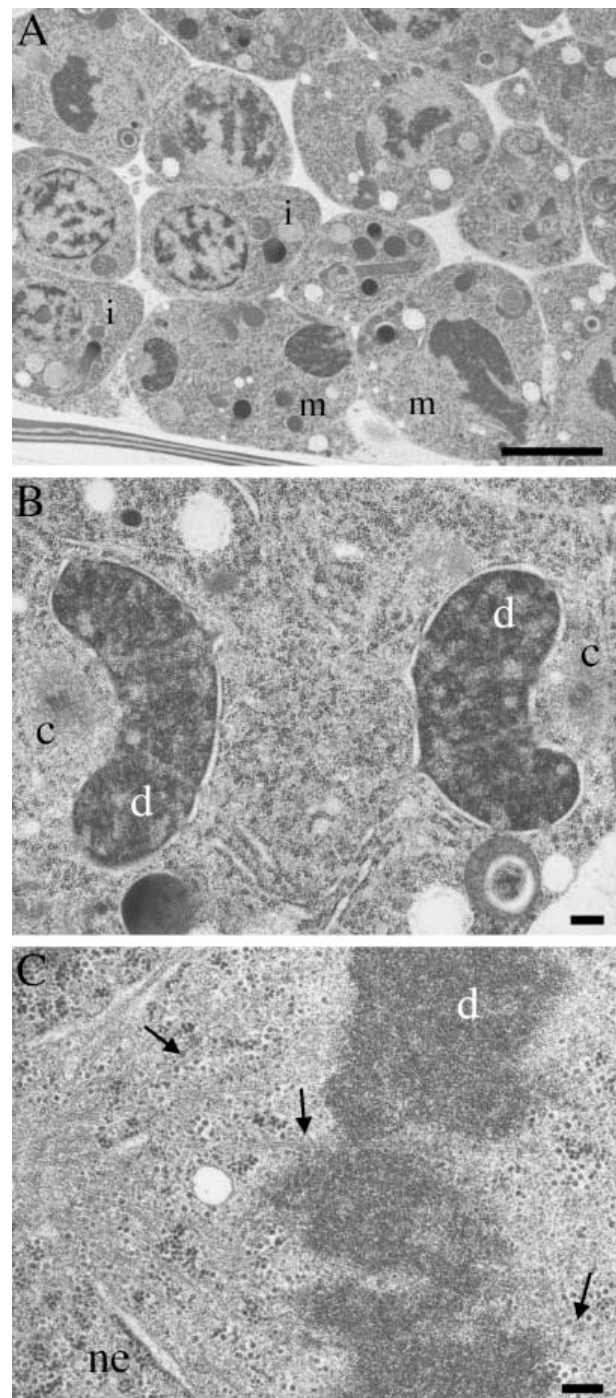


Fig. 4. Early *C. elegans* embryo in a thin-layer embedded whole-mounted wild-type worm. (A) Electron micrograph showing cells in interphase (i) and in mitosis (m). (B) Mitotic cell in telophase. Two centrioles (c) and the condensed DNA (d) are visible. (C) Ultrastructural details of a cell in metaphase. The partially dispersed nuclear envelope (ne) surrounds the DNA (d). Spindle microtubules (arrows) are visible. Wild-type hermaphrodites were high-pressure frozen. Specimens were freeze-substituted in acetone containing 1% osmium tetroxide and 0.1% uranyl acetate and embedded in Epon/Araldite. Scale bars = 0.25 μ m.

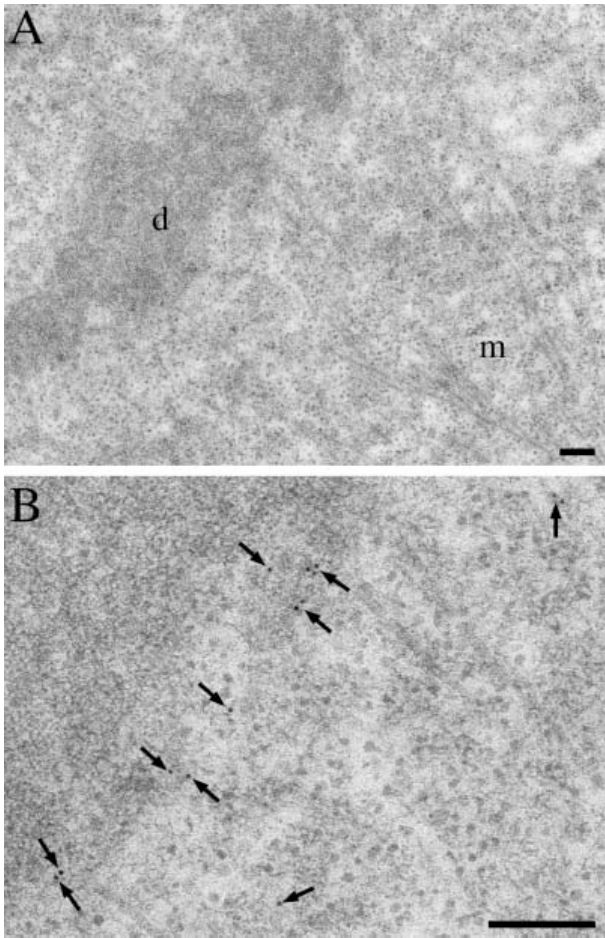


Fig. 5. Immunogold labelling in the early *C. elegans* embryo. (A) Longitudinal section through a metaphase spindle showing condensed DNA (d) and microtubules (m). (B) Details of the immunolabelling at higher magnification. The antibody recognized a kinetochore protein along the 'surface' of the condensed DNA. Wild-type worms were cryofixed by high-pressure freezing, freeze-substituted in acetone containing 0.2% glutaraldehyde and 0.1% uranyl acetate, and infiltrated with LR White. Sixty- to 70-nm sections were immunolabelled with antibody to Kn1-1p and 10-nm gold secondary antibody (arrows). Scale bars = 0.25 μ m.

Electron tomography of selected embryos

We used selected high-pressure frozen, thin-layer embedded worms to demonstrate the three-dimensional (3-D) reconstruction of early embryo ultrastructure by electron tomography (O'Toole *et al.*, 2002, 2003). Tomography is based on the use of serial, tilted views of a semi-thick section to create a computer-generated volume that can be sliced and imaged in any orientation. Figure 6(A) shows a selected, 2.14- μ m-thick tomographic slice through a portion of a mitotic spindle from an early *C. elegans* embryo. The cell is well preserved and free of ice crystal damage. The DNA is dense and uniform, and portions of the nuclear envelope are evident. The centrosome is

also well preserved, and features such as the centriole pair and the surrounding pericentriolar material are intact. Numerous microtubules can be seen embedded in this pericentriolar matrix. Structures of interest can be modelled within the complete tomographic volume and their positions displayed in three dimensions (Fig. 6B,C). The trajectories of microtubules, the position of the nuclear envelope and the surface of the condensed chromatin were modelled. Two different views of the model are displayed. As shown in these models, the spindle pole sits outside a large opening in the nuclear envelope. Microtubules radiate out from the centrosome, with the majority facing the chromosomes. Microtubule ends were identified and their positions marked with a blue sphere. Although this tomographic reconstruction contained approximately 2.8 μ m \times 1.4 μ m \times 250 nm of cell volume, only a portion of this spindle was visualized. Serial section tomography of adjacent sections would be needed to reconstruct this entire spindle.

Discussion

The most critical part of high-pressure freezing is probably loading of the specimens. Some practical guidelines for specimen loading are clearly presented by Moor (1987) and some of the key points are briefly repeated here. (1) Specimens should be in optimal physiological conditions at the moment of freezing. (2) Most samples need to be loaded quickly to minimize physical and physiological disruptions. (3) The entire cavity of the specimen holder has to be filled. If there are air spaces, these will collapse and possibly crush the specimen and/or interfere with effective heat transfer. (4) If the planchettes available do not seem to fit the sample, special planchettes that do fit may have to be made. (5) If existing planchettes have to be used, non-penetrating cryoprotectants can be used to fill air spaces and facilitate heat transfer. In summary, if the sample is not freezing well, it is probably not the fault of the high-pressure freezer, but rather the condition of the specimen as it goes into the freezer. It is generally known in high-pressure freezing laboratories that poor freezing is frequently correlated with the state of the water in and/or around the sample. Specimens with high water content, such as some plant cells and cartilage, are difficult to freeze. Likewise, samples that are surrounded by aqueous solutions such as cell suspensions tend to freeze poorly. The two methods we have presented here help to overcome some of the difficulties associated with loading of *C. elegans* into the freezing planchettes. Choosing either one of these two methods, however, will largely be based on the type of analysis following specimen preparation.

Using capillary tubes for freezing

Nematodes were incubated, gently concentrated and continually observed in their natural medium until rapidly frozen in their living state by high-pressure freezing. Direct contact of the nematodes with 1-hexadecene or other cryoprotectants

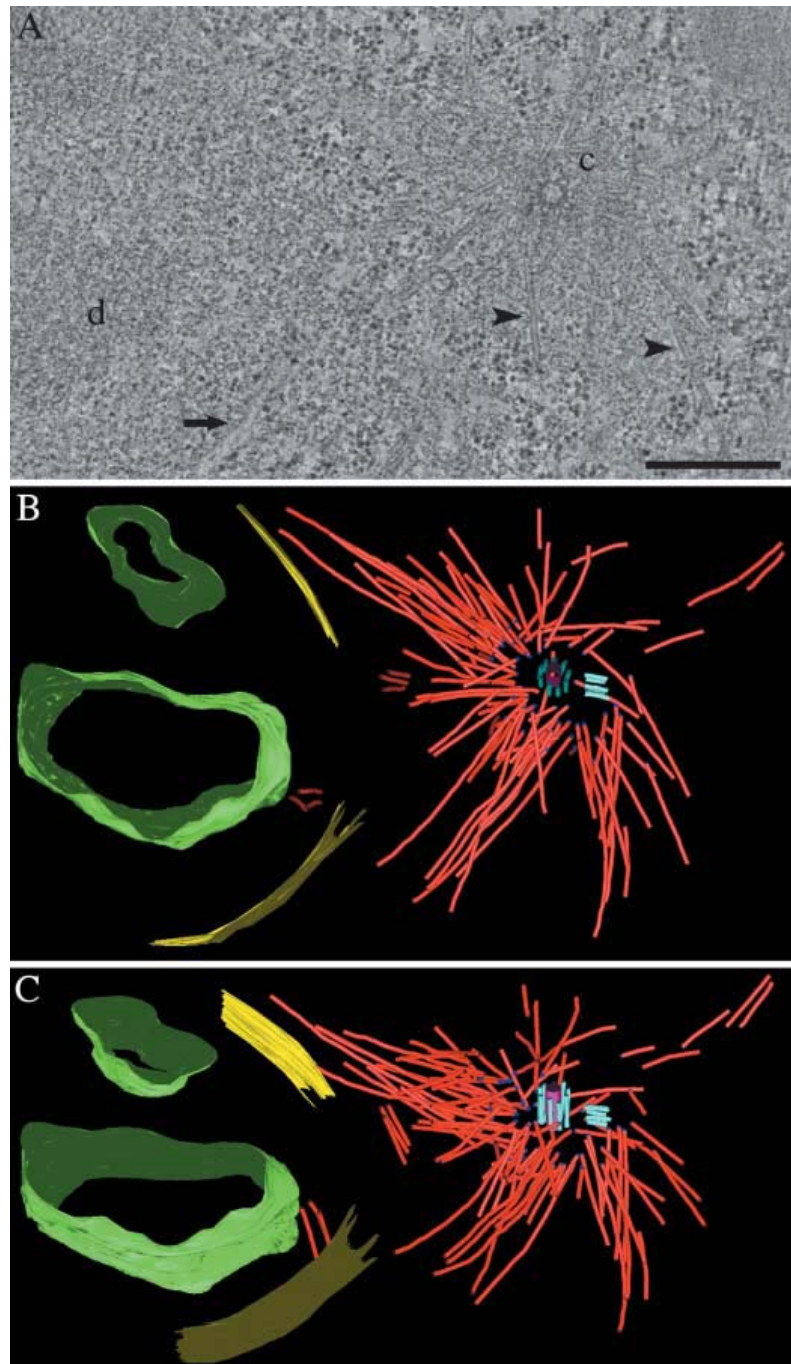


Fig. 6. Electron tomography of *C. elegans* ultrastructure. (A) Selected tomographic slice showing mitotic features in an early embryo. The centrosome (c), the condensed DNA (d) and a partially dispersed nuclear envelope (arrow) are visible. Microtubules are indicated by arrowheads. (B) Three-dimensional model of the same data set showing the complex array of microtubules (red) around the centrosomes (blue). The 'surface' of the DNA is modelled in 'green' and the nuclear envelope is modelled in 'yellow'. Minus ends of microtubules are indicated by blue spheres. (C) Horizontal rotation of the same 3-D model. Specimens for tomographic reconstruction were cryofixed by high-pressure freezing and freeze-substituted in acetone containing 1% osmium tetroxide and 0.1% uranyl acetate. Samples were embedded in Epon/Araldite. Scale bar = 0.5 μ m.

(Dahl & Staehelin, 1989; Studer *et al.*, 1989) was avoided. Nematodes, enclosed within cellulose capillary tubes and submerged under 1-hexadecene, remain alive for 7 h (observed by light microscopy). Upon direct contact with 1-hexadecene, nematodes stretch out and die in less than 5 min. Importantly, the hydrophobic 1-hexadecene is only marginally soluble in acetone at subzero temperatures. Ice crystals may grow and

distort the sample, if the substitution medium is prevented from dissolving the frozen sample at very low temperatures. The frozen 1-hexadecene therefore must be removed from the specimen prior to freeze-substitution. The capillary tube pores are water-filled and prevent the entry of 1-hexadecene.

Electron diffraction of cryosections of such prepared samples revealed vitrification of the nematodes and hexagonal ice

in the surrounding medium in most cases (Hohenberg *et al.*, 1994). It is important to note that the freezing quality was correlated with the concentration of the nematodes inside the capillary tubes; 40–50% of the capillary lumen should be filled with the worms. In the case of low nematode concentrations or the preparation of selected individuals or embryos, the application of solutions containing non-penetrating cryoprotectants (i.e. HES or Dextran) gave good results. The pattern of ice crystal formation in the frozen solution enclosing the nematodes is directly visible.

The advantages in using porous cellulose capillary tubes for the preparation of nematodes for high-pressure freezing are as follows. (1) The samples are cryoimmobilized in their natural environment, a procedure which retains structural information that can be correlated with the physiological state of the worms. Viability and vitality of the nematodes can be continually checked by light microscopy until freezing because capillary tubes are transparent. (2) The suspensions can be processed within a microcontainer of confined volume (about 0.5 L), avoiding repeated centrifugation during cryoprocessing. Loss of material is impossible because the containers are sealed. Nematodes of a single batch can be used for cryoimmobilization, cryosectioning and freeze-substitution. (3) This method ensures a very high and predictable yield of adequately and reproducibly high-pressure frozen samples. (4) Freeze-substitution and embedding procedures are not prolonged owing to the high porosity of the cellulose tubes. The pores have a variable molecular weight cut-off from 5 to 20 kDa, allowing the free passage of all substitution media and resin monomers. The disadvantages of this method can be summarized as follows. (i) It is not possible to select individual worms after high-pressure freezing/freeze-substitution. (ii) Specimens cannot be orientated before polymerization of the resin. In summary, the capillary tube method gives good freezing results. The use of this method, however, is limited when individual worms have to be selected for further analysis.

Thick paste/thin-layer embedding method

Using *E. coli* as the filler is very convenient because the worms are usually crawling through it on the food plate. This is their natural state and one can assume that the physiological conditions are excellent for the worms. However, the viscosity of the *E. coli* paste being used as filler in the planchettes is critical and on the food plates it is often not viscous enough. The same viscosity that is ideal for picking is good for filling. When using *E. coli* paste, a separate plate of viscous cells as the filler instead of what is on the plate with the worms should be used. If one has to work with worms in liquid, they have to be gently centrifuged first, before putting them on an agar plate. The agar will absorb the excess liquid and the worms can be picked off the plate as if they had been growing there. The overall requirement is to have intimate contact between the paste and

the worms during freezing. If the worms are surrounded by aqueous solutions, the transfer of heat will be impeded and they will not freeze well. Alternatively, a thick paste of bakers yeast can be used to fill the cavity of the freezing planchettes.

The advantages of the thick paste/thin-layer embedding method can be summarized as follows. (1) A large number of wild-type or mutant worms can be processed. Typically, 50–100 worms can be loaded into a specimen planchette (type A, 100 µm deep) for every freezing event. This method works best when worms are being 'picked' off food plates rather than being grown in liquid cultures. (2) Both types of pastes are easy to freeze well. In our experience, the yeast is usually better than the *E. coli* because in a thick paste the yeast probably act as tiny 'sponges', absorbing excess liquid from around the worms. (3) Specimen loading is fast. With a little practice, it is easy to load 50–100 worms into a planchette in 2 min or less. When working on an agar food plate, the paste will not dry out in that time. (4) Once through the freeze-substitution and resin infiltration procedures, it is possible to separate individual worms from the thick paste using a pair of fine tungsten needles to tease away the filling material during thin layer embedding. Worms should be spread on the slide so they are far enough apart to be cut out individually. (5) Single worms can be selected for (serial) microtomy. Following resin polymerization the worms are in a thin layer of resin on a microscope slide. This slide can be mounted in a high-quality light microscope and individual worms can be checked for stage of development (see Lonsdale *et al.*, 2001). This means that it is possible to work with mixed populations and select individuals for sectioning.

The disadvantages of this method may be summarized as follows. (i) It takes some practice to get the consistency of either the *E. coli* or yeast paste right and this is one of the major keys to success with the thick paste method. If it is too thick, it is difficult to mix with the worms. If it is too thin, it is not effective at heat transfer. One suggestion is to practise making different thickness of paste and use the thickest one that will cover the worms. It sometimes helps to mix the worms and paste on the agar food plate and load them together into the planchette, rather than adding them separately. It is also possible to add them separately, but the worms should be put in first, and then covered with *E. coli*/yeast paste. Working on an agar plate such as the one the worms are growing on can help to keep the paste hydrated. If the paste seems to be drying out, a little liquid medium can be added to rehydrate it. When done correctly, worms should be moving in the paste while putting on the covering planchette. (ii) Worms can be lost during steps of dehydration and resin infiltration. In contrast to the capillary method, specimens are not contained in sealed microtubes. Centrifugation steps are necessary to concentrate worms after each dehydration and infiltration step. (iii) It is easy to introduce 'handling traumas'. After freeze-substitution, worms have to be separated from the surrounding paste prior to flat embedding. This manipulation has to be done with care,

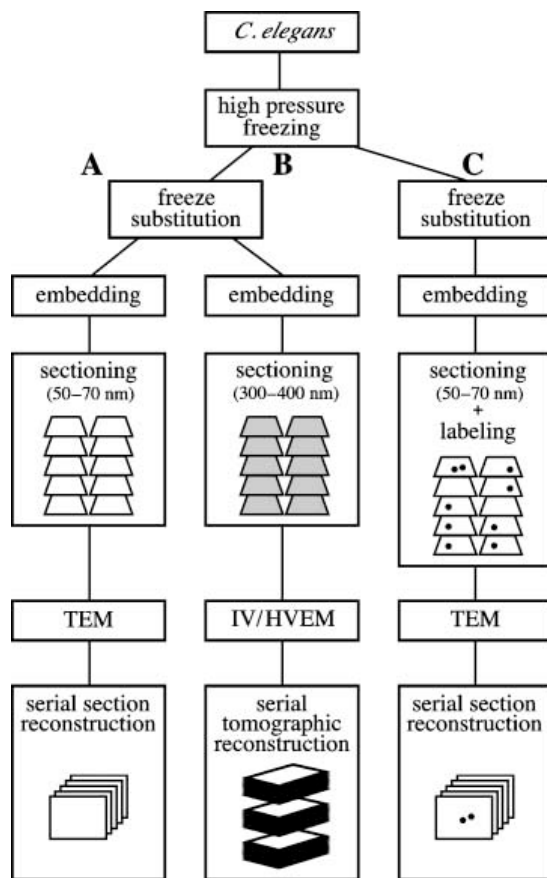


Fig. 7. Using selected, thin-layer embedded specimens for 3-D reconstruction and immunolabelling. To achieve an optimal preservation of *C. elegans* fine structure, high-pressure freezing is applied. (A) Thin sections are used for serial section reconstruction. (B) Semi-thick sections are cut for serial tomographic reconstruction. (C) Serial thin sectioning can be combined with immunolabelling to analyse the distribution of a specific protein in three dimensions.

because the freeze-substituted worms tend to be brittle and therefore 'break' easily. In conclusion, the thick paste method also gives good freezing results. As discussed below, it is recommended to use this method for example when cellular structures have to be identified in serial sections of embryos selected for electron tomography.

Three-dimensional reconstruction of spindle components in selected early C. elegans embryos

We have described the application of high-pressure freezing/freeze-substitution to immobilize, identify and reconstruct cellular features in early *C. elegans* embryos. Importantly, superior preservation of cellular fine structure is the first critical step in undertaking a 3-D structure study. The use of poorly fixed material can lead to artefacts, resulting in errors in the

final model and, ultimately, the interpretation of the 3-D geometry of cellular organelles. In principle, the third dimension can be reconstructed from serial sections with the limitation that the resolution perpendicular to the plane of the sections is no better than twice the average section thickness (McDonald *et al.*, 1996; Fig. 7). When combined with immunogold labelling, the distribution of a specific antigen can be demonstrated in three dimensions (Müller-Reichert *et al.*, 2003). As an alternative technique, electron tomography has evolved in recent years as the method of choice for a 3-D visualization of cellular fine structure. For example, the spindle pole body (Bullitt *et al.*, 1997) and the early mitotic spindle (O'Toole *et al.*, 1999) in *Saccharomyces cerevisiae*, the mammalian kinetochore (McEwen *et al.*, 1998), the centrosome in *Drosophila* (Moritz *et al.*, 1995) and the actin cytoskeleton in *Dictyostelium* (Medalia *et al.*, 2002) have been analysed by tomography. For a genetic system such as *C. elegans*, the combination of techniques described here has several advantages. First, this method allows serial sectioning of selected, resin-embedded whole mounted worms. Second, cellular components can be visualized *in situ* and modelled in three dimensions using appropriate software (Ladinsky *et al.*, 1999; O'Toole *et al.*, 1999; Marsh *et al.*, 2001). Third, montaging of data sets and serial tomography can be applied to cover larger areas and bigger volumes, respectively (Ladinsky *et al.*, 1999; Marsh *et al.*, 2001). In the future, 3-D reconstruction by electron tomography will be important for characterizing wild-type and mutant ultrastructure in genetic systems such as *C. elegans* and, definitively, high-pressure freezing will continue to play a key role in obtaining excellent ultrastructural preservation for these types of 3-D studies.

References

- Brenner, S. (1974) The genetics of *Caenorhabditis elegans*. *Genetics*, **77**, 71–94.
- Bullitt, E., Rout, M.P., Kilmartin, J.V. & Akey, C.W. (1997) The yeast spindle pole body is assembled around a central crystal of Spc42p. *Cell*, **89**, 1077–1086.
- Dahl, R. & Staehelin, L.A. (1989) High pressure freezing for the preservation of biological structure: theory and practice. *J. Electron Microsc. Techn.* **13**, 165–174.
- Dernburg, A.F., McDonald, K., Moulder, G., Barstead, R., Dresser, M. & Villeneuve, A.M. (1998) Meiotic recombination in *C. elegans* initiates by a conserved mechanism and is dispensable for homologous chromosome synapsis. *Cell*, **94**, 387–398.
- Desai, A., Rybina, S., Muller-Reichert, T., Shevchenko, A., Hyman, A.A. & Oegema, K. (2003) KNL-1 directs assembly of the microtubule binding interface of the kinetochore in *C. elegans*. *Genes Dev.* (in press).
- Echlin, P., Skaer, H.B., Gardiner, B.O., Franks, F. & Asquith, M.H. (1977) Polymeric cryoprotectants in the preservation of biological ultrastructure. II. Physiological effects. *J. Microsc.* **110**, 239–255.
- Favre, R., Hermann, R., Cermola, M., Hohenberg, H., Müller, M. & Bazzicalupo, P. (1995) Immuno-gold-labelling of CUT-1, CUT-2 and cuticulin epitopes in *Caenorhabditis elegans* and *Heterorhabditis* sp. processed by

- high pressure freezing and freeze-substitution. *J. Submicrosc. Cytol. Pathol.* **27**, 341–347.
- Hall, D.H. (1995) Electron microscopy and three-dimensional image reconstruction. *Meth. Cell Biol.* **48**, 395–436.
- van Harrevelde, A. & Crowell, J. (1964) Electron microscopy after rapid freezing on a metal surface and substitution fixation. *Anat. Rec.* **149**, 381–386.
- Hohenberg, H., Mannweiler, K. & Sleytr, U.B. (1994) High pressure freezing of cell suspensions in cellulose capillary tubes. *J. Microsc.* **175**, 34–43.
- Howe, M., McDonald, K.L., Albertson, D.G. & Meyer, B.J. (2001) HIM-10 is required for kinetochore structure and function on *Caenorhabditis elegans* holocentric chromosomes. *J. Cell Biol.* **153**, 1227–1238.
- Jones, T.J. & Gwynn, I.A. (1992) A method for rapid fixation and dehydration of nematode tissue for transmission electron microscopy. *J. Microsc.* **164**, 43–52.
- Kirkham, M., Müller-Reichert, T., Oegema, K., Grill, S. & Hyman, A.A. (2003) SAS-4 is a *C. elegans* centriolar protein that controls centrosome size. *Cell*, **112**, 575–587.
- Kremer, J.R., Mastronarde, D.N. & McIntosh, J.R. (1996) Computer visualization of three-dimensional image data using IMOD. *J. Struct. Biol.* **116**, 71–76.
- Ladinsky, M.S., Mastronarde, D.N., McIntosh, J.R., Howell, K.E. & Staehelin, L.A. (1999) Golgi structure in 3 dimensions: functional insights from the NRK cell. *J. Cell Biol.* **144**, 1135–1149.
- Lonsdale, J.E., McDonald, K.L. & Jones, R.L. (2001) Microwave polymerisation in thin layers of London Resin White allows selection of specimens for immunogold labelling. *Microwave Techniques and Protocols* (ed. by T. Giberson & R. S. Demaree), pp. 139–153. Humana Press, Totowa, NJ.
- Marsh, B.J., Mastronarde, D.N., Buttle, K.F., Howell, K.E. & McIntosh, J.R. (2001) Organellar relationships in the Golgi region of the pancreatic beta cell, line, HIT-T15, visualized by high resolution electron tomography. *Proc. Natl Acad Sci. USA*, **98**, 2399–2406.
- Mastronarde, D.N. (1997) Dual-axis tomography: an approach with alignment methods that preserve resolution. *J. Struct. Biol.* **120**, 343–352.
- McDonald, K.L. (1994) Electron microscopy and EM immunohistochemistry. *Meth. Cell Biol.* **44**, 411–444.
- McDonald, K. (1999) High-pressure freezing for preservation of high resolution fine structure and antigenicity for immunolabeling. *Electron Microscopy Methods and Protocols* (ed. by N. Hajibagheri), pp. 77–97. Humana Press, Totowa, NJ.
- McDonald, K. & Müller-Reichert, T. (2002) Cryomethods for thin section electron microscopy. *Meth. Enzymol.* **351**, 96–123.
- McDonald, K., O'Toole, E.T., Mastronarde, D.N., Winey, M. & McIntosh, J.R. (1996) Mapping the three-dimensional organization of microtubules in mitotic spindles of yeast. *Trends Cell Biol.* **6**, 235–239.
- McEwen, B.E., Hsieh, C., Matteyses, A.L. & Rieder, C.L. (1998) A new look at kinetochore structure in vertebrate somatic cells using high-pressure freezing and freeze substitution. *Chromosoma*, **107**, 366–375.
- Medalia, O., Weber, I., Frangakis, A.S., Nicastro, D., Gerisch, G. & Baumeister, W. (2002) Macromolecular architecture in eukaryotic cells visualized by cryoelectron tomography. *Science*, **298**, 1209–1213.
- Moor, H. (1987) Theory and practice of high pressure freezing. *Cryotechniques in Biological Electron Microscopy* (ed. by R. A. Steinbrecht & K. Zierold), pp. 175–191. Springer Verlag, Berlin.
- Moritz, M., Braunfeld, M.B., Fung, J.C., Sedat, J.W. & Alberts, B.M. (1995) Three-dimensional structural characterization of centrosomes from early *Drosophila* embryos. *J. Cell Biol.* **130**, 1149–1159.
- Müller-Reichert, T., Sassoon, I., O'Toole, E., Romao, M., Ashford, A.J., Hyman, A. & Antony, C. (2003) Analysis of the distribution of the kinetochore protein Ndc10p in *Saccharomyces cerevisiae* using 3-D modeling of mitotic spindles. *Chromosoma*, **111**, 417–428.
- O'Toole, E., McDonald, K., Hyman, A. & Müller-Reichert, T. (2002) High-voltage electron tomography of the centrosome in *Caenorhabditis elegans*. *Microsc. Microanal.* **8** (Suppl. 2), 880CD–881CD.
- O'Toole, E.T., McDonald, K.L., Mäntler, J., McIntosh, J.R., Hyman, A.A. & Müller-Reichert, T. (2003) Morphologically distinct microtubule ends in the mitotic centrosome of *Caenorhabditis elegans*. *J. Cell Biol.* (in press).
- O'Toole, E.T., Winey, M. & McIntosh, J.R. (1999) High voltage electron tomography of spindle pole bodies and early mitotic spindles in the yeast, *Saccharomyces cerevisiae*. *Mol. Biol. Cell.* **10**, 2017–2031.
- Priess, J.R. & Hirsh, D.I. (1986) *Caenorhabditis elegans* morphogenesis: the role of the cytoskeleton in elongation of the embryo. *Dev. Biol.* **117**, 156–173.
- Rappleye, C.A., Paredez, A.R., Smith, C.W., McDonald, K.L. & Aroian, R.V. (1999) The coronin-like protein POD-1 is required for anterior-posterior axis formation and cellular architecture in the nematode *Caenorhabditis elegans*. *Genes Dev.* **13**, 2838–2851.
- Shepard, B. & Clark, C. (1976) Structure of the anterior alimentary tract of the passively feeding nematode *Pratylenchus penetrans* (Nematoda: Pratylenchidae). *Nematologica*, **31**, 321–334.
- Spurr, A.R. (1969) A low-viscosity epoxy resin embedding medium for electron microscopy. *J. Ultrastruct. Res.* **26**, 31–43.
- Studer, D., Michel, M. & Müller, M. (1989) High-pressure freezing comes of age. *Scann. Microsc. Suppl.* **3**, 253–269.
- Ward, S., Thomson, N., White, J.G. & Brenner, S. (1975) Electron microscopical reconstruction of the anterior sensory anatomy of the nematode *Caenorhabditis elegans*. *J. Comp. Neurol.* **160**, 313–338.

Structural changes at microtubule ends accompanying GTP hydrolysis: Information from a slowly hydrolyzable analogue of GTP, guanylyl (α,β)methylenediphosphonate

THOMAS MÜLLER-REICHERT*, DENIS CHRÉTIEN, FEDOR SEVERIN, AND ANTHONY A. HYMAN

Cell Biology Program, European Molecular Biology Laboratory, Meyerhofstrasse 1, Postfach 1022.09, D-69117, Heidelberg, Germany

Communicated by Kai Simons, European Molecular Biology Laboratory, Heidelberg, Germany, December 29, 1997 (received for review December 12, 1997)

ABSTRACT Microtubules are dynamic polymers that interconvert between periods of slow growth and fast shrinkage. The energy driving this nonequilibrium behavior comes from the hydrolysis of GTP, which is required to destabilize the microtubule lattice. To understand the mechanism of this destabilization, cryo-electron microscopy was used to compare the structure of the ends of shrinking microtubules assembled in the presence of either GTP or the slowly hydrolyzable analogue guanylyl (α,β)methylenediphosphonate (GMPCPP). Depolymerization was induced by cold or addition of calcium. With either nucleotide, we have observed curled oligomers at the ends of shrinking microtubules. However, GDP oligomers were consistently more curved than GMPCPP oligomers. This difference in curvature between depolymerizing GDP and GMPCPP protofilaments suggests that GTP hydrolysis is accompanied by an increase in curvature of the protofilaments, thereby destabilizing the lateral interactions between tubulin subunits in the microtubule lattice.

Microtubules are polar macromolecules composed of tubulin α - β heterodimers (1). The head-to-tail alignment of these tubulin dimers forms protofilaments, which are juxtaposed to form the cylindrical microtubule wall (2). Microtubules show alternating phases of growth and shrinkage. The interconversion between these phases is unpredictable, a process known as dynamic instability (3–7). GTP hydrolysis is thought to play a key role in regulating this dynamic behavior of microtubule growth and shrinkage. GTP bound to β -tubulin is hydrolyzed to GDP during—or soon after—microtubule assembly (8–10). The resulting GDP microtubule lattice is unstable. In contrast, work with nonhydrolyzable analogues of GTP has shown that a GTP-like lattice is stable (11, 12).

How does GTP hydrolysis destabilize the microtubule lattice? There is some evidence that tubulin can take up different conformational states according to its nucleotide state. The GTP- and GDP-bound states of tubulin in the dimeric form differ by Raman spectroscopy (13) in α -helix and anti-parallel β -sheet content. Analysis of tubulin structure by cryo-electron microscopy (EM) has shown that in the presence of a nonhydrolyzable analogue of GTP, guanylyl (α,β)methylenediphosphonate (GMPCPP), the average length of the tubulin dimer is 0.3 nm longer than in microtubules consisting of GDP-tubulin (14). These data combine to suggest that GTP hydrolysis changes the conformation of the tubulin dimer.

How could structural changes in the tubulin dimer induced by GTP hydrolysis destabilize the microtubule lattice? It has been known for a long time that the structure of microtubule

ends is different between growing and shrinking phases. Microtubules grow by elongation of tubulin sheets that later close to form the cylindrical wall (15–17), whereas microtubules depolymerize by coiling of individual protofilaments and end-wise release of curled oligomers (18–20) with a radius of curvature of about 18–20 nm (19). Combined with the data discussed above, suggesting that tubulin could take up two conformations, the striking images of curled oligomers during depolymerization suggested the following model: when liganded with GTP, tubulin is in a “straight” conformation. Upon GTP hydrolysis, the tubulin molecule would tend to adopt a “curved” conformation (21). This model was developed by Mandelkow *et al.* (19) to suggest that GTP hydrolysis, by increasing the curvature of the protofilaments, forces them to peel off the microtubule wall and that this change in curvature is the driving force for microtubule depolymerization. These models suggest that the GTP protofilament should be less curved than GDP protofilaments. However, individual GTP protofilaments have never been observed by electron microscopy.

Here, we have looked at the curvature of protofilaments liganded with GMPCPP, a nonhydrolyzable analogue of GTP, to trap protofilaments in the GTP state (12, 14). We have compared this curvature with that of protofilaments liganded with GDP. We show that both GDP and GMPCPP protofilaments are curved during microtubule disassembly. However, GDP protofilaments are more curved than GMPCPP protofilaments. This result suggests a difference in structure between GTP and GDP protofilaments and is compatible with the model suggesting that an increase in curvature could drive microtubule depolymerization.

MATERIALS AND METHODS

Tubulin Preparation and GMPCPP Synthesis. Calf brain tubulin was purified by two cycles of assembly/disassembly in the presence of glycerol and subsequent phosphocellulose chromatography as described previously (22). Tubulin concentration was determined from video-microscope measurements using an association constant of $3.8 \mu\text{M}^{-1}\text{s}^{-1}$, thus measuring the concentration of active tubulin (23). Axonemes were isolated from *Tetrahymena thermophila* (24). GMPCPP was synthesized as described (12), except that the final product was purified by two rounds of precipitation in ethanol. Tubulin assembly was performed at 37°C in BRB80 (80 mM Pipes/1 mM EGTA/1 mM MgCl_2 , pH 6.8 with KOH) + 1 mM GTP or 0.1 mM GMPCPP.

Cryo-EM. The ends of shrinking microtubules were analyzed on self-assembled microtubules according to the methods of Chrétien *et al.* (17). For observation of cold-

The publication costs of this article were defrayed in part by page charge payment. This article must therefore be hereby marked “advertisement” in accordance with 18 U.S.C. §1734 solely to indicate this fact.

© 1998 by The National Academy of Sciences 0027-8424/98/953661-6\$2.00/0 PNAS is available online at <http://www.pnas.org>.

Abbreviations: EM, electron microscopy; DIC, differential interference contrast; GMPCPP, guanylyl (α,β)methylenediphosphonate.

*To whom reprint requests should be addressed. e-mail: reichert@embl-heidelberg.de.

depolymerized GDP microtubules, tubulin concentration was adjusted to 9 mg/ml, and the microtubules were assembled for 3.5 min at 37°C. A 4- μ l sample was then transferred to the holey carbon-coated grid, and depolymerization was initiated by lowering the temperature of the sample to about 4°C using a cold stream of air blown onto the specimen. We checked the extent of evaporation by measuring the conductivity of a 1 M NaCl solution under these conditions. Evaporation was limited to 15% over the 30 sec needed to cool the specimen. GMPCPP microtubules were assembled at a tubulin concentration of 0.4 mg/ml for 30 min and subsequently depolymerized for 1 min on ice to ensure that all microtubules were in the shrinking phase. Using the same tubulin concentration for GMPCPP as was used for GTP resulted in an extensive end to end annealing of the microtubules that render the analysis of the ends impossible. For calcium-induced depolymerization, GDP microtubules were assembled at either 5 mg/ml or 9 mg/ml tubulin concentration for various times, and GMPCPP microtubules were polymerized for 1 h at a tubulin concentration of 0.4 mg/ml. Depolymerization was started by mixing rapidly 9 volumes of microtubule solution with 1 volume of a 10 \times stock of CaCl₂ to give a final concentration of either 4 or 40 mM. The sample was then rapidly transferred to a prewarmed carbon-coated grid and prepared for cryo-EM. Storage and observation of the samples were performed as described previously (17). The structure of microtubule ends and of depolymerization products was analyzed on enlarged prints. Radii of curvature were determined by overlaying circles of defined curvature on the prints.

Site Occupancy of GMPCPP Microtubules. Microtubules were polymerized from 300 μ l of 5 mg/ml tubulin preincubated with GMPCPP on ice for 15 min (GMPCPP tubulin) for 30 min at 37°C. The nucleotides were extracted as described (25) and analyzed on a monoQ 1.6/5 column using a SMART system (Pharmacia). The column was equilibrated with BRB80, and the sample was loaded and eluted with 20 column volumes of gradient 0–400 mM NaCl in BRB80. GTP, GDP, and GMPCPP separated well. Because GMPCPP tubulin is free of GTP, the tubulin concentration was calculated using the N-site GTP. The site occupancy of GMPCPP was calculated by comparing GMPCPP with GDP. GMPCPP site occupancy was 70%. To increase the site occupancy to 90%, tubulin was equilibrated with GMPCPP using a desalting column HR 10/10 (Pharmacia). The column was pre-equilibrated with 10 ml of 100 μ M GMPCPP in BRB80. Two hundred microliters of cycled tubulin (15 mg/ml) in 100 μ M GMPCPP in BRB80 was loaded. Protofilament curvature during depolymerization was examined at high site occupancy. No difference in curvature of the protofilaments was noticed when microtubules depolymerize (data not shown).

Video-Enhanced Differential Interference Contrast (DIC) Light Microscopy. Video-DIC light microscopy was performed as described previously (17) to analyze the depolymerization rates of axoneme-seeded microtubules. Measurements included both plus- and minus-ended microtubules. We

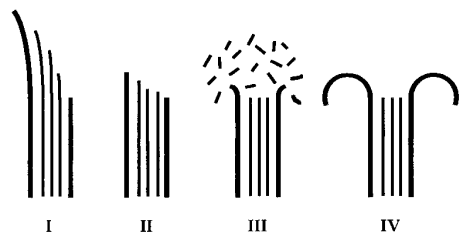


FIG. 1. Classification of microtubule ends as observed by cryo-EM. Four classes of ends were defined: I, curved sheets; II, tapered or blunt ends; III, tapered or blunt ends surrounded by a "cloud" of oligomeric structures; and IV, ends showing curved oligomers.

have used special homemade metal chambers to induce cold depolymerization of the microtubules. Long microtubules

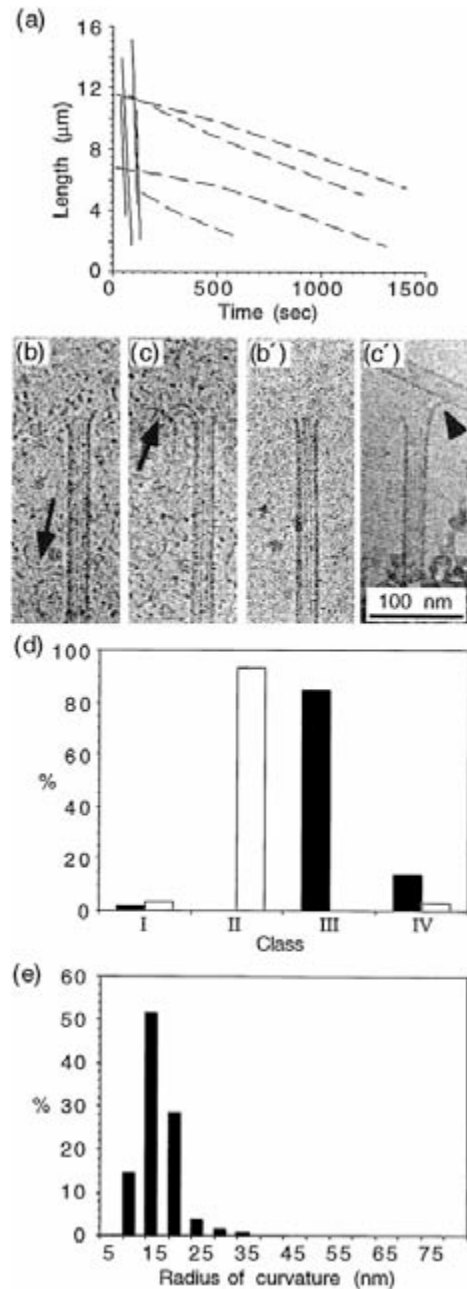


FIG. 2. Cold-induced depolymerization of GDP and GMPCPP microtubules. (a) Length versus time plots of GDP (plain lines) and GMPCPP microtubules (dotted lines) obtained by video-DIC light microscopy. Depolymerization rates of $-20.3 \pm 4.9 \mu\text{m}/\text{min}$ and $-0.3 \pm 0.1 \mu\text{m}/\text{min}$ were measured for GDP and GMPCPP microtubules, respectively. (b, c) Ends of depolymerizing GDP microtubules. Curved oligomeric structures are indicated by arrows. (b', c') Ends of depolymerizing GMPCPP microtubules as observed by cryo-electron microscopy. The arrowhead in (c') shows a curled end. (d) Percentage of end types observed after cold depolymerization of GDP (black bars) and GMPCPP microtubules (open bars). About 85% of the GDP microtubule ends showed oligomeric structures, and 95% of the GMPCPP microtubules showed tapered or blunt ends. (e) Curvature of the oligomers observed during cold depolymerization of GDP microtubules. The average radius of curvature was $19 \pm 4.1 \text{ nm}$.

were allowed to grow at 37°C by placing the specimen chambers on a thermostated plate. To induce microtubule depolymerization, the specimen chambers were mounted on the stage of the light microscope, and metal blocks were placed on top of the specimen chambers. The metal blocks and both the objective and the condenser of the light microscope were cooled by a solution containing ~80% water and ~20% methanol using a brass collar and cooling tubes. The temperature inside the specimen chamber could be accurately controlled using a fine thermocouple. The lowest temperature achieved was 7°C. The temperature could be reduced from 37°C to 7°C in about 3–4 min. The conditions used for assembly were as described for the cryo-EM experiments, except that the tubulin concentrations were 1.8 and 0.25 mg/ml for assembly in the presence of GTP and GMPCPP, respectively. To examine calcium-induced disassembly of microtubules, we used glass chambers made of a glass slide and a coverslip (5). The microtubules were allowed to grow at 37°C as before, and the specimen chamber was placed on the stage of the microscope. The stage, the objective, and the condenser were heated using a homemade device to ensure a temperature of 37°C

inside the specimen chamber. Depolymerization was induced by perfusing a large volume of prewarmed tubulin at the same concentration (and in the same buffer as was used for assembly) and containing either 4 or 40 mM calcium. The tubulin concentration was 2 mg/ml and 0.1 mg/ml for assembly in the presence of GTP and GMPCPP, respectively. Analysis of the video sequences and rate measurements was performed as described (17).

RESULTS

We wanted to examine the structure of GMPCPP microtubules to investigate whether the curvature of protofilaments during disassembly was changed by GTP hydrolysis. Study of the depolymerization products of GMPCPP microtubules is hampered by the fact that under normal conditions of isothermal dilution, GMPCPP microtubules do not depolymerize. We destabilized GMPCPP microtubules using either cold depolymerization or calcium (12). To confirm that GMPCPP microtubules depolymerize in the presence of cold or calcium without hydrolysis, we labeled the γ phosphate of GMPCPP

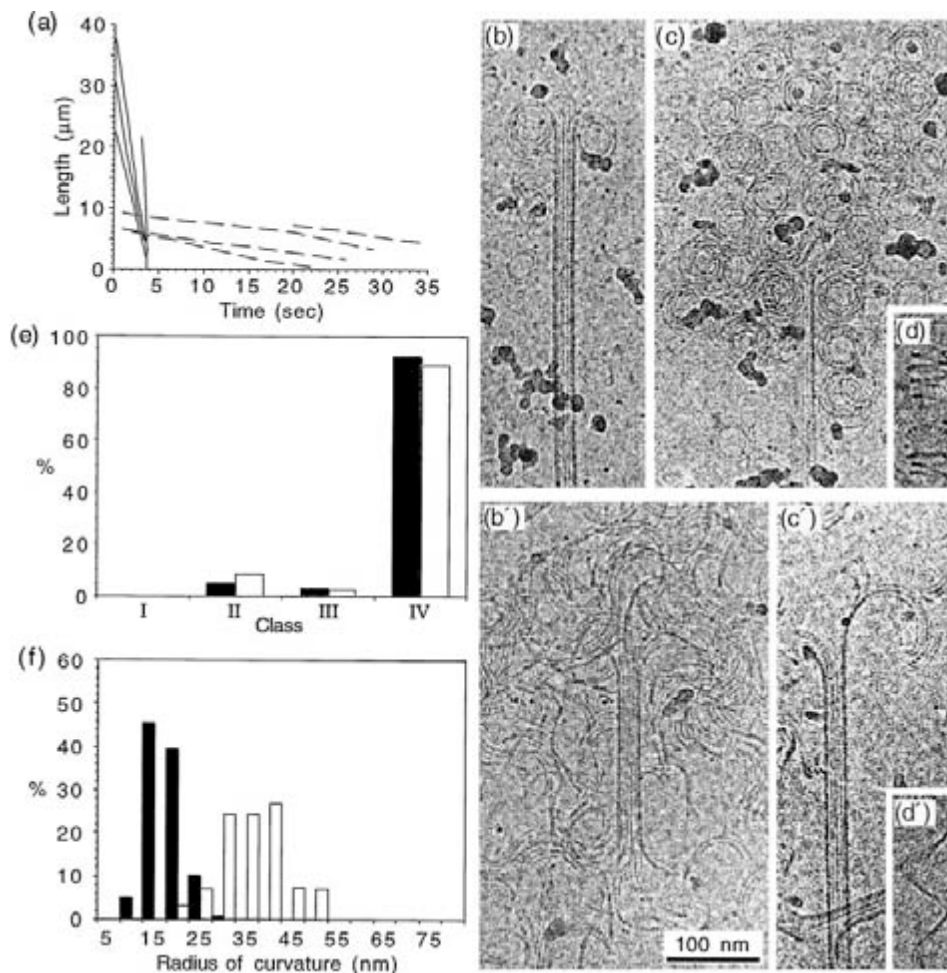


FIG. 3. Depolymerization of GDP and GMPCPP microtubules in the presence of 4 mM calcium. (a) Length versus time plots of GDP (plain lines) and GMPCPP microtubules (dotted lines). Depolymerization rates of $-611 \pm 125 \mu\text{m}/\text{min}$ and $-13.0 \pm 3.2 \mu\text{m}/\text{min}$ were measured for GDP and GMPCPP microtubules, respectively. (b–d) Depolymerization products of GDP microtubules. (b'–d') Depolymerization products of GMPCPP microtubules. Curved oligomeric structures (b, b', c, c') and spirals of protofilaments (d, d') were observed in both cases. (e) Percentage of end types observed after calcium depolymerization of GDP (black bars) and GMPCPP microtubules (open bars). About 90% of both GDP and GMPCPP microtubule ends displayed curved oligomers. (f) Curvature of the oligomers observed during calcium depolymerization of the GDP (black bars) and GMPCPP microtubules (open bars). The average radius of curvature was $20 \pm 4.1 \text{ nm}$ and $38.6 \pm 7.1 \text{ nm}$ for GDP and GMPCPP oligomers, respectively.

with ^{32}P . Trace amounts of $[\gamma\text{-}^{32}\text{P}]\text{GMPCPP}$ were added during polymerization in the presence of GMPCPP. GMPCPP microtubules were recovered by sedimentation through sucrose, and GMPCPP hydrolysis was monitored by thin layer chromatography (12). Although calcium and cold induced depolymerization of microtubules, neither induced detectable hydrolysis of GMPCPP (data not shown and ref. 12). Because GTP is hydrolyzed in the microtubule lattice to GDP, the structures observed at the depolymerizing ends of GTP microtubules reflect disassembly of a GDP tubulin lattice. Therefore, microtubules assembled in the presence of GTP will be called GDP microtubules. Similarly, microtubules assembled in the presence of GMPCPP will be called GMPCPP microtubules. Microtubules were grown in the presence of either nucleotide and subjected to cold or to calcium. The shrinking rates were measured using video-DIC light microscopy, and the depolymerization products were analyzed using cryo-EM. To better quantify the effects of GTP hydrolysis on microtubule ends, four classes were defined (Fig. 1): I, ends showing outwardly curved sheets; II, blunt or slightly tapered ends; III, blunt or slightly tapered ends surrounded by a cloud of oligomeric structures; and IV, ends showing curved oligomeric structures. Although class I is characteristic of growing microtubules and class III and class IV are characteristic of shrinking microtubules, class II can be seen in either growing or shrinking microtubules.

Cold-Induced Depolymerization. The destabilization of microtubules by cold was characterized initially using video-DIC light microscopy. Microtubules were nucleated from axonemes in the presence of either nucleotide and cooled to 7°C on the stage of the light microscope. Length versus time plots of cold-depolymerizing GDP and GMPCPP microtubules are given in Fig. 2*a*. GDP microtubules were found to shrink at a rate of $-20.3 \pm 4.9 \mu\text{m}/\text{min}$, whereas GMPCPP microtubules depolymerized very slowly at a rate of $-0.3 \pm 0.1 \mu\text{m}/\text{min}$. To characterize the structure of the ends by cryo-EM, microtubules were self-assembled in a test tube. Samples of microtubules assembled in the presence of GTP were transferred to the EM grid and subjected to a cold stream of air to lower the temperature to $\sim 4^\circ\text{C}$ before vitrification. Cold-depolymerizing GDP microtubules observed by cryo-EM showed 85% of microtubules surrounded by a "cloud" of depolymerization products (Fig. 2*b* and *d*) or short and curved oligomers (Fig. 2*c* and *d*). Oligomeric structures were also observed in the background (Fig. 2*b* and *c*, arrows). The average radius of curvature of the curved GDP oligomers was $19.0 \pm 4.1 \text{ nm}$ (Fig. 2*e*).

GMPCPP microtubules were incubated for 1 min on ice before cryo-EM preparation due to the very low rate of shrinkage. A total of 95% of the cold-depolymerized GMPCPP microtubules were identified with tapered or blunt ends (class II) (Fig. 2*b'* and *d*) and showed occasionally short and curved extensions (Fig. 2*c'*, arrowhead); the remaining microtubules showed very short and curved extensions (class IV). Very few products of depolymerization could be identified in the background. The curved structures observed at the ends of GMPCPP microtubules were too short to be measured accurately.

Calcium-Induced Depolymerization. Because the rate of depolymerization of GMPCPP microtubules induced by cooling was too slow to identify a significant number of depolymerization products, we decided to induce depolymerization using calcium. To measure the depolymerization rates, long microtubules were grown from axonemes, and the specimen chambers were perfused with a prewarmed tubulin solution containing 4 mM calcium. Fig. 3*a* compares the length versus time plots of microtubules depolymerized in the presence of 4 mM calcium (note the difference in time scale with Fig. 3*a*). GDP microtubules depolymerized at $-611 \pm 1.25 \mu\text{m}/\text{min}$ compared with $-13.0 \pm 3.2 \mu\text{m}/\text{min}$ for GMPCPP microtu-

bles. Cryo-EM showed that both the GDP and GMPCPP microtubules depolymerized by release of curved oligomers comprising ring-like structures (Fig. 3*b*, *b'*, *c*, and *c'*) and spirals of protofilaments (Fig. 3*d* and *d'*). Roughly 90% of both GDP and GMPCPP microtubules could be identified with curved oligomers at their ends (Fig. 3*e*). The main difference between GDP and GMPCPP oligomers was found in their radii

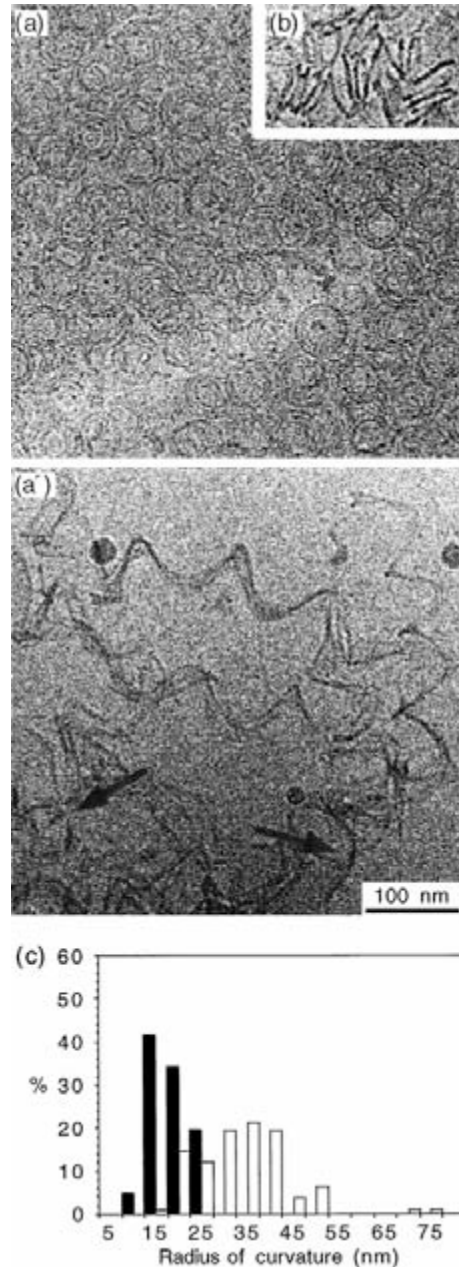


FIG. 4. Depolymerization of GDP and GMPCPP microtubules in the presence of 40 mM calcium. (*a*, *b*) Depolymerization products of GDP microtubules. Curved oligomers (*a*) and spirals of protofilaments, seen as a side view (*b*), were observed. (*a'*) Depolymerization products of GMPCPP microtubules. Long spirals of protofilaments as well as curved oligomers (arrows) were observed in the background. (*c*) Curvature of the oligomeric products of GDP (black bars) and GMPCPP microtubules (open bars). The average radius of curvature was $21.2 \pm 4.3 \text{ nm}$ and $36.2 \pm 10.1 \text{ nm}$ for the GDP and GMPCPP oligomers, respectively.

Table 1. Rates of depolymerization of GDP and GMPCPP microtubules and radius of curvature of oligomers

Conditions	GDP microtubules		GMPCPP microtubules	
	Rate, $\mu\text{m}/\text{min}$	Radius, nm	Rate, $\mu\text{m}/\text{min}$	Radius, nm
Cooling	-20.3 ± 4.9 (8, 163)	19.0 ± 4.1 (140)	-0.3 ± 0.1 (8, 274)	ND
4 mM Ca^{2+}	-611 ± 125 (7, 90)	20.0 ± 4.1 (163)	-13.0 ± 3.2 (12, 176)	38.6 ± 7.1 (160)
40 mM Ca^{2+}	ND	21.1 ± 4.3 (123)	-72.0 ± 45.0 (3, 60)	36.2 ± 10.1 (108)

The rates of depolymerization were measured on individual microtubules using video-DIC light microscopy. The two numbers in parentheses indicate the number of microtubules analyzed and the number of rate measurements performed. The radii of curvature were measured on oligomers present at the ends of shrinking microtubules or in the background of the cryo-EM images. The number in parentheses indicates the number of measurements performed. Mean values are given \pm their standard deviation. ND, not determined.

of curvature (Fig. 3*f*). The mean radius of curvature was 20.0 ± 4.1 nm for the GDP oligomers and 38.6 ± 7.1 nm for the GMPCPP oligomers.

Although the shrinking rate of calcium-depolymerized GDP microtubules was 20-fold greater compared with cold-depolymerized GDP microtubules, the radius of curvature of the oligomers remained constant at ≈ 20 nm in both conditions. We asked whether the curvature of the oligomers released from the ends of shrinking GMPCPP microtubules was also independent of calcium concentration. To increase the rate of depolymerization, we increased the calcium concentration to 40 mM. Under these conditions, the rate of depolymerization of GDP microtubules was too fast to be accurately determined. We observed only a cloud of depolymerized oligomers, either coiled oligomers and rings (Fig. 4*a*) or spirals (Fig. 4*b*). The radii of curvature was 21.1 ± 4.3 nm (Fig. 4*c*). Under the same conditions, GMPCPP microtubules depolymerized at -72 ± 45 $\mu\text{m}/\text{min}$. The depolymerization products were mostly long spirals of protofilaments; some curved oligomers could be observed in the background (see arrows in Fig. 4*a'*). We found radii of curvature of 36.2 ± 10.1 nm for the GMPCPP oligomers as seen at 4 mM calcium. Thus, the radius of curvature is independent of calcium concentration, suggesting that we have revealed the intrinsic curvature of the protofilaments. We conclude that protofilaments of GDP microtubules are more curved than those of GMPCPP microtubules.

DISCUSSION

In this paper, we have investigated the mechanisms by which GTP hydrolysis destabilizes microtubules by examining the structure of protofilaments at microtubule ends, with and without nucleotide hydrolysis. To compare the structure of protofilaments in a "GTP-like" conformation with those in a "GDP-like" conformation, we have trapped the GTP state using the nonhydrolyzable analog of GTP, GMPCPP. Previous studies have shown that the properties of GMPCPP microtubules are very similar to those of microtubules polymerized in the presence of GTP (12, 14). Therefore, GMPCPP as well as other nonhydrolyzable analogues can be considered to mimic closely the GTP form of tubulin. Our results show that during depolymerization, protofilaments released from the ends of GMPCPP and GDP microtubules are curved. The degree of curvature seemed to be independent of increasing rates of depolymerization; although a 10-fold increase in calcium concentration increases the rate of depolymerization by about 5-fold, the radius of curvature does not increase (Table 1). Furthermore, the radius of curvature for cold and calcium depolymerization is the same. Taken together, these data suggest both that we are seeing the intrinsic curvature of the protofilaments and that calcium destabilizes microtubules by other mechanisms such as weakening of interprotofilament bonds (19, 26).

Nevertheless, GMPCPP protofilaments have a different curvature from GDP protofilaments. The most likely reason for this result is that the conformation of tubulin subunits

liganded with GMPCPP is different from that of subunits liganded with GDP. This idea is consistent with previous results obtained on the structure of GMPCPP and GDP microtubules (14). Tubulin molecules in GMPCPP microtubules were found to be ≈ 0.3 nm longer than in GDP microtubules. In analogy to the proposed existence of a "straight" GTP and a more "curved" GDP conformation (21, 27), this size change was interpreted as a difference in curvature between GMPCPP and GDP subunits, although a change in the bond angle between the tubulin dimers could not be excluded (14). With the recent high resolution structure of tubulin from zinc sheets, it should be possible in the near future to understand the exact structural differences between GMPCPP tubulin and GDP tubulin.

Our data support the model that microtubules are destabilized by an increase in curvature of protofilaments induced by GTP hydrolysis (21). Whereas previous models have proposed a change in protofilament structure from straight to curved (19), we have shown that a GMPCPP, and therefore probably a GTP protofilament, is not straight but has an intrinsic curvature of its own. Thus, during polymerization, the curvature of GTP protofilaments is probably constrained within the microtubule lattice. How could the change in curvature induced by GTP hydrolysis destabilize microtubules? The microtubule wall is stabilized by interactions between protofilaments and destabilized by the tendency of protofilaments to curl away from the lattice (14, 18, 19). The curvature change induced by GTP hydrolysis must be constrained within the microtubule lattice. This constraint would induce mechanical strain on the lateral interactions between protofilaments in the microtubule wall. Thus, our data support the idea in which some of the chemical energy from GTP hydrolysis is stored in the lattice as mechanical strain, ready to be released when depolymerization is triggered (19, 28, 29).

We thank Tim Mitchison and Joe Howard for helpful discussions on the work and T. Ashford, J. Bereiter-Hahn, S. Cohen, S. Eaton, P. Gönczy, M. Glotzer, R. Heald, and S. Reinsch for reading the manuscript. This work was supported by the European Molecular Biology Organization (long-term fellowship to T.M.-R.).

1. Avila, J. (1990) *Microtubule Proteins* (CRC, Boca Raton, FL).
2. Amos, L. & Klug, A. (1974) *J. Cell. Sci.* **14**, 523–549.
3. Mitchison, T. & Kirschner, M. (1984) *Nature (London)* **312**, 237–242.
4. Horio, T. & Hotani, H. (1986) *Nature (London)* **321**, 605–607.
5. Walker, R. A., O'Brien, E. T., Pryer, N. K., Sobeiro, M. F., Voter, W. A., Erickson, H. P. & Salmon, E. D. (1988) *J. Cell Biol.* **107**, 1437–1448.
6. Cassimeris, L., Pryer, N. K. & Salmon, E. D. (1988) *J. Cell Biol.* **107**, 2223–2231.
7. Sammak, P. J. & Borisy, G. G. (1988) *Nature (London)* **332**, 724–726.
8. Carlier, M.-F., Didry, D., Simon, C. & Pantaloni, D. (1989) *Biochemistry* **28**, 1783–1791.
9. Purich, D. L. & Kristoffersen, D. (1984) *Adv. Protein Chem.* **36**, 133–212.
10. Kirschner, M. W. (1978) *Int. Rev. Cytol.* **54**, 1–71.

11. Caplow, M., Ruhlen, R. L. & Shanks, J. (1994) *J. Cell Biol.* **127**, 779–788.
12. Hyman, A. A., Salser, S., Drechsel, D. N., Unwin, N. & Mitchison, T. J. (1992) *Mol. Biol. Cell* **3**, 1155–1167.
13. Audenaert, R., Heremans, L., Heremans, K. & Engelborghs, Y. (1989) *Biochim. Biophys. Acta* **996**, 110–115.
14. Hyman, A. A., Chrétien, D., Arnal, I. & Wade, R. H. (1995) *J. Cell Biol.* **128**, 117–125.
15. Erickson, H. P. (1974) *J. Cell Biol.* **60**, 153–167.
16. Simon, J. R. & Salmon, E. D. (1990) *J. Cell Sci.* **96**, 571–582.
17. Chrétien, D., Fuller, S. D. & Karsenti, E. (1995) *J. Cell Biol.* **129**, 1311–1328.
18. Kirschner, M. W., Williams, R. C., Weingarten, M. & Gerhart, J. C. (1974) *Proc. Natl. Acad. Sci. USA* **71**, 1159–1163.
19. Mandelkow, E. M., Mandelkow, E. & Milligan, R. A. (1991) *J. Cell Biol.* **114**, 977–991.
20. Warner, F. D. & Satir, P. (1973) *J. Cell Sci.* **12**, 313–326.
21. Melki, R., Carlier, M.-F., Pantaloni, D. & Timasheff, S. N. (1989) *Biochemistry* **28**, 9143–9152.
22. Ashford, T., Andersen, S. & Hyman, A. A. (1988) in *Cell Biology, a Laboratory Handbook*, ed. Celis, J. E. (Academic, San Diego), 2nd Ed., Vol. 2, pp. 205–212.
23. Mitchison, T. & Kirschner, M. (1984) *Nature (London)* **312**, 232–237.
24. Porter, M. E. & Johnson, K. A. (1983) *J. Biol. Chem.* **258**, 6575–6581.
25. Field, C. M., Al-Awar, O., Rosenblatt, J., Wong, M. L., Alberts, B. & Mitchison, T. J. (1996) *J. Cell Biol.* **133**, 605–616.
26. Tran, P. T., Joshi, P. & Salmon, E. D. (1997) *J. Struct. Biol.* **118**, 107–118.
27. Howard, W. D. & Timasheff, S. N. (1986) *Biochemistry* **25**, 8292–8300.
28. Mickey, B. & Howard, J. (1995) *J. Cell Biol.* **130**, 909–917.
29. Hyman, A. A. & Karsenti, E. (1996) *Cell* **84**, 401–410.

6.2 List of publications

Original publications

O'Toole, E. T., M. Srayko, A. A. Hyman, and T. Müller-Reichert. 2006. Role of *C. elegans* katanin in acentrosomal spindle assembly. *Science*. (submitted).

Özlu, N., M. Srayko, K. Kinoshita, B. Habermann, E. T. O'Toole, T. Müller-Reichert, N. Schmalz, A. Desai, and A. A. Hyman. 2005. An essential function of the *C. elegans* orthologue of TPX2 is to localize activated Aurora A kinase to mitotic spindles. *Dev. Cell*. 9, 237-248.

Dammermann, A., T. Müller-Reichert, L. Pelletier, B. Habermann, A. Desai, and K. Oegema. 2004. Centriole assembly requires both centriolar and pericentriolar material proteins. *Dev. Cell*. 7, 815-829.

Pelletier, L., N. Özlu, E. Hannak, C. Cowan, B. Habermann, M. Ruer, T. Müller-Reichert, and A. A. Hyman. 2004. The *Caenorhabditis elegans* centrosomal protein SPD-2 is required for both pericentriolar material recruitment and centriole duplication. *Curr. Biol*. 14, 863-873.

O'Toole, E. T., K. L. McDonald, J. Mäntler, J. R. McIntosh, A. A. Hyman, and T. Müller-Reichert. 2003. Morphologically distinct microtubule ends in the mitotic centrosome of *Caenorhabditis elegans*. *J. Cell Biol*. 163, 451-456.

Müller-Reichert, T., H. Hohenberg, E. T. O'Toole, and K. McDonald. 2003. Cryoimmobilization and three-dimensional visualization of *C. elegans* ultrastructure. *J. Microsc.* 212, 71-80.

Desai, A., S. Rybina, T. Müller-Reichert, A. Shevchenko, A. Shevchenko, A. Hyman, and K. Oegema. 2003. KNL-1 directs assembly of the microtubule-binding interface of the kinetochore in *C. elegans*. *Genes Dev*. 17, 2421-2435.

Kirkham*, M., T. Müller-Reichert*, K. Oegema*, S. Grill, and A. A. Hyman. (* joint first authors). 2003. SAS-4 is a *C. elegans* centriolar protein that controls centrosome size. *Cell*. 112, 575-587.

Müller-Reichert, T., I. Sassoon, E. O'Toole, M. Romao, A. J. Ashford, A. A. Hyman, and C. Antony. 2003. Analysis of the distribution of the kinetochore protein Ndc10p in *Saccharomyces cerevisiae* using 3-D modeling of mitotic spindles. *Chromosoma*. 111, 417-428.

McDonald, K., and T. Müller-Reichert. 2002. Cryomethods for thin section electron microscopy. *Meth. Enzymol*. 351, 96-123.

Cheeseman, I. M., M. Enquist-Newman, T. Müller-Reichert, D. G. Drubin, and G. Barnes. 2001. Mitotic spindle integrity and kinetochore function linked by the Duo1p/Dam1p complex. *J. Cell Biol*. 152, 197-212.

Müller-Reichert, T., D. Chrétien, F. Severin, and A. A. Hyman. 1998. Structural changes at microtubule ends accompanying GTP hydrolysis: information from a slowly hydrolyzable analogue of GTP, guanylyl (α,β) methylenediphosphonate. *Proc. Natl. Acad. Sci. USA*. 95, 3661-3666.

Müller-Reichert, T., and H. Gross. 1996. Microscopic analysis of DNA and DNA-protein assembly by transmission electron microscopy, scanning tunneling microscopy and scanning force microscopy. *Scan. Microsc. Suppl.* 10, 111-121.

Müller-Reichert, T., H.-J. Butt, and H. Gross. 1996. STM of metal embedded and coated DNA and DNA-protein complexes. *J. Microsc.* 182, 169-176.

Gilson, E., T. Müller, J. Sogo, T. Laroche, and S. M. Gasser. 1994. RAP1 stimulates single- to double-strand association of yeast telomeric DNA: Implications for telomere-telomere interactions. *Nucleic Acids Res.* 22, 5310-5320.

Müller, T., E. Gilson, R. Schmidt, R. Giraldo, J. Sogo, H. Gross, and S. M. Gasser. 1994. Imaging the asymmetric DNA bend induced by Repressor Activator Protein 1 with scanning tunneling microscopy. *J. Struct. Biol.* 113, 1-12.

Butt, H.-J., T. Müller, and H. Gross. 1993. Immobilizing biomolecules for scanning force microscopy by embedding in carbon. *J. Struct. Biol.* 110, 127-132.

Müller, T., and J. Bereiter-Hahn. 1991. Demonstration of calcium in dermal melanocytes of *Xenopus laevis* and *Poecilia reticulata* with electron energy-loss spectroscopy and electron spectroscopic imaging. *J. Microsc.* 162, 141-146.

Book chapters

Müller-Reichert, T., M. Srayko, A. A. Hyman, E. O'Toole, and K. McDonald. 2006. Correlative light and electron microscopy of early *C. elegans* embryos in mitosis. *Cellular Electron Microscopy* (ed. by J. R. McIntosh). (submitted).

McDonald, K. L., M. Morphew, P. Verkade, and T. Müller-Reichert. 2006. Some practical observations regarding high pressure freezing. *Methods in Molecular Biology*. (in press).

Pelletier, L., T. Müller-Reichert, M. Srayko, N. Özlü, A.-L. Schlaitz, and A. A. Hyman. 2004. The *C. elegans* centrosome during early embryonic development. *Centrosomes in Development and Disease* (ed. by E. Nigg), pp. 227-250. Wiley-VCH, Weinheim.

ERKLÄRUNGEN

Hiermit erkläre ich, dass die vorgelegte Habilitationsschrift von mir persönlich angefertigt und ohne andere als die darin angegebenen Hilfsmittel angefertigt, sowie die wörtlich oder inhaltlich übernommenen Stellen als solche gekennzeichnet wurden. Die der Habilitationsschrift zugrunde liegenden Publikationen wurden in Zusammenarbeit mit den genannten Autoren angefertigt. Die Publikationen über SAS-4 (Kirkham et al., 2003), SPD-2 (Pelletier et al., 2004) und TPXL-1 (Özlu et al., 2005) wurden im Labor von Herrn Prof. Dr. A. Hyman (MPI-CBG) erstellt. Alle elektronenmikroskopischen Experimente dazu wurden von mir durchgeführt. Die dafür notwendige EM-Methodik (Müller-Reichert et al., 2003) wurde von mir modifiziert bzw. entwickelt. Die Arbeit über SAS-5/SAS-6 (Dammermann et al., 2004) ist im wesentlichen im Labor von Frau Dr. K. Oegema (UCSD) durchgeführt worden. Mein Beitrag in dieser Zusammenarbeit erstreckt sich auf die EM-Analyse der Zentriolenduplikation und die Immunmarkierungen. Die Darstellung der Mikrotubuli in vitrifiziertem Eis (Müller-Reichert et al., 1998) wurde von mir am EMBL (Heidelberg) erstellt. Die Elektronentomographie des mitotischen Zentrosoms (O'Toole et al., 2003) und die Strukturanalyse der meiotischen Spindel in *C. elegans* (O'Toole et al., 2006) wurden in enger Kooperation mit Frau Dr. E. O'Toole (CU) auf meine Initiative hin und unter meiner Federführung durchgeführt. Bei diesen Arbeiten bin ich daher als korrespondierender Letztautor genannt. Alle tomographischen Daten (Kippserien) wurden im "Boulder Laboratory for 3-D Electron Microscopy of Cells" (Boulder, USA) in Zusammenarbeit mit Frau Dr. E. O'Toole erstellt. Die Kalkulation der Tomogramme, die Modellierung in 3-D und die Quantifizierung der Daten wurden zusammen erarbeitet.

Dr. Thomas Müller-Reichert

Dresden, den 31. März 2006